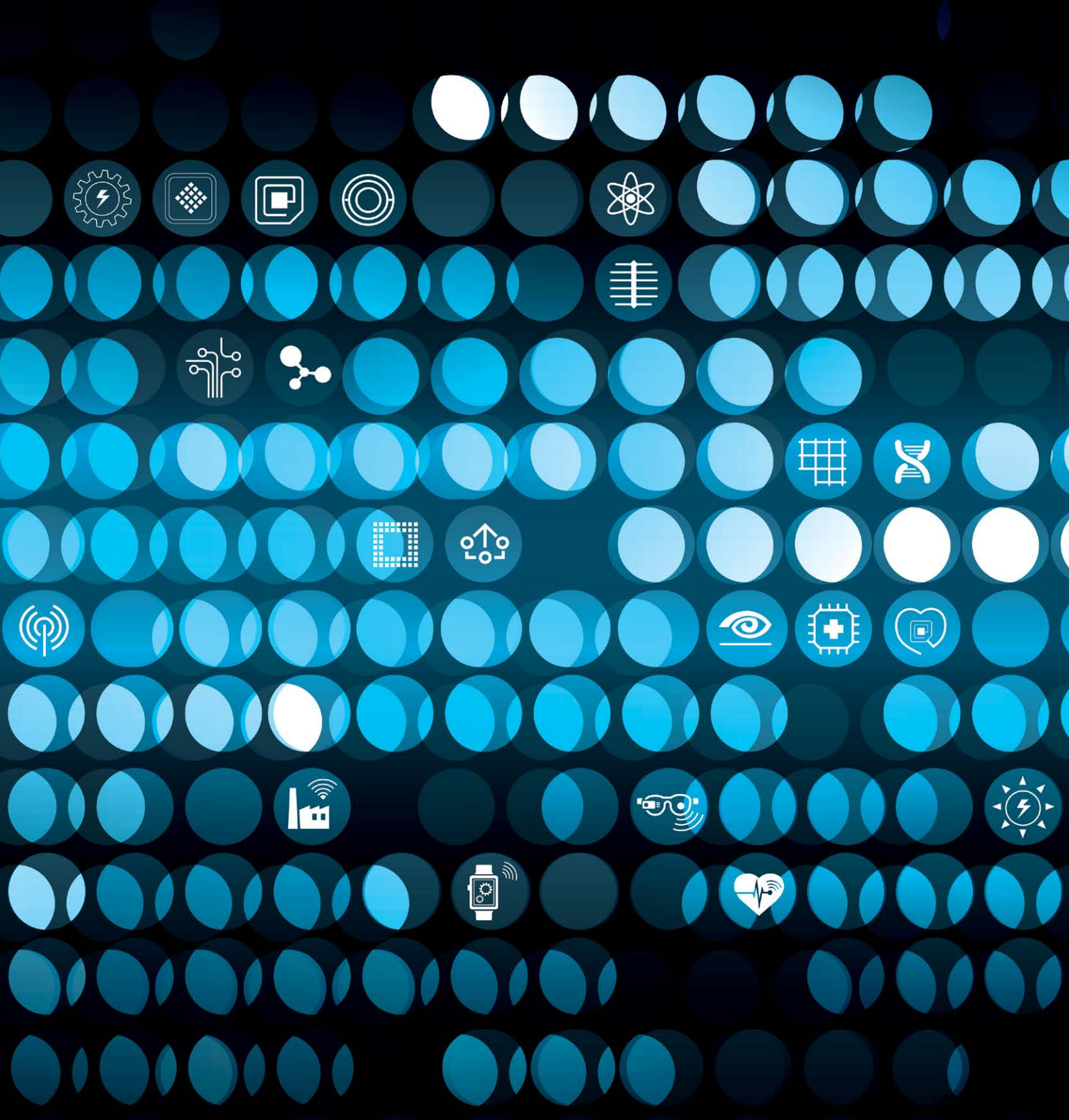




SCIENTIFIC AND
TECHNICAL REPORT
2015



CSEM SA

CSEM SA is a private, non-profit research and technology organization (RTO). Our mission is to ensure the competitiveness of the Swiss economy through the transfer of technologies and know-how from fundamental research to industry.

A 440 strong workforce, with extremely impressive academic backgrounds and often with industrial experience, dedicates its passion to this mission. In this way, CSEM effectively contributes to the process of innovation and its diffusion, which require increasingly close interaction between the world of science and technology and the marketplace.

By bringing to maturity the technologies initiated by its academic partners, CSEM gives all of Swiss industry access to the best in Swiss research. Thanks to the Heterogeneous Technology Alliance (HTA), co-founded by CSEM, we also guarantee access to an even broader range of technological expertise at the European level. In this way, CSEM ensures rapid and concrete technology transfer. CSEM-developed technology platforms offer industry a whole range of solutions to meet market needs and surpass client expectations—from healthcare, watchmaking, aerospace, and security, to consumer electronics, food, energy, and the environment.

CONTENTS

PREFACE	7	SURFACE ENGINEERING	37
MULTIDISCIPLINARY INTEGRATED PROJECTS—MIPS			
Wear-a-Watt—Energy Autonomy for the Wearables	12	Innovative Thin-film Optics for Solid-state Lighting	40
FlatVision—Imaging Optics in Confined Spaces	13	Large-area Plasmonic Substrates Based on Ordered Metallic Nanostructures	41
LiLoTrack—Short-term Forecasting and Storage for Optimal Management of PV Electricity	14	Fabrication of Sub-micron High Contrast Gratings in Hard Semiconductors or Dielectrics	42
muTish—Towards a Cell Sorter for Medium Sized Biological Entities	15	Manufacturing of High-added Value Micro-nanostructured Plastic Components	43
MOFETs II—MHz-operating Organic Field Effect Transistors II	16	Icephobic Coating Associated with Low-power Electromechanical De-icers	44
HybSi—Silicon Hybridization Process for Watch Industry and Precision Mechanisms	17	Sol-gel based Pressure Sensitive Paint for Wind Tunnel and Aeronautics Application	45
MEMSPlant Sense—Miniaturized Implantable Pressure Sensor	18	Sensors and Systems for Wound Care Management	46
MiniNOB—Miniaturized Wearable System for NOBP Measurement	19	DEMOX—a Miniature Non-invasive Optical Oxygen Sensor	47
SMAC 2P—Towards a Flat Form Factor Miniature Atomic Clock	20	Impedance Measurement for 3D Cell Culture Models	48
MICROSYSTEMS	21	Air Pretreatment Platform for Indoor Air Quality Monitoring	49
Microstructuring of Bulk Metallic Glass	23	Automation of Traditional Sample Preparation for Oil, Milk, and Nuts	50
MEMS Scanner with Integrated Position Sensors	24	Integrated and Automated Sample Preparation to Monitor Small Organic Pollutants	51
MEMS Mirror for High Power, Large Angle, 2D Laser Steering	25	Surface Functionalization for Solvent-free Capture and Release of Molecules	52
Design of a MEMS Gas Chromatograph	26	Supercritical CO ₂ Treatment as a Novel Sample Preparation Method for the Analysis of Nanoparticle Content in Sunscreen Agents	53
MEMS Accelerometer with Remote Optical Readout for Power Generator Monitoring	27	UV Absorption and Multi-angle Light Scattering Detector System for Nanoparticle Analysis	54
Advanced Structural Investigation of SiGe Heteroepitaxially Grown Crystal Arrays	28	Functionalization of Teflon Surfaces	55
Cleanroom Compatible Micro-structuring of Silicon using Ultrashort Pulsed Laser Systems	29	Optodex as a Linker to Functionalize Textiles	56
Nondestructive Raman Spectroscopy for Hermetic Package Reliability Analysis	30	Automated Monitoring of Micro-bioreactors	57
MEMS Narrow Band IR Emitters	31	Compact Optical Setup for Wide-field Fluorescence Lifetime Imaging	58
Monitoring Cell Traction	32	Development of a Protein-coated Hydrogel Microcarrier for Stem Cell Expansion	59
ACTION—Active Implants for Optoacoustic Natural Sound Enhancement	33	New Materials for Disposable Sensors	60
Furnace-free Micro-joining with Reactive Nanofoils	34	A Patch for Estimating Exercise Intensity by Monitoring Lactate in Sweat	61
Process Development for Integrating Electronics in Textiles	35	Multi-purpose Bi-directional PC Interface for Printed Electronics Systems	62
WiseSKIN: Wireless Sensor Skin for Tactile Prosthetics	36	PV-CENTER & ENERGY MANAGEMENT	63
		Organic and Printable Photovoltaics at CSEM	66
		Light Management for OPV	67
		Development of Highly Conductive Transparent Materials for PV Applications	68
		White Solar Modules: from Prototypes to Industrial Products	69
		Photovoltaics for Hydrogen Production	70

Perovskite Upscaling: from Cells to Modules	71	Stratospheric Observatory for Infrared Astronomy (SOFIA): Flight Spare Mechanism for the Secondary Mirror	102
Demonstrating Advanced PECVD Reactor for Uniform Coating on both Sides of a Substrate	72	GENEQUAND, a Novel Watch Regulator based on Compliant Mechanisms	103
Metallization and Interconnection for Competitive Silicon Heterojunction Solar Cells	73		
Platform for High-efficiency Silicon Heterojunction Solar Cells	74		
Plastics Compounding Platform and the Formulation Development of PV Module Packaging Materials in CSEM	75	ULTRA-LOW-POWER INTEGRATED SYSTEMS	105
Optimization of Quality of Supply in Demand–Response Schemes	76	A 1 M-Pixel 2000 Frames/s Image Sensor	107
Design and Control of DC Microgrid for Integrating PV in Built Areas	77	Towards the Industrialization of the SunTracker	108
Electrical Energy Optimization at District Level	78	Feature Selection in Support Vector Machines for Cars and Pedestrian Detection	109
Adaptive and Predictive Air Conditioning Control	79	Scale-invariant Object Recognition from Industrial Light-field imaging	110
SYSTEMS	81	System-on-chip for Nanometric-range, High-speed Optical Positioning Measurement	111
Validation Results of the Long-term Medical Survey System (LTMS-S) for Antarctica	83	HearRestore: Nanotracking for Image-guided Microsurgery	112
ECG12CS—12-lead ECG Monitoring System with Cooperative Sensors	84	Efficient Delineation of Curvilinear Networks from Biological Images	113
Activity-specific Step Counting and Energy Expenditure Models using 3D Wrist Acceleration	85	Data Muling for Remote Monitoring	114
A Medical Compliant Wearable Monitoring System for 12-Lead ECG	86	IR-UWB in Intra-satellite Communications	115
Cuffless Blood Pressure Monitoring: CSEM's Portfolio of Non-occlusive Technologies	87	A Wireless Sensor Network for Safe Ship Evacuation	116
Wrist-worn Optical Heart Rate Monitoring: a Comprehensive System Approach	88	WiseFly Routing—Reliability and Self-organization for Wireless Sensor Networks	117
Reliability of Integrated IMUs for Elbow-like Motion Patterns	89	Robust and Accurate Clock Synchronization for Wireless Sensor Networks	118
A Human Centred Design Approach for System Integration of Wearables	90	Using Smart Phones for Remote Powering and Charging of Miniature Wireless Nodes	119
LuCa Phantom Vent V2.0	91	Securing Wireless Links on Resource-limited Devices	120
Ultra-precision Manufacturing of XXL Parts	92	Motion Sensing Behind Walls and Obstacles Using Radio Waves	121
Self-adaptation and Pre-maintenance Strategy in Industrial Production	93	A 6-8 GHz IR-UWB Transceiver ASIC in 65 nm CMOS for Ranging Applications	122
Robotic System for Integration of Electronics into Textiles	94	A Miniature Timing Module Embedding its XTAL within the CMOS Substrate	123
In-situ Tissue Identification by Ultrasonic Pulse Echo Analysis	95	Bluetooth Low Energy, from Integrated Circuit to Application	124
A Platform for a MEMS-based Laser Pointing System with Position Feedback	96	icyTRX-55, an Evolution of the Bluetooth Low Energy (BLE) RF IP	125
Integrated System and Proof of Concept of X-ray Phase Contrast Imaging for Inspection of Composite Materials	97	A Modeling Technique for Simulating Power Supply Noise Coupling in a Complex System	126
Miniaturized Flash Imaging Lidar for Space Robotic Assessment of Precision Force Actuators and Non-contact Force Sensors for Astronomical and Medical Applications	98	An Off-chip Capacitor-free LDO with Fast Transient Response	127
Optical Reference Cavities for Frequency Stabilization of Lasers	99	A Versatile Sensor Interface for IO-Link Applications	128
Atomic Gyroscope for Enhanced Navigation	100	Design and on-Silicon Characterization of a 6T SRAM Memory Operating at Subthreshold Voltage	129
	101	Telemetry Unit for a Neuro-prosthesis Stimulation Chip	130

ANNEXES **131**

Publications	131
Proceedings	133
Conferences and Workshops	138
Research Projects	140
Swiss Commission for Technology and Innovation (CTI)	142
European Commission Projects	145
European Space Agency (ESA), Swiss Space Office and CNES Projects	147
Industrial Property	149
Collaboration with Research Institutes and Universities	149
Teaching	153
Theses	154
Commissions and Committees	155
Prizes and Awards	158

PREFACE

Dear Reader,

It is again a great pleasure to present you with our scientific report: a review of the state-of-the-art applied-science research carried out at CSEM including the highlights of our 2015 research activities. In these pages, you will find numerous examples of how we're continuing to expand as a preeminent research and technology organization, transforming science into groundbreaking technologies and championing innovation in industry.

I also hope that it will encourage you to work more closely with CSEM in the creation of innovative products.

Even if this report is only the "tip of the iceberg" of our accomplishments—since we have to respect our customers' confidentiality requirements—I still hope that you will enjoy reading it, and that doing so gives you a real sense of how CSEM engineers can, by using their creativity and innovation, help industry and society to prepare for the future.

I would like to take this opportunity to thank personally our partners and my colleagues for their efforts and their dedication to what is very much a joint endeavour. We all contribute to the technological excellence of CSEM—day after day, together.

Mario El-Khoury

CEO, CSEM SA

MULTIDISCIPLINARY INTEGRATED PROJECTS—MIPS

Harry Heinzelmann

An important part of CSEM's research activities is carried out within the framework of its five research programs—namely, **Microsystems, Surface Engineering, Integrated Systems, Ultra-Low-Power Integrated Systems, and PV-Center & Energy Management**. These research programs are constantly advanced, reviewed, and adapted to emerging trends and expected future demand from industry. They are presented in detail in the following pages.

Often, however, innovation needs to be driven by a multidisciplinary effort in order to build technology platforms across these separate research programs. For many years CSEM has encouraged collaborative projects of this kind—**Multidisciplinary Integrated Projects (MIPs)**. MIPs are characterized by their high degree of interdisciplinarity and their high level of maturity (high technology readiness level (TRL)), which allow them to demonstrate novel applications with high market potential in relatively short amounts of time. Approximately one quarter of CSEM's annual R&D effort is applied within the MIP program.

The MIP program is re-evaluated every year and consists of ongoing projects and new proposals in a healthy balance that allows quick response times to new market needs. In this way, the MIPs complement CSEM's five topical research programs in an ideal way. The MIP program enables CSEM to offer its industrial clients an even richer portfolio of technologies beyond the possibilities of its individual research programs. Ideally, one deliverable of a MIP is a demonstrator with specifications close to those demanded by industry.

In 2015 a total of 10 projects were carried out. An overview of 9 of these projects is given here; each MIP is presented in more detail on the following pages.

Wear-a-Watt—Energy Autonomy for the Wearables

The goal of the project Wear-a-Watt is an energy harvesting solution integrated into a wristband that could be deployed across different fields of activity, including medtech, the watch industry, and other wearables in general. The proposed solution will integrate a PV cell, a wristband, power management, and the communication of messages to a smartphone.

The solution should be able to work in low illumination environments. Preliminary tests show that power densities in the range of 15-20 $\mu\text{W}/\text{cm}^2$ can be harvested with a single junction, amorphous solar cell with an illumination of approximately 200 lux (typical home lighting level). This would therefore yield up to 400 μW on a typical bracelet of 15-20 cm^2 in dimly lit environments and correspondingly more in a well-lit office (2 mW at 1000 lux) or in full sunlight (over 50 mW, accounting for some shading losses).

The project brings together PV technology, substrate surface structuring technologies, and power management and communication technologies. The first year demonstrator will display the energy harvester's state of charge and in the second year it should periodically communicate with a smartphone allowing the energy harvested by the device to be

visualized. This energy harvesting solution will help extend the autonomy of various devices ranging from watches to wireless sensors. The flexible PV bracelet (or a different form factor) will be dimensioned with respect to the selected application.

FlatVision—Imaging Optics in Confined Spaces

This project aims at developing an ultra-flat imaging system based on a very thin diffractive periscope. The FlatVision system will enable images to be taken of objects of interest in situations where only very limited space is available. It is composed of a very thin, flat periscope made from a wave guide and including specific in- and out-coupling sub-micrometer structures and an imaging structure based on micro-lenses. This periscope-type device will allow an image to be transferred from limited space areas to connected detectors or cameras.

Such a wave guide periscope offers advantages over current flat imaging systems based on CCD linear scanner technology, which are limited to a thickness of at least 2 to 5 mm by their silicon and packaging requirements. The possibility of taking images through thin slits (1 mm) such as the interspaces between teeth is interesting for medical applications.

LiLoTrack—Short-term Forecasting and Storage for Optimal Management of PV Electricity

The technology developed in LILOTRACK will provide a solution for the two main issues related to the integration of photovoltaics into power networks: the variability of generation and demand and the discrepancy between them. LILOTRACK is primarily aimed at buildings with flat roofs, which represent around 40% of the European PV market, and aims to enable end users to maximize the share of energy produced on-site by dynamically increasing production when necessary through orientation of the modules toward the sun. It will also allow the peak power exchanged with the grid to be reduced, which will strongly influence future electricity bills.

From a power system perspective, this technology will make PV energy generation more predictable, and reduce the risks of voltage deviations and reverse power flows. This makes LILOTRACK an attractive solution also for distribution network operators.

muTish—Towards a Cell Sorter for Medium Sized Biological Entities

CSEM previously developed the technology CellFactor for sorting biological objects of sizes above 500 μm . The project muTish pushes this technology toward smaller objects with sizes of between 100 μm and 500 μm . Further, an additional sorter module based on fluorescence contrast-mode object classification makes possible the sorting and dispensing of biological objects into smart well plates with integrated sensors for sample monitoring over long time periods.

The project brings together CSEM's expertise in fluid handling, automation, vision algorithms, bio-sensing, and printing technologies. The demonstrator is a low-cost, tabletop apparatus for the sorting of medium-sized objects/cells into smart well plates with integrated monitoring.

MOFETs II—MHz-operating Organic Field Effect Transistors II

The main objective of MOFETs_II is the further optimization of organic field-effect transistors (OFETs), begun in the MOFETs project in 2014. As a demonstration, their integration into digital circuits—for example as disposable and low-power digital circuits on foils—will be shown. Potential applications exist in memory and display fabrication, the consumer electronics market, and sensing.

HybSi—Silicon Hybridization Process for Watch Industry and Precision Mechanisms

HybSi 2015 is a continuation of HybSi 2013 and 2014, with the goal of further developing technologies for the integration and hybridization of silicon-based components in high-precision micro-mechanisms on the macro scale ("macroMEMS"). To this end, HybSi will also deal with combining additive manufacturing and MEMS technologies.

The main challenges include materials and processes, assembly techniques, tools for assembly, and shock protection strategies:

1. Work on materials and processes for additive manufacturing is aimed at providing materials and process choices that are complementary to DRIE/silicon for fast prototyping and small volume production. The same aims apply with regards to the implementation of new assembly, packaging, and shock-protection strategies for MEMS and MacroMEMS, and for the laser macro-machining of macroMEMS from different materials such as silicon, zerodur, or metallic glasses.
2. Novel concepts of mechanical interfaces help facilitate the assembly of macroMEMS. Some interfaces will be directly produced in silicon (DRIE) while others will be developed using additive manufacturing methods. Experimental characterization of the assemblies resulting from different techniques (strength and aging tests) help qualify the results.
3. As a novel tool optimized for the handling and assembly of macroMEMS parts, an innovative gripper has been designed and fabricated. The goal is the integration and implementation of this specific gripper into an existing die-bonding machine for the handling of silicon parts.
4. Shock protection is essential for highly fragile macroMEMS parts. The approach followed here is the incorporation of dedicated shock-protection features into the macroMEMS component, starting from the early design phase. Some concepts are being proposed and evaluated.

The above developments are focused on those hybridization challenges that are typical to the watchmaking industry.

MEMSplant Sense—Miniaturized Implantable Pressure Sensor

The MEMSplant projects aims to develop long-term (more than five years) implantable, membrane-based MEMS devices. The primary target application is an implantable pressure sensor used mainly for hypertension patients, brain implants, or for prosthetic vascular grafts. The sensor will continuously log data—without the intervention of any external device—at

regular intervals and can be read when needed using an external reader. Such a sensor will make possible the analysis of heart/brain/artificial bypass functions over long periods of time. This work will lead to a more generic platform for miniaturized, active, long-term implants, including for spinal cord stimulation, deep brain stimulation, cochlear implants, optical neuro-stimulation, optical pacemakers, (implantable) microphones, vision prostheses, and glucose monitoring.

The technical deliverables of the project include electro-thermal proximity and mechanically coupled sensors, a reliable package of size 1.5mm x 3mm with four integrated feedthroughs, a miniaturized pump with optimized power consumption, a reliable helium leak testing method, and energy harvesting using PV cells, which is being tested with skin models. The first demonstrator will be based on a long-term implantable pressure sensor using two different sensing principles.

MiniNOB—Miniaturized Wearable System for NOBP Measurement

MiniNOB, launched in 2015, is a three-year MIP targeting the development of a TRL-5 miniaturized wearable system for the continuous measurement of non-occlusive mean blood pressure (NOBP). MiniNOB is built on the results obtained in several previous MIPs, in particular PULSEMON and MONIMIP. Cooperative sensors require a significant increase in technology with respect to the state of the art or to competitive products, but they offer a measurement power for wearable systems that by far exceeds that of classical solutions. Furthermore, they can be miniaturized and manufactured at a low cost. A large part of this necessary increase in technology was addressed in a previous MIP—MONIMIP.

MiniNOB targets the development of cooperative sensors focused on the measurement of NOBP. The system will consist of four low-cost, low-power, highly integrated cooperative sensors clipped on and connected via a conductive garment fitting the chest. NOBP will be computed by a smartphone from other relevant physiological signals (ECG, impedance, and PPG) transmitted via BTLE. The intended use of the product is the continuous monitoring of the blood pressure of outpatients. As the application is medical, the project is executed under ISO 13485 in order to maximize its value for future customers.

SMAC 2P—Towards a Flat Form Factor Miniature Atomic Clock

SMAC 2P furthers the series of developments and constant progress already made with regards to the technologies required by miniature atomic clocks. The targeted application of this project is the implementation of an atomic clock into a wristwatch for the Swiss watchmaking industry. The other applications that will profit from this development are those that require ultra-stable time bases/frequency references while putting major emphasis on compactness and low power consumption. Such applications are typically portable and operate using battery power. They include handheld GPS receivers; portable, high-precision inertial measurement units (IMUs), including gyroscopes, accelerometers, and a time base; small satellites; high-end wireless communication systems (frequency agile systems); certain avionics applications (in particular unmanned aerial vehicles (UAVs)); and elements of natural resource exploration (oil and gas in particular). The future demonstrator consists of a miniature atomic clock with dimensions (L x W x H = 15 x 15 x 5 mm³), power consumption (30 mW), and

frequency stability ($<10^{-9}$ @ 1s) compatible with implementation in a wristwatch or in other portable devices.

Development in SMAC 2P will be focused during an initial phase (2015) on improving the reliability and yield of atomic vapor cell manufacturing, increasing the technology's maturity and lowering the power consumption of the ASIC, and on consolidating and integrating the low-temperature, co-fired ceramics (LTCC) based low-power physics package. A second phase, foreseen for 2016, will allow for optimization and characterization.

Wear-a-Watt—Energy Autonomy for the Wearables

J. Bailat, D. Dominé, N. Blondiaux, G. Cattaneo, L. Sansonnens, L.-E. Perret-Aebi, S. Nicolay, R. Pugin, M. Dadras, A. Luu-Dinh, R. Ferrini, M. Correvon, P.-F. Rüedi, J. Deng, M. Morgan, P. Albert, A.-S. Porret, J. Krauss, C. Bosshard, C. Ballif

CSEM is developing ultra-low power solutions and high performance flexible thin film silicon photovoltaic cells to prepare for tomorrow's autonomous watches and other wearables. The project demonstrator will consist of a watch which measures the energy harvested per day and the instant power produced. These data will be used to size autonomous applications for wearables.

No more chargers and no more wires: the multi-interdisciplinary project Wear-a-Watt builds on the strengths of CSEM in its five research programs to create an ultra-low power wearable system which can operate off the energy harvested from its environment only. The device consists of a wristband with custom made flexible solar cells which powers the electronics embedded in the watchcase.

In the first part of the project, lab prototypes (in Figure 1) are designed and produced to assess the amount of energy available under different illumination conditions. Since the amount of harvested energy strongly depends on the habits, the environment of the watch bearers and the seasons, a statistical study from tests 'au porter' will be realized to assess the variability of the amount of energy the bearers may collect.

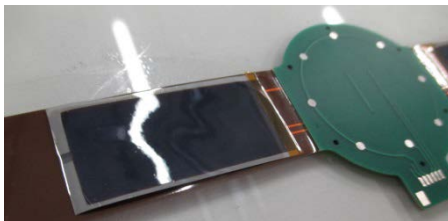


Figure 1: Flexible solar cells and flexible PCB in a lab demonstrator to benchmark the performance of solar cells embedded in wristbands.

The thin film solar cells developed purposely for this study are deposited on nano-imprinted transparent substrates. They show excellent performance even at low illumination levels which is one of the most important features for powering wearables since users may spend very little time out in the sun. A first performance evaluation based on the flexible cells produced at CSEM is presented in Figure 2. At low illumination of 260 lux, the wristband still produces over 140 μW . With two different—winter and summer—scenarios, the energy harvested per day varies from 12 to 40 Joules per day, which is enough to power applications such as activity tracking, notifications, etc.

Table 1: Predictions of harvested power and energy for 12 cm^2 of flexible solar cells with the performances shown in Figure 1.

Illumination	10% of 1 sun	1000 lux	250 lux	25 lux
1 cm²	0.6 mW	50 μW	12 μW	1 μW
12 cm²	7.2 mW	600 μW	144 μW	12 μW
Scenario 1: 5.2 mWh/day	0.2 hour (12min)	5 hours	5 hours	5 hours
Scenario 2: 12.5 mWh/day	1 hour	8 hours	3 hours	3 hours

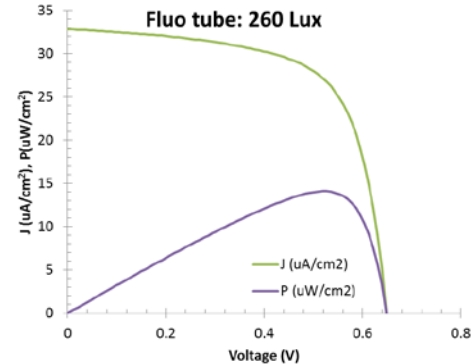


Figure 2: Performance of flexible solar cells at low illumination. A power of 14 μW can be harvested per square centimeter of active PV area under low indoor illumination of 260 Lux.

Based on these first steps, an autonomous wearable system is designed. The applications will target different fields: med-tech, advanced watches, sports watches, internet of things, etc. System integration including feedthrough to the watchcase and cell encapsulation are currently addressed with the aim to comply with the chemical, physical and mechanical conformity standards relevant to watch wristbands. An ultra-low power system for energy management and wireless communication has been designed using, in the current stage, leading edge commercial off-the-shelf components (Figure 3). CSEM is also developing a chip to further optimize energy harvesting from the rigid and flexible photovoltaic cells including several of CSEM's ultra-low power blocks as the icyTRX, an ULP transceiver, and icyflex2, an ULP processor. The chip will be implemented in 2016.

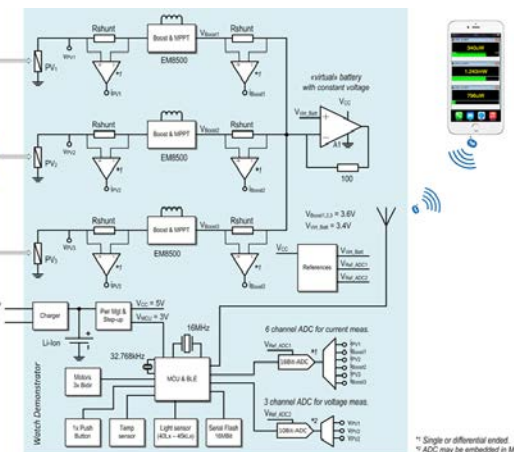


Figure 3: Block-diagram of the energy harvesting monitoring system, taking advantage of the outstanding performances of the new energy harvesting chip EM8500 from EM Marin SA.

FlatVision—Imaging Optics in Confined Spaces

G. Basset, C. Hofer, P. Volet, S. Cattaneo, C. Schneider, A. Luu-Dinh, M. Krieger, B. Gallinet, N. Glaser, D. Hasler, R. Ferrini

Because of technological limitations, miniaturizing imaging systems below the millimetric scale is highly demanding. However, different industries such as medical endoscopes, industrial Quality Control (QC), and micro-robotics are requiring further miniaturized vision systems. CSEM is developing an innovative disposable endoscope based on extra flat flexible polymer slabs used as multimode waveguides. These can be produced with low-cost roll-to-roll production technologies and can be easily customized by patterning, coating and printing techniques according to the specifications of the target application. In order to couple the light (i.e. the image) in and out of the waveguide, diffractive subwavelength gratings are used. These nano-scale optical structures enable a highly efficient and controlled light trapping by total internal reflection, while minimizing the distortion and scattering due to defect near the edges of polymer slabs.

Continuous miniaturization of vision system is driven by the needs of markets of consumer electronics and medtech. Recent developments includes camera as small as 1 cubic millimeter and stereoscopic camera module as small as 2.2x1x1 mm^[1]. Further miniaturization of silicon image sensors, such as CMOS and CCD, is a complex task due to the material and processes involved. CSEM is developing a new endoscopic vision sensor based on disposable and flexible polymer slabs to address current unmet needs by further miniaturizing imaging endoscopes.

In order to reduce further the size of endoscopes, the light sources and imaging system are left out of the endoscope and a polymer slab is used as a multimode imaging waveguide. The waveguide is used to transport light illumination to the objects and to transport back a part of the light reflected from the objects, the imaging beam, by using total internal reflection. Polymer slabs thinner than 200 µm, could be tested and validated as a fully functional endoscope, illuminating and imaging objects at the same time.

In order to couple the illumination and the imaging beams in and out of the polymer slab, extremely flat (< 1 µm) diffractive optical couplers are used. The diffractive optical couplers are made of subwavelength gratings^[2] that can be totally embedded in a polymer matrix. They can be nano-patterned on the polymer surface using established techniques (i.e. hot embossing, UV casting) that are compatible with industrial high volume production lines.

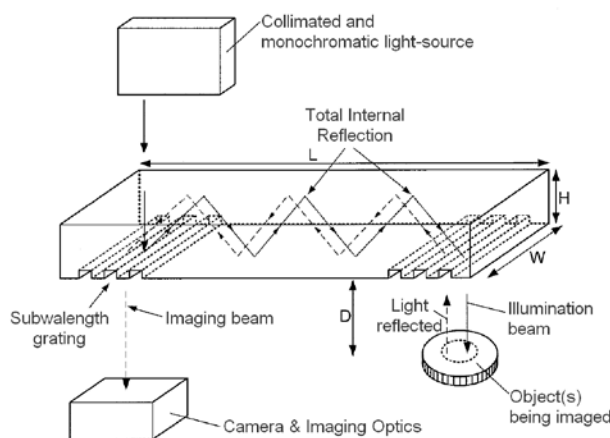


Figure 1: Sketch of a slab waveguide diffractive endoscope.

^[1] NanEye camera from CMOSIS are in pre-production when this article is written. Intra-heart endoscopy during surgery was demonstrated: www.youtube.com/watch?v=KwfknUbpGcg

A sketch of shows the components and the optical path for such a polymer slab endoscope in Figure 1.

The distinctive features of these innovative endoscopes are i) the possibility to achieve an endoscope thickness below 200µm, ii) the ability to record lateral images in confined spaces, iii) the ability to image samples (e.g. biological tissues, objects) in direct contact with the polymer slab, with no minimum imaging distance, and iv) the compatibility with high volume fabrication techniques that can enable the cost-effective production of disposable endoscopes.

A first implementation is a flat line-scanning endoscope acquiring a sequence of 1D images by a scanning movement, with which 2D images are reconstructed by software stitching. The first images acquired with polymer slab thinner than 200µm with an aspect ratio above 150 ($L>150^*H$) exhibits a resolution below 100µm. Such a thin polymer waveguide with its diffractive coupler and an example of acquired image is shown in Figure 2.

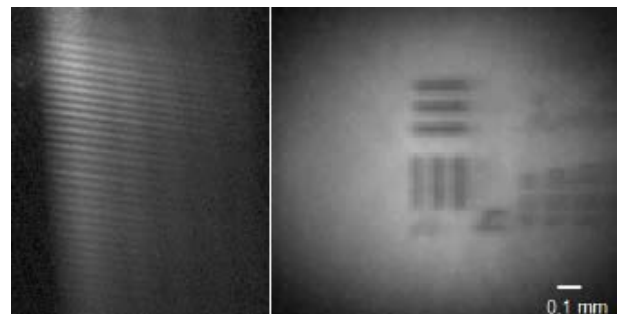


Figure 2: Left: 1D image of an optical target with thin horizontal lines. The thickness of the individual lines is below 100 µm. The thin polymer foil used as an illumination and imaging waveguide is thinner than 200µm ($H<200\mu\text{m}$). Right: Example of 2D image acquired with a diffractive endoscope of a test target reconstructed by stitching 1D images.

These results are highly promising, for example for the development of ultra-thin disposable endoscopes made of thin polymer slab waveguides, having the bulky light sources and imaging system out of the confined spaces being imaged. First prototypes having thicknesses below 200µm exhibit good optical resolution. A fully automated 2D scanning endoscope is currently being developed and tested in various medical and industrial applications

^[2] Patent applications WO2015062641 & WO2014016343

LiLoTrack—Short-term Forecasting and Storage for Optimal Management of PV Electricity

P.-J. Alet, V. Musolino, S. Majerus, Y. Stauffer, M. Boegli, S. Pernecker, A. Hutter, M. Höchemer, S. Widmer, G. Gruener, L.-E. Perret-Aebi, C. Ballif

This project combines energy and power management in relation to photovoltaic (PV) systems on timescales which range from sub-second to one day. The whole system is best suited for mid-sized buildings; the components which have been developed in the project can also add value to most commercial or utility-scale: full-sky image analysis and machine learning for short- and medium-term forecasting, and control of ramp rates with storage for grid integration.

Reduced costs of photovoltaic (PV) systems across the world make it increasingly attractive for households and companies to use their own production rather than purchase electricity from the grid. Maximizing this self-consumption of PV electricity requires managing the energy flows between generation, loads, and storage over at least one day. On the other hand, the challenges in terms of grid integration of PV are related to the instant power exchanged with the grid in terms of absolute values and variations. Managing these challenges therefore requires a very responsive control loop operating on a second timescale.

In this project an integrated management system is being developed with its three components: observation, forecasting, and action. A demonstrator has been installed in one of CSEM's regional centers in Alpnach. Its power chain includes a set of PV modules on single-axis trackers, module-level DC/DC converters with maximum-power-point tracking (MPPT), short-term storage in the form of supercapacitors, and a programmable inverter. Figure 1 shows the central electrical components of the demonstrator.

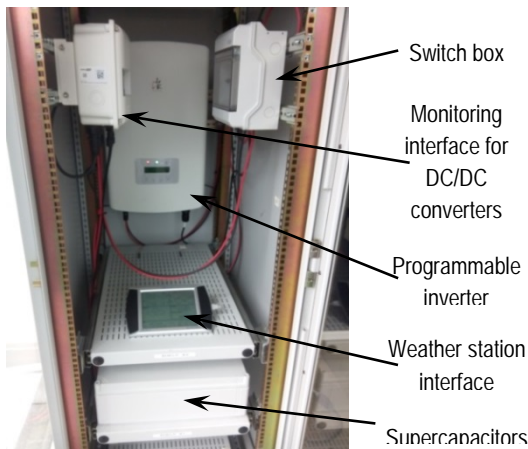


Figure 1: Power and energy management cabinet as installed in the demonstrator.

Performing lifecycle tests on the storage components is desirable to determine the effects of this application on their lifetime, and to integrate this knowledge in the optimal control system. Existing standards have been developed for very different applications such as electric vehicles. New current profiles have been developed in this project to reflect the specificities of our application (Figure 2). A representative set of battery technologies is currently under test with these new profiles.

The energy management system is implemented in a pocket computer running a lightweight Linux distribution (Raspberry Pi). Commercial components (consumer-grade weather station, DC/DC converters, and power meters) generally provide data with a time resolution between one and fifteen minutes and use

proprietary protocols. To monitor the state of the system, custom interfaces have therefore been implemented in the energy management platform to aggregate information from these components.

In addition, a 360° fisheye camera captures full-sky images. These images are analyzed in real time to estimate the current and near-future levels of irradiance. The most challenging situation is when passing clouds cross an otherwise clear sky. This situation represents about 40% of the days in Neuchâtel. It is handled by using pattern recognition techniques to identify clear areas. Cloud motion direction is estimated by comparing subsequent images.

A self-training algorithm was developed to predict energy consumption over 24 h with a 15 min resolution. It is based on support vector regression (SVR) and takes as input information such as occupancy, outdoor temperature, solar radiation, and actual energy consumption. The algorithm continuously adapts its forecasting model to follow seasonal changes and weekly/daily patterns. The algorithm was validated on synthetic and real data with a correlation coefficient between 0.6-0.95, depending on the pattern of energy consumption.

As the PV modules individually operate at their maximum power point and the load is a constraint, possible actions from the control system are charging or discharging the storage elements, adjusting the position of the single-axis trackers, or modifying the operating point of the inverter. Due to the time resolution of most available data to the energy management system, charging and discharging of the storage elements for management of rapid power fluctuations are separately triggered based on the DC voltage. This control has been programmed in the power converters themselves. In the laboratory integration of the components prior to their installation on site, a reduction in ramp rates from 4200 W/s to 15 W/s was demonstrated.

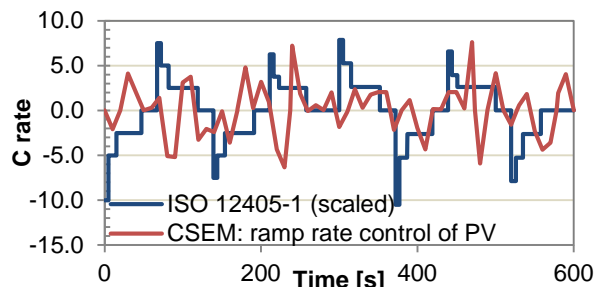


Figure 2: Current profiles for cycle life test on batteries derived from automotive standards (ISO 12405-1, scaled down for single cells) and developed by CSEM for ramp-rate control of PV.

muTish—Towards a Cell Sorter for Medium Sized Biological Entities

S. F. Graf, K. Weggelaar, N. Schmid, R. Limacher, I. Kastanis, S. Widmer, M. Höchemer, C. Hofer, S. Cattaneo, S. Generelli, L. Barbe, D. Migliorelli, D. Caminada, N. Glaser, F. Schleiss, M. Schnieper, H. F. Knapp, P. Steiert, M. Krieger, H. Heinzelmann

With the demand to replace, reduce and refine (3Rs) animal testing, higher quantities of 3D human tissue models will be used in future drug development and toxicity testing. These tissues are too large for conventional flow cytometers and therefore currently have to be manually manipulated. CSEM is thus developing an automated system, which characterizes and sorts individual spheroid tissue models in a size range of 200 to 500 µm. In addition a smart well plate is developed for long-term monitoring pH, lactate and glucose levels of such microtissues.

With this project CSEM's CellFactor technology was extended towards medium sized cells/cell clusters. In the past, this technology was designed for large objects in the size range of 500 to 2000 µm e.g. Zebrafish eggs or Xenopus oocytes and used viscous drag forces for transportation (patented). The extension towards 200 to 500 µm sized samples enables to handle biological entities such as microtissues or cell-spiked alginate beads. Conventional cell sorters do not cover these size ranges, because they are designed for sorting single cells, up to few tens of micrometers in size. Furthermore, they are built for very high throughput which is most often not a hard requirement for larger entities. Finally, conventional cell sorters can have low yields and typically require a huge number of cells to start with. In contrast, CSEM's CellFactor technology is designed to work with only a few up to several thousand entities and can sort them all reliably without loss. Real-time image based analysis and/or fluorescent detection can be used as a sorting criteria. To offer a robust fluidic setup, sensors for inline process control are also developed. Additionally, to offer the complete cycle of analysis, a smart well plate is being developed which allows long-term monitoring of pH, lactate and glucose in each individual well.

The fluidic system (see Figure 1) is designed such that the samples are cycled between two sample containers. In-between the two containers, an image based inspection or fluorescent analysis of the samples takes place. If a sample fits the predefined sorting criteria, a small crossflow of about 20 µl ejects the sample into a well plate. The cycling offers a continuous analysis until all entities have been sorted.



Figure 1: Symmetric flow cell for continuous measurements.

To keep the cost of the system low, the fluorescent module is designed to work with high power LEDs, a highly sensitive photo diode and dedicated optics to measure the very weak signals. Figure 2 shows the module currently optimized for green fluorescent signals (Fluorescein).

To further increase process stability of the fluidic setup, a sensor which measures the impedance of the passing entity is in development. In the lower MHz range, the differences between various cells and air bubbles are detectable. Figure 3 shows a first design of the inline detector.

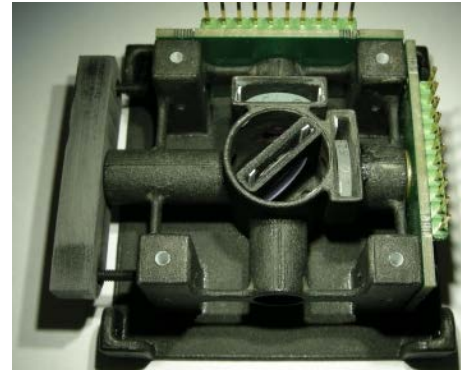


Figure 2: Cost-efficient fluorescence module.

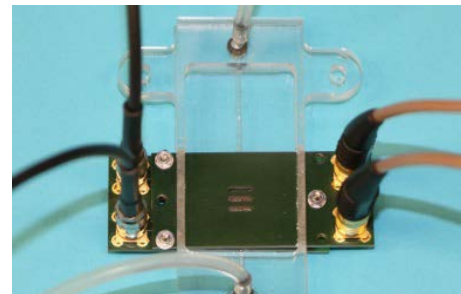


Figure 3: Inline sensor discriminating between air, bubbles and cells.

The smart well plate (see Figure 4) for subsequent long-term monitoring is thermoformed from PMMA substrates with pre-printed electrodes. The electrodes are bio-chemically modified with stable functional layers sensitive to pH, lactate or glucose, to provide long shelf-life and stable monitoring. In parallel to the development of the functional layers of the sensors, a new concept for a printed, solid state reference electrode is being developed to minimize the drifts.

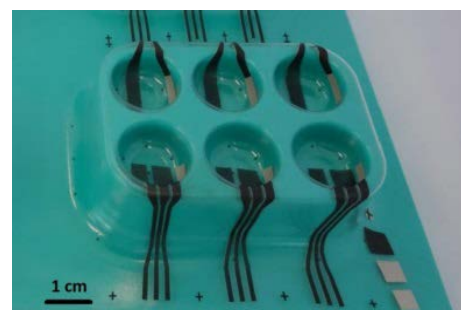


Figure 4: Thermoformed smart well plate with printed electrodes.

The technologies described were designed in close contact with our lead users hepia and fGen which work with neurospheres and alginate beads, respectively. In a next step, the novel cell sorter will be tested and evaluated with our lead users.

CSEM would like to thank the Swiss Federation and the MCCS Micro Center Central Switzerland for their financial support and FHNW for the thermoforming.

MOFETs II—MHz-operating Organic Field Effect Transistors II

N. Marjanović, F. Zanella, F. Herzog, Z. Szamel, A. Bionaz, J. Tillier, O. Sereda, S. Nicolay, D. Ruffieux, G. Nisato, R. Ferrini

CSEM's sub-micrometer-channel organic field-effect transistors (MOFETs) technology – a combination of Hot Embossing Nanoimprint lithography (HE-NIL, standard industrial process) and self-aligned patterning of source and drain contacts – is under continuous optimization. After successfully downscaling the dielectric thickness (<50 nm), the current focus is set on proper selection of the semiconductor and the system integration. A ZnO suspension was casted onto CSEM's semiconductor screening platform. Preliminary results show operational transistors and environmental stability. The system integration was performed by using so-called inkjet gate array approach enabling higher system yield. This integration approach applied to MOFET technology can potentially deliver faster and low operating voltages organic circuits thus opening new opportunities for CSEM (e.g. RFID tags and smart printed circuits boards).

Organic Field Effect Transistors (OFETs), which can be fabricated with high throughput technologies on flexible and disposable substrates, can provide an alternative to inorganic amorphous silicon TFTs (a:Si TFTs). High performing OFETs with switching frequencies in MHz-range and low operating voltages are sufficiently good for display backplanes, RFID tags or disposable sensors.

The aim of MIP MOFETs II project was to further enhance CSEM's state-of-the-art organic field effect transistors (OFETs) technology (see Figure 1) by selecting proper semiconductor, with higher mobility and environmental stability and to demonstrate improved system integration yield by using so-called inkjet gate array approach.

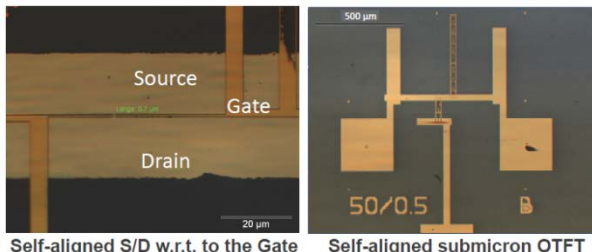


Figure 1: CSEM's sub-micrometer channel OTFTs technology.

Recently amorphous oxide semiconductors, which can also be printed, started drawing more and more attention as an alternative transistor active layer with respect to the traditionally used polymer-based semiconductors. We have tested a ZnO suspension casted by blade-coating on top of Si/SiO₂ dies with pre-patterned Au source /drain electrodes.

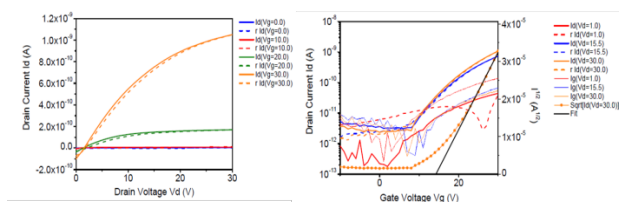


Figure 2: Typical output and transfer characteristics of the first batch of ZnO based OTFTs on the dedicated test substrates.

The resulting ZnO printed film shows a typical OTFTs behavior, illustrated in Figure 2. However, the preliminary resulting field-effect mobility is still low e.g. in the range of 10⁻⁶ cm²/Vs. Therefore, further material/solvent testing need to be continued in order to achieve vacuum-deposited a:Si performances. Afterwards this material should be tested on the MOFETs' transistor stack. This work is in progress.

The second objective of this project was the demonstration of the MOFETs integration capabilities, through a digital circuit. A recent integration approach, the so-called inkjet gate array [11], was applied in a fault-tolerant design. This approach is illustrated in Figure 3.

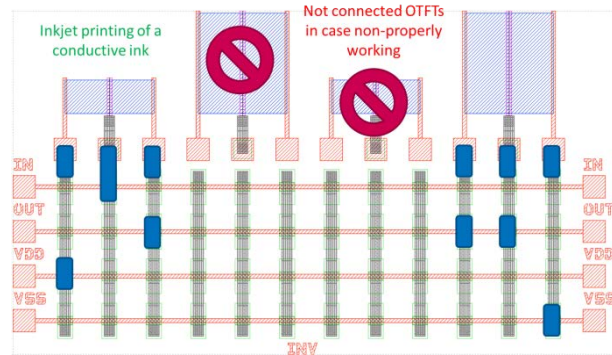


Figure 3: Inkjet Gate Array approach illustrated on Zero-V_{gs} Inverter.

As shown, only the properly working OFETs will be connected to the interconnections/bus lines, while non-working ones will remain disconnected. This interconnection process will be done by inkjet printing (blue areas in Figure 3). As the result, the system integration yield can be maximized.

Finally, the demonstrator, a capacitive sensor digital interface (illustrated in Figure 4), was designed with the above-mentioned integration approach and is under fabrication.

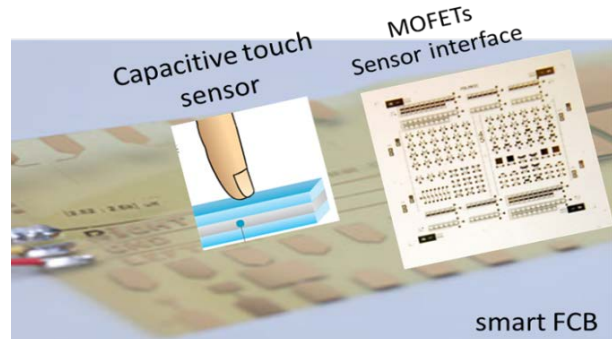


Figure 4: MOFETs II demonstrator concept.

This demonstrator provides an interface on foil to printed capacitive sensors. The modulation of the sensor capacitance, for example due to externally applied pressure, is detected in the frequency domain and indicated in a digital manner through an LED indicator. The demonstrator highlights the yield-increasing integration approach on MOFETs' technology.

[1] J. Carrabina, et al., "Inkjet gate array: Novel concept to implement electronic systems", LOPE-C, Munich, May 26, 2014

HybSi—Silicon Hybridization Process for Watch Industry and Precision Mechanisms

F. Barrot, G. Musy, J. Kruis, P. Gentsch, P. Theiler, L. Giriens, F. Cosandier, J. Kaufmann, J. Goldowsky, S. Lani, F. Cardot, S. Widmer, P. Glocker

Centimeter scale high precision mechanisms and systems can greatly benefit from the high precision micro-structuration of silicon and its good mechanical properties. Important Swiss industrial sectors such as the watch industry and scientific instrumentation are particularly concerned by this approach which is opening up new opportunities. However, silicon being a brittle material, its handling and its assembly with other materials is a true hybridization challenge. Combining its expertise in the domains of precision mechanisms and micro-manufacturing techniques, CSEM is taking up the challenge to become the Swiss competence center for the design, manufacturing, assembly and characterization processes of hybrid silicon based micro-mechanisms.

Using microfabrication techniques inherited from the microelectronic sector, it is possible to produce, with a micrometric precision, large quantities of centimeter scale mechanical parts made out of silicon, also referred to as MacroMEMS. Sectors such as the watch industry can benefit from this approach [1] which does not only offer an alternative option for the production of precise parts, but also opens up new opportunities for innovations [2]. However, due to the brittleness of silicon, its handling and assembly with other materials is a delicate task.

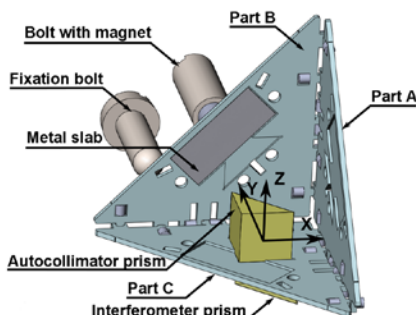


Figure 1: 6 DOF repeatability measurement of 3D puzzle like assembly of centimeter scale silicon parts.

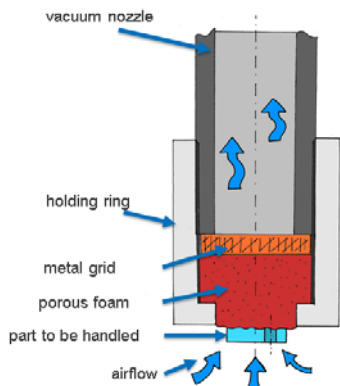


Figure 2: Proposed gripper for the handling of fragile silicon parts.

CSEM has been working on this hybridization challenge over the past few years. As far as the assembly is concerned, a 3D assembly methodology (Figure 1) based on a puzzle like assembly approach with interconnection features directly

integrated in the design of silicon parts has been implemented and experimentally validated. With this approach it has been shown that a challenging 3D assembly of silicon parts can be achieved with submicron repeatability [3].

As far as the handling his concerned, a gripper design has been proposed (Figure 2) for the handling of delicate MacroMEMS silicon parts, such as those comprising flexure hinges. The concept is based on a vacuum gripper featuring a foam interface to avoid damaging the part during manipulation. Coupled with a vision system to detect the orientation of the handled part, this micromanipulation strategy paves the way towards a semi-automated assembly of MacroMEMS.

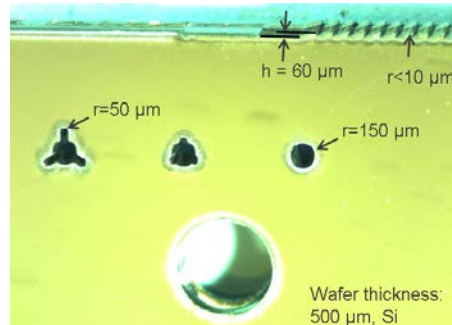


Figure 3: MacroMEMS laser micromachining.

Besides assembly and handling of MacroMEMS parts, CSEM has also investigated the potential of laser micromachining for fast prototyping of silicon based MacroMEMS parts. This serial production approach is not a substitute to the classical DRIE (Deep Reactive Ion Etching) approach; the idea is to offer an alternative to DRIE for the fast production of small quantities of MacroMEMS parts made out of silicon. The first machining tests show the potential of the approach (Figure 3): small size mechanical features that could be found in a watch mechanism have been successfully machined with a surface roughness Ra of 170 nm.

This strategic activity is performed in the frame of a multidivisional research program and CSEM would like to thank the Swiss Confederation and the Canton of Neuchâtel for their financial support.

[1] S. Jeanneret, A. Dommann, N. F. de Rooij, "Procédés de micro-fabrication avec application horlogère, développements récents", SSC, 2008

[2] F. Barrot, P. Genequand, I. Kjelberg, T. Hamaguchi, "Un nouveau régulateur mécanique pour une réserve de marche exceptionnelle", SSC, 2014

[3] J. Kruis, P. Gentsch, P. Theiler, F. Barrot, F. Cosandier, S. Henein, "6 DOF repeatability measurement setup for measuring position of assembled silicon parts with nanometric resolution", EUSPEN, 2015

MEMSPlant Sense—Miniaturized Implantable Pressure Sensor

R. Jose James, M. Fretz, G. Spinola Durante, P. Niedermann, L. Löfgren, J. Schleuniger, J. Gobet, T. Parkel, M. Sénéclauze, C. Bosshard, R. Eckert, M. Despont, S. Mohrdiek

The project focusses on developing a platform for long term implantable miniature wireless sensors. The sensor targeted here is an implantable wireless pressure sensor for blood pressure monitoring of patients with e.g. acute heart diseases. The challenges of developing miniature active implantable medical devices (AIMD) are numerous including the limited number of materials, low temperature packaging, miniaturization of electronics, powering, and leak and long term reliability testing. This project addresses each of these challenges.

Memsplant Sense project focuses on technologies needed for developing a miniature long term AIMD. The AIMD developed is an implantable pressure sensor. Potential applications of the demonstrator are in-vivo pressure monitoring in hypertension patients and in the brain. The main technologies developed in the project are the miniaturization of the electronics and wireless units, the packaging of the electronics with long term biocompatible materials, non-destructive leak testing, energy harvesting and long term reliability testing.

There are two pressure sensing concepts developed here, thermal proximity and mechanical coupling based pressure sensing (Figure 1). The thermal proximity sensor works on the principle of deflection measurement of a biocompatible membrane using a proximity sensor using silicon micromachining techniques at CSEM. The mechanical coupling method (patent pending) works on the principle of coupling between a biocompatible membrane and a pressure sensor membrane using a polymer material. The principle was demonstrated with a sensitivity of 40 $\mu\text{V}/\text{mbar}$ (Figure 2).

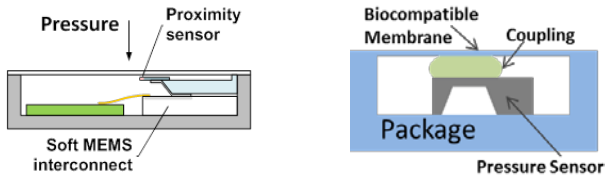


Figure 1: Thermal proximity (left) & mechanical coupling (right) pressure sensing concepts.

The package and membrane are made from sapphire. The cavities of the package are manufactured on wafer level. Sealing of the pressure sensor is done using a laser based bonding technique. This low temperature sealing ($< 100^\circ\text{C}$) was tested to be leak tight ($< 10^{-12} \text{ mbar}^*\text{l/s}$) with a good shear strength (110 MPa), and a good yield (> 90%). The fine pitch ($< 400 \mu\text{m}$) feedthroughs developed here are also leak tight ($< 10^{-12} \text{ mbar}^*\text{l/s}$) with good shear strength (110 MPa). The feedthroughs are fabricated using pins made of materials that are usually used for biocompatible feedthroughs like platinum and alloys. The via of the feedthrough has been tested to have low contact resistance ($\sim 1 \Omega$) with a via diameter as low as 100 μm . An example of a sealed package is displayed in Figure 2.

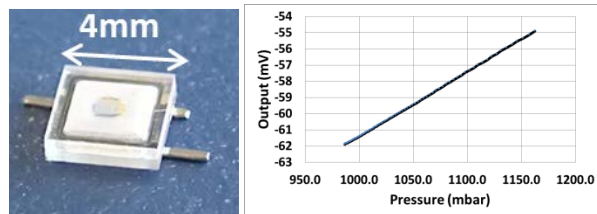


Figure 2: Implantable pressure sensor (left) and its sensitivity (right).

The wireless powering and data communication is implemented using two options, 1) using a miniature passive RF chip with a size of 2.5 mm x 2.5 mm and 2) using the Icycom platform which is capable of processing and storing data. The passive RF chip has been demonstrated with the pressure sensor. Work is going on to increase the communication range with the use of a miniature antenna.

A non destructive hermeticity test method based on FTIR quantitative measurement of the ingress of a tracer gas into the cavity was implemented. For the package the results were in good agreement with the conventional membrane deflection method while showing a lower detection limit, presently estimated at $2 \times 10^{-12} \text{ mbar}^*\text{l/s}$ (Figure 3). This opens the way to the individual control of manufactured chips to ascertain a 10-year life time in the body.

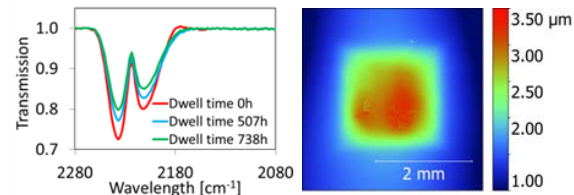


Figure 3: FTIR N_2O absorption spectra in the cavity (left) and deformation of the membrane (white light interferometry) (right).

The concept of energy harvesting, by implanting packaged photovoltaic (PV) devices directly under the skin has been studied. The optical properties of different artificial skin models (Figure 4) have been measured and a skin model with skin-like optical properties has been selected for the purpose of PV testing. Figure 4 shows estimated power densities of a set of PV technologies under standard sun spectra, as seen through 1.5 mm of fair skin.

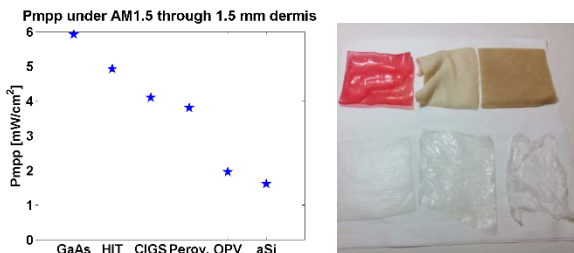


Figure 4: Maximum power density under standard sun spectra as seen through 1.5 mm skin (left); Skin models (right).

In summary, a platform for the miniaturization of AIMD has been developed. The required technologies can be adapted for many different in-vivo wireless sensing applications.

The project team acknowledges the funding provided by the Swiss Confederation, the Canton of Basel-Landschaft and the Canton of Graubünden.

MiniNOB—Miniaturized Wearable System for NOBP Measurement

O. Chételat, A. Bischof, C. Meier, E. Haenni, J.-A. Porchet, J. Solà, M. Rapin, M. K. Augustyniak, Y. Zha

MiniNOB is a three-year MIP (2015–2017) targeting the development of a TRL-5 miniaturized wearable medical device for the continuous measurement of non-occlusive mean blood pressure (NOBP) and multi-lead electrocardiogram (ECG). The device consists of four low-cost low-power highly-integrated cooperative sensors clipped in and connected by a conductive fitting chest garment (e.g., a bra or a vest). The intended use of the product is the continuous monitoring of blood pressure and ECG of outpatients. The project is executed under ISO13485 in order to maximize its value for future customers active in the medical market.

As shown in Figure 1 (upper left corner), state-of-the-art products use an inflatable cuff to measure NIBP (non-invasive blood pressure) and adhesive gel electrodes to measure multi-lead ECG. CSEM's current technology (upper right corner) does not use an inflatable cuff (except for a short calibration) to measure blood pressure but instead relies on a continuous surrogate of non-occlusive mean blood pressure (NOBP) computed from ECG, impedance cardiography (acquired with the same electrodes as ECG), and chest photoplethysmography for pulse arrival time (PAT). It has been shown^[1] during clinical trials that this CSEM's patented approach has performances compliant with the British Society of Hypertension (grade A) for more than two weeks after a single calibration manoeuvre.

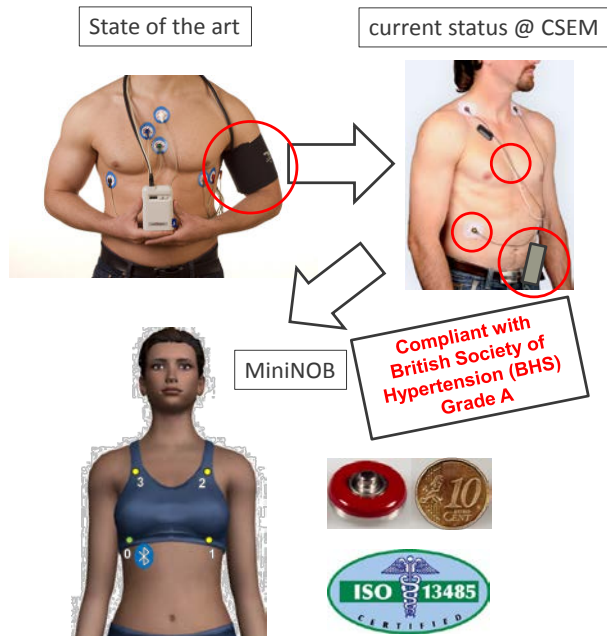


Figure 1: State of the art (product), current development status at CSEM, and project MiniNOB that targets the development of a medical device consisting of only four button sensors embedded in a vest or bra to simultaneously and continuously measure NOBP (cuffless blood pressure) and ECG. The red circles show the progressive simplification and increase of wearability of the device.

[1] J. Solà, et al., "Wearable PWV technologies to measure Blood Pressure: eliminating brachial cuffs" Engineering in Medicine and Biology Society (EMBC), 2013 35th Annual International Conference of the IEEE, pp. 4098–4101

[2] M. Rapin, et al., "Cooperative dry-electrode sensors for multi-lead biopotential and bioimpedance monitoring" Physiol Meas. 2015 Apr, 36(4):767-83

MiniNOB (as shown in the bottom of Figure 1) targets to measure NOBP and multi-ECG with the same approach but from only four dry-electrode miniaturized cooperative sensors embedded in a bra or vest (no cables, no explicit electronics box, no adhesive gel electrodes).

The cooperative sensor approach^[2] is also a CSEM's patented technology that allows one to drastically simplify cabling and connectors while keeping the best signal quality. In MiniNOB, the four cooperative sensors will have each only one contact with the skin and one with the garment. The latter will embed a single electrical connection that will be unshielded and only weakly insulated so as to significantly reduce the integration challenges and thereby costs and risks of unreliable measurements.

The sensors are miniaturized thanks to a dedicated ASIC developed in the project. The ASIC will be able to allow digital communication between the sensors so that all sensors work in perfect synchronisms^[3] and so that all measured signals are concentrated to a single sensor. The latter will be equipped with Bluetooth for communications with the external world. The ASIC will also contain the ECG and impedance frontends, as well as circuits for efficient power management and support for photoplethysmography measurement.

The MiniNOB device is developed according to our quality system for the development of medical devices certified compliant with ISO13485. The fulfilment of such high-quality standard will significantly increase the demonstrator value for customers active in the medical market and reduce the time to market of their product based on this technology.

In addition to NOBP and multi-lead ECG developed in full compliance with ISO13485, the device can easily be extended with other signals, such as heart rate, respiration rate, chest SpO2, core body and skin temperatures, activity, etc. as in the LTMS-S development^[4], but in a more integrated version.

In conclusion, MiniNOB is offering a medical device able to improve the diagnostic and treatment of outpatients suffering from heart and cardiovascular diseases with a smart garment featuring exceptional level of ease-of-use and comfort for the measurement of high-quality ECG and NOBP.

[3] O. Chételat, et al., "Synchronization and communication of cooperative sensors", 37th Annual International Conference of the IEEE Engineering in Medicine and Biology Society—EMBC2015, Milan (IT), 25–29 August 2015

[4] O. Chételat, et al., "Clinical validation of LTMS-S: a wearable system for vital signs monitoring", 37th Annual International Conference of the IEEE Engineering in Medicine and Biology Society—EMBC2015, Milan (IT), 25–29 August 2015

SMAC 2P—Towards a Flat Form Factor Miniature Atomic Clock

J. Haesler, H. Birol, T. Overstolz, B. Gallinet, J. Pierer, L. Giriens, T. Herr, L. Zulliger, L. Voruz, L. Balet, S. Lecomte

CSEM's Swiss miniature atomic clock (SMAC) prototypes have successfully been assembled but suffer from excessive thermal losses. CSEM's engineers are thus working on improved thermal efficiency (thermal design and improved vacuum levels). In order to open the way to the integration of MACs in portable devices, CSEM is presenting the first building blocks of a MAC physics package with a height of less than 5 mm.

The design, the fabrication, the assembly and the preliminary vacuum encapsulation of CSEM's Swiss-MAC have been reported for the past years.

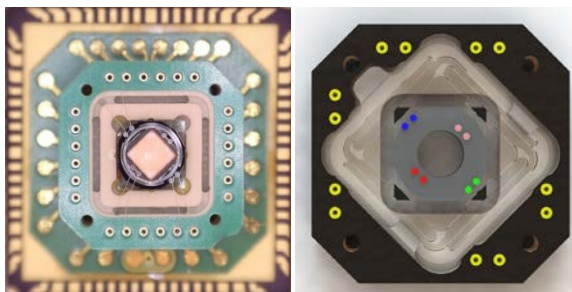


Figure 1: Physics package of the Swiss-MAC (right); Design of a thermally optimized atomic vapor cell holder (left) [less than 5 cm³].

A full Swiss-MAC has been successfully assembled and encapsulated with which first Coherent Population Trapping (CPT) clock signals have been measured. Further physics packages are currently being assembled in order to continue the characterization process and to assess the assembly reliability. The initial Swiss-MAC prototype suffers from excessive thermal losses. Thereofore, CSEM is currently working on developing smart solutions for improved thermal efficiency, especially for the atomic vapor cell holder^[1], as illustrated in Figure 1. In addition, decreasing the overall size of the Swiss-MAC, especially its height, is currently at the center of CSEM's development activities related to miniature atomic clocks. It has been shown that a height of less than 5 mm for the MAC physics package is requested in order to be integrated in portable devices like GNSS receivers, mobile phones, tablets or even watches.

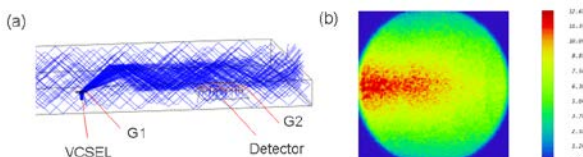


Figure 2: Optical simulations of CSEM's patent pending planar waveguide approach with gratings for a flat form factor MAC.

Such a flat packaging is made possible by planar arrangement of the individual components (cell, laser and detectors) next to each other's as opposed to stacking them. In this configuration, the optical connection is achieved via a planar multimode waveguide structure with gratings (G1 and G2) for input and output light coupling. Optical simulations (Figure 2), prototype manufacturing and first lab proof of principle showed to be very promising. This waveguide structure relies on a patent pending technology developed by CSEM.

This new physics package needs to provide means of integrating the waveguide approach as well as to provide smart assembly solutions, high flexibility in terms of electrical routing, low thermal conductivity and to be vacuum compatible. Low temperature co-fired ceramics (LTCC) showed to be the material of choice. Thanks to CSEM Brazil's LTCC production line in Belo Horizonte, preliminary manufacturing of LTCC cavities and holders was realized according to the flat form factor design developed for the SMAC. By means of an appropriate optimization of the manufacturing processes and by means of a methodical LTCC tapes selection, the LTCC team confirmed the feasibility of the atomic clock physics package in ceramics.

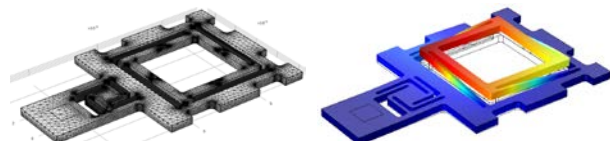


Figure 3: Mechanical simulations of the LTCC based atomic clock.

The detailed design of the LTCC based flat form factor SMAC has thus been engineered. Mechanical simulations (Figure 3) showed to be compliant with the request of a height of less than 5 mm, still providing enough stiffness.

The first LTCC fabrication batches were recently finalized as illustrated in Figure 4. Their characterization is ongoing and first assembly tests are expected in a near future.

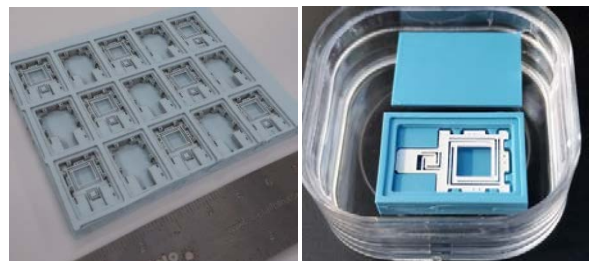


Figure 4: LTCC batch fabrication of the main LTCC physics package building blocks (cavity, holder and cap).

Thanks to the development presented in this paper and to very promising results for extended life-time atomic vapor cells at CSEM, the full prototype of a flat form factor SMAC is expected in the coming two years. Parallel and complementary developments for a ceramic based SMAC prototype are being conducted in collaboration with the European Space Agency (ESA) and VTT in Finland.

CSEM would like to thank the Swiss Confederation, the Canton of Neuchâtel, the Canton of Basel-Landschaft and the Cantons of Central Switzerland for their financial support as well as CSEM Brazil for the collaboration.

^[1] L. Zulliger, "Thermal and Structural Optimization in a Miniature Atomic Clock", Projet de Master, EPFL-CSEM, 2015

MICROSYSTEMS

Michel Despont

Today, MEMS technology is used almost everywhere in devices that sense and monitor our environment and control some of the actions that make up our daily lives. It plays an essential role as an interface with the user or the environment. The technology is used to fabricate a large variety of devices representing a market size approaching USD 10 billion. As an example of how MEMS technology has penetrated our daily life, today's cars use up to 30 or more different MEMS-based devices for monitoring and controlling engine functions as well as for safety, navigation, and passenger comfort. Similar trends can be seen in portable devices; the most recent smartphones contain dozens of MEMS-based sensors. Moreover, global technology trends such as of the Internet of Things (IoT) will also require massive use of connected sensors and promise large new markets for MEMS technologies, including building automation, healthcare and the life sciences, consumer & home automation, transportation, industrial and environmental monitoring, security, and retail and logistics. All of these markets are looking for autonomous, low-power, small form-factor and low-cost sensor and actuator devices.

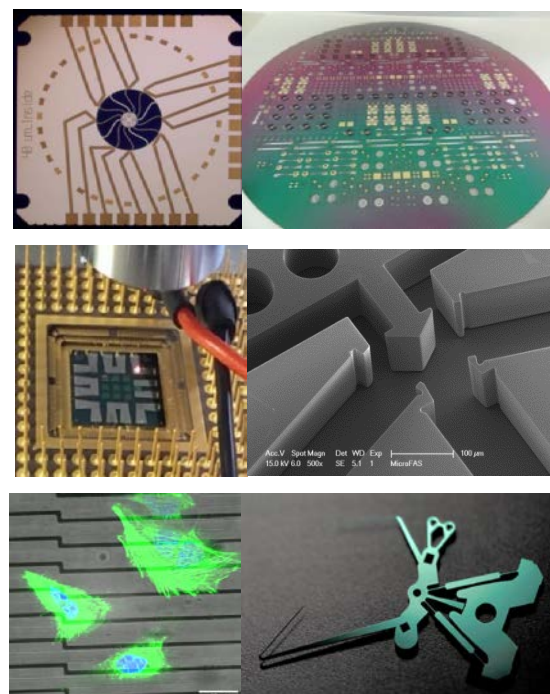
As MEMS processes are often derived from those used in the fabrication of microelectronic circuits, one could imagine that similar low-cost, high-volume manufacturing could be achieved for MEMS-based devices through process standardization. In reality, however, MEMS require many different processes and custom packaging solutions, making it difficult to have a common technology platform because, on the one hand, the extreme variety of physical effects used in MEMS devices necessitates a unique set of processes and materials and, on the other hand, there is an extreme fragmentation of the market with large differences in requirements regarding cost, time to market, form-factor, operating environment, and performance. Hence, a customized MEMS technology scheme is often developed for each specific application. Moreover, as MEMS devices have mechanically functional structures and in their role as sensors are exposed to the environment, reliability and lifetime need much more attention than they do in purely CMOS-based devices. Therefore, the industrialization of such devices is extremely critical and necessitates significant know-how in MEMS technology, packaging, material science, and reliability. With such know-how, acquired over decades, and a track record in bringing MEMS technology to the market, CSEM is uniquely positioned to be an essential partner in bringing ideas to market for many Swiss, high-tech SMEs active in the MEMS field.

CSEM's unique selling point is its cross-disciplinary approach, which blends microelectronics and system integration. Reliability and quality control are also key components of CSEM's MEMS concept and are differentiators of the center's R&D offering to industry. Partnerships are also a key CSEM strategy for speeding up developments and providing access to critical skills to best serve our customers. Hence, CSEM is increasing its collaboration with EPFL's Center of MicroNanoTechnology (CMi) and co-members of HTA—the Heterogeneous Technology Alliance (CEA-LETI, the Fraunhofer Microelectronics Alliance, and VTT). Likewise,

CSEM enjoys a strong and strategic collaboration with both Swiss federal institutes of technology, and with EMPA (the Swiss Federal Laboratories for Materials Science and Technology), and PSI—the Paul Scherrer Institute (natural and engineering sciences).

The global objective of the MEMS program is to establish MEMS device micro-fabrication and packaging technologies for CSEM's partners and to offer to Swiss and international industries a full product-development platform from feasibility demonstration of new device ideas to industrialized, qualified fabrication processes including the production of mature devices in small volumes. Therefore, the activities of this program are aimed at continuing to excel and to build up new competences in MEMS technology—in particular for application fields such as watch technologies, scientific instrumentation, optoelectronics, and medical device technology—with a strong focus on packaging, reliability, and cost reduction for demanding applications.

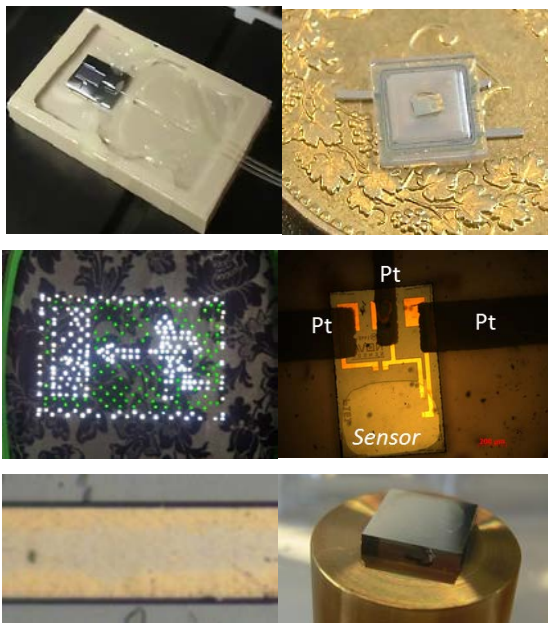
To address the demand for MEMS technology, the program comprises two main activities: (1) *Design & Process* and (2) *Integration & Packaging*.



A selection of developments pursued at CSEM in the Design & Process activity. From upper-left to lower-right: compliant structure with integrated strain sensors for a micromirror, 6" wafer with a variety of Si-Au hybrid watch micro-components, plasmonic-based chip with an array of narrow band IR emitters, MEMS part of an optical-based accelerometer (splitting mirror and fibers positioning elements), cells adhering on soft MEMS force sensors for cells study, Si-part of the "Genequand" escapement.

The *Design & Process* activity deals with the development and industrialization of specific MEMS in a wide spectrum of applications. The global objective of this activity is to maintain a state-of-the-art platform capable of developing and fabricating reliable MEMS products, from prototypes to small volume production or technology transfer. This platform, at the service of Swiss SMEs and industries, consists of a fully equipped MEMS fabrication clean room, a reliability laboratory, and an R&D infrastructure focusing on the investigation of advanced and novel MEMS-based devices. Today, developments are being pursued in the fields of watches and timekeeping, instrumentation and aerospace, and health, biotech, and lifestyle. These are the domains in which Swiss industry is highly successful at a global level and that have a large impact on the Swiss economy.

For industrial applications, reliability is of the utmost importance and CSEM's reliability and microstructure characterization capabilities are a powerful tool for supporting process development in order to eliminate defect- and stress-generated failure modes and performance limitations. The continuous improvement and systematic documentation of development and production process flows within ISO-9001 ensure the successful exploitation of the technology platforms developed. This enables a systematic approach to MEMS development from feasibility demonstration, via prototyping, to industrialization.



A selection of developments pursued at CSEM in the *Integration & Packaging* activity. From upper-left to lower-right: optical accelerometer package with Si-MEMS chip and placement of optical fibers, sapphire-titanium hermetic package with Pt-feedthroughs, LED integration in textile for signage applications, tactile sensor in a soft package, Au-Sn transient liquid phase bonding, MEMS chip bonafide.

The *Integration & Packaging* activity focuses on (i) the development of new integration platforms for CSEM's customers, and (ii) the realization, for clients, of new products based on these platforms. The chosen approach allows CSEM to serve a large number of customers in different application fields and markets. Its primary objectives are the integration of active MEMS dies, sensors, and actuators into prototype systems and products for different applications and markets.

The activity addresses today's global packaging challenges in sensor platforms for medical and environmental monitoring and for the integration of measurement solutions for harsh environments and for optoelectronics. The integration of microsystems continues to be a key element of many future high technology application areas. Hybrid integration technologies—from embedded silicon in polymer to M(O)EMS—find broad uses in markets such as healthcare and energy. Combined with hermetic sealing and embedded self-testing, they open up additional applications for sensors in harsh environments, such as in the medical field. In addition, miniaturization in optoelectronics continues to be an innovation driver from devices to architecture.

The valorization of the MEMS program is leveraged through CSEM's multidisciplinary capabilities and system approach and is naturally strongly linked to the research programs Systems (novel mechanical watch mechanisms, precision mechanics, or miniature atomic clocks), Ultra-Low-Power Integrated Systems (ASICs), and Surface Engineering (chemical and biosensors). This adds unique value as all aspects of a system can be included early in its development.

Highlights

Despite the wide diversity of available infrared light sources, there is no equivalent—in the infrared—of a light emitting device (LED): that is to say, a compact light source having a limited spectral linewidth and good directionality and being easy to manufacture and inexpensive. Combining nanophotonics—for controlling light at the wavelength scale—and MEMS technology, CSEM has demonstrated a novel thermal infrared emitter, with controllable linewidth and directionality, that has the potential to be fabricated at low cost for applications such as gas sensing.

Within a CTI project with MC-monitoring SA, a MEMS-based optical accelerometer with remote readout has been developed for the vibration monitoring of turbo and hydro power generators. The package has been designed according to the harsh environmental requirements of strong electromagnetic fields, high temperatures of up to 155°C, and a hydrogen-rich atmosphere. The advantages of the solution are the high rejection of the common mode signal thanks to a differential intensity signal approach, precise manufacturing of MEMS technology, and a low-cost, high-yield system assembly process.

Structures based on flexible guides are particularly suitable for providing precise, frictionless movement, without the use of lubricants and without wear, as is desirable in mechanical watches. However, viable solutions require a material with excellent mechanical properties and precise fabrication capabilities. This can be achieved with state-of-the-art silicon MEMS technology. At the forefront of this technique, CSEM has developed silicon-based microcomponents for the escapement and the oscillator of a revolutionary regulator invented by Pierre Genequand and jointly developed with Vaucher Manufacture Fleurier. An exceptional power reserve of over one month has been achieved in a mechanical movement.

Microstructuring of Bulk Metallic Glass

P. Niedermann, M. Dadras, A. Pezous, J. Kettkaew •, W. Chen •, J. Schroers •, M. Despont

Results of molding of a Pd-based bulk metallic glass are presented, using microfabricated silicon as a mold. This molding technique, which is reminiscent of polymer injection molding, is expected to allow the fabrication of components such as elastic elements with outstanding mechanical properties.

Bulk metallic glasses (BMGs) are a novel class of material that holds high promise for applications as microparts such as springs. They are characterized by slow crystallization kinetics, which make it possible to produce them from the melt in thicknesses of several mm. Alternatively and uniquely amongst metals, they can be molded in a so-called supercooled liquid state, where they exist in viscous form analogous to injection molding of thermoplastics^[1]. Their material properties in the amorphous state are outstanding. In particular, they have a high elastic limit and excellent resistance against corrosion^[2].

This makes micro-molding an interesting possibility for fabricating microparts with superior mechanical properties. Here, an injection type molding in silicon was explored and the molded parts characterized by TEM and X-ray diffraction.

A variety of BMG materials are known, with different degrees of processability, mechanical properties, and characteristic temperatures. Figure 1 shows the main classes of the materials with their elastic limit and Young's modulus values. Remarkably, the material classes lie on a line corresponding to a deformation of 2%, which is much higher than for steel.

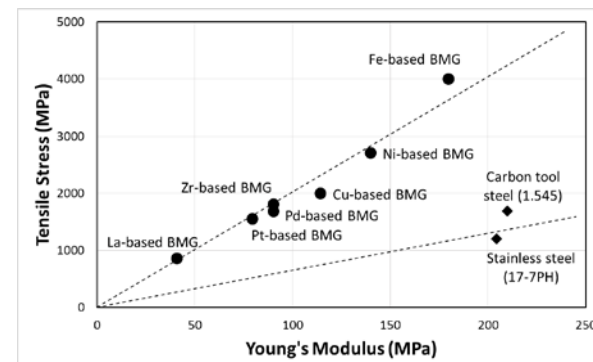


Figure 1: Tensile stress and Young's modulus of the main BMG material classes.

The Pd-based and Zr-based BMGs are the most readily available BMGs and have a high glass-forming ability. Their mechanical properties make them good spring materials, whereas Fe-based BMGs are known to be brittle. The Pd-based material of atomic composition Pd₄₀Cu₃₀Ni₁₀P₂₀ with its record high glass forming ability was used for this work.

A first class of molds was made by bonding two silicon wafers, with the first wafer containing injection holes and the second one, the mold of the parts to be formed. As Figure 1 shows, the molds could be successfully filled by pressing the raw BMG material (PdCuNiP alloy) into the injection holes under vacuum.

The silicon was removed by wet chemical means. It can be seen that very fine details were reproduced, namely, vertical ripples that are characteristic of the dry etching of the walls of the silicon mold.

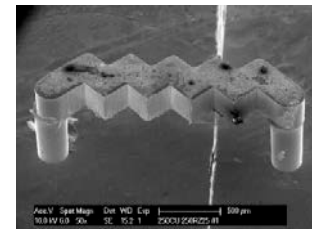


Figure 2: Molded PdCuNiP structure of zigzag shape, showing the injection structures.

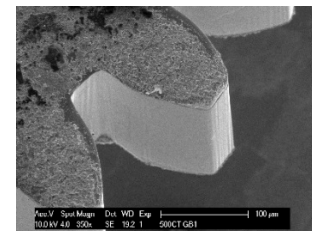


Figure 3: Detail of a molded gear, with vertical ripples characteristic of the (non-optimized) dry etching that was used for the fabrication of the mold.

The resulting finely replicated shape indicates that the material remained amorphous for a long enough time to completely fill the mold. The resulting parts were also investigated by TEM, EDX and XRD. TEM images showed them to be primarily amorphous, whereas XRD showed both fully amorphous state as well as residual crystallinity, indicating that the crystallization limit was reached in some cases (Figure 4).

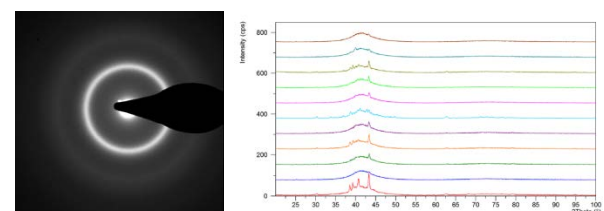


Figure 4: TEM image and XRD theta-2theta curves, indicating mainly amorphous state with residual crystallinity in some samples.

EDX analysis confirmed the composition of the material, and was able to detect defects such as occasional Si residues from the mold as well as gold residues on the top of the parts that are also visible in the SEM image of Figure 1. These defects can be eliminated by improved processing and using direct wafer bonding for the molds.

• School of Engineering & Applied Science, Yale University, USA

[1] J. Schroers, Adv. Mater. 22 1566 (2010)

[2] A. Inoue, A. Takeuchi, Acta Mat. 59 2243 (2011)

MEMS Scanner with Integrated Position Sensors

S. Lani, D. Bayat, A. Guillet, P.-A. Clerc, M. Despont

A position feedback has been integrated in a 2D micro mirror device for high optical power applications and high precision vector display. The developed solution consists of doped silicon piezoresistive sensors integrated directly on flexible parts of the membrane.

Scanning and beam deflecting devices present high interest for various applications like picoprojectors, LIDARs or galvo-scanners. For beam deflecting devices, the actuation is, in general, made with a DC analog signal. The investigated, basic device was previously described by Ataman, *et al.*^[1] and consists of a mirror fixed on silicon springs where a permanent magnet is attached. The MEMS scanner concept is presented in Figure 1 and the fabricated system in Figure 2.

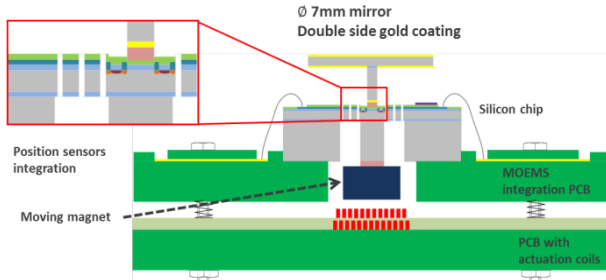


Figure 1: 2D tilting electromagnetic deflecting mirror concept.

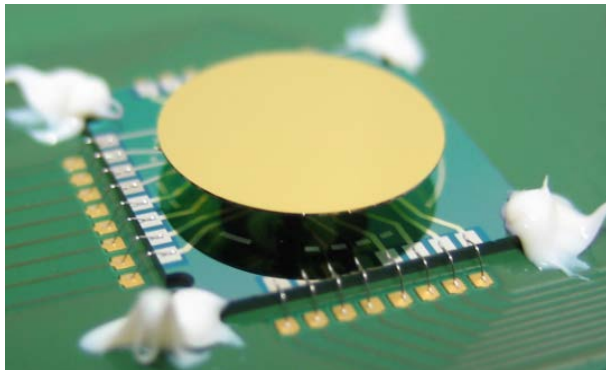


Figure 2: Assembled MEMS scanner with integrated position sensors.

The system is composed of a coated silicon mirror assembled on a silicon chip having a deformable membrane integrating the position sensors and assembled on a PCB to ensure electrical interconnections. The actuation is insured by two pairs of coils enabling a 2D analog tilting capability. It has a large tilt angle of +/- 9° and high resistance to optical power with a combination of a specific membrane design and reflective coating. To achieve a fine positioning of the mirror a sensor is needed that could, in general, be optical, capacitive, magnetic, thermal or piezoresistive. The most adapted sensing solution to the design

and cost target was piezoresistive sensors, consisting of four silicon doped resistances arranged in a Wheatstone bridge to decrease the effect of resistance variation with temperature. One of the resistances is placed on a part of the device having a deformation proportional to the tilt angle, on a flexible arm of the membrane. A total of four Wheatstone bridges are required to obtain the tilt angle and the tilt direction.

The performance of the piezoresistive sensors is evaluated by measuring the output signal of the piezoresistors as a function of the tilt of the mirror and the temperature. White light interferometry was performed for all measurements to measure the exact tilt angle. The minimum detectable angle with such sensors was 30 µrad (around 13 bits for an output voltage resolution of 20 µV) in the range of the minimum resolution of the interferometer. The tilt reproducibility was 0.0186%, obtained by measuring the tilt after repeated actuations with a coil current of 50 mA for 30 min, and the stability over time was 0.05% in 1 h without actuation. Electrical noise measurements were performed on the MEMS device with a probe station, an x1000 homemade signal amplifier and an HP3562a dynamic signal analyzer. To control the amplifier level, a standard resistance of 5.6 kΩ was measured to calibrate the measurement system. A typical noise figure is depicted in Figure 3, giving a noise close to a standard resistance (5nV/√ Hz). Accordingly, at the targeted sampling frequency for position control of 20 kHz, the noise level is below 1 µV. With an improved electrical design (low noise amplifier, improved wires) a 16 bit resolution corresponding to several µrad resolutions can be achieved.

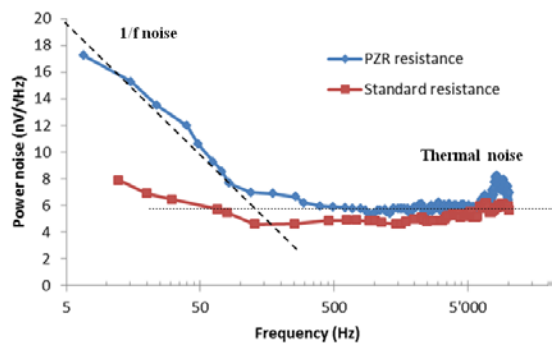


Figure 3: Noise level of a piezoresistor bridge.

^[1] C. Ataman, S. Lani, W. Noell, N. de Rooij, "A dual-axis pointing mirror with moving-magnet actuation", J. Micromech. Microeng. 23 (2013) 025002

MEMS Mirror for High Power, Large Angle, 2D Laser Steering

A. Hoogerwerf, D. Bayat, V. Revol, K. Krasnopski, T. Burch

A MEMS mirror has been developed for large angle, 2D steering of high power laser beams. Besides space applications, such mirrors can also be used for laser scribing and other laser patterning methods.

Within the JEM-EUSO project [1] a MEMS mirror for 2D laser steering has been developed, with the following key specifications:

- optical actuation angle: +/- 30° in both directions
- maximum settling time: 100 ms
- laser source: 355 nm (tripled Nd-YAG), 20 mJ, 15 ns pulses

The short wavelength of the laser source, combined with the high energy of the pulses, requires the mirror surface to have a minimum size in order to prevent laser-induced damage to the mirror surface. The mirror material chosen was coated quartz. The quartz itself is transparent to the laser light, so it cannot be damaged. Very good, high reflectivity coatings (> 99%) are available on this material. The laser source will be spread over a 2.4 mm diameter beam, so that the energy density of the light will remain below 1 mJ/mm². The mirror surface should have a diameter of at least 3 mm to be able to reflect all light from the laser in all possible directions.

The mechanical actuation angle of the mirror is half the optical actuation angle: +/-15°. The laser will impinge on the mirror at a 45° angle. As a result, the mechanical actuation angle in the actuation direction perpendicular to the plane of incidence of the laser light should be +/-21° in order to achieve the +/- 15° actuation in this direction.

The flexible material chosen for the suspension of the mirror is silicon. Silicon, when properly machined, has excellent mechanical and fatigue properties, which make it, therefore, well suited for space applications. Furthermore, it can be machined in batch processes with high precision.

The design of the flexible structure has been inspired from the work on a robotic arm actuator [2] and is depicted in Figure 1. In this figure, the mirror is transparent and will be clamped between two silicon holders in the middle of the structure. Each holder is connected by three spiral beams to a frame. The spiral beams are rigid with respect to lateral motion and are flexible for out-of-plane bending movements. Therefore, when the two frames are laterally displaced with respect to each other, a tilting of the mirror occurs. This can be understood by the fact that the spiral beams are stiff for a lateral motion, so that the lateral movement of the frame results in an almost identical lateral movement of the mirror holder. This lateral movement can only be accommodated by an out-of-plane rotation of the mirror. This rotation is possible because the spiral beams are flexible for out-of-plane movements.

The design has been simulated extensively using the Comsol finite element package. The actuation force can be as high as 1 N and the relative movement of the frame will be around 1 mm. Only magnetic actuation can deliver this amount of force over such a distance. Therefore, actuation voice coils from BEI Kimco will be used for actuation, with the goal of replacing these coils with a custom solution in the future.

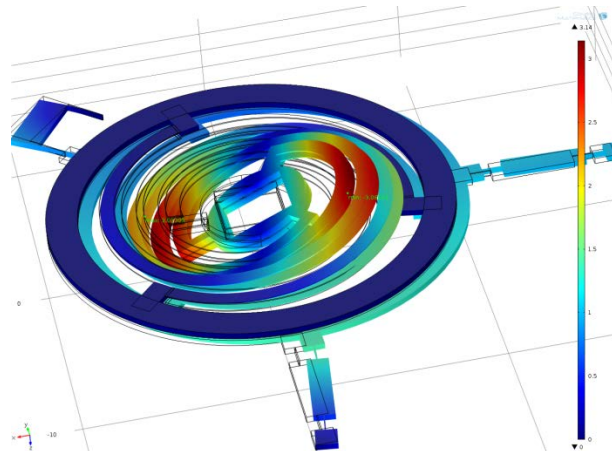


Figure 1: The actuation mechanism for the MEMS mirror.

It has been found that the structure exhibits a small piston movement that needs to be damped. This damping is achieved by making the side of the mirror conductive and placing a permanent magnet below the mirror. The piston movement of the mirror relative to the magnet induces Eddy currents in the conductive layer around the mirror, and these Eddy currents are converted into heat by the resistivity of the layer, thus absorbing the energy of the piston movement.

The launch conditions were also simulated, and the vibrations in the mirror risk breaking the spiral beams. A clamping mechanism was therefore designed to fix the mirror in place during launch. The resulting structure is depicted in Figure 2. The fabrication of this structure is foreseen for 2016.

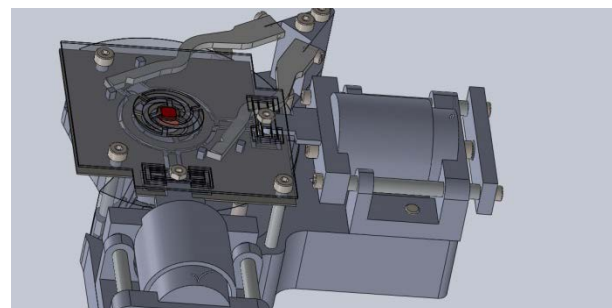


Figure 2: The complete MEMS mirror with actuation and clamping.

[1] T. Burch, et al., "A Platform for a MEMS-based Laser Pointing System with Position Feedback", this report page 96

[2] L. Rubbert, "Conception de mécanismes compliant pour la robotique chirurgicale", Ph.D. Thesis, University of Strasbourg, 2012

Design of a MEMS Gas Chromatograph

A. Hoogerwerf

A miniaturized gas chromatography system was developed with all components fabricated with MEMS technology. The low weight of the system makes it well suited for space applications but also for other applications, such as food quality control and explosive detection.

A miniaturized gas chromatography (GC) system is being developed that consists of a pre-concentrator, a separation column, and a thermal conductivity detector (TCD). All three elements are fabricated with MEMS technology, which enables batch fabrication with very small feature sizes. When combined with gas handling and a vacuum pump, this system can be used to detect and identify different compounds in gases.

The pre-concentrator is a small chamber that is filled with an absorbing material. During the absorption phase, the chamber is cooled with an external Thermo-Electric Cooler (TEC) to temperatures below ambient, thus facilitating the absorption of the different gas compounds. Once sufficient compounds have been absorbed, the absorbing material is heated through the direct heating of pillars that are placed at regular intervals in the chamber. The heating is very rapid, resulting in a sharp desorption peak of the absorbing material. Tenax® has been selected as the absorbing material, because of its good absorption characteristics and its widespread use in GC applications. Small chambers were made and filled with Tenax®, as shown in Figure 1. The white material in the left and right thirds of the chamber is Tenax®. The center of the chamber could not be filled due to the asymmetric placement of the relatively large access hole (encircled in red). A re-design of the pre-concentrator is currently underway to improve the Tenax® filling characteristics.

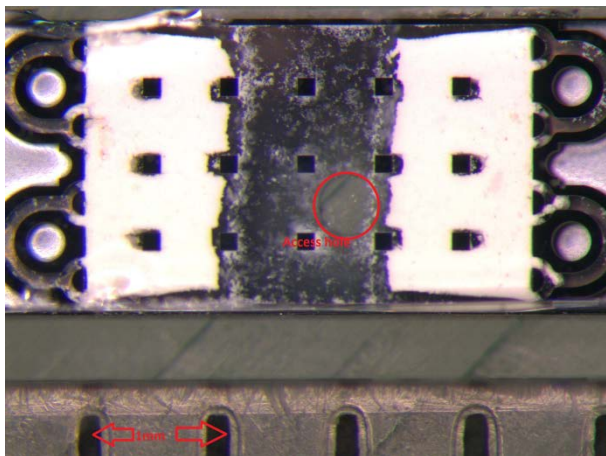


Figure 1: A pre-concentrator chamber partially filled with Tenax® (white).

The MEMS separation column was made by etching a long serpentine-shaped channel in silicon. A glass lid is anodically bonded to the silicon to form the column. The drawback of these columns so far, has been that it is very difficult to obtain a uniform coating of the stationary phase on the walls of these columns. The uniform thickness of the stationary phase is of paramount importance for the separation characteristics of the column. New techniques like Atomic Layer Deposition (ALD) and Molecular Vapor Deposition (MVD) allow the uniform coating of the columns, as they deposit the stationary phase one molecular layer at a time. The columns were fabricated, as depicted in Figure 2, and the deposition tests have begun.

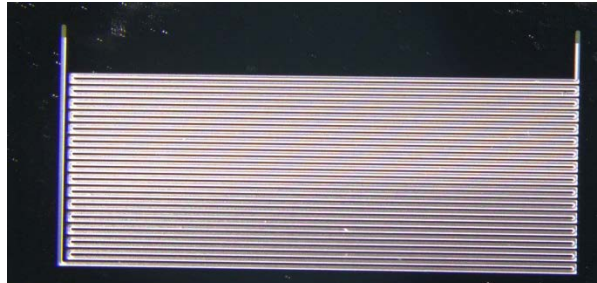


Figure 2: Test column structures.

The detection of the gases eluting from the column is done by a TCD. The TCD consists of four platinum resistors that are suspended two by two over two separate channels. A reference gas is led through one channel, and the gas eluting from the columns through the second channel. The temperature dependence of the platinum resistors is used to set their temperatures at a value slightly above the temperature of the gas. When particular compounds, having different thermal characteristics, elute from the column, the temperature of the resistors in that channel changes and, thus, so do their resistance values. This can be detected electrically by placing the four resistors in a Wheatstone bridge configuration.

The particularity of the TCD developed here is that it is designed to be flip-chip bonded to the end of the column, reducing the dead volume to an absolute minimum. As a result, there will be no peak broadening at the end of the columns. The fabrication of the TCD and its attachment to the columns is currently underway.

An easily overlooked aspect of the MEMS GC system is that it requires leak-tight gas connections of the silicon parts to conventional metal tubing. Therefore, multiple tests are underway to assure a reliable connection between silicon and the metal tubes. A first test result is shown in Figure 3, where a metal tube has successfully been inserted in a silicon chip.

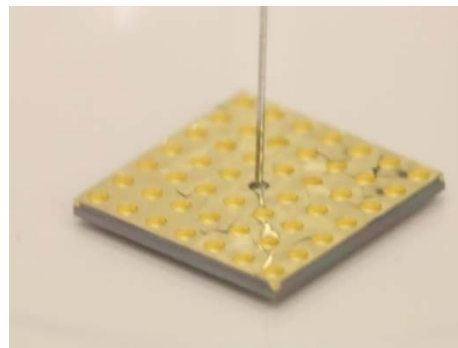


Figure 3: A metal tube attached to a gold-covered silicon chip.

MEMS Accelerometer with Remote Optical Readout for Power Generator Monitoring

M. Tormen, B. Timotijevic, Y. Pétremand, M. Lützelschwab, D. Bayat, O. Dubochet

A MEMS-based accelerometer with a remote optical readout is presented. Advantages are simplified electronics, high rejection of the common mode signal and high measurement linearity, low production cost for the accelerometer chip, low cost and high yield for the system assembly.

Miniaturized accelerometers with a remote optical readout are required devices for the continuous monitoring of vibrations inside power generators. In turbo and hydro generators, end-winding vibrations are present during operation, causing undesirable out-of-service repairs in the long run. Continuous monitoring of these vibrations is, therefore, mandatory. The high electromagnetic fields in the generators impose the use of devices immune to electromagnetic interferences.

A MEMS accelerometer with a remote optical readout has been developed. Solutions have been proposed in the past [1, 2, 3]. The advantages, compared to state-of-the-art devices for such applications, are the following: simplified electronics when compared to wavelength or phase-based measurement systems; high rejection of the common mode signal and high measurement linearity thanks to a differential intensity signal approach; a low cost MEMS chip given the reduced number of fabrication steps and the number of chips per wafer (more than 400 on a 6" wafer); a low cost and high yield system assembly thanks to a simple and robust assembly process; low barriers to market-entry, since the reduced package volume is compatible with the already allocated space in turbo generators. For electromagnetic immunity, no metal is present in the sensor head.

Fabrication of the MEMS chip (Figure 1) starts from a 6 inch SOI (Silicon-On-Insulator) wafer. It is composed of a seismic mass, suspended through springs, with opened regions to introduce a damping gel, and of a 2-facet mirror, moving with the seismic mass, redirecting the optical signal from an input fiber into two output fibers. In order to reduce the system dimensions, the two output fibers were placed at 70 deg. with respect to the input fiber.

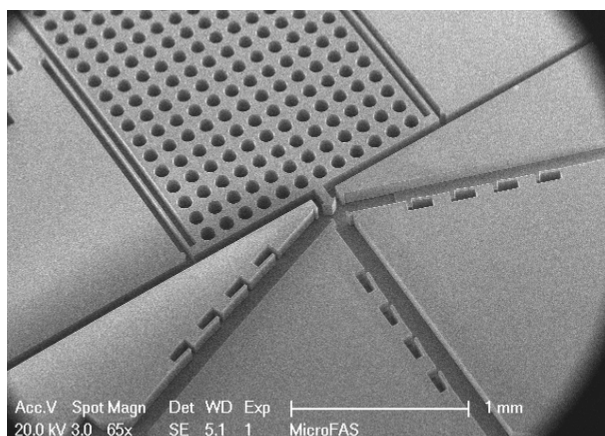


Figure 1: SEM picture of the fabricated device.

- [1] B. Guldmann, "Micromachined fiber optic accelerometer based on intensity modulation", PhD thesis, University of Neuchâtel, 2001
- [2] Y.-G. Lee, *et al.*, "Performance of a single reflective grating-based fiber optic accelerometer", Meas. Sci. Technol. 23 045101, 2012

The package provides a solid base for the interface between the MEMS device and the optical fibers. In terms of possible materials for the package, metal parts are excluded because of the strong electromagnetic fields present in the generators; moreover, temperatures of up to 155 °C and a hydrogen rich atmosphere (5 bars) represent further constraints in the choice of the package material. PEEK was chosen as the package material because of its physical and chemical properties as well as its adequate machinability. The optical fibers are completely molded in UV curable adhesive, thereby providing an effective strain relief. The output fibers are placed at an angle of 70 deg. with respect to the central input fiber. The fiber alignment is done using a six axis alignment stage with an arbitrary pivot point. For mechanical protection, a glass lid is added to the package at a final step. Figure 2 shows the fully assembled device with connectorized fibers.

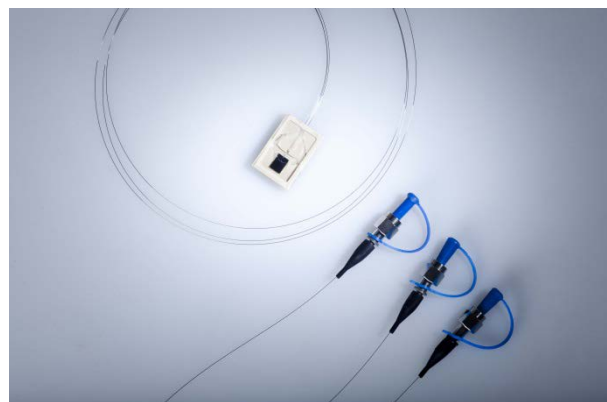


Figure 2: Fully assembled and connectorized optical accelerometer sensor.

The first resonance frequency is designed to be above 1 kHz, and squeeze air film damping was introduced to flatten even further the frequency response in the range of interest (10 Hz-400 Hz). Roughly 30 prototypes have been tested at this stage.

In conclusion, a MEMS-based accelerometer with a remote optical readout has been developed. Advantages of the present solution are the high rejection of the common mode signal thanks to a differential intensity signal approach, low cost for the MEMS chip given the number of chips per wafer, low cost and high yield system assembly thanks to a simple and robust assembly process.

- [3] Z.-Z. Yang, *et al.*, "High sensitivity fiber optic accelerometer based on folding F-P cavity", Proc. SPIE 8914, International Symposium on Photoelectronic Detection and Imaging 2013: Fiber Optic Sensors and Optical Coherence Tomography, 891411, 29 August 2013

Advanced Structural Investigation of SiGe Heteroepitaxially Grown Crystal Arrays

I. Marozau, F. Isa •, A. Jung • T. Kreiliger •, G. Isella ••, H. von Känel •, P. Niedermann, O. Sereda

Imaging sensors directly coupled to readout units form an area of growing technological interest. One example concerns devices for X-ray imaging and inspection, ranging from medical diagnostics and cancer therapy to non-destructive testing of all kinds of goods (quality assurance, security). A new approach towards X-ray detector fabrication, based on epitaxially grown Ge and SiGe crystal arrays, has helped to overcome the problems of crystal defects, layer cracks and wafer bowing. High resolution X-ray diffraction is a powerful tool to investigate the structural quality and strain condition in the three-dimensional SiGe crystal arrays heteroepitaxially grown on Si.

Monolithic integration of SiGe semiconductors on Si substrates is an easy and efficient way to combine specific optical and electronic properties of SiGe with the advantages of Si-based CMOS technology. This approach requires fabrication of high-quality dislocation-free heteroepitaxial SiGe layers on Si, which is a very challenging task due to the relatively large lattice mismatch between Ge and Si of about 4%. To overcome this difficulty, it was recently proposed to use pillar-patterned Si substrates for the growth of three-dimensional micron-size Ge and SiGe crystal arrays, which have been shown to be almost dislocation-free [1, 2] (Figure 1).

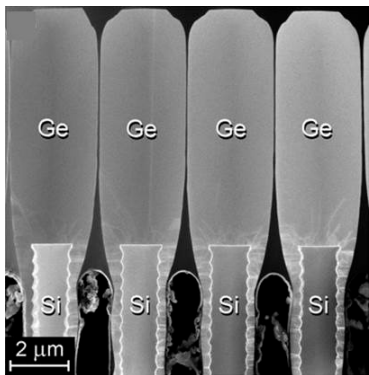


Figure 1: Cross-section view SEM micrograph of Ge three-dimensional crystal array grown on pillar-patterned Si substrate [2].

High resolution X-ray diffraction (HRXRD) was applied to study the epitaxial quality and strain state of such SiGe crystal arrays, in which the Ge content gradually increased from 0.5 at.% at the interface with the substrate to 40 at.% at the surface. Utilization of parallel monochromatic X-ray beam and narrow-acceptance-angle analyzer in combination with the high resolution goniometer, enables very precise analysis of tiny crystal lattice distortions by HRXRD. In particular, reciprocal space mapping of asymmetric crystallographic reflections allows a separate determination of in-plane and out-of-plane unit cell parameters and calculation of the corresponding strains in epitaxial samples.

An analysis of the $\omega/2\theta$ diffraction patterns (shown in Figure 2) and the corresponding rocking curves suggests that the SiGe crystals are epitaxially grown on Si substrates and exhibit a high structural quality. The crystals reveal a small tilt of up to $\sim 0.1^\circ$ with respect to the surface normal, which is probably due to slightly eccentric deposition geometry. The Ge content of 40.9 at. % was calculated for the top SiGe layer from the position of its crystallographic reflection (Figure 2). This value is in a good agreement with the expected target value of 40 at. %. Figure 3 shows an example of a reciprocal space map

(RSM) around the asymmetric (115) reflection. A comparison of the experimentally acquired data with the theoretical calculations reveals that the crystals are fully strain-relaxed through their whole height of $\sim 30 \mu\text{m}$. The calculated in-plane and out-of-plain strain values for the top $\text{Si}_{0.6}\text{Ge}_{0.4}$ layer are very small ($\sim 0.01\%$).

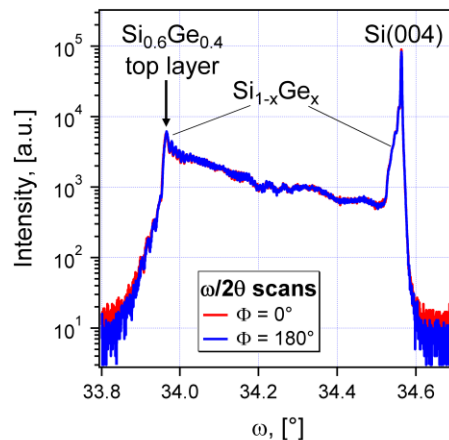


Figure 2: $\omega/2\theta$ XRD patterns of graded SiGe crystals on Si. Two measurements were performed at different Φ angles to account for the crystals tilt effect for calculation of the Ge content.

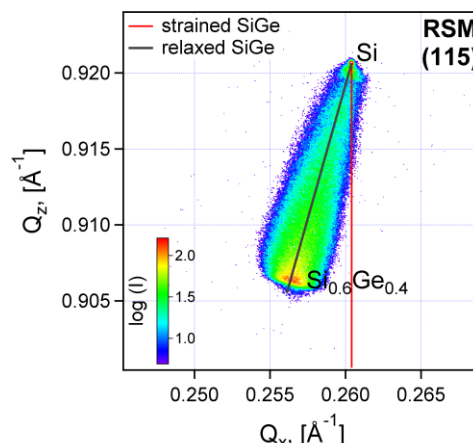


Figure 3: Reciprocal space map measured around the (115) asymmetric Bragg reflection. The theoretically calculated evolution of the reciprocal lattice parameters in case of fully strained and fully relaxed SiGe is shown with red and dark grey lines, respectively.

Performed structural analysis of the SiGe crystals provides valuable information for understanding the performance of this functional component for the development of a novel X-ray detector.

• Laboratory for Solid State Physics, ETHZ, Zurich, Switzerland
•• L-NESS, Como, Italy

[1] C.V. Falub, et al., Science, 335 (2012) 1330-1334

[2] C.V. Falub, et al., Thin Solid Films, 557 (2014) 42-49

Cleanroom Compatible Micro-structuring of Silicon using Ultrashort Pulsed Laser Systems

S. Berchtold, J. Kaufmann, K. Imhof •, B. Jäggi ••, T. Kramer ••, B. Neuenschwander ••, J. Auerswald •, O. Dubochet, T. Bewer •

The increasing demand of the watch industry to manufacture small high precision parts in Silicon leads to new manufacturing strategies. This report describes the development of such strategies using UV, green and IR ultrashort pulsed laser systems in combination with a cleanroom surface post treatment to improve cut and surface quality. All related work was done in the framework of the CTI project PICOFAB.

With ultrashort pulsed laser (USP) it is possible to machine hard and brittle materials with high Young's modulus, small specific weight and high wear resistance, like Silicon or ceramics, efficiently and with high precision.

In recent years major advancements have been made in the development of laser processes with high quality cutting edges and surfaces. Here we examined cutting of Silicon chips with three laser systems using different beam sources (UV, Green, IR). The UV (located at CSEM) and Green (project partner TRUMPF) laser systems use Galvo scanners for beam deflection, whereas the IR (project partner BFH) system is equipped with a trepanning optic. Laser cutting is followed by a cleanroom iterative etching and thermal oxidation procedure to remove residuals and to reduce the surface roughness. Table 1 lists laser system parameters and compares the sample quality parameters before and after post processing.

Table 1: Comparison of surface roughness before and after cleanroom post processing.

Ultrashort pulse laser [pulse length]	Surface roughness before treatment Ra [nm]	Surface roughness after treatment Ra [nm]
UV (343nm) [6ps]	177	158
Green (515nm) [6ps]	212	176
IR (1030nm) [900fs]	981	271

Figure 1 shows a Silicon sample cut with the UV USP laser system after the oxidation step and before the etching. The taper angle (which should ideally be 90°, here it is >86°) can be clearly seen on the right chip edge.

The taper angle can be further improved by using a trepanning optic. Challenging is the evaluation of the right cutting strategy to achieve a uniform and high quality cut.

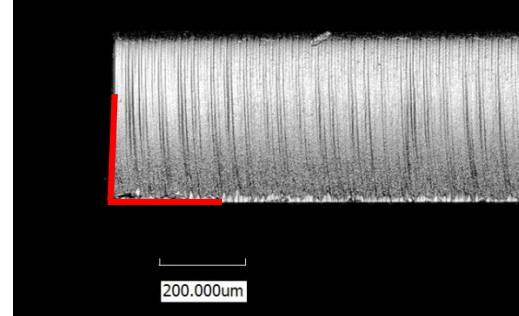


Figure 1: TruMicro UV manufactured Silicon cutting edge with thermal oxide layer. Taper angle >86° marked on the right side.

Using such an optimum laser cutting strategy, and applying the cleanroom treatment we achieve a result as can be seen in Figure 2, with a taper angle of 90° and a surface roughness Ra below 300 nm.

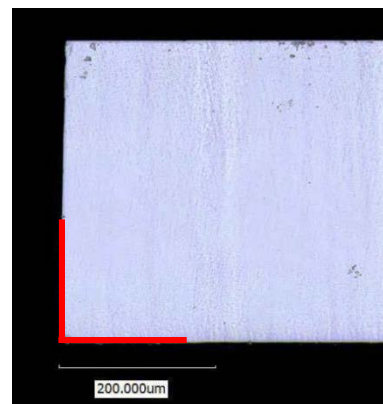


Figure 2: TruMicro IR manufactured Silicon cutting edge with a taper angle of 90°.

We could demonstrate that a combination of cleanroom technologies and USP laser cutting improves quality and precision of cutting edges for Si chips. The lasering process determines the initial surface structure. This structure will then influence the efficiency of the post process treatment. Therefore the coordination of both processes—laser and surface treatment—is essential to get the best out of both technologies.

The work has been supported by the Swiss Commission for Technology and Innovation CTI (project Nr. 16049.1 PFNM-NM PICOFAB). CSEM thanks them for their support.

• TRUMPF Maschinen AG, Baar

•• BFH Bern University of Applied Science, Institute for Applied Laser, Photonics and Surface Technologies ALPS

Nondestructive Raman Spectroscopy for Hermetic Package Reliability Analysis

J. Gobet, T. Overstolz, S. Karlen, J. Haesler

The capabilities of nondestructive Raman spectroscopy for reliability analysis are demonstrated with the case study of a rubidium (Rb) gas cell.

Hermetic packages are mandatory for MEMS applications such as accelerometers or pressure sensors, as well as for implantable medical devices. A quantitative analysis (nature and partial pressure) of the gases inside such sealed cavities is thus critical for reliability assessment. A simple and nondestructive technique would thus be a valuable complement to the sensitive but quite complex and destructive residual gas analysis (RGA) method.

Confocal Raman spectroscopy was proposed as a means to analyze gases in devices having an optical access to the sealed cavity [1]. Raman is a vibrational spectroscopy complementary to infrared spectroscopy (IR). It has, in particular, the crucial capability of measuring diatomic gases, the vibrations of which are forbidden in IR but allowed in Raman spectroscopy.

We report here on the development of Raman as a practical tool to study rubidium gas cell reliability and lifetime issues. Such cells are used for miniaturized atomic clock (MAC) and developed at CSEM within the Swiss-MAC [2] project. Our cells (Figure 1) are batch fabricated and filled with metallic rubidium (Rb) by UV irradiating RbN₃ deposited and sealed in the cavities.

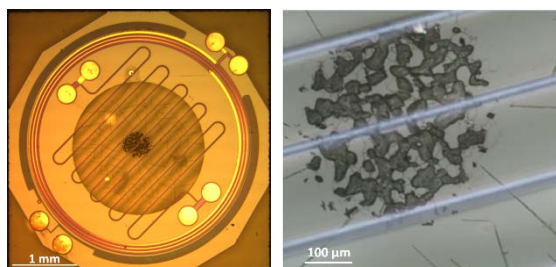
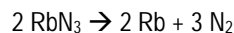


Figure 1: Pictures of the rubidium gas cell and the deposited RbN₃.

The presence of metallic rubidium in the cells is assessed by measuring the absorption spectra of the Rb vapor. In some cells, a loss of the Rb signal was observed and was assumed to be related to Rb oxidation by oxygen or water i) generated during the anodic bonding process or ii) desorbed from the glass covers while operating the cell at ~ 100 °C. In order to elucidate the failure mechanism, Raman spectroscopy is used here to measure the partial pressures of nitrogen (N₂), oxygen (O₂) and hydrogen (H₂) inside the cells. N₂ is present after UV irradiation due to the decomposition reaction:



The nitrogen pressure thus gives a direct indication of the UV irradiation yield. O₂ and water vapors cannot be present simultaneously with metallic rubidium because of the direct formation of rubidium oxides. Oxygen would, nevertheless, still be detected in cells without metallic rubidium. The presence of

H₂ is an indication of the presence of water inside the cell as it is a product of the reaction of Rb with water.

The confocal Raman configuration is schematically depicted in Figure 2. Thanks to an optimized calibration procedure, a detection limit of 5 mbar could be achieved. This value is sufficient with regard to i) the ~ 120 mbar of N₂ generated by the formation of 1 µg of Rb in the ~3 mm³ cell, ii) the ~ 80 mbar of O₂ necessary to oxidize Rb completely, or iii) the ~ 40 mbar of H₂ generated by the reaction of Rb with water.

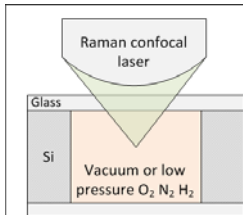


Figure 2: Confocal μRaman analysis inside the sealed cell cavity.

The absence of measurable quantities of O₂ or H₂ in our experiments led to the conclusion that formation, desorption or penetration of O₂ or water inside the cavity can be excluded as the main cause for the loss of the rubidium signal. A different mechanism has thus been postulated, and it is currently being further investigated.

The same Raman configuration was used in order to analyze in-situ the composition of the RbN₃ salt deposited in the sealed cavities. A batch of contaminated cells could thus be identified. The incriminated RbN₃ salt (Figure 3) was then removed from further fabrication lots.

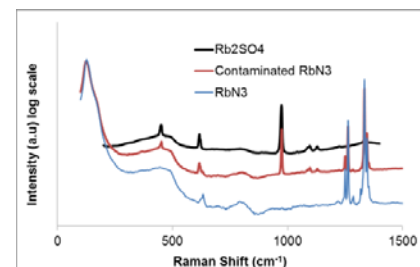


Figure 3: Raman spectra of pure RbN₃ and RbN₃ containing Rb₂SO₄.

Confocal Raman spectroscopy was successfully applied as a practical and nondestructive analytical method for atomic gas cell reliability analysis. The same method can thus be extended and used for the assessment of hermetic packages with an optically transparent window.

This research is performed within the frame of a multidivisional research program, and CSEM would like to thank the Swiss Confederation and the Canton of Neuchâtel for their financial support.

[1] W. H. Weber, *et al.* "Using Raman microscopy to detect leaks in micromechanical silicon structures", Applied spectroscopy, vol. 51, no. 1, pp. 123–129, 1997

[2] T. Overstolz, *et al.* "Highly Integrated, Miniaturized Gas Cell for Atomic Clocks," CSEM Scientific and Technical Report (2013), 28

MEMS Narrow Band IR Emitters

R. P. Stanley, B. Timotijevic, R. Eckert

With nanophotonics, we play with light on the wavelength scale. With MEMS, we can fabricate silicon machines to manipulate light. The two meet at infrared wavelengths where the wavelength scale structuring matches with MEMS fabrication technology. We show that the combination of plasmonics and MEMS leads to novel thermal infrared emitters with a controllable linewidth. We contrast these emitters with other thermal emitters currently on the market and discuss the reasons for the improvements seen as well as the challenges in further improving thermal emitters.

LEDs are efficient and cheap light sources with good spectral purity. Over the last ten years they have slowly replaced tungsten light bulbs, which have dominated interior lighting since the days of Edison. The problem with light bulbs is that they are thermal sources, and only some of the radiation is emitted at visible wavelengths, with the rest being lost as heat.

At infrared wavelengths, the equivalent of a light bulb remains the source of choice for cost-sensitive applications. All of the drawbacks that light bulbs have in the visible also exist in the infrared. LEDs in the infrared are very inefficient due to leakage currents and the lack of direct band gap materials.

The goal of this work is to use techniques from nanophotonics to create MEMS thermal emitters that are wavelength selective. Thermal emission is given by the temperature and emissivity of the hot object. The emission spectrum is normally the product of the blackbody radiation spectrum (broad) times the material emissivity (flat). The only parameter that can be engineered is the emissivity. From Kirchoff's law, the emissivity is proportional to the absorption of the material.

Our approach is to take a weakly absorbing material and make it selectively absorbing at a given wavelength. There are two classes of weakly absorbing materials: transparent materials and highly reflective materials. In the infrared, most highly conducting metals are also highly reflective and have a very low emissivity. We can change this dynamic by texturing the metal.

The famous enhanced optical transmission of light through sub-wavelength metal holes relies on surface waves travelling a long distance over the metal. If this distance is sufficiently long, the wave is absorbed rather than transmitted. This resonance effect can be tailored by varying the periodicity of the holes, the size and shape of the hole, and also the thickness of the metal layer.

Following these principles, we manufactured a MEMS emitter according to specific design parameters. The emitter is based on a SiN membrane that is a few hundred nanometers thin and a thin metal (Pt) film on its sides. The metal layers play the role of a heating element, but it also allows for the surface plasmon propagation. The emitting area is scalable, and in the chosen design, 1 mm x 1 mm. The devices were processed in clean rooms and characterized with respect to state of the art emitters.

The MEMS emitter indeed shows emissions that are much narrower than a thermal source. In addition, the device can be modulated at 20 Hz with rise times in the order of several milliseconds.

Figure 1 shows an image of a functioning device. Some light emission is visible in the image. The spectral response was measured using a Fourier Transform Infrared Spectrometer (Bruker Vertex 70) and compared with a commercial blackbody source. From this, we can derive the emissivity as a function of wavelength. As seen in Figure 2 the emissivity shows a narrow

peak at the design wavelength (7.8 microns) and a very flat, low emissivity at shorter wavelength. We have designed similar devices that operate at 4.3 and 6.1 microns.

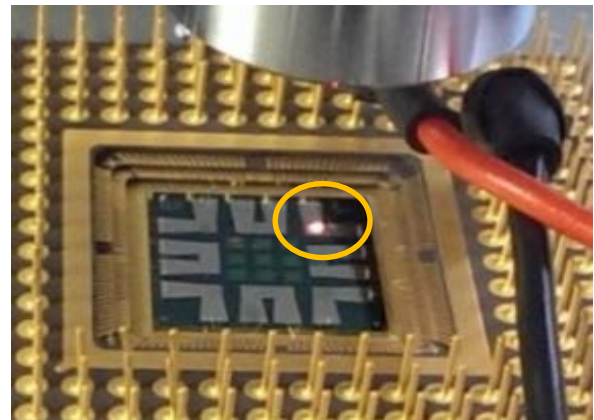


Figure 1: An image showing a working MEMS emitter. The white spot is visible light emission from the hot emitter. The MEMS emitter is housed in a large test package and is under an infrared Fourier transform microscope.

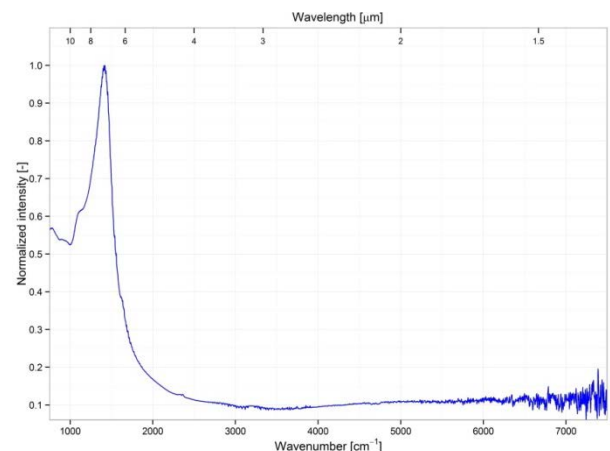


Figure 2: The emissivity of an MEMS thermal emitter using CSEM's hole array technology. The figure shows the emission as a function of wavelength (μm , top axis), and wavenumber (cm^{-1} , bottom axis). Note the low emissivity (0.1) across a wide range of wavelengths in comparison to the high emissivity peaked at $7 \mu\text{m}$ (1300 cm^{-1}).

In conclusion, we show that an inexpensive MEMS membrane can be designed and microfabricated to have a narrow spectral emission. Not only is the technology cost effective, but it enables the development of low power sources for gas detectors.

CSEM has filed a patent on the technology.

Monitoring Cell Traction

F. Sorba, M. Gazzon, R. Ischer, M. Liley, C. Martin-Olmos

CSEM is developing hybrid stiffness microelectromechanical systems (MEMS), which combine materials with elastic moduli that differ by several orders of magnitude. The goal is to develop a very sensitive mechanical device that is able to both detect and apply extremely small forces on large numbers of living biological cells in parallel.

Europe needs to respond to the growing challenge of chronic diseases: cancer, diabetes, chronic respiratory and cardiovascular diseases, all affecting the aging quality of the population and increasing health care costs. In order to address this challenge, not only are more effective therapeutic agents necessary, but also better tools for early diagnoses.

Mechanobiology is potentially a powerful approach to the recognition of early stages of many chronic diseases. Numerous mechanoreceptors, such as extra cellular matrix molecules, transmembrane proteins, cytoskeleton, exist in the cells and tissues of our body, and many diverse diseases are associated with changes in their mechanical properties. These mechanical properties open a new perspective on disease development, and thus, new possibilities for early diagnosis.

However, in order to advance significantly in this field, a measurement device is needed [1] that is capable of:

- Real-time measurements
- Parallel operation
- Incubator compatibility

Our goal in this project is to develop high throughput and easy to use measurement platforms for the mechanobiology of single cells (Figure 1). In contrast to existing, mostly optical, methods, we intend to determine the cell's mechanical properties electrically. An electrical approach allows parallel measurements and easy computerized data acquisition.



Figure 1: A platform tool that can be plugged into a PC for operation, data acquisition and analysis is highly preferred by the end users for its simplicity.

The first challenge is to detect the traction forces exerted by living cells on their culture support. Single cells exert very small forces (in the range of 1-40 nN [2]). A measurement device will require materials with alike Young's Moduli and structures with extremely low spring constants to produce measurable deformations with such small forces. For this reason,

softMEMS devices using very low Young's Modulus polymers are good candidates for the measurement platform.

A first series of softMEMS devices was fabricated using SU-8 as a structural material (Figure 2). SU-8 is biocompatible, stable in an aqueous environment, and chemically inert. These properties, together with its mechanical properties (4 GPa), make it an ideal candidate for this application.

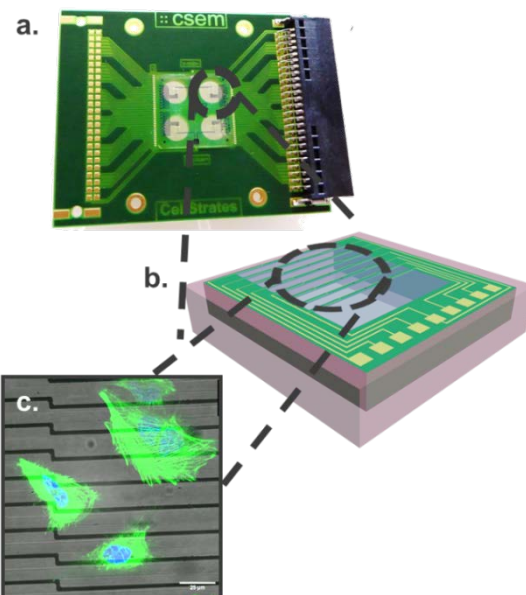


Figure 2: A softMEMS device for measurement of cell mechanical properties. a) A disposable PCB serves as mechanical support for the soft biocompatible chip and provides electrical connection for data acquisition; b) Schematic drawing of the hybrid polymer chip; c) Fluorescence image of osteoblast cells successfully attached to the flexible beams in the sensing areas of the chip.

The current softMEMS device uses gold wires as gauges embedded in self-standing SU-8 beams for detection of cell traction forces. Changes in the resistance of the wires occur when the beams are deformed.

Currently, the development of highly sensitive and multiplexable circuitry is in progress, together with the design of a method to calibrate the platform. A robust setup, like the one CSEM is envisioning with this project, has great potential to be used by a large variety of laboratories and clinics; and it will have a large impact on both the knowledge of fundamental processes of single cells and the early detection of diseases.

Financial support by the Swiss National Science Foundation (SNF) is gratefully acknowledged (Ambizione project No 154900).

[1] J. Guck, E. R. Chilvers, *Science Translational Medicine* 5, 212 (2013)

[2] O. du Roure, et al., *PNAS* 102, 7 (2005)

ACTION—Active Implants for Optoacoustic Natural Sound Enhancement

M. Fretz, R. Jose James, G. Spinola Durante, T. Burch, S. Bitterli, S. Mohrdieck

The European project ACTION builds on the recent discovery that relatively low levels of pulsed infrared laser light are capable of triggering activity in hair cells of the partially hearing cochlea (optoacoustic stimulus). New implants based on this technology will rely on novel packaging concepts: miniature biocompatible and hermetic packages are required to protect the (VCSEL) light source. The challenge is to make them sufficiently small to fit inside the cochlea. Optoacoustic cochlear implants have the potential to provide better hearing quality than state of the art devices as they generate a sound wave inside the cochlea rather than electrically stimulating the nerves.

State of the art cochlear implants rely on electric signals to stimulate the auditory nerve fibers. These signals are provided by electrodes which are inserted in the cochlea. There are limiting challenges associated with this approach: High electric current densities can damage the tissue, electric interference with the environment may occur and high-frequency artefacts are introduced into electrical signals recorded during stimulation. Furthermore, the performance is limited by the extent to which the electric field can be controlled by the position of the electrode and by the field shaping capabilities of the device.

An optoacoustic (OA) single channel device has the potential to replace the hearing aid in electro-acoustic stimulation, freeing up the inner ear and offering the patient a greater degree of freedom. In patients with mixed hearing loss (conductive component), the OA -device can help too, as it bypasses the middle ear by generating the sound waves inside the intra-cochlear fluid.

The OA device requires that a VCSEL or other laser source be placed inside the body for a prolonged period of time. This poses the challenge of hermetically sealing the VCSEL in a biocompatible and long-term stable package (Figure 1). The space constraints in the cochlea further impose restrictions on the package with regard to size. To date, no packages are commercially available which would meet all the requirements. The challenges of the project are to develop such packages along with a flexible substrate, which carries the metal tracks needed to connect the VCSELs to the driver hardware. Development of the driver hardware and software are further tasks of the project.

CSEM focuses on the development of the hermetic package, the flexible substrate and contributes to the development of the hard- and software for the laser driver.

A first long term implantable hermetic package made from sapphire and Pt feedthroughs has been demonstrated. A similar package made from the same materials is being manufactured. Its outer dimensions are designed to be 0.6 mm x 1.2 mm laterally and 0.6 mm in height. This device will fit inside a cochlea (assuming a tubular structure) of 0.8 mm diameter. The internal components (VCSEL and focusing lens) are being developed by our consortium partners. In first lab tests we showed that acoustic waves inside an aqueous fluid can be generated with the output light of a VCSEL at around 1550 nm.

We further work on the development of a long term implantable flexible substrate. It provides electrodes to stimulate nerves and measure responses of nerves as well as space to accommodate hermetically packaged VCSELs for optoacoustic stimulation. Fabrication of the substrate is based on batch and automatable process steps. Figure 2 shows laser-structured electrodes which belong to an array of substrates. (Further

process steps follow). These developments allow for reduced manufacturing costs. It also reduces the dependence on the availability of qualified and trained personnel as it reduces the number of manual intervention steps to a minimum.

The substrate comprises both distal and proximal end electrodes (metal structures), a flexible but non-stretchable member to protect the metal structure from strain, and a soft silicone coating to insulate the metal, protect the tissue from damage, and add robustness for handling. The substrate can also be equipped with bond sites for hermetically packaged VCSELs or sensors that need protection from the body. It is therefore possible to fabricate a substrate that combines stimulating/recording electrodes and active components in one device.

The joining of biocompatible and hermetically packaged VCSELs/sensors and flexible substrates opens up new potential treatment options through a combination of electrical and optical stimulation not just for hearing impaired but for patients who could benefit from neural stimulation.

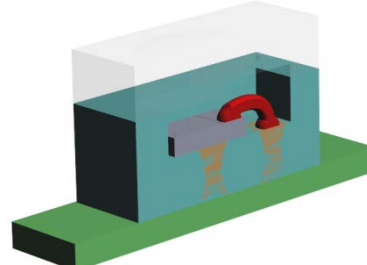


Figure 1: Sketch of a package with a cavity to accommodate a VCSEL (cross section). The package is made from a sapphire box (turquoise) and lid (translucent). The wire bond is represented by a red line. The feedthroughs (orange) connect the VCSEL to the flex substrate (green).

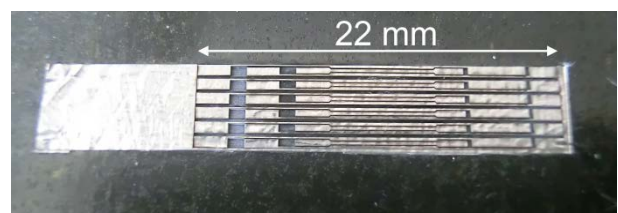


Figure 2: Array of substrate electrodes. Batch and automated processes are developed to manufacture new, reliable and flexible implantable substrates.

The research leading to these results has received funding from the European Union Seventh Framework Program FP7/2007-2013 under grant agreement n° FP7-ICT-611230.

Furnace-free Micro-joining with Reactive Nanofoils

G. Spinola Durante, R. Jose James, K. Krasnopski, U. Lang •

Reactive nanofoils are multi-layer foil materials that deliver energy in a fast and controlled fashion for micro-joining with typical bonding times of milliseconds. Applications can be found in many industrial areas like semiconductor, industrial, energy, medical and other market segments. Focus of this R&D activity is to develop a long-term reliable interconnection with customer-specific chip and substrate requirements.

Micro-joining technologies are well established in the semiconductor and in the mechanical industries. Dedicated soft solder and brazing alloy solutions require to be performed in reflow-ovens, diffusion bonders or in general in heat-controlled environments. This is a limiting factor in a number of interesting cases for the industry segments above mentioned. In principle to join two components it is required to have only a heater foil and two solderable layers according to Figure 1.

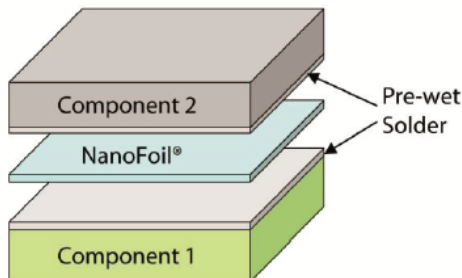


Figure 1: bonding configuration using Ni/Al-based Nanofoil® (Courtesy: Indium Corporation).

A furnace-free approach is considerably simple and enables to mount small components on large substrates without the burden of having a large oven. Large components also have a large thermal mass and most processes are easily limited by time due to cost and to technical reasons. Nanofoil® enables micro-joining with a heat wave travelling speed in the range of 5 mm/ms, independently of the substrate size and volume, making it possible to join components of very different geometric scale.

The fast nanofoils reaction also allows performing low-temperature bonding as the heat is only delivered to melt the solder layer and not to heat the bulk of the components to be joined. Simulations were performed to confirm that dissimilar materials with large thermal mismatch can be bonded with lower stress in the bulk of the component^[1]. A typical application of Nanofoils is the bonding of > 10 cm sputtering high purity metal targets onto a copper holder for cooling purposes.

The specific Ni/Al Nanofoils material selected in this work has a specific advantage for both soft soldering and brazing. Nickel is an excellent wetting material for an extended range of solders and brazing alloys.

The foil is originally developed for large heatsink bonding, with a pricing which is highly competitive specifically on mm scale as compared to conventional furnace based bonding. This enables new applications where the extra accepted packaging costs are very low.

Focus of CSEM work is to investigate material combinations, bonding process parameter including pressure, temperature and cover-gas atmosphere to achieve a reliable and hermetic interconnect. The test dummies are prepared according to specific industrial areas requirements. A laser cutting process has been developed at CSEM which does not trigger the Nanofoil inherent exothermic reaction, in order to achieve the correct preform dimensions (Figure 2a). In Figure 2b the hybrid bonding of an AlN submount on a stainless steel substrate is shown.

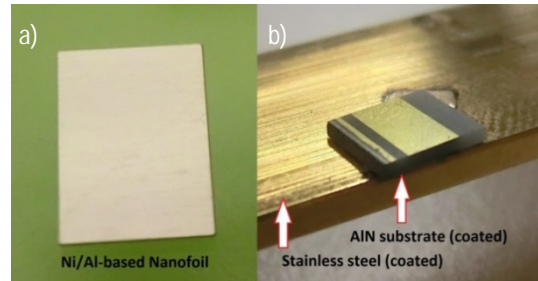


Figure 2: a) Laser-milled Nanofoil®; b) Sample bonded with Nanofoil®.

Many issues have to be tackled, depending on the selected chip and substrate combinations: de-adhesion of layers, partial bonding of Nanofoils and reliability issues like cracking of the multi-layer stack and low pull-strength and low shear-strength. Normed material testing is available at HSLU and through collaboration with CSEM will provide useful insight to the developed bonded configurations. (see Figure 3).

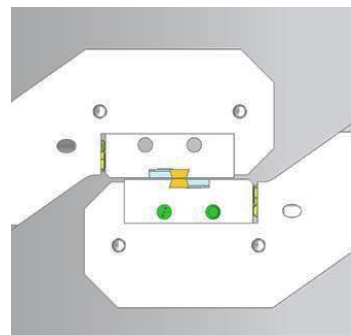


Figure 3: Lap-shear Testing fixture for bonded samples in yellow color (courtesy: HSLU).

CSEM can offer process development to any customer willing to test this new technology. Customization including samples specification and preparation, laser-cutting of Nanofoils is readily available.

• Hochschule Luzern - Technik & Architektur, CC Mech. Systeme

[1] www.techbriefs.com/dl/2013.php?i=15647&d=1

Process Development for Integrating Electronics in Textiles

M. Lützelschwab, S. Widmer, P. Glocker, A. Steinecker

CSEM developed a process which facilitates the insertion of electronic devices into textiles. The goal was to fabricate a demonstrator featuring a curtain, which incorporates an "EXIT" sign consisting of 400 LEDs. The exit sign should be hardly recognizable when switched off but should light up brightly in case of an emergency. This EU-Project was generally aiming to explore options for industrialized embedding of electronics into textiles, opening up a wide range of completely new applications.

The integration of rigid electronic devices into flexible uneven structures is a non-trivial task for the assembly process, particularly if several components have to be placed in close proximity and in considerable quantities. An interdisciplinary team was involved, including specialists in robotics as well as packaging. This report focuses on the packaging part.

Figure 1 shows the main achievement, which is the "EXIT" sign demonstrator, comprising about 400 LEDs inside a curtain showing an emergency case with the lights being switched on.

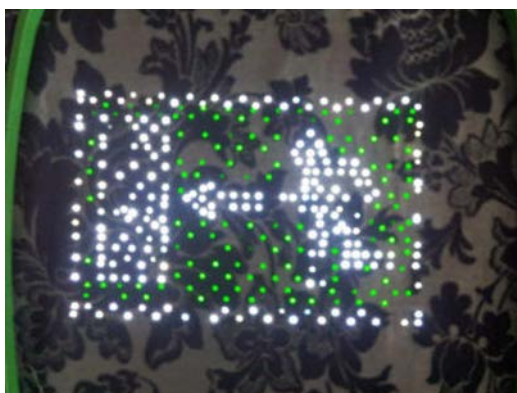


Figure 1: 400 assembled LED's showing EXIT sign.

The features of the LED device are of the same magnitude as the textiles features, thereby making the assembly process more challenging. Figure 2 gives an impression about the dimension of the LED device with respect to the textile and its conductive tracks seen from the backside.

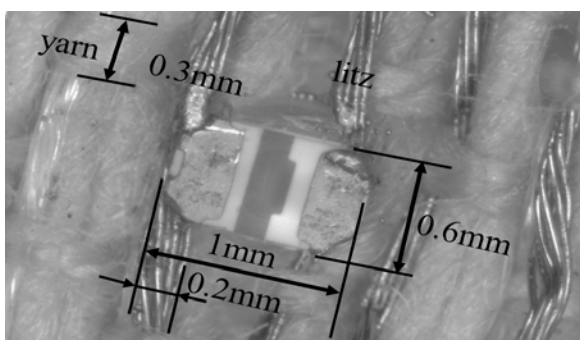


Figure 2: Image of an assembled LED.

The LED device is held by a tungsten vacuum gripper during the insertion process. Its fixation and proper guidance strongly depends on the momentum that is exerted during the insertion process on the LED device having a pyramidal mount. This means that the shape of the pyramid plays a crucial role on the insertion yield. Several iteration steps by the LED device's

manufacturer^[1] were required to find the ideal shape to achieve the anticipated yield.

Figure 3 shows an overview of the assembly process.

The left hand side (1) shows an LED with a glued polymer pyramid. This device is integrated into the textile that is depicted below which features a Cu litz on its surface. The LED device is then inserted into the textile and soldered to the Cu litz to establish electrical and mechanical contact (2). In a last step the tip of the pyramid is molten and flattened to further enhance the mechanical connection between textile and LED device as well as improving the optical output.

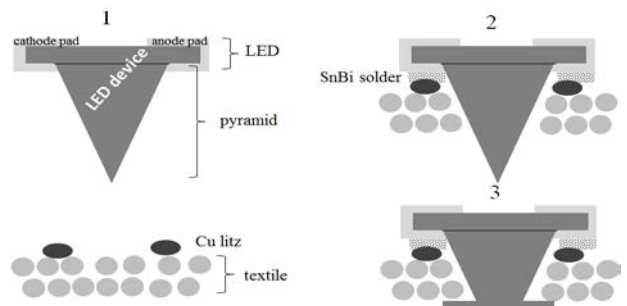


Figure 3: Illustration of the bonding principle.

Different melting and glass transition temperatures of the materials play an important role for the process development. Figure 4 shows the different values. Due to this, the process times and conductivity of the different parts and interfaces needed to be well investigated to keep the LED device intact and to ensure no detrimental effects appear on the textile.

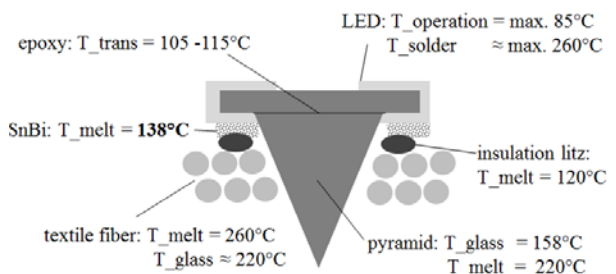


Figure 4: Melting and glass transition temperature for the different components of the LED device and textile.

Several demonstrators were fabricated with a placement yield better than 95%. Good results concerning reliability were obtained.

The research leading to these results has received funding from the European Union Seventh Framework Program FP7/2007-2011 under grant agreement n° 258724.

^[1] PEP, Centre Technique de la plasturgie et des Composites, Bellignat, France

WiseSKIN: Wireless Sensor Skin for Tactile Prosthetics

J. Baborowski, P. N. Volpe, A. Bionaz, M. Despont, J. R. Farserotu

A sense of tactility is needed to provide feedback for the control of prosthetic limbs and to perceive the prosthesis as a real part of the body. WiseSkin embeds wireless tactility sensors into the cosmetic silicone coating of prostheses. The silicone (PDMS) is structured to host PCBs integrating the sensors and their associated electronics.

The goal of the project is to reestablish a sense of tactility, which is needed to provide feedback for the control of prosthetic limbs and to perceive the prosthesis as a real part of the body. WiseSkin embeds wireless tactility sensors into the cosmetic silicone coating of prostheses. This part of the project is dedicated to the development of the Miniaturized Sensor Module. This module is the base element for the tactile sensing of the subject. Several modules (typically three per finger) are to be placed on the prosthetic. The targeted module includes the pressure sensor, microelectronic controller and radio placed on the common PCB. The module is connected to the artificial skin via the conformal power distribution layer (CPDL). Recently, several aspects have been developed:

- Flexible interconnections obtained on the PDMS substrates by the metallization using the Pt implantation (i-Pt);
- 3D soft (i-Pt on PDMS) interconnections between the pressure sensor (top side) and the external connectors;
- Tests and calibration of the sensors embedded in the PDMS skin with flexible interconnections (Prototype "0");
- Concept, design and the manufacturing of the miniaturized 3D PCB dedicated for the Prototype "1" and "2".

A general concept of the module is shown in Figure 1. The individual module consists of a sensor module embedded in artificial skin and connected via CPDL. The tactile sensor is placed on the top of the module and the electronic part on the bottom. The 3D PCB is customized in order to fit with the architecture of the module.

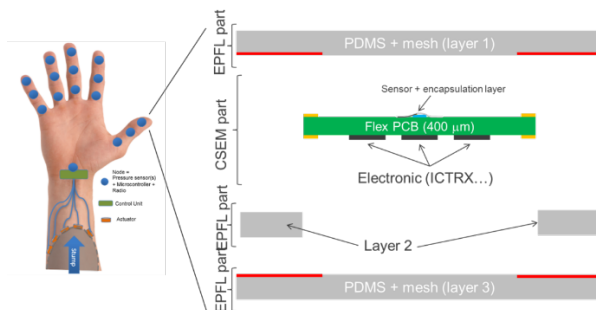


Figure 1: A general concept of the sensing module and integration with CPDL.

Figure 2a shows the single pressure sensor (GE-P161 type, top view) embedded in the PDMS. The PDMS interface (150 μm thick) contains the conducting Pt paths (black lines on Figure 1a) making the electrical connections between the sensor and the external measurement unit. The tight integration between the sensor and PDMS is obtained by plasma activated bonding. The resistivity of the connections (less than kOhm) is compatible with the functionality of the piezoresistive sensor. Figure 2b represents a global view of the Prototype "0". In this case, the sensor module is integrated on the 3 x 3 cm² silicon support and a standard PCB for the preliminary tactile tests.

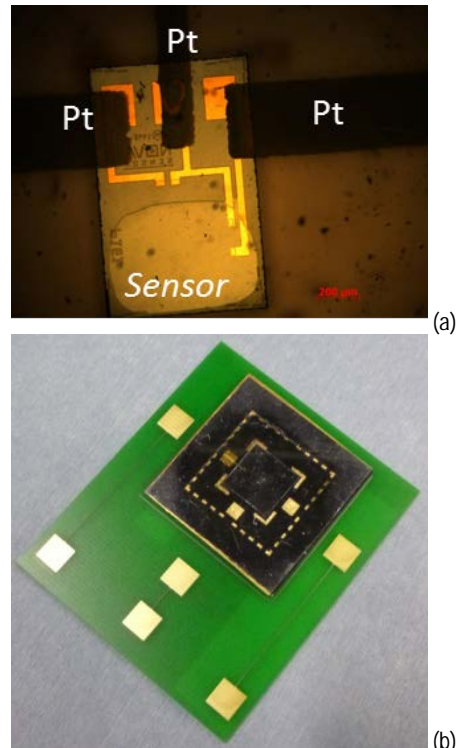


Figure 2: (a) Close view of the GE-P161 sensor embedded in the PDMS with the soft interconnections; (b) Global view of the prototype "0".

The first tactile tests were done at the laboratory level by applying pressure with a finger on the top of the sensor and reading the output voltage (Figure 3). The sensor embedded in the PDMS and connected via the soft Pt paths is sensible enough to transmit the quite large range of the applied pressure. The robustness of the module (mechanical and electrical) was satisfactory, and the tests have been repeated with a dozen of sensing module units. The calibration of the sensor module is still ongoing.

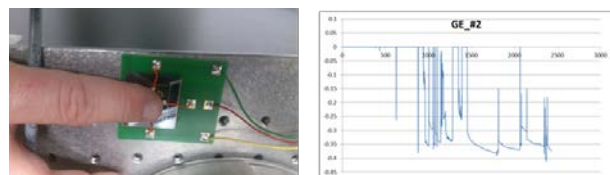


Figure 3: Laboratory level tactile tests performed on the Prototype "0" and the output signal recorded in function of different pressure levels applied.

SURFACE ENGINEERING

Stéphane Follonier

CSEM's Surface Engineering program (SE) addresses several global technology trends in engineered surfaces, including **nano-textured surfaces**, with applications ranging from super-hydrophobic coatings to embedded nano-grating security features; **printed electronics**, with applications ranging from printed, hybrid electronic systems to printing on flexible substrates; and **bio-functional surfaces**, with applications ranging from intelligent, disposable wound dressings to 3-D cell cultures on microbeads.

To address these trends and to simultaneously provide Swiss industry with continuous, unique innovation in surface engineering, the SE program focuses both on the novel properties of engineered surfaces in order to deliver breakthrough surface effects and on such surfaces' "up-compatible" manufacturing processes in order to bridge the gap separating technology platforms and industrial applications and to drive adoption of these surface technologies by industry. As a result, the program balances

- scientific competencies—in the design, modelling, prototyping, and testing of surface properties—by modifying surface material composition and/or geometrical surface structures, and
- technical expertise in manufacturing processes with a focus on processes that are compatible with industry manufacturing standards for large volume manufacturing.

CSEM's scientific competencies in production-relevant tools and processes for modifying surface material composition focus on surface chemical modification (covalent grafting of polymers, of functional silanes, or of biomolecules; sol-gel chemistry; and functionalization of mesoporous films) and on deposition techniques (screen printing, gravure and inkjet printing, dip and bar coating, slot die coating, oxygen plasma, electro-spinning, plasma enhanced CVD and low-pressure CVD, PVD multi-chamber, and MVD).

CSEM's scientific competencies in production-relevant tools and processes for geometrical surface structuring focus on surface patterning (laser scribing and microstructuring, reactive ion etching, and holography submicron optical patterning) and on replication processes (hot embossing and UV curing, COC rapid prototyping, and injection molding). This expertise is completed by production-relevant methods in the field of structure origination (including top down micro- and nanolithography and the combination of self-assembly and dry etching).

These focuses translate into the program's vision: To research and develop engineered surfaces and interfaces through surface material composition and/or geometrical surface structures using processes compatible with large-scale manufacturing and respecting quality comparable to laboratory prototypes

As stated in this vision, CSEM uniquely focuses both on novel properties and on the associated manufacturing processes necessary for a rapid adoption by industry. This attention to scalable production processes ensures the smooth transfer of

the engineered surfaces from the labs to fab. It distinctively positions CSEM in the surface engineering community as the link between research and industrial applications.

As an example of this approach and its impact on the Swiss pharmaceutical industry, the program is developing tools and processes to embed security features into medicines during their production. Within the Surface Engineering program, micron and sub-micron-resolution diffractive gratings, micro-barcodes, and high-level security holograms have been transferred directly into the steel molding and embossing tools used in the production of medicines, without chemical or biological additives and at no extra cost with regards to production lines (i.e., the lines remain fully compatible with the original processes so that no additional approval from regulatory agencies is required).

As previously stated, the CSEM Surface Engineering program balances scientific expertise in engineering surfaces with technical expertise in "up-compatible" manufacturing processes in order to produce a significant positive impact for Swiss industry. Without this dual focus, surface engineering would remain in the lab.

Therefore, the first global objective of the Surface Engineering program is a scientific understanding of surface engineering, elaborated by targeting the research and development of functionalized surfaces and interfaces with novel physical, optical, chemical, biological, electrical, and mechanical properties and their integration into devices and systems.

The second global objective—upscale, up-compatible manufacturing processes—is achieved by targeting the research and development of cost-effective manufacturing technologies and processes and their transfer to Swiss industry, including to the watchmaking, life sciences and food, energy and environment, medical and sport, aeronautics, transportation, and security sectors.

In executing its vision, achieving these two objectives will be the keys to the success of the Surface Engineering program and will allow the program to directly help in generating high added value within Switzerland.

Engineering surfaces implies a knowledge of many scientific disciplines ranging from the chemical to the biological, and from the optical to the mechanical, while incorporating electrical engineering. The Surface Engineering program is built on the abovementioned five key disciplines grouped into the three pillars of opto-mechanical, biochemical, and electrical properties that constitute the three activities of the Surface Engineering research program—namely, *Nanosurface Engineering*, *Biosurface Engineering*, and *Printable Electronics*.

Nanosurface Engineering is composed of the following topics:

- Micro-/nano-manufacturing technologies
- Functional nanocoating
- Nanophotonics engineering

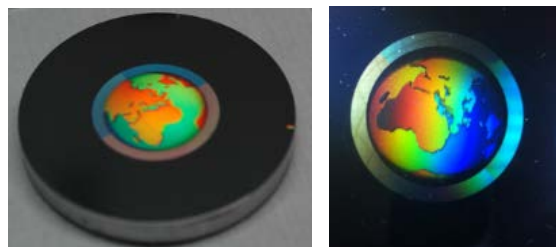
Biosurface Engineering is composed of the following topics:

- Cell handling
- Sensors
- Sample handling

Printable Electronics is composed of the following topics:

- Printable electronic processes and components
- Design, modelling, and testing
- Application and hybrid integration

The focus of the *Nanosurface Engineering* activity is the development of reliable processes for the fabrication of submicro- and/or nanometric structured surfaces, films, and components with enhanced performance or unique physical, chemical, or biological properties. In line with the dual objectives of the program, the *Nanosurface Engineering* activity focuses on understanding the link between physical, chemical, and biological properties and the characteristics of a surface at the nanometer scale, and works toward the development of reliable processes for the fabrication of submicro- and/or nanometric structured surfaces, films, or components with enhanced performance or unique properties. A third pillar is the integration of such surfaces into devices or systems, for example plasmonic devices.



Durable micro-nanostructured stainless steel insert for injection molding for the serial production of plastic components incorporating micro- or nano-scale functional features.

The *Biosurface Engineering* activity provides integrated solutions to our partners in the form of smart consumables based on low-cost manufacturing processes for biomolecule detection and cell and sample handling. The activity focuses on the development of technology platforms in its three topics of cell handling, sample handling, and sensors. By bringing together competences and technologies from numerous disciplines—surface chemistry, fluidics, cell biology, electrochemistry, electronics, optics, and mechanical design—the activity offers unique solutions to its customers. *Biosurface Engineering* has a strong emphasis on proprietary technologies and on the use of manufacturing processes suitable for upscaling.

The focus of the *Printable Electronics* activity is additive manufacturing for large area, lightweight, flexible, and hybrid electronics. The activity is a set of emerging technologies including new materials, process equipment, and devices based on novel additive manufacturing processes, which make possible large area, lightweight, flexible, distributed electronics. *Printable Electronics* creates a flexible and broad technology base—ranging from materials via processes to device development—to support Swiss companies across the value chain.

These activities are interlinked to provide our customers with better integrated solutions at the system level. An example of such an inter-activity success is our *in vitro* models of biological barriers for the evaluation of drug nanocarrier uptake and for nanotoxicology assessments, created by combining

- silicon nanoporous membranes (nano- activity) with
- stand-alone bioreactors (bio- activity) and
- electronic and microfluidic equipment

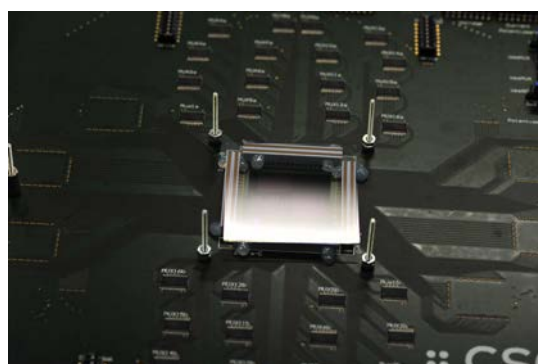
to measure, *in situ* and continuously, transepithelial electrical resistance (TEER). This non-invasive method can be used to ascertain the quality of a barrier model such as the lungs, intestine, skin, cardiovascular system, or the blood–brain barrier.

Highlights

It is clear that the surfaces of solids do not have the same properties as their bulk counterparts. Surfaces interact with their environment, so tailoring their properties is key to durability, reliability, efficiency, and quality in the following application fields: watchmaking, life sciences and food, energy and the environment, medical and sport, aeronautics, transportation, and security.

The successes of the Surface Engineering program encompass a number of industrial processes and products that rely today on technologies transferred from CSEM in the past. Highlights include:

- CSEM's **injection molding replication** via holographic steel inserts with micro- and nanometer scale surface modification allowing for the injection molding of plastics with grating periods down to 270 nm on non-planar surfaces tested on a real production line with a record production of up to 3 million pieces (by our industrial partner).
- CSEM's **disposable electro-chemical sensors**, created by printing electrically conductive inks on flexible substrates, by screen printed manufacturing, and by further passivating their surfaces with—for example—ion selective membranes, making possible the fabrication of disposable electro-chemical sensors for cell culture monitoring.
- The **Revelation System®**, which introduces an ingenious mechanism based on polarizing discs with anti-reflective sub-wavelength structures that reveal a watch's mechanism while it is on your wrist.



Organic photodiode array (center) and matrix driving electronic testing board.

Today, CSEM's Surface Engineering program is positioned to offer solutions to industry by providing novel surface properties and novel production processes to address major global trends. Surface engineering has served, serves, and will continue to serve Swiss industry in these areas by:

- Enabling Swiss companies, especially SMEs, to contribute to and benefit from the emerging field of surface engineering by offering a proof of concept and prototyping lab environment.
- Enabling Swiss equipment and material producers to benefit from the developments in the nano-, bio-, and printed electronics fields.
- Manufacturing prototypes and small series to demonstrate relevant applications.

CSEM's Surface Engineering program has certainly made a strong, positive impact on both the scientific and the industrial community. It is well aligned with key Swiss and European initiatives and—ultimately—has led to the transfer of several successful technologies to Swiss industry, thus completing the innovation cycle by helping bring innovative products to market.

Innovative Thin-film Optics for Solid-state Lighting

O. Fernandez, R. Ferrini, A. Lücke, A. Luu-Dinh

The point-like nature of the LEDs imposes the use of either inefficient and bulky light scattering sheets or of costly short-pitch LED arrays to achieve the spatial luminance uniformity required by large-area luminaires for professional lighting. Here we present an innovative thin form-factor light management (LM) system comprising a highly engineered combination of diffractive, refractive micro and nano-optical elements. The developed solution is compatible with large-area, low-cost roll-to-roll manufacturing.

The presence of light emitting diodes (LEDs) in the lighting domain is expected to reach a penetration rate of 56% by 2016 [1]. This rapid shift towards LED technology brings enormous business opportunities since LED-based light sources can still benefit from a significant amount of R&D efforts in different aspects.

One of these aspects is the design and realization of planar large-area panels used in e.g. the Professional Lighting domain, where the light emitted by the LEDs needs to be spatially homogenized over the entire emitting area not only efficiently but also maintaining a thin form factor of the module.

Commercial products of this kind today use either edge-lit or backlit configuration and both approaches have severe disadvantages. The former is compatible with thin profiles but requires a rather high density of LEDs to achieve the required light output and the luminance uniformity is typically rather low. On the other hand, back-lit configuration is compatible with high luminance uniformity and acceptable efficacy levels only if the diffuser is set away from the LED a distance larger than the LED pitch.

In the framework of the LASSIE-FP7 project CSEM is developing a light management concept which is a hybrid of the two above. The LASSIE-FP7 concept is based on light in-coupling and subsequent out-coupling into and from a thin-film waveguide using a backlit configuration.

In LASSIE-FP7 LM system, the light emitted by a collection of blue LEDs is coupled into a thin-film (0.5 mm), flexible transparent waveguide through diffractive in-coupling pixels ($3 \times 3 \text{ mm}^2$) replicated on the surface of the former. The LED board is in a backlit configuration with respect to the waveguide and both in close proximity ($\sim 0.2 \text{ mm}$).

Similarly to the edge-lit approach, the in-coupled light travels inside the waveguide based on total internal reflection (TIR), until it is disrupted by the presence of out-coupling structures and escapes.

With the waveguide at close distance from the LED board and the in-coupling pixels aligned to the LEDs, a substantial amount of the light is in-coupled inside the waveguide (Figure 1). In addition, each in-coupling pixel contains large number of sub-pixels ($0.1 \times 0.1 \text{ mm}^2$) positioned in a chessboard arrangement (Figure 2) which ensures in-plane light in-coupling.

Out-coupling pixels are, for instance, replicated in-between adjacent in-couplers, allowing the effective emissive area to increase (see Figure 3).

Before leaving the lighting module, blue light is down-converted into a high-quality white light using a thin-film (50-500 μm thick) color changing foil (CCF) also in close proximity to the waveguide. The CCF, produced and supplied by BASF, comprises a series of proprietary (Lumogen®) organic dyes. These are extruded into a polymer matrix in a finely tuned concentration according to the color target.

The presented LM system is compatible with large-area, cost-effective, roll-to-roll manufacturing.

The research leading to these results has received funding from the European Union Seventh Framework Programme FP7/2007-2013 under grant agreement No. 619556, project LASSIE-FP7.

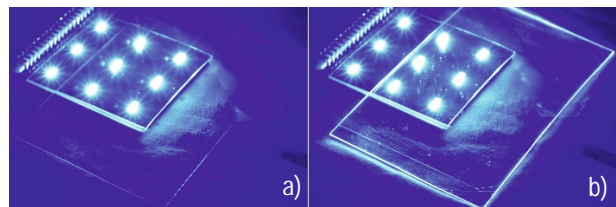


Figure 1: a) 0.5 mm thickness PC foil sitting on top of a 3x3 LED board (VTT); b) 0.5 mm thickness PC foil with replicated in-coupling pixels on the same LED board: the glowing edges in indicative of the in-plane light in-coupling.

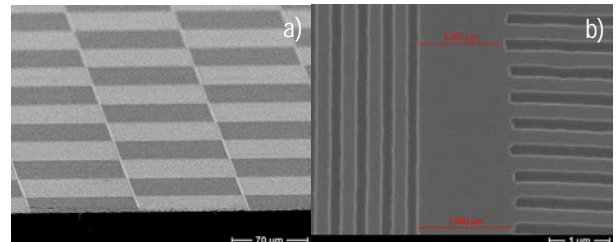


Figure 2: a) SEM picture of an in-coupling pixel showing a number of sub-pixels; b) Close-up SEM picture of two adjacent sub-pixels with mutually perpendicular groove orientation and nearly perfect overlap.

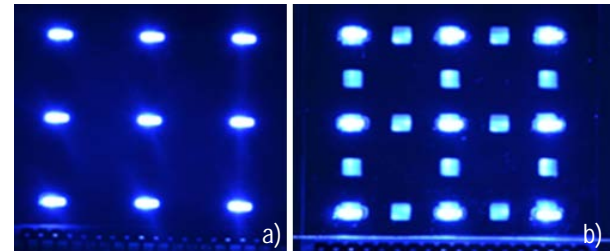


Figure 3: a) picture of the LED board; b) picture of the same LED board with CSEM light management foil on its top surface.

[1] Prasad, A. 2015 Year of (LED) Light. LED professional 47, pp. 32-36 (2015)

Large-area Plasmonic Substrates Based on Ordered Metallic Nanostructures

L. Duempelmann, F. Lütolf, D. Casari, A. Luu-Dinh, G. Basset, B. Gallinet

We present the fabrication of large-scale plasmonic substrates based on UV casting or hot embossing. Such plasmonic structures are very promising in the field of structural color, sensor, solar cell or light harvesting applications.

Plasmonics is the field of light interaction with metallic nanostructures mainly in the visible and NIR. Specifically sub-wavelength light confinement enables such interactions, leading to strong field enhancement in close vicinity. This results in a resonant spectral interaction, which is strongly dependent on the surrounding media. These properties make plasmonics very promising for optical security, color filter, sensing or light harvesting applications respectively.

Recent examples show the potential of plasmonic substrates, but to date fabrication of such plasmonic structures is very challenging or requires expensive and serial fabrication techniques. Our aim is to develop plasmonic structures in industrially relevant dimensions and with cost-effective processes.

For fabrication of ordered sub-wavelength structures we utilize laser interference lithography, capable of creating a large-area (5cm x 5cm) master structure. With the use of an in-house step-and-repeat robot we can upscale this master manifold, reaching up to 20x the original area (1m x 1m), see Figure 1. This area is fully roll-to-roll compatible and can be utilized for rapid and cost-effective mass-production.

Replication of the structures is done either with UV casting in UV curable sol-gel or via hot embossing into plastic both by using the master structure. Subsequently a variety of metals at distinct angles can be deposited. Finally the structures are embedded in e.g. UV curable sol-gel for protection in ambient conditions.

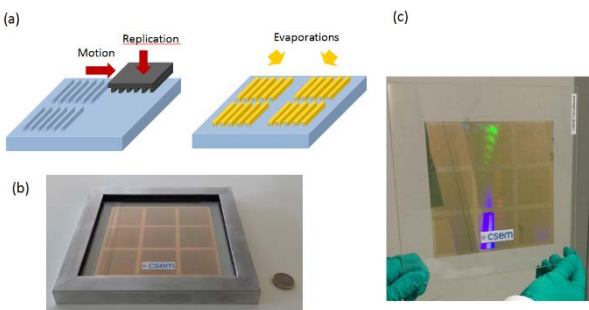


Figure 1: Plasmonic nanostructures fabricated with a step-and-repeat UV casting process. a) Replication and evaporation process; b & c) 15 cm x 15 cm sample.

The ordered metallic nanowires (range of the visible wavelength) interact with the light in such that a resonant condition leads to appearance of a color. Figure 2 shows how this resonance not only depends on the kind of metal used, but also whether the structure is embedded or not. Moreover the resonance depends on the polarization and the incidence angle of the impinging light, but more importantly on the structure of the nanowire themselves.

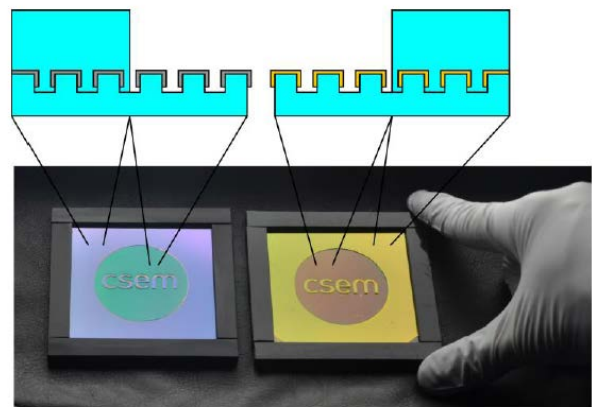


Figure 2: Photograph of aluminum (left) and gold (right) evaporated samples containing plasmonic structures. The image also shows the contrast between embedded (border and letters) and air interfaced parts (circular area) of the structure.

Figure 3 shows a stretch sensor, which changes the appearance upon elongation. Replication of the mold master was done in polyurethane allowing high elasticity of the substrate, provided with metallic nanostructures and subsequently embedded PDMS. The color change is caused by the increased distance of the metallic nanowires, resulting in a shift of the plasmon resonance.

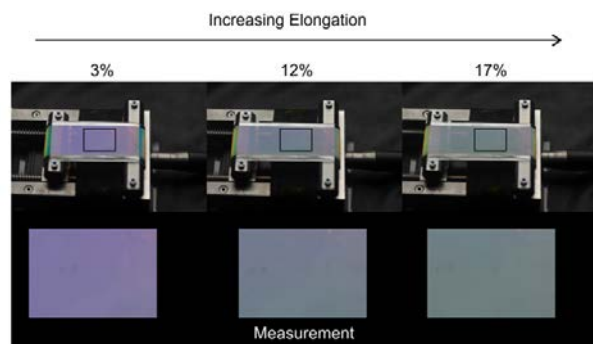


Figure 3: Visible response of the stretch sensor for elongations of up to 17%.

Overall we demonstrate a fabrication process of large-scale plasmonic substrates compatible with industrial roll-to-roll process. Adaptability of the substrates to different applications such as color filters or sensors is granted by modification of the fabrication process. This paves the way for industrialization of plasmonic substrates with great potential in future applications.

Fabrication of Sub-micron High Contrast Gratings in Hard Semiconductors or Dielectrics

G. Basset, C. Schneider, A. Luu-Dinh, R. Ferrini

Subwavelength gratings are of high interest in optical system because of their unique capabilities to provide high chromatic dispersion, high reflectance or transmittance dichroism and high polarization selectivity. Among sub-wavelength gratings, gratings with a high contrast between the refractive indexes of the slow and fast optical materials, called High Contrast Gratings (HCGs), are of particular interest because of their compact design and very effective optical properties. Many optical systems integrate HCGs, for instance spectrometers, laser beam combiners and polarization-selectivity laser cavity mirrors. However, their accurate fabrication in hard semiconductors or dielectric materials is challenging. A new process-flow was developed to accurately etch any hard dielectric or semiconductor based on hard masking, Reactive Ion Beam Etching (RIBE) and lift-off.

The high contrast of refractive indexes used in HCGs is obtained by a patterned etching process in a layer made of a high contrast dielectric or semi-conductor material. The gratings grooves are filled with air or another gas, or sealed in vacuum to maximize the refractive index contrast of the final structure. As the optical properties of dielectrics and semiconductors have large chromatic variations, different optical materials with a high refractive index must be used according to the wavelength range of interest.

As an example, for wavelengths greater than 1.15 μm in the infrared domain, silicon is commonly used because of the extended process know-how developed for the semiconductor and MEMS industry. Silicon processing tools are broadly available and well-known processes using chemically reactive plasma, Reactive Ion Etching (RIE), enable smooth and deep etching of silicon. However, optical systems using wavelengths shorter than 1.15 μm , for example using visible light, require other high refractive index materials exhibiting a high transparency.

Commonly used materials include the following dielectrics; titanium dioxide (TiO_2), tantalum pentoxide (Ta_2O_5) and Hafnium Oxide (HfO_2). Etching tantalum pentoxide (Ta_2O_5) films is challenging as chemically reactive plasma does not allow an efficient etching process. This is why only ion bombardments in high-vacuum such as Argon Reactive Ion Beam Etching (Ar-RIBE) allow its nano-structuration. However, a re-deposition of the heavy tantalum atoms is intrinsic to this process. This can be seen on the Scanning Electron Microscopy (SEM) image in Figure 1 after removing the organic nano-imprint resist used for the patterning.

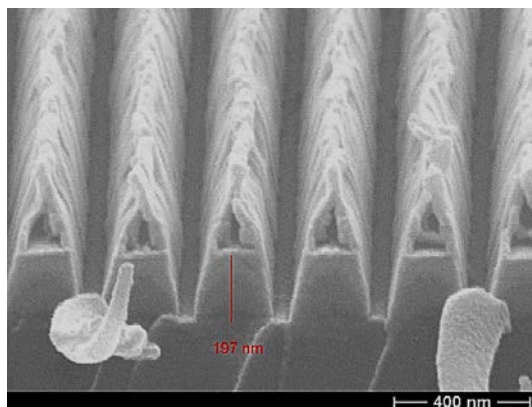


Figure 1: Cross-section image using SEM of a subwavelength grating etched by RIBE in Ta_2O_5 after nano-imprint resist removal by solvent. A massive material re-deposition can be observed on the ridges.

In addition to optical design, CSEM is able to prototype and produce HCGs in hard dielectric and semiconductor materials required by specific and advanced optical systems. Different process steps can be engineered to minimize the re-deposition and to further remove these residues. For example, multiple grazing angles Ar-RIBE allows to etch most of the redeposited material, as can be seen in Figure 2.

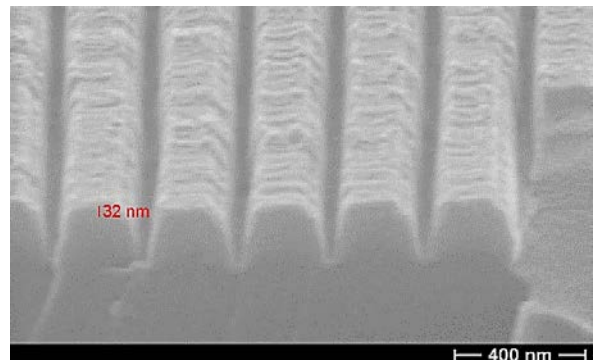


Figure 2: SEM cross-section of a Ta_2O_5 subwavelength grating after top polishing by grazing angle Ar-RIBE.

However, the top interface of the grating layer has still a large roughness making it unsuitable for assembly using bonding with other optical coatings or gratings. In order to minimize the roughness of the top interface of the grating, a combination of hard-masking, Ar-RIBE and lift-off process was developed and optimized, as can be seen in Figure 3.

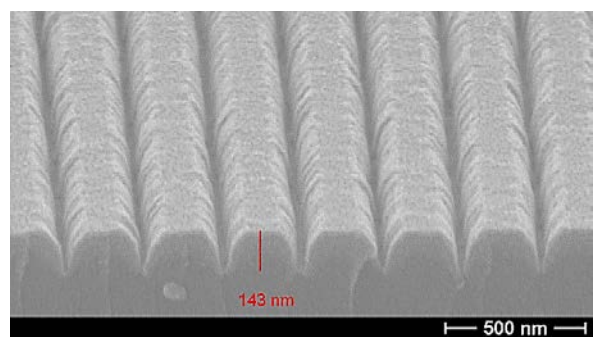


Figure 3: SEM cross-section of a Ta_2O_5 subwavelength grating manufactured by RIBE, hard masking and lift-off. The original top interface of the layer is left intact, enabling a low roughness making it suitable for being bonded.

Using this novel process, high quality sub-wavelength gratings can be manufactured in any hard dielectric or semiconductor material, for which RIBE is an enabling etching process. The top grating interface is the original film top interface, having a low roughness similar to the one of the initial film.

Manufacturing of High-added Value Micro-nanostructured Plastic Components

N. Blondiaux, R. Pugin, P.-F. Chauvy •, M. Diserens •, S. Dessors ••, L. Tenchine ••, P. Vuillermoz *

We report on the latest developments of the Interreg project PIMENT. The main goal of this project is to combine state-of-the-art metal micro- and nanostructuring techniques with injection molding for the fabrication of functional plastic components. A first phase was dedicated to the development of metal micro and nanostructuring techniques with the challenge of processing both planar and non-planar surfaces. The second phase focused on the production of micro-nanostructured plastic parts by means of injection molding. Micro and nanostructures were designed for two case studies: a bio-diagnostic platform and for decorative effects.

The main objective of the project PIMENT is to foster innovation in the field of micro-manufacturing and injection molding. This transnational Interreg project gathers specialists from French and Swiss companies and research centers with the goal of producing high-added value micro-nanostructured plastic parts by injection molding. There is indeed a growing trend to develop more advanced processes for the fabrication of functional products by means of injection molding. The high throughput of this technique and the recent breakthroughs in terms of replication accuracy have made it a standard for the production of nanostructured parts and devices such as optical data storage media and holographic structures for anti-counterfeiting. Beyond these examples, surface micro/nanostructuring has real potential to control additional surface properties such as adhesion, wetting, biological-matter interactions.

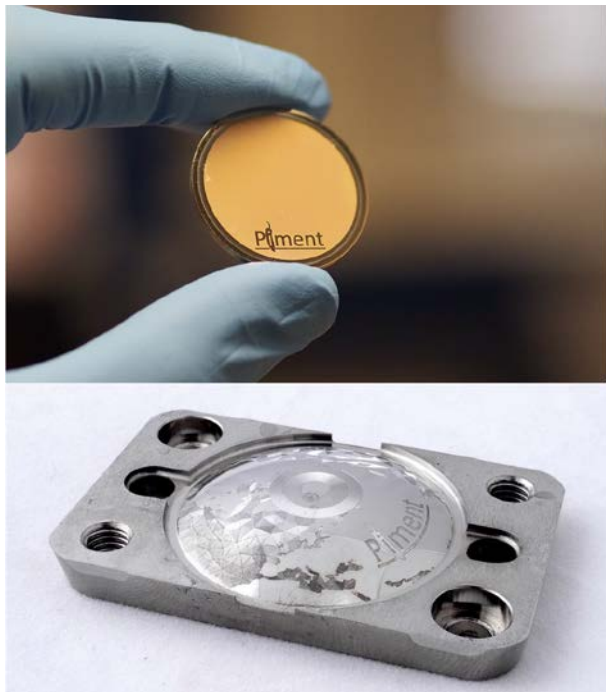


Figure 1: Photographs of a nanostructured stainless steel coin (top) and a microstructured mold steel (1.2343) insert (bottom), both fabricated during the project.

Well-established tooling techniques such as electroforming are currently used to produce micro/nanostructured mold inserts. However, there have been problems of integration into injection molds, especially when non-planar parts must be produced.

- Micropat SA, Suisse, www.micropat.ch
- Pôle Européen de Plasturgie, France, www.poleplasturgie.net

One of the key challenges addressed during the project PIMENT is the development of a new process chain for the fabrication of micro/nanostructures on planar and non-planar steel mold inserts.

Three types of inserts (flat, curved and micro-structured) have been used for two final applications: a bio-diagnostics platform and a watch glass. On the first demonstrator, the goal was to integrate micro/nanostructures on the detection spots of the bio-diagnostics platform to increase its sensitivity. The structures were fabricated on detection spots located in a microfluidic channel. For the second demonstrator, a curved insert was fabricated and surface microstructures were integrated for decorative purposes. The microstructures were designed to induce a change in pattern upon rotation and tilt. Figure 1 presents photographs of two micro and nanostructured steel inserts made during the project.

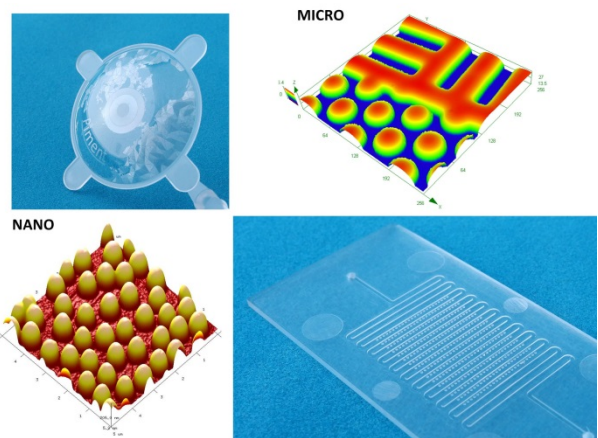


Figure 2: (top) Photograph and interference microscopy image of a micro-structured plastic replica produced by injection molding; (bottom) Scanning electron microscope image and photograph of nanostructured samples made for the bio-diagnostics platform.

For the fabrication of plastic replica, hot embossing and injection molding have been used. In Figure 2, photographs, atomic force microscopy and interference microscopy images of plastic replica produced during the project are presented.

The Interreg IVa project PIMENT is funded by the European Regional Development Fund, the OFES, and on the Swiss side, by the cantons of Neuchâtel and Vaud. We thank them for their support.

* Vuillermoz SA, France, www.vuillermoz-sa.com

Icephobic Coating Associated with Low-power Electromechanical De-icers

E. Scolan, A. Bionaz, N. Blondiaux, R. Pugin, S. Grimm •, D. Szabo •, M. Schneebeli •

Low ice adhesion coatings have been fabricated and tested regarding wettability and erosion resistance. Structured samples have been scaled up to A4 size to reduce the energy consumption of de-icers. These coatings may be applied to protect outdoor and indoor surfaces from freezing.

Ice adhesion and accretion on surfaces such as aircraft present long-recognized problems with respect to safety, efficiency and operational costs. Current active ice removal methods, such as electromechanical de-icers, are often based on breaking already-formed ice layers. In addition to their undesired weight and design complexity, these active anti-icing approaches require substantial energy for their operation. Passive solutions such as icephobic coatings have also been evaluated with varying success. Recently, coatings preventing ice accretion have been the subject of more attention stimulated by the remarkable water repellent properties of superhydrophobic surfaces. If superhydrophobic coatings are also not able to fully prevent ice accretion, the development of highly efficient hybrid low power systems combining active electromechanical de-icers and passive icephobic coatings remains highly promising to reduce the ice adhesion. This development and the design optimization of a hybrid solution require a deeper understanding of the links between superhydrophobicity and anti-icing properties.

To this end, the ICEAGE project was aimed at evaluating superhydrophobic coatings regarding ice adhesion reduction and erosion resistance in combination with electromechanical de-icers. Two types of nanostructures (pillars and holes) with two lateral sizes (100 and 500 nm) were created with selected resins, regarding their elasticity and structurability (Figure 1). These nanostructures were generated by combining nanosphere lithography, etching, and replication techniques. Hydrophobization of the replicated nanostructures was then performed to confer them superhydrophobic property. Holey samples are expected a) to be more erosion-resistant than pillared ones, and b) to prevent the formation of strongly adhering 'Wenzel ice' (ice penetrating inside the structures).

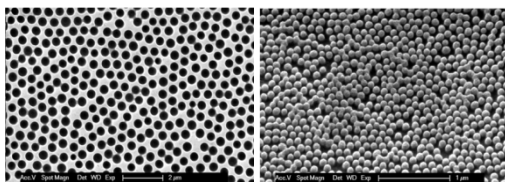


Figure 1: SEM pictures of structures of 500 nm large holes (left) and 100 nm pillars (right).

Produced samples have been tested regarding the ice adhesion, and the resistance to cracking and erosion. Based on agreed specifications, dedicated set-ups have been designed and fabricated by our partner WSL-SLF. The samples all exhibited good cracking resistance (no delamination), along with an exceptionally low ice adhesion (shear strength < 50 kPa), ten times lower than the ice adhesion of reference surfaces, i.e. aluminum and commercial coatings (Figure 2). Moreover, this ice adhesion of the ICEAGE samples remains low over a large temperature range down to -45 °C. Finally, the

erosion test demonstrated that the holey samples with a large size (500 nm) exhibited the best erosion resistance of the structured samples. Nevertheless, erosion resistance may be improved by selecting a more appropriate resin. In addition to indoor tests, outdoor exposure and bombardment with a snow gun were carried out. Surprisingly, the small pillared sample (100 nm) showed a good resistance to this testing. In addition, all the nanostructured samples resisted very well to the snow gun test compared to the reference samples, confirming the ranking of the ice adhesion test.

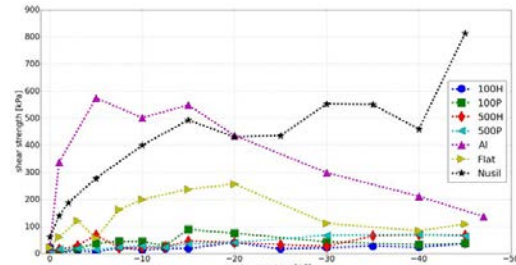


Figure 2: Dependence of adhesion strength on temperature between 0 and -50 °C. 100/500=structure size in nm; H=holes, P=pillars.

The low ice adhesion nanostructured layer is intended to be coated on the metallic surface of an electromechanical de-icer. Based on experimental conditions proposed by the industrial partner Zodiac Aerotechnics, vibration modes of a coated aluminum plate have been determined to shed the ice layer.

In order to prepare a more realistic ice wind tunnel test, large samples (A4 sized) were prepared with two highly promising nanostructures: 500 nm large holes (due to their higher resistance to abrasion) and 100 nm large pillars (due to their resistance to outdoor exposure). A step-and-repeat process was designed to form these large area samples from an elementary 7x7 cm² sized nanostructured block. After the hydrophobization step performed by MVD™, the samples produced exhibit a superhydrophobic behavior (Figure 3). These large area samples are expected to be evaluated in the icing wind tunnel to confirm the excellent anti-icing performance in the lab. These coatings will impact not only aeronautics, but will also benefit to outdoor (e.g. windmills, antennas, solar panels) and indoor infrastructures (e.g. freezers, condensers).



Figure 3: Picture of water droplets rolling off a large scale sample.

• WSL-SLF, www.slf.ch

Sol-gel based Pressure Sensitive Paint for Wind Tunnel and Aeronautics Application

E. Scolan, A. Grivel, R. Pugin, M.-C. Merienne •, Y. Le Sant •, Y. Michou •, M. Lyonnet •

A new unsteady Pressure Sensitive Paint (PSP) based on a nanostructured sol-gel coating has been developed and tested on a steel model of a civil aircraft in a transonic wind tunnel of ONERA. The results, which are in good agreement with pressure measurements, make this nanoporous coating a promising PSP to study aircraft models in unsteady conditions.

Pressure Sensitive Paint (PSP) is a global surface pressure measurement for a large domain of velocities from low speed to supersonic steady state flows. The fundamental operating principle of PSP is the oxygen quenching of luminescence from luminophores dispersed in the paint. Light intensity emitted by the paint is measured by a photodetector, providing a global map of pressure distribution over the probed surface. The extension of the PSP technique to unsteady measurements is a new challenge that requires the development of new paints with a response time several orders of magnitude below that of conventional PSP. Among the several ways to reduce the response time of the paint while maintaining a high sensitivity to pressure and a high intensity of luminescence, the most efficient are based on the introduction of porosity within the coating to increase the diffusivity of O₂. A fast responding PSP based on porous anodized aluminum (AA-PSP) with the dye adsorbed on the surface, achieving a very short response time ($t \sim 100s \mu s$) has been developed. However, sensitivity to humidity, the low intensity of emission, and the limiting structuration process (immersion in an acid bath of Al parts) make this approach difficult to implement.

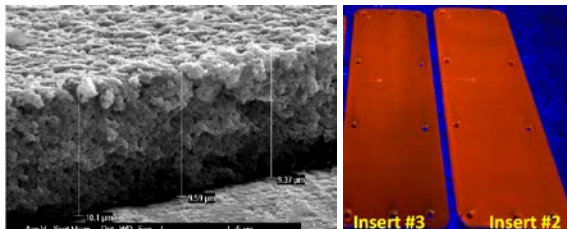


Figure 1: (Left) SEM micrograph of the nanoporous silica layer cross-section of a sample similar to insert #3 (10 μm thick); (Right) Fluorescence pictures (excitation 365 nm) of nano-PSP homogeneously treated inserts #2 and #3.

In order to address those issues, a new method has been investigated at CSEM: to develop a sol-gel based nanoporous pressure sensitive paint (nano-PSP) with low response time and high luminescent intensity, which would provide an increased frequency bandwidth (> 2 kHz). As a result, the influence of some nanoporous film features on the sensing performances was established (Figure 1). More specifically, the pore diameter and the total pore volume have a decisive effect on the sensitivity of dye loaded films for O₂ concentration measurement. Moreover, the high film transparency enables optical measurements. Finally, the films contain a crosslinked polymer that improves their mechanical resistance. All these characteristics make these nanoporous films relevant candidates for the optical measurement of O₂ pressure in a transonic wind tunnel. For this purpose, a few challenges have been addressed. First, the nanoporous PSP composition was

designed in order to obtain suitable pore sizes enabling low response times, film thickness for an optimal luminescence intensity, and mechanical stability to support the wind impact. Secondly, the functionalisation process with the luminescent dye was modified to improve the sensitivity to O₂, the luminescence intensity and homogeneity over the whole surface area. Finally, nanoporous layer deposition and functionalisation processes have been scaled up to cover non-even substrates with a homogeneously distributed luminescence and O₂ sensitivity.

The first generation of this PSP has a pressure sensitivity around 0.35 %/kPa, which is lower than that of the AA-PSP. However, its luminescence intensity is about three to five times higher than that of the AA-PSP, resulting in a favourable compromise for a fast acquisition rate, which requires short exposure time. This first generation of nanoporous PSP was tested on a civil aircraft in the ONERA S2MA transonic wind tunnel. PSP measurements were achieved at a frame rate up to 5000 fps (Figure 2). Useful results as RMS, PSD and coherence maps were obtained and compared favourably with those of pressure sensors. PSP measurements provide a high density of spatial information over a large area, which is difficult to achieve with pressure sensors. These results have been presented at the well-known AIAA aeronautics conference [1].

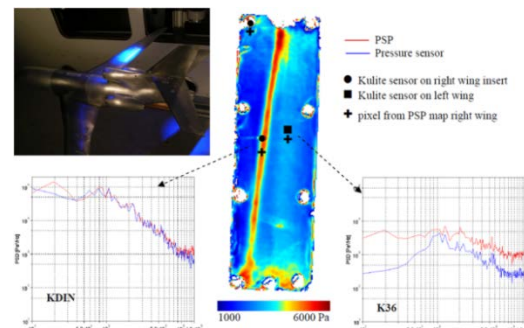


Figure 2: RMS map and PSD from nano-PSP (Insert #3). Pressure $P_{lo} = 185$ kPa, speed $M = 0.875$, incidence $\alpha = 1.11^\circ$, acquisition frequency $F_{acq} = 5000$ fps. Photograph of the insert on the model.

However, this first generation of nanoporous PSP can still be improved. Since the test was conducted in a wind tunnel, a second generation of the nanoporous PSP has been under development. The pressure sensitivity has been improved while maintaining the high luminescence intensity of the first generation. A wind tunnel test of this new generation is scheduled for late 2015. Future developments will aim at reducing the temperature sensitivity and improving the usability on larger 3D surfaces.

• ONERA, France

[1] Y. Michou, B. Deleglise, F. Lebrun, E. Scolan, A. Grivel, R. Steiger, R. Pugin, M.-C. Merienne, Y. Le Sant, Proc. 31st AIAA 2015, 2408

Sensors and Systems for Wound Care Management

G. Voirin, R. Smajda, G. Dudnik, M. Correvon

In the frame of the SWAN-iCare European project, a monitoring system was developed to allow patients with hard-to-heal ulcers to return home and to be looked after by their physician without needing to visit the hospital very often. Some parameters are monitored continuously and others are controlled during the home care nurse's regular visit.

Some diseases lead to recurrent pathologies, such as diabetic foot ulcers for patients suffering from diabetes or venous leg ulcers for patients with blood circulation problems. These hard-to-heal wounds require long and expensive treatments. One effective treatment consists of applying a negative pressure on the wound bed, where suction will evacuate the secretion, the bacteria and debris, and will enhance the revascularization, thus speeding up the healing process. In order to make this therapy possible in the patient's home, a system is being developed by the European project SWAN-iCare [1].

The system is mainly composed of three parts (Figure 1):

- One subsystem that is applied to the wound with a device that creates the negative pressure, and several integrated sensors that measure several wound parameters.
- A second subsystem composed of a network of devices to be used daily or when the wound dressing is changed.
- A third part consists of an informatics system where the monitored parameters are stored. They can be consulted by the health care staff through an internet connection. The two first subsystems send the information through a GPRS connection.

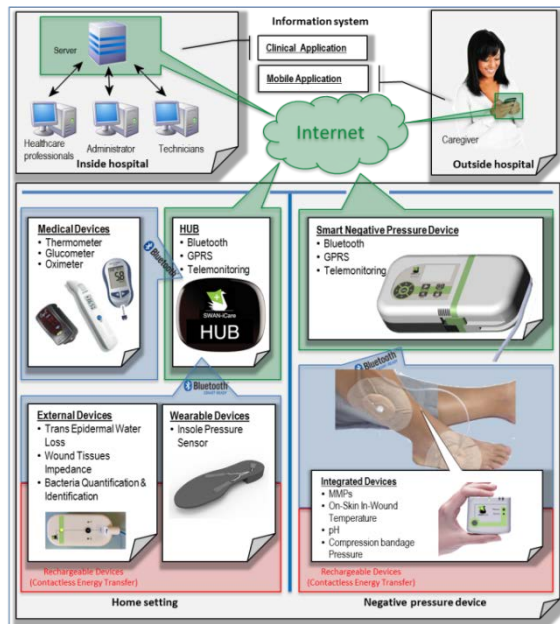


Figure 1: System for wound care management.

In this project, CSEM is developing the negative pressure device electronics and several sensors. One of the sensors measures the pressure that the patient applies on his or her foot when standing or walking. Diabetic patients often suffer from neuropathies that lead to a loss of sensation in their lower

extremities. With the insole pressure sensor, the wound care physician would be informed about the pressure the patient applies and can advise him or her how to take care for better healing of the ulcer or for preventing a new ulcer. Figure 2 depicts how the insole pressure electronics with the three sensors were integrated in the shoe of a diabetic patient.

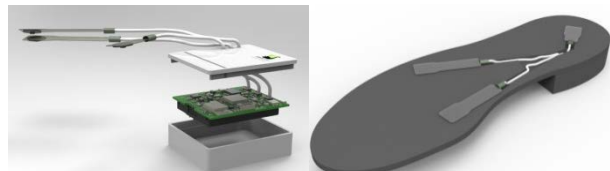


Figure 2: Insole pressure device: electronics and sensors (left), integrated in the shoe insole and heel (right).

CSEM has also developed the electronics for Trans Epidermal Water Loss (TEWL) measurement. Based on a demonstrator device designed and fabricated in partnership with the University of Pisa, CSEM developed the device adapted to the SWAN-iCare system with a Bluetooth connection to the home setting. Figure 3 shows the TEWL device delivery kit.



Figure 3: Trans epidermal water loss device.

For measurements related to the wound healing status, CSEM is developing a fiber optic biosensor for matrix metalloproteinase (MMP) monitoring. It is composed of a modified optical fiber: one part of its cladding is replaced by a colored gelatin that can be digested by the gelatinase family of the MMP [2]. When active gelatinase are in contact with the modified fiber, its transmission is modified at the absorption wavelength of the colored gelatin. MMP activity is estimated after analysis of the transmission change with time.

Thanks to wireless communication, the SWAN-iCare system offers the possibility for wound management care physicians and nurses to monitor their patients remotely. At home, the patient will have a level of control and safety equivalent to that found at the hospital, with the comfort of the home environment and the support of relatives.

This work is supported by the EU-funded FP7 ICT-317894 SWAN-iCare project.

[1] www.swan-icare.eu

[2] Patent application EP2565630

DEMOX—a Miniature Non-invasive Optical Oxygen Sensor

G. Weder, R. Ischer, M. Favre, R. Smajda, P. Albert, M. Liley

An innovative oxygen reader has been developed to determine oxygen concentration rapidly, efficiently and non-invasively. Originally developed to monitor dissolved oxygen in real time in cell and tissue cultures, the DEMOX optical reader is a versatile device that enables oxygen measurements for many different applications such as medical air monitoring, food and beverage process control or water quality.

Molecular oxygen is a prerequisite for almost all life. Since respiration is vital for cells, tissues and organs, measurement and control of oxygen levels is of particular importance in the life sciences. Traditionally, oxygen concentration has been measured electrochemically, while more recently, optical sensors have become more widely used. The working principle of these optical sensors is based on selective quenching of fluorescent dyes in the presence of oxygen. One of the major advantages of optical oxygen sensing is that oxygen concentration can be determined relatively non-invasively. An additional advantage is that oxygen is not consumed by the sensing process.

For several years, CSEM has followed a multi-disciplinary approach to the development of effective sensing solutions for gaseous and dissolved oxygen by combining chemistry, optical and electronics integration, signal processing, packaging and life applications. Currently, the miniaturization of sensors together with their readers is a critical factor of success in many application fields.

CSEM's optical oxygen sensors are based on the functionalization of thin mesoporous silica-based films with selective dye indicators such as ruthenium complexes. Thanks to their high porosity and surface area, the mesoporous sensing films have both a high optical density and fast response times. The sensing films can easily be produced using large-area industrial techniques. They are biocompatible, can be sterilized by autoclaving, and can be fixed to the inner surfaces of transparent disposable plastics, glassware or bioreactors. The only requirement is an optical access to sensing films in contact with the sample, and the oxygen concentration can be measured non-invasively through the wall of the container while avoiding any contamination of the sample (Figure 1).



Figure 1: Fluorescent oxygen sensor in a tissue culture flask.

An extra compact reader called DEMOX has been designed and produced in a format very similar to a microscope objective (Figure 2a). It can be directly mounted on the inverted microscopes used routinely in biology (Figure 2b). The microscope facilitates alignment between sensor and reader while ensuring a stable and constant optical environment for reliability.

The quantitative determination of oxygen concentration is based on a frequency-domain lifetime measurement. The sensing films are excited by a blue square-modulated LED and the emitted fluorescence has a similar waveform but is phase-shifted with respect to the excitation curve. The amplitude of the phase-shift is directly dependent on the concentration of

oxygen. The optimum measuring range for the sensors is from 0% to 21% oxygen with an accuracy of $\pm 0.13\%$ at 1% oxygen and $\pm 0.48\%$ at 10% oxygen. The precision is $\pm 0.07\%$ oxygen. The response time in gaseous environment is around two seconds.

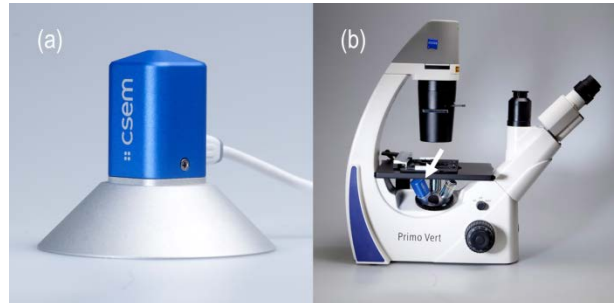


Figure 2: DEMOX reader on its support (a) and mounted on an inverted microscope (b).

The DEMOX reader has been developed to monitor oxygen in real time in cell cultures (Figure 3), but it enables oxygen measurements in many other contexts such as biotechnology, pharmaceuticals or environmental research. It can be used, for example, for the quality control of air and water, and for the process control of food or beverages, as well as for diagnosis in applied and basic research. A clear advantage of this "objective-like" device is its compatibility with most commercial microscopes that are regularly used in biology.

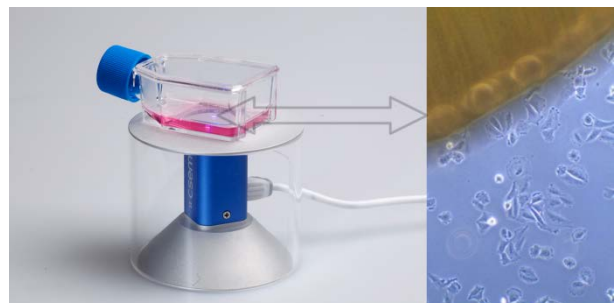


Figure 3: Oxygen control in a human osteosarcoma cell culture.

The combination of this new miniature reader with inexpensive sensing materials provides an innovative oxygen meter that opens new applications in health and environmental monitoring. The solution is highly customisable in terms of power supply, wireless communication or e-reading on mobile devices.

The Demox oxygen sensor was awarded the BioInnovation-Eclosion prize 2015.

Impedance Measurement for 3D Cell Culture Models

M. Favre, M. Giazzon, R. Ischer, G. Andreatta, D. Bayat, M. Liley

Cells grown in a 3D environment have proven to behave in a manner closer to in vivo tissues. Compared to 2D cell cultures, these improved models have several applications such as drug development, toxicity testing or tissue engineering. Measuring the impedance is a non-invasive and real-time technique to monitor cell activities inside 3D constructs. CSEM is currently developing a bioimpedance chamber with integrated electrodes for 3D hydrogel scaffolds.

In vitro 3D cell culture is increasingly used to better mimic in vivo tissues. It has shown an improvement over growing cells on 2D surfaces, but the observation of cellular activities inside the 3D cell culture is much more challenging. Optical microscopy is unsuitable for thick 3D constructs or can only be used as an endpoint analysis with sectioning of the sample.

Electrical impedance spectroscopy (EIS) is a good candidate to get better insight into what is going on inside a 3D construct. This technique consists of applying a defined alternative current and measuring the electrical impedance at different frequencies. The presence of cells, which can be modeled with a resistance (cytoplasm) in parallel with a capacitance (cell membrane), will influence the measured impedance. EIS has potential for simultaneous structural characterisation of 3D scaffolds and evaluation of cellular behaviour (cell proliferation, response to chemicals).

CSEM is developing a biochamber for 3D hydrogel scaffolds with embedded electrodes. COMSOL multiphysics simulations were performed to understand the influence of the electrode shapes, numbers and localisation in the system. Sensitivity distribution of the impedance describes how effectively each region contributes to the measured impedance signal. Depending on the electrode configurations, the measured impedance reflects the whole sample (Figure 1a) or only one region in the sample (Figure 1b). The spatial resolution of the impedance measurement may be enhanced by using an array of electrodes around the conducting volume of interest.

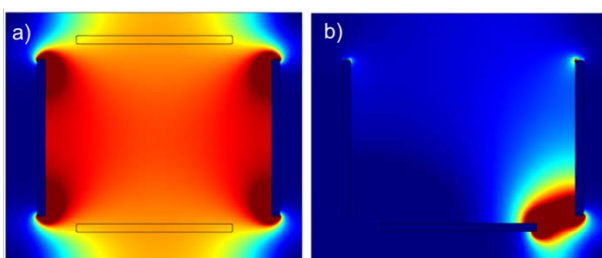


Figure 1: Sensitivity field distribution from COMSOL simulation. Scale from blue (no sensitivity) to red (high sensitivity). a) Sensitivity on the whole sample. b) Sensitivity only in one spot.

The fabricated culture chamber consists of a polycarbonate holder with two microfabricated electrode plates (Figure 2a). A mixture of hydrogel and cells is injected in the chamber between the two electrode plates. Polymerization of the gel is done directly inside the chamber. Platinum electrodes are then connected to an impedance analyzer.

Two different configurations of electrodes were designed. The simplest one consists of a four-point impedance measurement—two electrodes injecting the current and two measuring the voltage. The impedance in this case will give an estimation of the number of cells in the entire scaffold. The second configuration consists of six electrodes on each side of

the chamber in order to be able to gather information on the spatial distribution of the cells inside the scaffold.

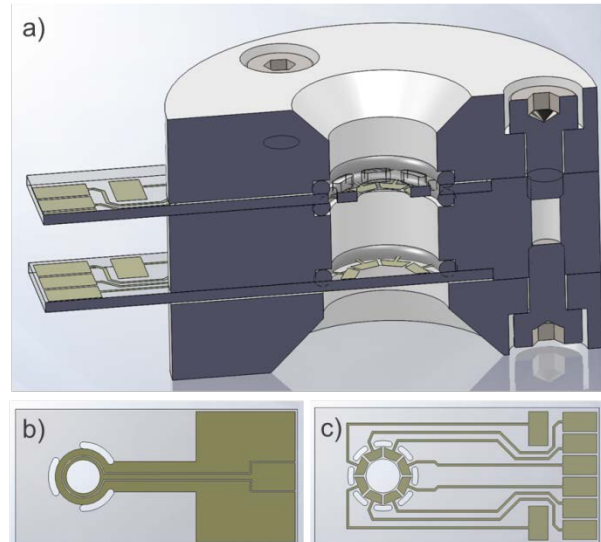


Figure 2: a) Cross-section of biochamber with integrated electrodes; b) Design with 2 electrodes (for one side); c) Design with six electrodes (for one side).

3D cell cultures are used more and more in cell biology as they mimic better the physiological conditions. There is no standard method yet to observe cells inside the scaffold to obtain information on the cell viability, proliferation and migration. As a real-time and non-invasive method, impedance spectroscopy can be a good candidate for the monitoring of large 3D cell culture.

This work is partly funded by NanoTera. CSEM thanks them for their support.

Air Pretreatment Platform for Indoor Air Quality Monitoring

E. Hammes, P. Ryser •, H. F. Knapp

A humidity stabilization and gas delivery system which delivers equal quantities of gas to three sensors simultaneously was developed at CSEM. To date, it has been successfully used to test and calibrate gas sensor prototypes. It has also been incorporated into the prototype Air Quality Monitor of the European project INTASENSE.

Many diseases including sick building syndrome, respiratory problems and cancers can be caused by exposure to high concentrations of toxins commonly used in modern building materials, paints, glues and furniture. To minimize exposure to these toxins, it is important to have air exchange with the outside environment. However, this is usually not energy efficient because the air must be heated or cooled. The purpose of the Intasense Project was to resolve this problem by creating a device which determines the current quality of air within the building (Figure 1). This information could then be used to control the ventilation system within an energy efficient building. CSEM designed and constructed the fluidic platform which includes a humidity buffering system, and is able to deliver equal quantities of gas to three sensors simultaneously. To date it has been used in two versions of the Intasense Prototype [1] and used to calibrate novel gas sensors.

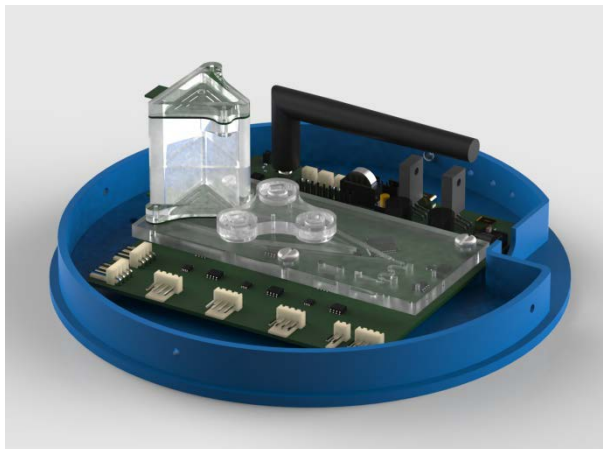


Figure 1: CAD drawing of the fluidic platform integrated into the Intasense prototype.

In both of these applications simultaneous delivery of equal quantities of the sample gas are required for optimal gas sensor signal processing: equal quantities are required so that the amount of analyte in contact with each sensor is the same and simultaneous delivery allows all three sensors to respond concurrently. This was achieved by creating a computational model of gas flow through the system, conducting a parameter sweep and then selecting the optimal set. To confirm that the model and machine error was not significant, a Greco-Latin square design was used to test the platform. This test showed that gas delivery to each channel was equal within statistical boundaries [2].

• Laboratoire de Production Microtechnique, EPFL, CH

[1] www.intasense.eu

[2] E. Hammes, et al., "The Transport Phenomena behind the INTASENSE Indoor Air Quality Monitor Product Design". American Society of Chemical Engineers, 2015

Another major challenge was buffering humidity fluctuations without loss of analyte gas. This was necessary, because the Intasense platform's gas sensors are also sensitive to humidity fluctuations [3]. To prevent a false positive caused by a rapid humidity increase, a reversible adsorbent was placed upstream of the gas sensors. However, there was concern that the adsorbent may remove analyte gasses. To optimize the tradeoff between humidity buffering and loss or delay analyte signal, a computational model of adsorption and desorption of gasses within the filtration system is under development. It is being experimentally tested using benzene, carbon monoxide, formaldehyde and nitrogen dioxide. Preliminary results of the model as compared to the experiments can be seen in Figure 2.

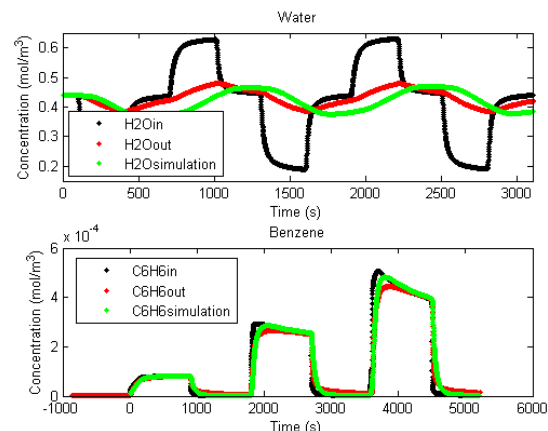


Figure 2: Results of the Computational model of analyte adsorption and desorption from the gas stream as it passes through the humidity buffer.

In this figure, the inlet gas concentration and humidity, shown in black, were measured by metal oxide semiconductor sensors and Sensirion THS 75 sensors respectively. The measured outlet concentration is shown in red. Experimental inlet concentrations are used as the inlet concentrations in the computational model. The simulated outlet concentration is depicted in green. Work is ongoing to further perfect this model.

To date ten platforms have been delivered to laboratories throughout Europe. Three are being used to test and calibrate gas sensors [4], the remaining elements have been used to create prototypes of the Intasense air quality monitor.

[3] E. Hammes, et al., "A Smart Air Quality Monitor for Energy Efficient Buildings". Smart Systems Integration, 2015

[4] G. G. Mandayo, et al., "The INTASENSE Project Approach for Toxic Gas Detection Indoors." International Congress on Architectural Envelopes, 2015

Automation of Traditional Sample Preparation for Oil, Milk, and Nuts

S. F. Graf, J. Goldowsky, T. Volden, H. F. Knapp

Food analysis for insecticides, antibiotics or mycotoxin residues always have a foregoing sample preparation step to transform the food sample into form which can be processed by the respective sensor. This can include concentrating the analytes, filtering the sample to remove solids, transfer analytes from solid materials to solvents, remove fatty sample part etc. In many cases problematic solvents as e.g. Acetonitrile or Hexane are required, hence food analysis is currently performed in dedicated laboratories. Having an on-site analysis system with integrated automated sample preparation could minimize food waste by not contaminating perfectly fine food with contaminated food.

On-site food sample preparation is difficult because of its complexity and the use of problematic solvents. Evaporators, centrifuges and shakers are often required for these processes. This project's goal is to move sample preparation from the laboratory to sites like farms where milk is collected for further processing at a production site. If contaminants are present in the milk, it would simply not be added to the already collected clean milk and thus not contaminate the whole load. In a first step of this project the preparation processes for oil, milk and nuts were modified to work with solid phase extraction (SPE) which is more suitable for automation. In SPE, analytes in the sample bind to a solid phase matrix because of their specific affinity. The analytes can then be eluted from the solid phase matrix using appropriate solvents. In a second step of the project, the common process steps for the three completely different food types were selected as shown in Figure 2, i.e. preparation of the SPE; binding the analytes in the SPE, washing the SPE and finally eluting the analytes and transporting them to the detection unit. For the time being, the preceding divergent process steps (Figure 1) of the different food types i.e. grinding, adding solvents, shaking and extracting, will be done manually.

Food Type	Grind	Add solvent	Shake	Extract
Nuts				
Oil	NA			
Milk	NA		NA	

Manual steps

Figure 1: Preceding sample preparation steps for nuts, oil and milk.

Prep	Bind	Wash	Elute

Automated steps

Figure 2: Common automated preparation steps using SPE.

Standard laboratory systems for SPE concentration and filters use vacuum to drive the liquid. Because of this the process is slow, as only less than 1 bar pressure difference can be applied. Our system is equipped with an independent pressure driven dispensing module^[1] (patent pending) which can create a pressure difference of up to 1.5 bar (higher pressures in development) and precisely dose volumes from 100 µl up to

several milliliters. After the sample is introduced via a pipette, the system takes over, preconditions the SPE, and pushes the sample through the SPE into waste. The SPE is then automatically washed and the analytes eluted with a defined volume and then guided towards the detection unit. A breadboard prototype based on the schematics in Figure 3 was tested and then miniaturized into a cartridge (Figure 4).

The pretreatment unit will be combined with the sensor unit based on an optical biosensor functionalized with aptamers to sense smallest contaminations in milk, oils or nuts. The combined system will be a portable setup which allows performing measurements on-site. At a later stage, this system will be customized for each food type to also automate the current manual steps.

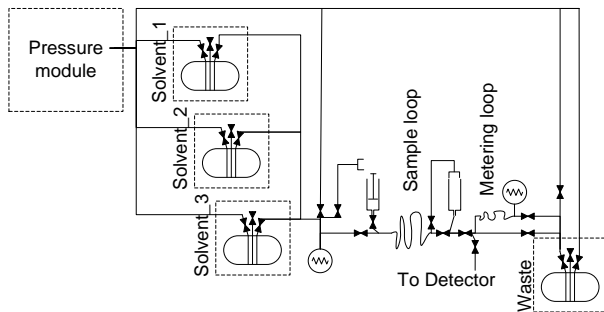


Figure 3: Schematics of the pretreatment system.



Figure 4: Drawing of the microfluidic cartridge for the sample preparation unit. H 76 mm x W 75 mm x D 80 mm. Not included in the figure are the electronics, tubing and liquid bottles for solvents and waste which are required for the complete system.

This work was supported by the Swiss federation, MCCS Micro Center Central Switzerland, and the European Commission (FP7-611528 BIOFOS). CSEM thanks them for their support.

^[1] S. F. Graf, J. Goldowsky, H. F. Knapp, "Compact, Pressure-based Flow System for Sequential Actuation of Fluids with Integrated Flow Monitoring", CSEM Scientific and Technical Report (2014), 114

Integrated and Automated Sample Preparation to Monitor Small Organic Pollutants

S. Heub, N. Tscharner, L. Barbe, S. Follonier

A fully automated and portable platform for on-site sample preparation is being developed within the EU project RADAR to monitor endocrine disruptive compounds in water and food processes. Solid phase extraction is performed on a microfluidic device that enables the manipulation of small volumes of solution and fast sample preconcentration. The method is suited for sample preparation for analysis using biodetection methods, from standard well-plate format to label-free optical biosensors.

Endocrine disrupting compounds (EDCs) are a family of pollutants originating mostly from the degradation of plastics, smokes and drugs. Today, it is proven that they cause feminization of aquatic species in contaminated lakes and rivers, which increases human health concerns. Within the European RADAR^[1] (Rationally Designed Aquatic Receptors) project, the development of an integrated and automated sample preparation platform is required prior to optical label-free detection for on-site monitoring of those compounds.

The portable sample preparation system that is being developed performs fully automated liquid sample collection, filtration of particles, removal of gas bubbles, enrichment of the target compounds and delivery of the different buffer solutions and reactants to the biosensor.

Since EDCs are found at very low levels in the environment (< 1 ppb = 1 ng/ml), i.e. below the limit of detection (LOD) of most biosensors, a preconcentration step is required. Methods based on solid phase extraction (SPE) are the most efficient in terms of separation and enrichment. However, SPE techniques are adapted to detection by chromatography and mass spectrometry and imply the use of organic solvents through many time-consuming steps. For biosensing monitoring purposes, the speed of the process, availability of the resources and final buffer conditions are critical aspects.

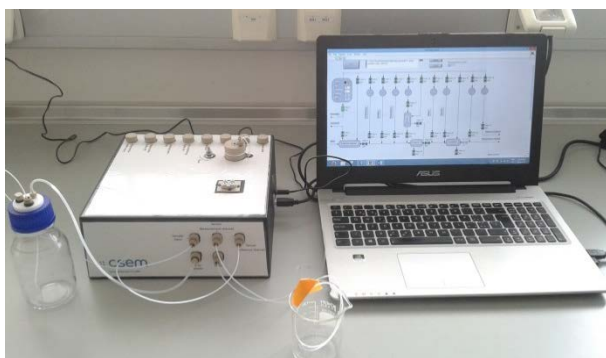


Figure 1: The sample preparation unit (SPU) as used in a laboratory.

A fully automated platform (Figure 1) was developed adapting and integrating a SPE method^[2]. This system can be used independently or on-line with a biosensor. The main element of the instrument is the polyether ether ketone microfluidic device (Figure 2) that enables facile control of small fluid volumes.

Compared to traditional SPE procedures, our method requires smaller volumes of solution (3-30 ml sample, 20 µl eluent minimum), it is faster and user-friendly. Another key advantage is its full compatibility with immuno-detection methods by providing an enriched sample in an aqueous buffer with low solvent content. Finally, our instrument offers the possibility to adapt the parameters of the SPE procedure to provide the preconcentration factor required for any immunoassay.

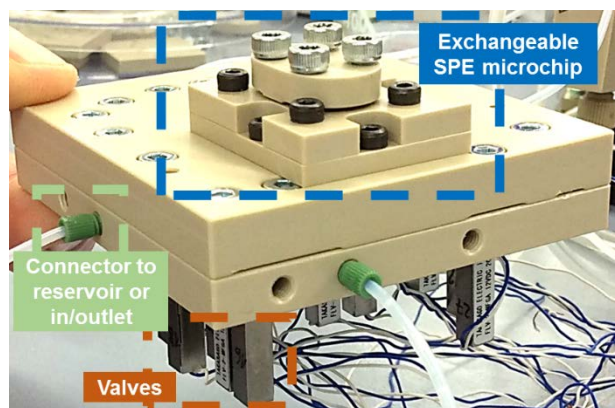


Figure 2: Picture of the PEEK microfluidic device (dimensions 7 x 6.5 cm long and 2.5 cm thick including the SPE microchip).

Our method was successfully applied to seawater samples spiked with 50 ng/l of 17 β -estradiol. Our method was compared with a bench-top SPE procedure performed by the Rikilt Institute for Food Safety in the Netherlands. The molecule was detected using a label-free receptor assay on a surface plasmon resonance (SPR) biosensor. Satisfactory results were obtained with our instrument (Table 1), with a considerable reduction in the time needed for the sample preparation.

Table 1: Comparison of method and results obtained with the SPU and a bench-top procedure from RIKILT, with E2 in seawater samples, detected with a receptor assay on a SPR platform.

Method	Sample volume	SPE eluent	Time	Recovery
Bench-top	50 ml	1 ml solvent 100 vol%	≥ 2 h	68 %
SPU	30 ml	84 µl solvent 60 vol%	20 min	58 %

The next development steps will focus on the mechanical robustness of the instrument. The method will be applied to other EDCs and liquid sample matrices, such as drinking water, beer and milk.

[1] www.fp7-radar.eu

[2] S. Heub, L. Barbe, S. Follonier, P.S. Dittrich, "Fully automated and portable platform for integrated extraction and pre-concentration of toxins and pollutants from liquid samples", Proc. of the 18th micro-TAS conference, 2014.

Surface Functionalization for Solvent-free Capture and Release of Molecules

S. Heub, X. Mao, L. Barbe, S. Follonier

A microfluidic platform for solvent-free extraction and preconcentration of pollutants from water has been developed. A microfluidic channel with embedded pillar array is functionalised with a thermo-responsive polymer. This sorbent enables capturing and releasing the analytes by changing the temperature. This technology is fit for analytical methods where the use of an organic solvent is prohibited, such as immunoassays.

Efficient and rapid capture and release of molecules are required in many fields, in particular for the development of grown cell films, clean-up, and biosensing applications. However the biological working environment often prohibits the use of organic solvents in the processing steps, as they can cause damage to the structure of the biological elements.

In this project, we focused on the preconcentration of molecules for their analysis in water samples using bioassays. Preconcentration is often required to bridge the gap between actual levels and limit of detection in the analytical method. It is usually performed by applying solid phase extraction techniques. The sample is flushed through a sorbent in which the analytes have an affinity. The target molecules are then desorbed using an appropriate solution of a given volume. Preconcentration is achieved when the final volume is smaller than the sample. However, this method often requires the use of organic solvents in the desorption step, which is not directly compatible with a detection method involving biological elements.

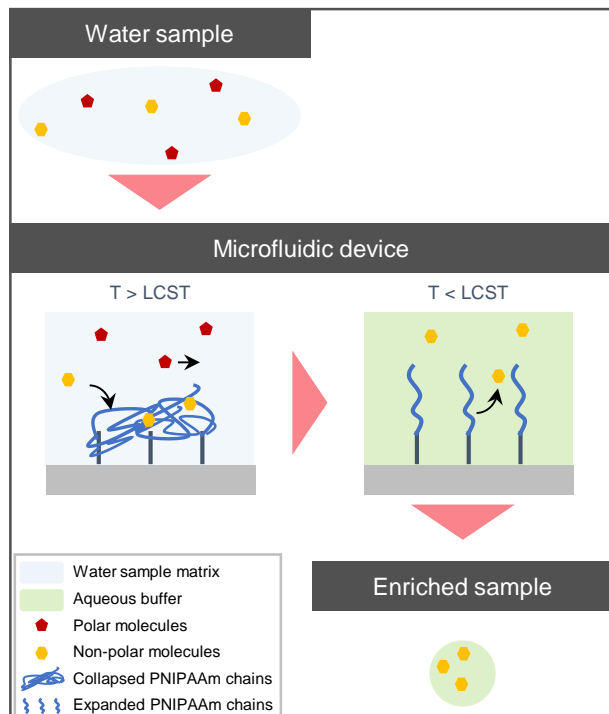


Figure 1: Illustration of the solvent-free extraction and release principle using the thermo-responsive polymer PNIPAAm, where T is the temperature in the microfluidic device and T_s is its switching temperature.

Here we developed a surface coating to enable solvent-free capture and release of molecules from aqueous media. Thermo-responsive polymers are macromolecules that undergo a change of conformation around their lowest critical solution temperature (LCST). Above this temperature, the polymer chains aggregate and become hydrophobic, while they expand in water (hydrophilic behavior) below this value. Such a polymer could be used to replace traditional hydrophobic sorbents.

Figure 1 illustrates the principle of sample preconcentration using a thermo-responsive polymer. Hydrophobic molecules will adsorb on the hydrophobic polymer film on the surface of the fluidic channel when heating above the LCST, while salts, ionic and polar molecules will not. The hydrophobic molecules could then desorb in a fresh aqueous buffer upon cooling below the LCST. High preconcentration factors could be achieved by applying this method in a microfluidic device, enabling the control of tiny volumes of solution.

A polydimethylsiloxane (PDMS) microfluidic device was fabricated and functionalized with Poly(N-isopropylacrylamide)^[1] whose LCST is about 32°C. The functionalization consists of the in-situ polymerization of the monomers. The microfluidic channel has embedded micropillars to increase the surface area. The film coating was observed by confocal microscopy as shown in Figure 2. The film density is homogeneous along the pillar walls. A capture and release proof of concept study was performed using a fluorescently labeled IgG biomolecule (IgG^*) in phosphate buffer saline (PBS). The molecule successfully adsorbed at $T > \text{LCST}$ and desorbed in fresh PBS for $T < \text{LCST}$ (Figure 2).

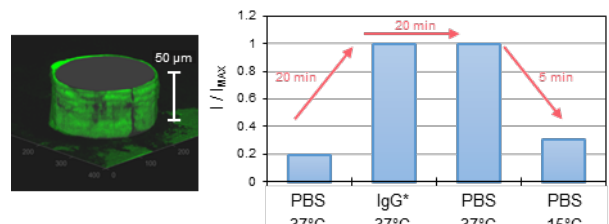


Figure 2: 3D image of a coated micropillar after the injection of IgG^* , obtained by confocal microscopy, and results of the capture and release study, with I/I_{Max} the relative fluorescence intensity.

The application of this method for smaller molecules in environmental samples will be investigated. New copolymers films will be explored to optimize the transition speed and the switching temperature. This project contributes to the development of new green analytical methods for environmental monitoring applications.

^[1] S. Heub, X. Mao, P.S. Dittrich, L. Barbe, "A functionalized poly(dimethylsiloxane) chip for solvent-free, temperature actuated solid phase extraction", Proc. of the 19th micro-TAS conference, 2015

Supercritical CO₂ Treatment as a Novel Sample Preparation Method for the Analysis of Nanoparticle Content in Sunscreen Agents

D. Müller •, S. Cattaneo, F. Meier ••, R. Welz ••, T. de Vries •••, M. Portugal-Cohen **, D.C. Antonio **, C. Cascio **, L. Calzolai **, D. Gilliland **, A. de Mello •

Today, a growing number of consumer products make use of the unique physical and chemical properties of nanomaterials. As the number of such products increases, the ability to thoroughly characterize their properties and functionality becomes critical. In particular, the recent regulatory efforts concerning the labelling of nanoparticle-containing products call for the development of simple and robust sample preparation protocols enabling a reliable detection and quantification of nanoparticulate ingredients in complex matrices. In this work, we demonstrate the use of supercritical carbon dioxide (scCO₂) as a method of sample preparation for the analysis of complex nanoparticle-containing samples—in our case, a model sunscreen agent with titanium dioxide nanoparticles. This novel treatment can be executed in a single step using a lab scale supercritical fluid extraction system and has important ecological as well as economic advantages over currently used sample preparation techniques involving organic solvents.

Supercritical CO₂ is well-known for its application in extraction processes and is commonly used to extract small and/or non-polar molecules from natural materials under very mild conditions (e.g. essential oils from herbs or caffeine from coffee beans). In these prior applications, however, the scCO₂ was used to dissolve and extract the compounds of interest. In this work, it is used as a novel sample treatment to simplify the matrix of a model sunscreen by removing unwanted components, thus keeping the target nanomaterials (in our case titanium dioxide nanoparticles) in the residual sample.

The method was developed and tested on a model sunscreen spiked with TiO₂ nanoparticles (Figure 1a). The sunscreen was placed on a Teflon support surrounded by a stainless steel holder with a small recess (Figure 1b) and the excess sunscreen was removed using a spatula. The Teflon support was then removed from its holder (Figure 1c) and placed in the extraction vessel of a lab scale supercritical fluid extraction system, where it was subjected to a constant flow of scCO₂. The minimal surface tension of scCO₂ allows for thorough sample penetration whilst maintaining the structure of the residual material. After treatment, the remaining sample (Figure 1d) was removed from the support (Figure 1e) and easily re-dispersed in an aqueous solution (Figure 1f).

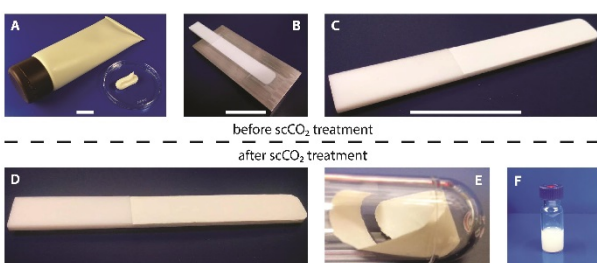


Figure 1: Model sunscreen at different stages before (A–C) and after (D–F) the novel supercritical CO₂ treatment. Scale bars are 25 mm.

After sonication, the re-dispersed sample was directly injected into an asymmetrical flow field-flow fractionation system (AF4) linked to UV and multi-angle light scattering (MALS) detectors.

As shown in Figure 2, the resulting UV curve allows a clear distinction between spiked and non-spiked sample. The black solid line is the signal obtained from the TiO₂ spiked sunscreen

after scCO₂ treatment and resuspension in water. A wide peak, indicating particles with a broad size distribution and hence, eluting over an extended separation period, is evident. For the blank model cream (black dotted line, treated in the same way), no significant signal was detected over the whole separation cycle. The size distribution was measured by MALS (red line), and was found to be very similar to that of the original TiO₂ suspension used to spike the samples. The measurements were verified by a Scanning Transmission Electron Microscope (STEM) and energy-dispersive X-ray spectroscopy (EDX) analysis.

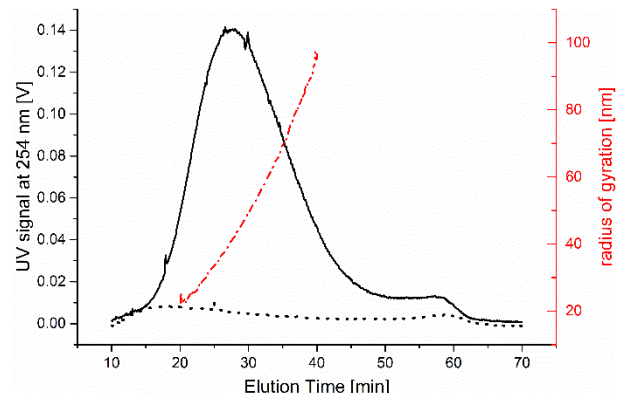


Figure 2: Elugram of the TiO₂ spiked (solid line) and blank (dotted line) model sunscreens, after scCO₂ treatment and resuspension in water. The red line shows the radius of gyration measured by MALS.

The results demonstrated that the novel scCO₂ sample preparation method allows a precise determination of the nanoparticle content of sunscreens, while essentially maintaining the size distribution of the nanoparticles. Although the method is demonstrated using a model sunscreen matrix, we expect it to be applicable to a wide class of consumer products.

This work is supported by the European Commission 7th Framework Programme (project SMART-NANO NMP4-SE-2012-280779). CSEM thanks them for their support.

• CSEM/ETH Zurich, Biochemical Engineering
•• Postnova Analytics GmbH, Landsberg am Lech, Germany
••• Feyecon Carbon Tioxide Technologies, Weesp, The Netherlands

* AHAVA Dead Sea Laboratories, Lod, Israel

** Joint Research Center (JRC), Ispra, Italy

UV Absorption and Multi-angle Light Scattering Detector System for Nanoparticle Analysis

C. Hofer, S. Cattaneo, D. Müller, S. Follonier

We report on the final integration of a UV absorption and Multi-Angle Light Scattering (MALS) detector system for the detection of nanoparticles in liquid suspensions. The advantages of the detector system are the compact optical design, the high sensitivity and the cost-effective and easily replaceable flow-through cartridges. The system was demonstrated with in-line measurements of liquid samples containing various nanoparticles.

Previously, we reported on the development of UV absorption and Multi-Angle Light Scattering (MALS) prototype systems, developed in the framework of the ongoing EU-FP7 project SMART-NANO (see CSEM Scientific Report 2014 and 2013). In the last year, the two prototype detectors were further developed and combined into a single detection system.

The improvements of the MALS detector covered both hardware and software aspects. To reduce the costs of the system, the solid state laser used in the previous prototype was replaced by a diode laser and the optical chopper was removed. Instead of the optical chopper, the diode laser is now modulated electronically. This resulted in a more robust system with no moving parts. The signal to noise ratio of the detector was further increased by removing ground loops in the electronic system. Another improvement is the higher modulation frequency of the laser diode, which increases the signal to noise level of the lock-in amplifier. The flow cell of the MALS system was also improved. The glue-bonded flow cell used in the previous prototype turned out too tricky to handle, leading to leakage in case of pressure increases in the system, or when using organic detergents/surfactants such as sodium dodecyl sulfate (SDS). To solve these problems, the MALS cell was redesigned. The new cell design features a clamped cylinder lens to the mechanical body with a gasket in between. The new design allows the use of organic solvents for cleaning and no leakage due to overpressure occurred.

The UV detector was also further optimized in several aspects. To improve the signal to noise ratio, the photodiode electronics were redesigned and packaged into a Faraday cage. To simplify the handling of the UV detector, an automated optical filter system was installed to reduce the higher order diffraction. In the previous prototype, the filter had to be exchanged manually. Furthermore, the user friendliness was improved by reducing the number of USB connections to the laptop from three connections (analog to digital converter card, monochromator and automated optical filter) to a single one. Figure 1 shows the inside view of the two detectors.



Figure 1: Inside view of the UV (left) and MALS (right) detectors.

For both instruments, a compact housing was designed. The main goals of the housing design was for it to be as small as

possible and that the measurement cell be easily accessible/removable without the need to remove any screws. Furthermore, a single GUI (graphical user interface) was developed. The GUI can control both instruments at the same time and show the measured data of the UV- and MALS-detector in the same graph. Finally, the analysis software was also improved in collaboration with the project partners.

Figure 2 shows the complete final system as it was delivered to our project partners.



Figure 2: Complete UV absorption and MALS detector system for nanoparticle analysis. The lock-in system used for MALS detection is visible on the right.

Preliminary calibration measurements were carried out at CSEM to verify the reliable operation of the detector system. The complete system was then delivered to JRC (Joint Research Center) Ispra, a partner in the project for in-depth testing and qualification of the two detectors within standard solutions and engineered nanoparticles (ENP) containing samples developed in the project. The characterization is ongoing. Figure 3 shows a first, preliminary measurement of BSA (Bovine Serum Albumin).

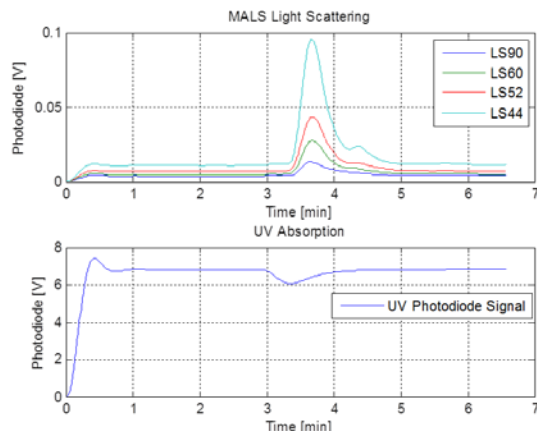


Figure 3: MALS (top) and UV (bottom) signals of BSA protein sample. The MALS data shows the light scattering signals collected at four different angles (90° , 60° , 52° and 44°). The UV data shows the data collected at 280 nm.

This work is supported by the European Commission 7th Framework Programme (project SMART-NANO ^[1], NMP4-SE-2012-280779). CSEM thanks them for their support.

^[1] www.smartnano.org

Functionalization of Teflon Surfaces

H. Gao, D. Caminada

The OptoDex® platform is a surface engineering technology developed by CSEM that integrates technologies from material science, surface chemistry, and biochemistry, and includes novel materials, controllable and well characterized surface chemistries for biomolecule attachment and surface passivation. The proprietary linker polymer technology brings unique properties to bioanalytics and generates valuable new material surfaces.

In a feasibility study we have shown that Teflon substrates can be functionalized using the OptoDex surface functionalization technology. Polytetrafluoroethylene (Teflon) has inherently low surface energy and poor polarizability due to its chemical structure. This means the surface cannot provide enough energy to bond with adherents such as adhesives and inks. Gas plasma surface treatment solves this problem by increasing the surface energy of polytetrafluoroethylene. This is achieved with the addition or substitution of polar chemical groups onto the surface.

The OptoDex® technology relies on the unique properties of photolinker polymers which immobilize probe molecules on material surfaces. Light activation of photolinker polymers leads to the generation of highly reactive intermediates, in particular photogenerated carbenes, which form covalent bonds with probe molecules on nearly any type of material.

In this study, the functionalization of Teflon surfaces was attained by combining a plasma treatment and the OptoDex® technology. Two coating processes were applied, adsorptive dip coating and dry-down coating, using fluorescence labelled OptoDex.

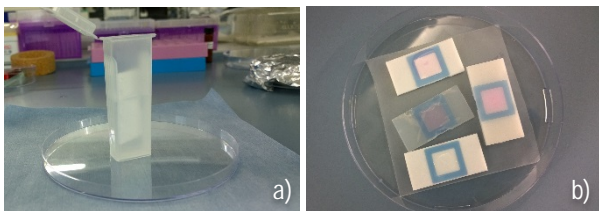


Figure 1: Coating processes. a) adsorptive dip coating, and b) dry-down coating.

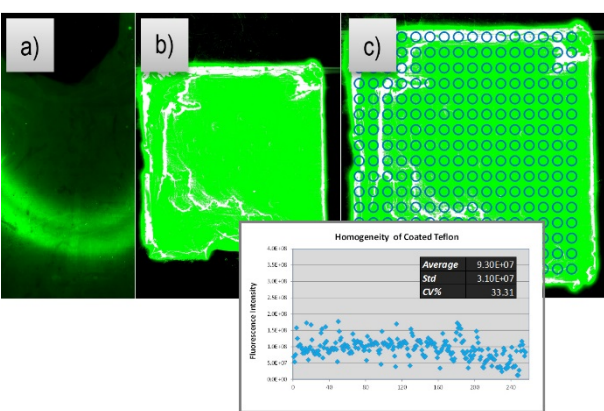


Figure 2: Image of fluorescence scanning. a) adsorptive dip coating; b) dry-down coating, and c) analysis of fluorescence image with GenePix quantification.

The fluorescence intensity was determined using GenePix Array Scanner (Excitation 535 nm and Emission 570 nm) and evaluated by localizing the grid onto the coating surface (16 col x 16 raw, $\phi = 600 \mu\text{m}$).

The functionalized Teflon samples showed that the surface became hydrophilic after OptoDex coating. The hydrophilic properties of OptoDex coated Teflon surfaces were analyzed with water contact angle measurements using the commercially available Tropfenkonturanalyse-System DSA30 (KRÜSS). One data point per second was collected via video analysis. There was no delay from start of measurement and data collection. Data was collected for approximately 10 s. Table 1 lists the values of contact angle before and after OptoDex coating.

	Before coating	After coating
Contact angle	103 ± 2.5	64.5 ± 0.83

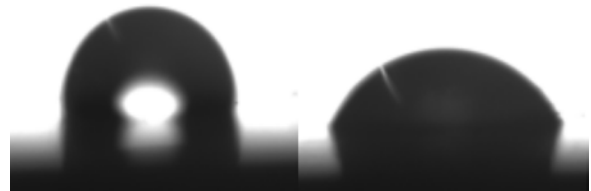


Figure 3: Image of contact angle measurement.

These tests proved that a modification of Teflon surfaces is feasible. Fluorescent images showed the homogeneity of the coating with Fluorescent-labelled OptoDex. The water adsorption properties (Figure 4) demonstrated the obtained hydrophilicity of the surface.

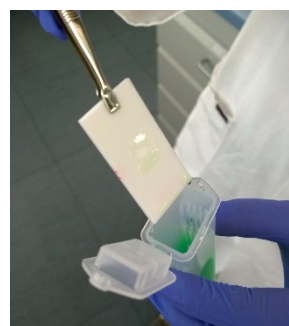


Figure 4: Photograph of hydrophilicity of OptoDex coated surface.

Pre-activation with plasma treatment is crucial to obtain good surface functionalization. In this feasibility study, the surface could be modified by pre-activation with air-plasma. In upcoming projects, the optimization of this pre-activation process will be explored, e.g. using oxygen plasma instead of air plasma. In order to obtain a more homogeneous coating of the surface, the coating processes will be optimized further.

OptoDex as a Linker to Functionalize Textiles

H. Gao, D. Caminada

CSEM's versatile surface biofunctionalization technology enables creating cost effective products with outstanding performance and stability. CSEM's patented linker polymer OptoDex® and related surface functionalization technologies cover a large scope of applications: from robust bioanalytics for *in vitro* diagnostics to biofunctionalization of implant surfaces and medical devices. OptoDex® immobilizes almost any biomolecule, in particular proteins, on an exceptionally large range of material surfaces. One single OptoDex® linker polymer provides up to 6 reactive sites, capable of establishing covalent bonds with the surface, the biomolecule or other OptoDex® polymers.

Wound healing is a complex process encompassing a number of overlapping phases, including inflammation, epithelialization, granulation tissue formation and tissue remodelling. The OptoDex® technology comprises widely applicable validated processes and procedures for bio- and nano-engineering of solid and soft surfaces. Covalent attachment of (bio) molecules to any type of surface is attained with carbene-based linker chemistries. Carbenes are highly reactive intermediates. Photochemically or thermochemically generated polymer-based carbenes act as molecular glue when brought into contact with, and activated in the presence of both target material and target (bio)molecules.

The covalent functionalization of textile for wound care dressings has been developed at CSEM using OptoDex®—an in-house surface bioengineering technology. Bio-functional molecules are covalently immobilized on textile surfaces while maintaining their specific activities.



Figure 1: Schematic of the OptoDex® technology: ① Adsorptive coating of surface with photolinker polymer; ② Addition of biomolecules; ③ Stress-less vacuum drying in OptoDex® embedding; ④ Dry state bonding by photoactivated linking polymers; ⑤ Rehydration reconstitutes functional biomolecule.

The advantages and features of the OptoDex® technology for surface bioengineering are:

- One step photoactivatable (or thermo-activateable) covalent crosslinking
- Bioactivity preserving dry-state immobilization
- Surface hydrophilization and functionalization
- Robust and long-term stable biosurfaces

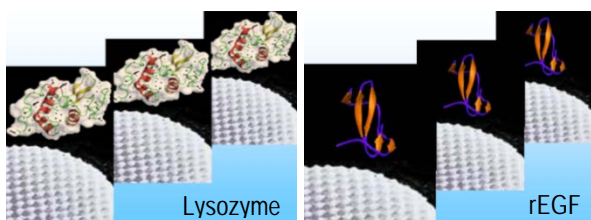


Figure 2: Biofunctionalized wound pad (polyester wound pad of Tissupor) with antimicrobial (lysozyme) or growth factor (rEGF).

In wound healing, antibacterial coatings play a crucial role. Bactericidal enzymes—lysozyme as an example—quicken the elimination of bacteria if present in open wounds. Lysozyme is a muramidase which is widely distributed in nature. Its antibacterial activity is related to its catalytic properties by breaking the cell wall components of Gram-positive bacteria. In its polymeric state or as a dextran conjugate, lysozyme reduces antimicrobial activity for both Gram-negative and Gram-positive bacteria. The system components—textile (polyester), lysozyme and photoactivated OptoDex—are biocompatible and immobilised lysozyme is stable at room temperature for at least 5 weeks and 18 months at 4°C. The enzyme stays catalytically active after photoimmobilization and sterilization with ethylene oxide.

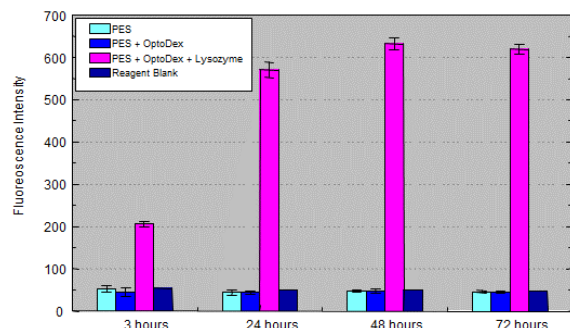


Figure 3: Lytic activity of photoimmobilised lysozyme on polyester wound pads is retained.

Besides anti-bacterial properties, the time required for complete wound healing, and the efficiency of the individual steps involved are crucial. With many overlapping functional properties, epidermal growth factor (EGF) orchestrates the recruitment and growth of fibroblasts, such as molecular presentation and its resulting cellular effects, termed matricrine stimulation, mimics juxtacrine cell stimulation. Covalent attachment of recombinant human EGF (rhEGF) onto woven textile has been achieved successfully using the OptoDex surface bioengineering technology. Modified textiles can be sterilized and NRK-49F fibroblast cell proliferation is attained with OptoDex-rhEGF grafted fabrics, whereas CHO cells—as expected for not transformed CHO cells—do not elicit rhEGF-graft mediated proliferation.

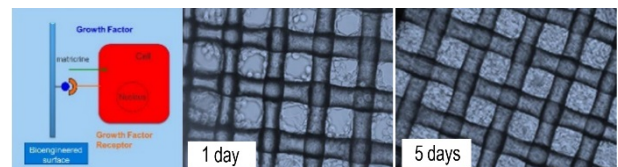


Figure 4: The images shown above document cell proliferation in the presence of a rhEGF grafted tissue scaffold. In this series of experiments, 10^6 cells were inoculated and were grown on the functionalized tissue scaffold. Images of cell culture were taken 1 day and 5 days after seeding.

Automated Monitoring of Micro-bioreactors

S. Generelli, J. B. la Cour, L. Barbe

The use of *in-vitro* micro-tissue models for toxicological assays is an ever-growing field. An automated sampling, handling and sensing platform was developed to be interfaced with a bioreactor in order to have an in-line detection system for cell culture supernatant.

The use of *in-vitro* micro-tissue models for toxicological assays is an ever-growing field. Spheroids are an example of a tissue model gaining popularity for this type of *in-vitro* testing. These tests are in general performed in multi-well plates, and biomarkers for toxicity assessment are often measured using well-plate-based assays. This approach can be used for the determination of a large panel of biomarkers, but is difficult when performing (semi)-continuous monitoring.

Within the EU project Hemibio^[1] (Hepatic Microfluidic Bioreactor), a hepatic tissue model system is being developed for *in-vitro* repeated dose toxicity up to 30 days. A set of sensors is integrated downstream from the micro-bioreactor where the tissue model is cultivated in order to maintain optimal culture conditions for the cells, monitor their metabolism and potential cell death and detect and quantify their response to exposure to potentially toxic compounds.

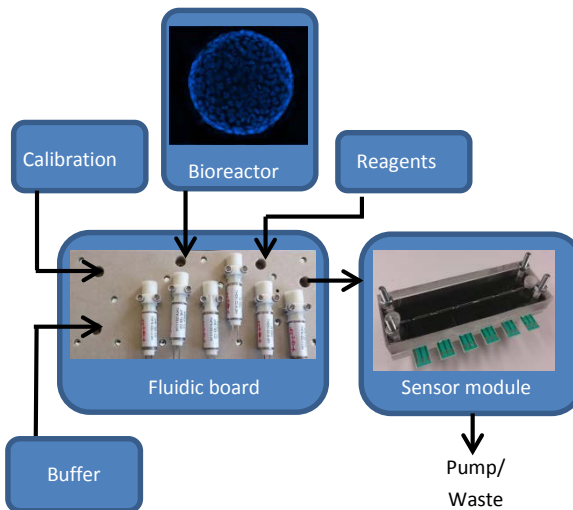


Figure 1: Schematic of the automated sampling and monitoring system. The custom-made sensing module designed for Hemibio, is capable of accommodating up to 6 sensors in a series and has a total volume in the channel of less than 50 μl .

The automated sampling, handling and sensing platform was designed by CSEM to be interfaced with the Hemibio bioreactor in order to have an in-line detection system, as illustrated in Figure 1. The sensor module is decoupled from the bioreactor, and placed after its outlet. In this way the cell culture is completely independent from the presence of sensors, which will not interfere with the biological material (and vice-versa). The modular concept allows for an easy exchange of the sensor in case of failing sensors, an easy re-calibration of

^[1] www.hemibio.eu, project funded by the Cosmetics Europe association and the European Union FP7, grant agreement Nr. 266777

sensors and as well the modularity in the choice of the sensors to be used for a specific experiment.

Given the unified dimensional footprint for all the electrochemical-based sensors, this panel of markers can be modified or expanded in the future, to specific metabolites related to diseases of interest, or even to different tissue models. The developed monitoring setup can be adapted to future new bioreactor designs.

Within the Hemibio project the selected parameters to be monitored with the sensor module are glucose, lactate, ALT (enzyme marker specific for hepatocyte cell death). Commercial fluorescence-based oxygen sensor beads were placed directly in the bioreactor.

The detection of ALT is indirect: the marker measured is a product of the enzymatic reaction catalyzed by ALT. The rate of production of this product provides the indication for the concentration of the enzyme present in the sample. The measurement of the product from the enzymatic reaction takes place over time, and requires the implementation of a reaction chamber, to allow time for the reaction to take place, and the implementation of multiple injection times.

Validation of the automated setup has been made by using cell culture supernatant withdrawn from the Hemibio bioreactor with HepG2 cells exposed to a toxic insult, by adding 200 μM rotenone and 0.4% DMSO to the perfusion medium. A clear increase in the signal for both oxygen and ALT is visible, (Figure 2^[2]), which indicates that these two parameters can monitor cellular damages after a toxic insult.

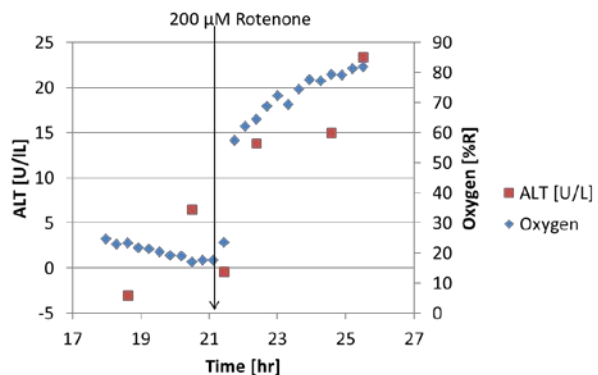


Figure 2: Monitoring of ALT and O_2 levels of a HepG2 culture before and after exposure to 200 μM rotenone^[2].

^[2] T. Gocht, M. Schwartz (Ed.), Towards the Replacement of *in-vivo* Repeated Dose Systemic Toxicity Testing, SEURAT-1 Annual Report Nr. 5, submitted for publication

Compact Optical Setup for Wide-field Fluorescence Lifetime Imaging

S. Cattaneo, C. Hofer, S. Emery, H.-R. Graf, A. Bischof, B. Schaffer

A compact optical setup for real-time, wide-field fluorescence lifetime imaging (FLIM) in the nano- to micro-second range was developed. The system is based on a fast lock-in imager and a modulated diode laser, and yields 2D maps of fluorescent lifetimes with nanosecond resolution. The prototype is considerably cheaper and easier to operate than commercial FLIM systems, opening the door to novel applications of fluorescence lifetime imaging.

Fluorescence lifetime imaging microscopy (FLIM) has been applied since the early 1990s for the mapping of molecular environment parameters (pH, ion concentration, oxygen content) and protein interactions in living cells, tissues and model organisms. More recently, the use and value of FLIM in medical diagnostics, histology and high-throughput pharmacological compound screening has been demonstrated. Despite its intrinsic value, the adoption of FLIM outside specialized research labs has been limited by the cost of the required instrumentation and by the expertise necessary for its maintenance and operation.

Solid-state image sensing with in-pixel demodulation, on the other hand, is a well-known technology for 3D imaging (TOF, time-of-flight). The existing products are applied with success in markets such as industrial metrology, robotics and safety. The technology also has large potential in the fields of life science and medical diagnostics, which, however, are still largely unexploited. The potential of lock-in pixels for fluorescence lifetime measurements was previously demonstrated by CSEM and others [1, 2]. These demonstrations, however, relied on expensive external components (microscope, external light source) and, therefore, partially shared the limitations of existing solutions.



Figure 1: Optical setup for wide-field FLIM, allowing a 2D map of fluorescence lifetimes with nanosecond resolution.

To promote a wide-spread application of FLIM outside of academic and research laboratories, a demonstrator incorporating all the necessary hardware components in a single, compact and cost-effective setup was developed within the Nano-Tera project FlusiTEx (Figure 1). The system consists

of a modulated solid-state light source (laser diode), a CMOS lock-in imager, optical components, electronics and software interfaces. The lifetime measurement is carried in the frequency domain (phase fluorometry). In this method, the fluorescence lifetime is obtained from measurements of the phase lag and demodulation of the emission as compared to the excitation light.

The setup was tested with various fluorescent dyes (rhodamine, dichlorofluorescein) in solution as well as in thin films. A 2D map of the fluorescence lifetime in the low nanosecond range could be obtained (Figure 2). The system was also tested with ruthenium-doped thin films used for oxygen sensing, with lifetimes in the microsecond range.

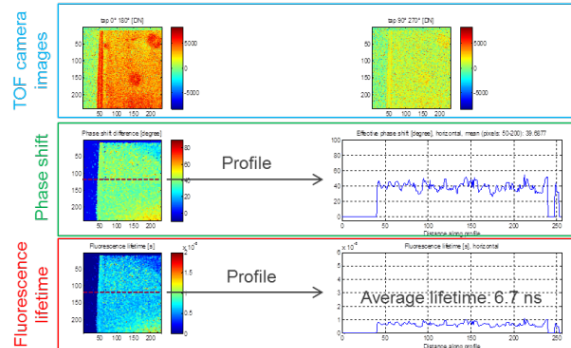


Figure 2: Fluorescent lifetime distribution of a fluorescein/rhodamine mixture (4:1 molar ratio). The sample was provided by EMPA.

The obtained results show that the combination of a fast lock-in imager with novel solid-state light sources has the potential to bridge the technological divide that limits the use of lifetime imaging in relevant areas that could benefit from its application.

As a next step, a more integrated prototype will be developed. The camera electronics will be redesigned based on a stacked PCB approach, including a base board, a FPGA processing module and a sensor head PCB. The camera will allow control of the modulation signal frequency, amplitude and offset of the illumination. The optical interface will also be further miniaturized. The complete, integrated FLIM prototype will be made available to application partners for characterization and testing.

CSEM thanks Nano-Tera for its financial support in the framework of the RTD project FlusiTEx.

[1] A. Esposito, *et al.*, Opt. Exp. 13 (2005), pp. 9812-9821

[2] L.-E. Bonjour, *et al.*, in Sensors, IEEE (2011), pp. 724-727

Development of a Protein-coated Hydrogel Microcarrier for Stem Cell Expansion

M. Håkanson, L. Barbe, H. Straub, R. Junuzovic, H. Zepik, H. Chai-Gao, D. Caminada

The methods for controlling stem cell cultures in drug discovery or tissue engineering have been steadily progressing. However, cost-effective strategies to expand a large number of stem cells while retaining their unique properties are needed. Within a project partly funded by a Eurostars grant [1], CSEM is developing a hydrogel microcarrier that can be used as a stem cell culture support in a stirred bioreactor. In this report the results of the first step of this project, the material selection, are presented.

For the expansion of stem cells, stirred bioreactors have shown several advantages over conventional stationary cultures. Firstly, the cell yield is higher and secondly the environment surrounding the cell is more homogeneous, reducing oxygen and metabolite concentration gradients to a minimum. In addition, the culture in a stirred bioreactor can be almost completely automated. This is not true for stationary 2D culture, with application limited to cell production. Still, there is currently no established method to culture a large population of cells using bioreactors. In this regard, CSEM together with the Swedish company Biolamina AB are developing a hydrogel microcarrier coated with a special stem cell supporting protein, LN-521, that should allow homogeneous 2D culture of pluripotent stem cells in stirred bioreactors. Biolamina develops and sells the recombinant LN-521. Within this project they will improve the production of the LN-521 to ensure enough supply coating of the microcarrier for example. CSEM is responsible for the development of the microcarrier, which consists of the following main parts:

- Material selection
- Microcarrier development
- Bioreactor culture protocol optimisation

In the first part of the project, different hydrogel materials were molded into 1 x 5 mm circular pads. The protein LN-521 was then linked to these materials by different strategies: covalently by binding to a specific functional group on the protein or non-specific via adsorption or absorption by immersing the dry gel in a protein solution. The quantification of the protein linkage by biochemical methods and the evaluation of the suitability of the material as a stem cell culture support determined if a material was suitable for the intended application. In this project, variations of eight chemically different materials were examined. For the optimization of the physical and biochemical properties of the material the following factors were varied: polymer concentration, crosslinking method and protein-binding method.

The hydrogel microcarrier formation was performed in a microfluidic flow focusing chip with two inlets for the aqueous phase and one for the oil phase.

Of all materials tested, CSEM identified one acrylamide-based candidate that can support the stem cell culture. Many of the tested materials did not support stem cell culture at all. For the

selected material, the protein was covalently linked to the material. The material has been tested extensively with pluripotent stem cells. The cells attach, grow and maintain their very motile phenotype when they are grown on this material (see Figure 1).

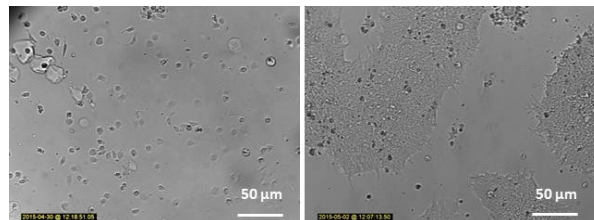


Figure 1: Pluripotent stem cells attach well to the laminin-functionalized acrylamide material; images at 1 and 48h after seeding.

Preliminary results showed that it is possible to make microcarriers out of this material in a relevant size range for cell culture (see Figure 2). The polymerization can be initiated by UV or by the addition of a chemical compound. Depending of the polymerization method the initiation is inside or outside of the chip.

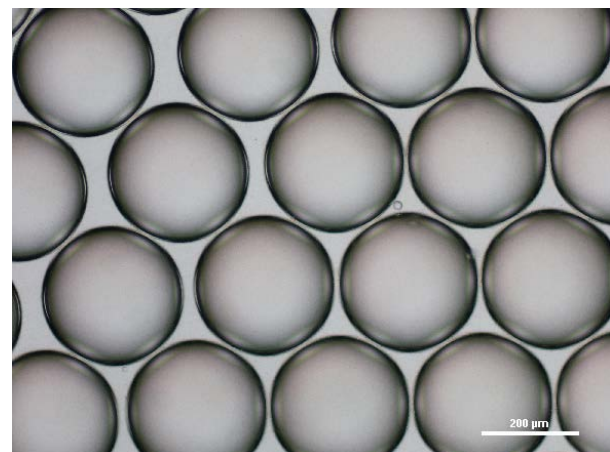


Figure 2: Acrylamide droplets with a very low size distribution produced by the microfluidic flow focusing setup at CSEM.

In the next step, the team at CSEM will set the conditions to produce larger amounts of polymerized acrylamide microcarriers. Next year, the consortia hope to deliver the first results on how well the LN-521 coated microcarriers support stem cell culture in stirred bioreactors.

[1] Eurostars project Production of LAMinin-521™ coated MICrocarriers for stem cell expansion (LAMMIC), No. 8 972

New Materials for Disposable Sensors

D. Migliorelli, S. Generelli, N. Glaser, M. Schnieper, D. Caminada

Nanocellulose derived from cellulose nanofibers is a material derived from wood and is the most common natural polymer. Because nanocellulose is transparent, light and strong, it can be used in place of plastic or glass, it is completely renewable and can be used in various industrial applications. Here, we investigate the use of this novel material as a substrate for printed electrodes.

Upcoming sustainable future technologies rely on the development of new materials. They must meet the technological requirement of showing physical and mechanical characteristics similar to or enhanced with respect to the materials currently in use. Another important aspect to be taken into account is that at the end of the life cycle, these products should be able to be reused, recycled or disposed in an environmental-friendly and sustainable way.

Flexible printed electronics are important because of their low cost, large scale, roll-to-roll manufacturing capability. The substrate is one major component – and the major waste – of the electronic device and its properties will determine if the device will be flexible or rigid, heavy or light, transparent or opaque. Regular paper and plastic are two commonly used flexible substrates for printed electronics; paper based on nanostructured material is an emerging sustainable, transparent and flexible substrate with excellent physical and chemical characteristics.

CSEM has tested nanocellulose as a substrate to print flexible electrodes, in order to create a renewable, flexible, cost-effective screen printed electrodes (SPEs) (Figure 1).

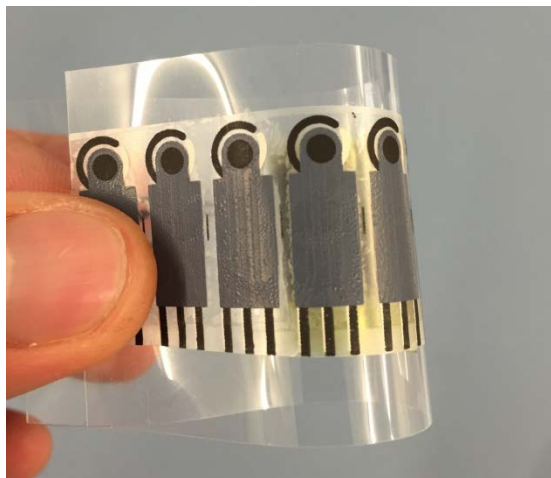


Figure 1: Screen printed electrodes printed on nanocellulose.

The first study focused on the evaluation of the electrochemical quality of the electrodes printed on nanocellulose. In this regard, the electrochemical behavior using ferro/ferricyanide (a reversible system) as an electrochemical probe was investigated with SPEs printed using cyclic voltammetry as a diagnostic technique. As shown in Figure 2, the peaks of the redox system of ferro/ferricyanide are clearly visible on the scans, and show good reversible behavior, as expected for measurement with a good quality sensor material.

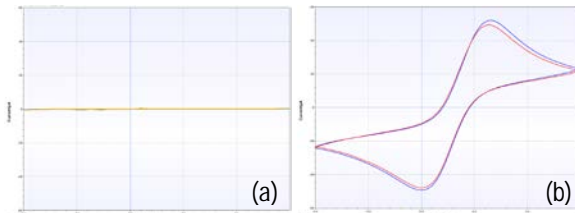


Figure 2: Cyclic voltammetry plots recorded using two different SPEs printed on nanocellulose. In KCl 0.1 M (a) in absence and (b) in presence of ferro/ferricyanide 5 mM, scan rate=50 mV/sec.

When the sensors are functionalized with an oxidase enzyme to produce, for example, glucose sensors, the active redox species used to quantify glucose is hydrogen peroxide (H_2O_2). In order to prove the full functionality of the printed sensors for this aim, we functionalized the sensors for the specific detection of H_2O_2 , and tested the response of the sensors in the presence and absence of H_2O_2 in buffer solution (Figure 3).

The change in the response of the sensor in the presence of H_2O_2 is clearly visible in Figure 3b, clearly different from the scans in Figure 3a. This indicates the possibility of using the sensors for quantification of H_2O_2 , thus making the nanocellulose based sensors a valuable alternative for less sustainable plastic substrates.

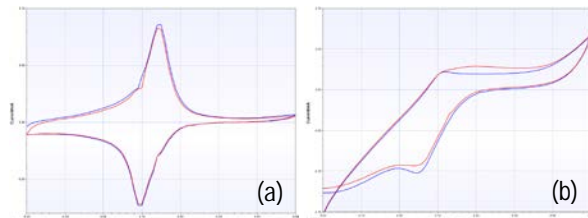


Figure 3: Cyclic voltammetry in PBS 0.05 M+ KCl 0.1 M, pH=7.4 (a) in absence and (b) in presence of H_2O_2 10 mM, scan rate=50 mV/s.

A Patch for Estimating Exercise Intensity by Monitoring Lactate in Sweat

D. Migliorelli, T. Parkel, N. Tscharner, S. Generelli

Recent developments in wearable sensor technologies have opened new frontiers in the monitoring of body parameters. Wearables could play a great role in markets such as sports and healthcare by continuously monitoring body parameters in sweat or other secreted body fluids. Wearable sensors can also provide feedback to their users about their lifestyle regarding physical activity and sports and in this way encourage a more active, healthier lifestyle.

The monitoring of sweat electrolyte concentrations can provide a great deal of information on the state of the human body. Typically, low water levels (dehydration) or low sodium concentrations (hyponatremia) should be immediately replenished to avoid detrimental effects to human health and reduced physical and mental performance.

Another important biomarker is lactate, an indicator of tissue oxygenation. During intensive physical activity the stored glycogen is consumed to produce lactate (glycolysis). Consequently, this parameter is of great importance in assessing physical performance in sports and health care applications.

CSEM has been active for many years in developing technologies for accurate, real-time and on-body, measurement of a variety of health indicators like heart rate, heart rate variability and blood oxygenation. These technologies include all aspects of the wearable from the sensor membranes to the electronics and algorithms collecting and analyzing the data. More recently, activities focusing on biocompatible, disposable sensing solutions for monitoring skin pH, conductivity, ion content, sweat rate and lactate levels have been initiated.

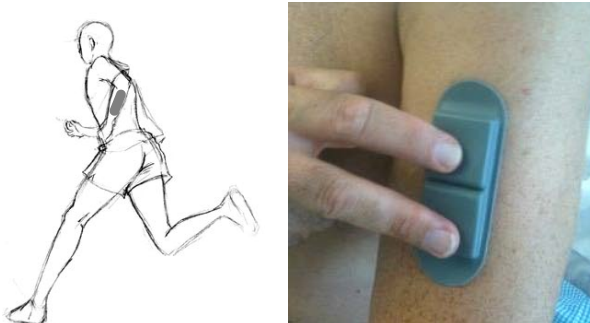


Figure 1: The ECHO patch (Kenzewear Inc. product, on the arm) is worn during exercise, and has the necessary electronics for the readout of the system. The data are either sent to the athlete's smartphone or stored within the patch for further transfer, after the training session (sketch by studiocyen.net).

In line with these activities, a smart patch able to read and store the information from the lactate sensors has been realised. The lactate sensor is based on screen printing technology, and is in contact with sweat, which gives a real-time readout of the concentration of lactate in sweat. The adhesive patch is placed on the athlete's body as shown in Figure 1.

The patch (Figure 2) will read lactate concentrations in real-time, and either store the data in the device until the end of the training session for further transmission to dedicated data storage and analysis software, or is sent in real-time to a mobile device. The continuous monitoring of lactate will thus alert the athlete of sub-optimal use of resources during physical effort.

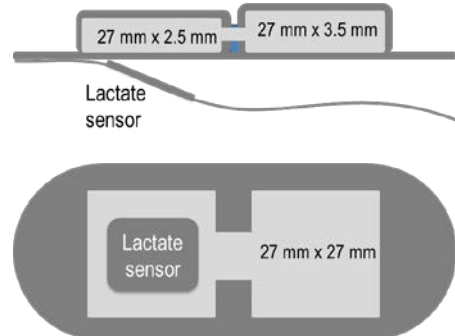


Figure 2: Side and bottom schematic view of the patch. In light grey the non-disposable core of the patch, with its dimensions. In dark grey the disposable part of the patch. Overall dimension 100 mm x 40 mm x 8.5 mm.

A lactate sensor is being developed to address the challenges of acquiring measurements in sweat. The focus of the current development is to obtain a stable and robust device for the detection of lactate in sweat in the concentration range of 1 mM up to 20 mM for a period of one to four hours. A calibration curve in the range of interest has been recorded in buffer solution and is depicted in Figure 3.

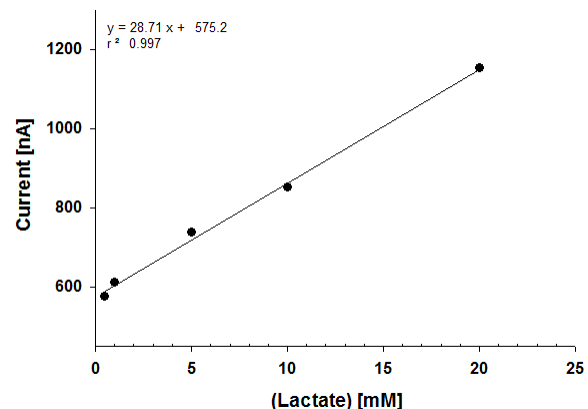


Figure 3: An example lactate calibration curve.

Multi-purpose Bi-directional PC Interface for Printed Electronics Systems

F. Zanella, J. Disser, R. Rossignol •, N. Marjanović, G. Nisato, R. Ferrini

CSEM has recently developed a multi-purpose bi-directional PC interface which allows the electrical characterization and driving of electronic matrix e.g. sensor (optical, chemical) arrays, imagers, display backplane, memories, etc. Its reading/writing capabilities, multi-channel addressing and Current-to-Voltage conversion not only help testing and optimizing the above mentioned electronic systems, but also ease the development of their dedicated custom driving units. The developed platform is here demonstrated to interface CSEM's first imager made of organic photodiodes (OPDs, 64 ppi resolution).

CSEM's TP-10 is an example of a fully automated testing & data analysis platform extracting electrical parameters of single thin-film devices, such as: transistors, diodes, resistors, capacitors and inverters. It was mainly designed for fast screening of new materials dedicated to printed electronics.

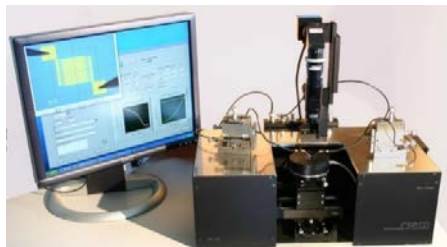


Figure 1: CSEM's TP-10 automated prober for single devices.

In addition to this well-recognized custom-made measurement platform for single thin-film devices, CSEM has developed another platform capable to drive sensor arrays, imagers, display backplane, memories, etc. This new platform is a multi-purpose bi-directional PC interface (see Figure 2) which comprises: i) a substrate holder with a non-permanent electrical interconnection, ii) a PCB with row drivers and a multiplexing system, iii) data acquisition instruments and iv) a PC user interface. Multi-channels addressing and Current-to-Voltage multi-channels conversion are possible.



Figure 2: CSEM's multi-purpose bi-directional PC interface platform.

The platform specifications are summarized in Table 1.

Table 1: Overview of the platform specifications

Channels	Range
32 analog inputs	-10V / +10V
16 voltage outputs	-10V / +10V
16 current outputs	0.1 / 20 mA
56 digital inputs / outputs	5V
Addressable matrix	Up to 512 x 512

As an example using this platform CSEM could address its first organic imager (photodetector array). The imager is made of a 32 x 32 organic photodiode (OPD) array and was tested with a printed grid on top of it as target (see Figure 3).

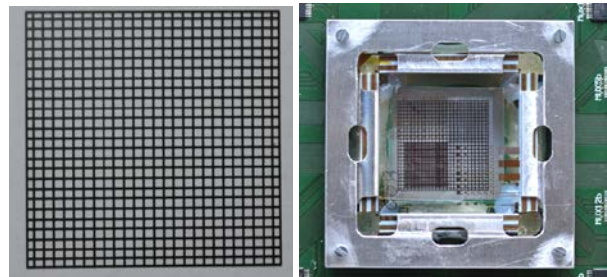


Figure 3: The target (left) and the 32x32 OPD imager (64 ppi) mounted on the platform for testing (right).

The measurements (Figure 4) show color lines representing the grid of the target as a voltage difference with respect to the reference voltage image acquired without the target.

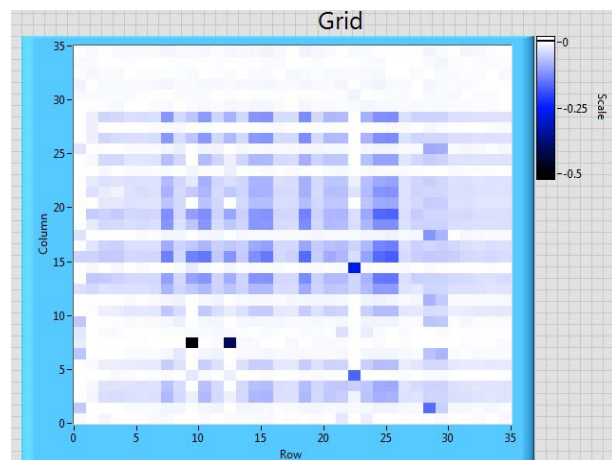


Figure 4: Visualization of the imaged grid target.

Last but not least the elements (hardware and software) of this multi-purpose platform can serve as a starting point for developing custom driving units dedicated to a particular device type (either imager or display) with particular specifications (e.g. number of rows/columns).

This work was funded by the European Community's Seventh Framework Programme under the grant agreement n°312792 (INGRESS project).

• Now at Institut d'Electronique et des Systèmes (IES), Université de Montpellier, France

PV-CENTER & ENERGY MANAGEMENT

Christophe Ballif

Worldwide, the PV sector continues to enjoy a steady annual growth, in the range of 10–15% in terms of new annually installed capacity. The major trend in the crystalline silicon field, which continues to dominate the PV front-end market, is stepwise increments in the technology used, for example upgrading production lines by introducing two or three additional tools to produce PERC (passivated emitter and rear contact) solar cells, introducing more busbars (4–5) to reduce Ag consumption, or moving to glass-glass laminates for lower costs and increased module reliability. There have also been several hidden improvements, for example in interconnection and metallization schemes, in the quality of c-Si material, and in the packaging materials of modules. New solar cell makers tend to opt for more advanced technologies, including n-type PERT or c-Si heterojunction (Kaneka, Silevo, Ecosolifer, CIC, AUO...). These technological developments are accompanied by changes at the PV system level, including bi-facial solar modules, or the massive introduction of one-axis tracking for large PV power plants. The "energy system" aspects are developing strongly, linked to the development of PV. Because PV is reaching production costs below retail grid parity (the local electricity price), storage systems are increasingly being installed in private homes, and—even though business models are not yet clearly established—larger, utility-scale storage systems, typically from 1 to 10 MW, have been installed all over the world, mostly as demonstration examples. All this is accompanied by various trends, including the monitoring and predicting output of PV power plants, the creation and management of virtual power plants, the rethinking of local networks, and the development of DC micro-grids. Integrated systems, incorporating storage and multiple energy sources, are increasingly being installed. One example is the increasing number of companies providing "container solutions", with PV, wind, batteries, and back-up diesel generators, and even possibility to connect to an external grid. Finally, we note that large PV solar parks have now achieved—in sunny countries—direct electricity production costs equivalent to or below the wholesale electricity price. Power purchase agreements are now being reached at a price of 5–7 US cts/kWh making, *de facto*, solar one of the lowest cost new sources of electricity (including when compared with new fossil fuel plants), but still leaving it not competitive with the marginal production costs of electricity generated with coal and gas, unless CO₂ pricing is taken into consideration. With the upcoming requirements for CO₂ emission reduction worldwide in mind, we can expect that solar and—later—storage at the large PV penetration level will definitely play a key role in energy solutions.

The long terms objectives of CSEM's PV-center and Energy Management program are:

- To provide cutting-edge innovation in the field of photovoltaic devices, realizing the best devices with a high potential for industrialization, and providing modules with the highest potential for adoption by the public in the built environment.
- To support the development of next-generation equipment and metrology systems, all along the value chain of

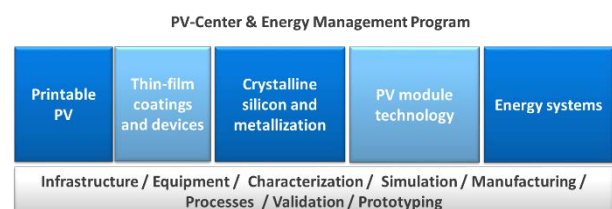
photovoltaics, creating a sustainable clean-tech value for existing and future CSEM customers.

- To provide new solutions for specialized devices, coatings, or materials with higher added-value, and for PV components with enhanced functionalities.
- To bring solutions to the energy/electricity management field as we transition toward a society essentially powered by renewables, in which energy efficiency and management will be realized through intelligent hardware and algorithms.

The program has also been strategically positioned via the entrance of Viteos and BKW as CSEM shareholders. CSEM has also continued developing initiatives launched in 2014, including in the XGW project and the OEE, and finalizing the establishment of the ESREC storage research center together with the Bern University of Applied Sciences (BFH). An immense effort has been made to relocate most of the program's equipment to new facilities that make possible a more efficient research and development program. In parallel, further new facilities (600 m²) for module manufacturing, reliability testing, plating, and sample annealing have been set up at Innoparc. Complementing the existing facilities for printed photovoltaics, CSEM in Neuchâtel is thus now equipped with state-of-the-art infrastructure.

At the national level, collaborations with other research institutes have been reinforced through the projects of the SNSF PNR70 program (PV2050 and Active Interface) and participation in SCCER-Furies, the CCEM-CH project PV-Connect, and the Nano-Tera projects Synergy and Shine.

Finally all activities are well connected to industry via direct mandates, and CTI and EU projects. In the last two years, around 30 companies have contracted the CSEM PV-center program for technological developments.



Schematic of the activities in the PV-center and Energy Management program.

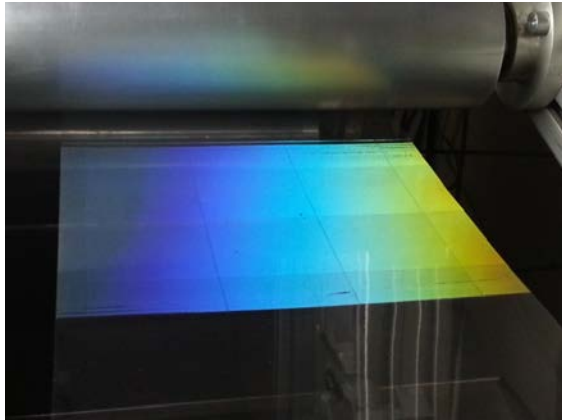
The program is organized into five activities that cover the full chain from prospective cell and module technologies up to fully integrated energy systems. These activities are strongly interlinked; the developments made in each activity can find applications in most of the other activities (e.g., solution process oxides can be used for crystalline cells).

Printable photovoltaics

This activity deals with breakthrough organic and inorganic printable materials and processing technologies that target applications with added design value and reduced environmental impact. These technologies address the additive

and mass customizable manufacturing of PV products with high levels of automation and reduced capital equipment costs. They are based on the following core competences:

- Solution-processed PV, including devices based on printed organic (e.g., conjugated semiconductors) and inorganic (e.g., perovskites, ZnO, Ag nanoparticles) materials for single multi-junction PV cells and modules.
- Light management with surface structuring and processes for enhancing the efficiency, design, and optical appearance of printable PV.
- Metrology with dedicated methods for evaluating the efficiency, mechanical properties, and lifetime-limiting factors of printable, flexible solution-processed PV.



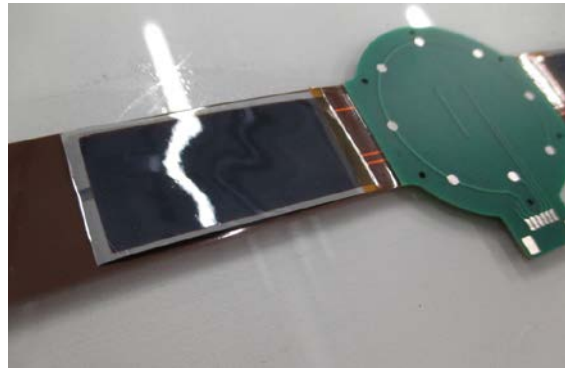
Large area light management: >25 cm-wide foil produced at CSEM.

Thin-film coatings and devices

This activity aims at developing next-generation thin-film devices based on layer stacks. Such layers can be used as electrodes, passivating layers in high-efficiency crystalline or thin-film solar cells (e.g., thin-film Si or CIGS), or directly as absorbers (perovskite or a-Si). The major goal is to provide world-class device manufacturing technology for tailored applications. The activity also covers PV cells for low-illumination applications (sensors and energy scavenging), and includes a baseline process for full-device thin-film Si and perovskite, and for full-size thin-film Si modules with monolithic interconnection (30x30 cm²) for OEM applications.

This activity is based on the following core competences:

- Physical and chemical vapor-deposition technologies—from the modelling of deposition processes to layer deposition and characterization.
- Inorganic materials and interfaces, transparent conductive oxides, and semiconductor materials.
- Design and fabrication of single and multi-junction devices and their characterization.
- PV cell architecture, design, and characterization; interconnection schemes in thin-film modules.



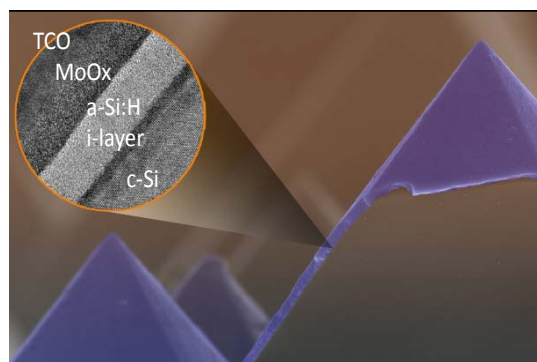
Thin-film silicon solar cells for energy harvesting solutions: mounted in the wristband of a lab prototype wristwatch.

Crystalline silicon and metallization

This activity aims at furthering crystalline silicon PV technology. The focus is on high-efficiency devices with passivated contacts and on reducing the cost of the metallization of PV devices. These devices are targeted for mass PV production, but can also find applications in specialty products.

The activity relies on the following core competences:

- Full control of manufacturing processes for silicon heterojunction solar cells with more than 22.5% efficiency.
- Knowledge of coating technologies, interfaces, and passivation layers.
- Expertise in low-temperature solar cell metallization techniques, including screen printing, stencil printing, copper plating, and ink-jet printing.
- Expertise in the simulation and characterization of layers, cells, and modules.
- A tool box for high-temperature operations processes including phosphorus diffusion, SiNx deposition, and passivating oxides.



Solar cells with 22.5% certified efficiency, without any doped p-type silicon layer (Geissbuheler, et al., APL 2015).

PV module technology

This activity targets cost reductions, increased reliability, and a higher acceptability of PV products in the built environment. It helps create new products by, for example, adapting existing mass market technologies.

The activity is based on the following competences:

- Extensive knowledge of polymers, adhesion, interfaces, lamination processes, material and polymer preparation, and additives.

- Knowledge and experience of simulating failure modes; general opto-electrical analysis.
- The design and integration of PV components into buildings.
- Testing methodology and reliability of PV modules.
- The design and fabrication of specialty product prototypes, including an ultra-lightweight PV generator for mobile applications and flexible crystalline PV modules.



First fully operational terracotta color roof—Neuchâtel.

Energy systems

The Energy Systems activity aims at developing solutions and products in two key areas—energy efficiency and power systems. Energy efficiency focuses on the building sector, where sensing and control technologies are developed for reducing energy consumption. The systems aspects cover the introduction and impact of innovative construction elements such as solar glazings and systems. “Power systems” looks at new solutions for managing the impact of massively decentralized electrical production and storage and at the associated intelligent integration of renewable energy into existing energy distribution infrastructures.

The activity is based on the following competences:

- Variety of designs of control algorithms.
- Knowledge of electricity markets and energy economics.
- Knowledge, testing, and modelling of energy system components, including storage, the design of small and large PV systems, and the modelling of these systems’ impact on local grids.
- The design and integration of multi-function PV components into buildings.



Assessment of grid resilience to large PV penetration.

Some achievements of the program

The targets set up for 2015 have in large part been met. Fully “printable PV”, tandem devices with 8.5% efficiency were realized. Baseline processes established for high-efficiency

thin-film silicon (>10% initial AM1.5 efficiency, and 17% indoor efficiency, up to 30x30 cm²) were used to realize several prototypes of rigid and flexible energy scavengers. The first laser-scribed perovskite modules were demonstrated. Four terminal measurements of tandem perovskites/c-Si cells with 22.8% were demonstrated, showing that—working together with the EPFL PV-lab—it is possible to optically improve c-Si (a base c-Si cell with 21.8%). The base process for heterojunction solar cells was steadily improved in the month before the aforementioned move to new facilities (>22.8% screen printed on 156x156 mm², measured using the GridTouch approach), and building blocks for advancing PV and energy management technologies were put in place (microcrystalline layers, advanced IBC structures, metal-oxide p-type contacts...), including back-contacted cells with over 21.5% efficiency. At the module technology level, CSEM has further worked on understanding and developing methods based on multi-wire approaches, which allow the cost of metallization to be reduced. In particular, competences in extruding polymer foil with the right formulations were applied to next-generation heterojunction modules, including—for example—multi-wire interconnections.

In parallel, strong progress was made with regards to the reliability of white and colored PV modules. In early 2016, a company—Solaxess—began the process of bringing the product to market. Further demonstration projects were also supported by this program, including the first roof integration of heterojunction modules in glass-glass laminates, and the spectacular PV façade at the CSEM HQ in Neuchâtel. At the building level, working on the control of ventilation systems we were able to show that energy savings can be made by respecting thermal comfort criteria from European standard EN 15251 for indoor environments. A series of micro-inverters and DC/DC inverters were tested and analyzed, identifying and quantifying issues such as poor wave shapes with high harmonic contents. Initial testing and modelling of li-ion batteries began on the 40-cell, 12-module test bench at the ESREC center, with the goal of quantifying the true performance and achievable costs of battery systems in real conditions, for example coupled to PV systems.



Picture taken at the inauguration of the new CSEM high-tech PV screen—the façade incorporates bi-facial heterojunction solar cells interconnected with multi-wire technology.

Organic and Printable Photovoltaics at CSEM

T. Offermans, M. Chrappa, L. Mühlbach, I. Zhurinsky, J. Schleuniger, B. Satilmis, N. Glaser, R. Ferrini, G. Nisato

The Printable PV activity at CSEM addresses disruptive, organic and inorganic printable materials and processing technologies that target applications with design added value and reduced environmental impact. The additive technologies developed are aimed at mass customizable manufacturing of PV products with high automation and reduced capital equipment cost. The objective is to provide Switzerland with know-how and technological options at the device design and process development level to support equipment developer, materials researchers and industrial suppliers as well as end users in the emerging field of printed PV.

Design and customizability of printable PV

The use of printing methods for the deposition of all layers required in an OPV stack allows direct patterning of all layers and thus printing of any desired shape of cell – and consequently module. The design feature of printed OPV is thus not only of aesthetic value but it allows the embedding of a module into an electrical device without limiting the design of the device. This opens up totally new market potential for printed OPV. In a design example below (Figure 1a), a module consisting of 9 interconnected cells in series were fabricated, by coating the photoactive layers on a flexible substrates, which were patterned in a single post-patterning step, followed by a screen printed top electrode.

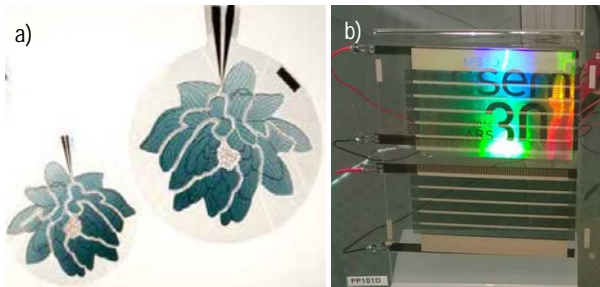


Figure 1: a) Free-shape modules; b) Module with integrated logo.

From small labscale cells to demonstrators

During the past years, CSEM has developed their printing and device fabrication capability from lab-scale single cells made by spin-coating in an inert gas on small 2.5x2.5cm glass substrates, through dr. blade coating in the ambient environment on increasingly larger substrates to complete modules printed on flexible substrates (Figure 2).



Figure 2: (left) 2.5x2.5cm spincoated cells on a glass substrate, (middle) 5x5cm blade coated cells on a glass substrate and on a flexible substrate, (right) a mini-module.

Recently, our first slot-die coated cells were fabricated with an efficiency of ~6% in a single junction using commercially available material, still on glass. Our current efforts focus on the transfer of the established processes for glass substrates to flexible substrate. Part of this transfer is complete. Using screen printing or inkjet printing metal grids that can be used for the bottom or the top grid were demonstrated (Figure 3).

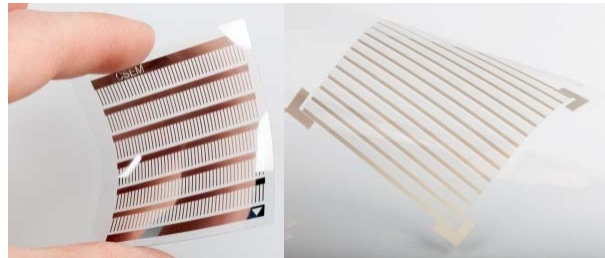


Figure 3: Example of (left) an inkjet printed silver grid, (right) a screen printed grid.

Module development

Such screen printed grid was integrated in one of our latest module demonstrators (Figure 1b). The module in the Figure 1b is fully printed on a flexible substrate, and encapsulated between flexible barriers. The performance of the device is 3-4% at the cell level. To generate an eye-catching effect, a foil with a nano-textured holographic logo (30 years CSEM) was integrated into the inside of the module, by lamination between the barrier foils.

Towards high efficiency printed tandem cells

To enable the next generation of OPV, a process was developed to fabricate tandem solar cells. Using the tandem architecture efficiencies well over 10% are expected to be feasible. Selected organic and inorganic materials were blade-coated on glass substrates from non-halogenated solvents at ambient conditions, and at temperature below 120°C. Nanometer control of the layer thicknesses (see Figure 2 for a TEM analysis of the stack) lead to an 8.5% tandem cell realized in our lab.

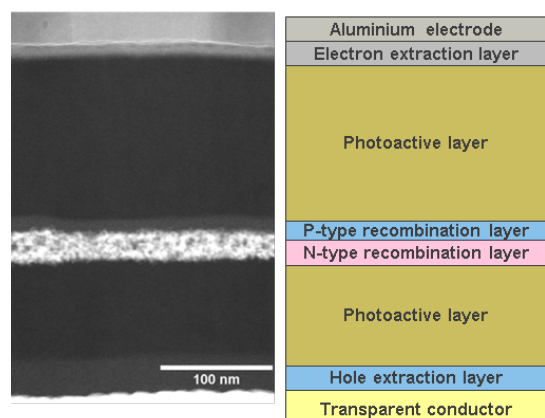


Figure 4: TEM cross-section and schematic representation of an 8.5% organic tandem cell.

We gratefully acknowledge support from the EU project Sunflower (Nr. 287594), Interreg project Rhin-Solar and the Canton of Baselland.

Light Management for OPV

J. Mayer, T. Offermans, B. Gallinet, R. Ferrini

Optical in-coupling gratings are designed and tested to improve the performance of thin film organic photovoltaics. The impact of the grating on the absorption in the active layer has been modeled and explained using a standard OPV cell architecture. Simulations predict an increase in absorption of up to 20 %, which shows to be independent from the chosen absorber material. Different structures have been applied on blade-coated devices and an efficiency improvement of 12 % could be validated. The angular performance of the structures was further measured, showing an increased stability of the enhancement for two dimensional gratings. In simulations of the current generation for different angles and illumination conditions, a total yearly increase of the harvested energy of 12 % is predicted, using an optimized grating. The fabrication of these structures, moreover, is compatible with roll to roll production techniques, which makes them an optimal solution for printed photovoltaics.

Organic photovoltaics (OPV) represent an emerging technology, which can enable cost-effective, flexible and light-weight energy-harvesting and which allows for fabrication with established printing techniques, like roll-to-roll. A remaining drawback, however, is the limited absorption of the thin polymer layers, which can be addressed by the use light-management structures, which increase the portion of the light that is absorbed in the device.

Most approaches for nanophotonic light-trapping thereby have a direct impact on the fabrication processes and the device architecture.^[1] Since diffraction gratings can be added on top of the light-incident interface (Figure 1), they can be fabricated fully independent from the OPV and therefore exhibit high potential for integration into roll-to-roll production. Moreover the gratings can be functional even when embedded into a matrix, which then provides protection against external environmental influences (e.g. scratching, dust, moisture).

In this work the optical interplay of the gratings and the multilayer stack was studied and revealed that in the thin films of OPVs the origin for the strong enhancement is not only the increased path-length, but also constructive interferences, which can be accessed with the diffracted light of the surface grating. Consequently, the resulting absorption enhancement induced by the grating is linked to the stack architecture and does not depend on the active material, which largely dominates the power conversion efficiency.

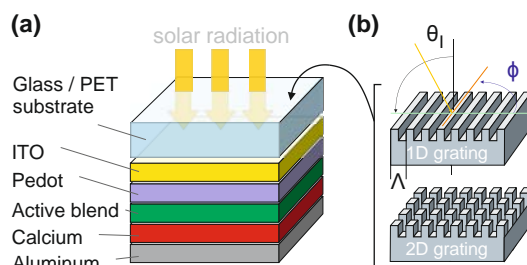


Figure 1: (a) Standard device architecture of an OPV. (b) A sub-micrometer line grating (1D) or crossed grating (2D) is fabricated at the light incident surface of the device.

The validation of the structures on blade-coated photovoltaic devices showed an enhancement of 12 % with respect to the reference which had an efficiency of 5.2%, measured under standard test conditions and straight incident light. Simultaneous computations and experiments are ongoing to further optimize these structures to exceed the predicted enhancement of 20 %. However, besides maximizing the absorption for straight incidence under AM 1.5G solar

illumination, a more general solution is pursued, accounting for the different ambient conditions in the final application. In angular dependent measurements of the generated current, especially the 2D grating has shown a good performance with low dependency on the incident polar and azimuthal angles, θ and ϕ .

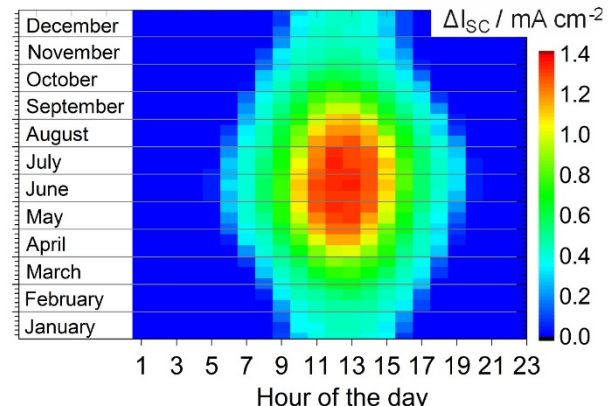


Figure 2: Hourly increase in the generated current for the standard OPV equipped with an in-coupling grating.

These results were used to model the hourly current generation over 365 days by considering also the respective illumination spectra in the location of Basel, Switzerland, obtained from the NREL database (Figure 2). By this means, a total yearly increase in harvested energy of 12 % could be simulated using the 2D in-coupling grating.

Continuing from the promising results of this proof-of-concept study, in a next step this added value of increased light-harvesting will be transferred on foils, which can be structured with diffraction gratings via hot-embossing (Figure 3).

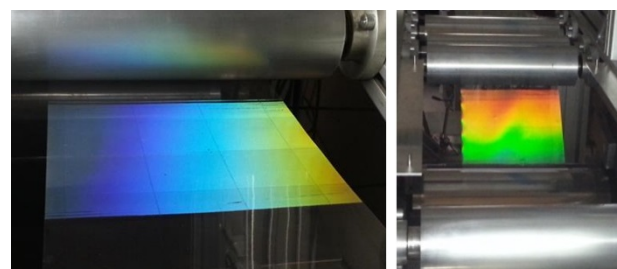


Figure 3: Hot-embossed diffraction grating as prospective light-management structure for roll-to-roll processed organic photovoltaics.

The work was partly funded by the European FP7 project SUNFLOWER (grant number 287594) and we thank the partners for their support.

^[1] J.-D. Chen, C. Cui, Y.-Q. Li, L. Zhou, Q.-D. Ou, C. Li, Y. Li, J.-X. Tang, "Single-junction polymer solar cells exceeding 10 % power conversion efficiency", Adv. Mat. 27 (2014) 1035

Development of Highly Conductive Transparent Materials for PV Applications

S. Nicolay, L. Sansonnens, D. Sacchetto, G. Christmann, L. Barraud, A. Descoeuilles, M. Despeisse, C. Ballif

In the framework of the CTI project TACOS, CSEM develops highly transparent and conductive electrode materials for PV applications.

In collaboration with the Meyer Burger group, CSEM develops electrode materials for the Silicon heterojunction technology (HJT). The high efficiency achieved with HJT solar cells rely on high quality n-type crystalline silicon wafer and on high quality surface passivation by amorphous silicon thin film for low bulk and surface recombination. In order to collect the generated photocurrent, a combination of a front transparent conductive oxide (TCO) electrode and silver printed fingers is used.

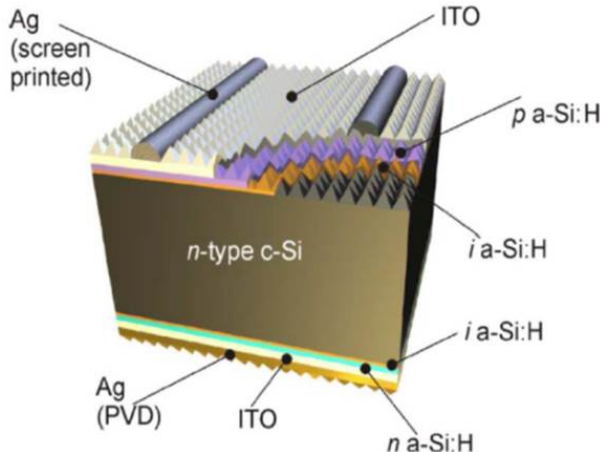


Figure 1: Schematic representation of a silicon heterojunction solar cell.

The front TCO for HJT solar cells has to fulfill the following criteria:

- Low sheet resistance in order to minimize the electrical losses during the lateral transport of the current
- Low absorbance in order to minimize the optical losses
- Ability to form a good ohmic contact with both the a-Si doped layer and the silver fingers
- TCO thickness determined in order to form a quarter wavelength anti-reflection layer

For TCO in general, a lower sheet resistance can be obtained by either increasing the TCO thickness, the carrier density or the carrier mobility. However, in the case of HJT solar cells, the optimum TCO thickness is determined by the anti-reflection condition while carrier concentration should be kept low to minimize the infrared parasitic absorbance of the TCO. Therefore the carrier mobility is the main TCO parameter that can be increased in order to fulfill all the imposed criteria on the front TCO.

Actually, sputtered indium tin oxide (ITO) is the most standard TCO used for HJT solar cell production. Among other materials, CSEM is evaluating sputtering of high indium content TCO such as pure In_2O_3 doped with hydrogen (IO:H) or still In_2O_3 with trace amount of tungsten (IWO) or Cerium (ICO:H), as well as indium free TCO such as aluminum doped zinc oxide (AZO). Figure 2 shows the maximum electron mobility achieved for each TCO for a carrier density around $2 \times 10^{20} \text{ cm}^{-3}$ and a thickness of 100 nm after annealing at 190°C. In comparison to the standard ITO, higher electron mobilities are obtained for

high indium content TCO, while a lower mobility has been obtained for the AZO indium free TCO. With both ICO:H and IO:H, it is possible to reach electron mobilities higher than $100 \text{ cm}^2/(\text{V s})$, but this necessitates the use of water vapor doping during the material sputtering, which makes the deposition process difficult to control and hence less reproducible.

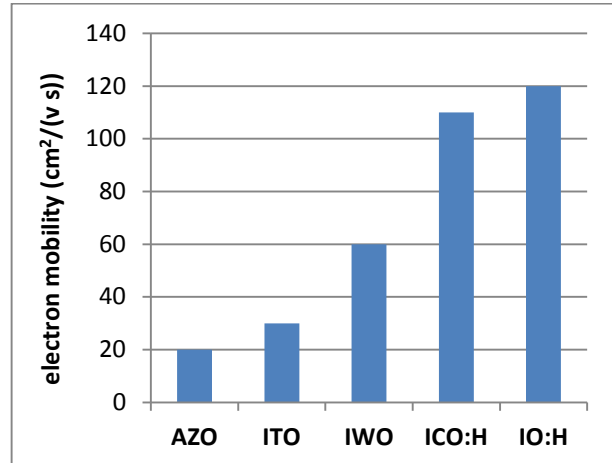


Figure 2: Carrier mobility for different TCO materials for a carrier density around $2 \times 10^{20} \text{ cm}^{-3}$ and a thickness of 100 nm after annealing at 190°C.

In terms of HJT solar cell efficiency, an absolute efficiency gain of 0.4% has been obtained with IWO in place of ITO while a reduction of the efficiency has been observed when replacing the ITO by AZO. These results have confirmed the possibility to increase the efficiency of HJT solar cell by using TCO with higher carrier mobility.

In the framework of the TACOS CTI project, CSEM and Meyer Burger also evaluate the industrialization potential of the different TCO for HJT solar cell production. For such evaluation, the final solar cell performance is an important criterion, but the following criteria have also to be taken into account:

- Raw material and sputtering target cost
- Process reproducibility
- Machine complexity
- Process tact time
- High reliability after module implementation

The final goal of the TACOS project is to find the best TCO in order to achieve the lowest cost of electricity production with silicon HJT solar module.

This work is supported by the Commission for Technology and Innovation (CTI) through the TACOS project.

White Solar Modules: from Prototypes to Industrial Products

J. Escarré, G. Cattaneo, L. Sansonnens, J. Bailat, L.-E. Perret-Aebi, S. Nicolay, C. Ballif

CSEM has developed white solar PV modules with conversion efficiencies above 10%. This innovative PV technology is particularly attractive for the BIPV market. In 2015 a company, Solaxess SA, has been founded to exploit this technology, and together with CSEM is now working on the industrialization of the technology.

Henry Ford's famous, "Any customer can have a car painted any color that he wants so long as it is black," is almost valid for solar panels as most of the actual installed PV modules are made from crystalline silicon solar cells interconnected by metallic ribbons and therefore present the same blue-black visual aspect with highly reflecting metallic ribbons.

In October 2014, CSEM has unveiled to the public its white or colored module technology. This technology is well suited for the BIPV market as Architects constantly demand new solutions to customize the color of PV elements to make them blend into the building skin.



Figure 1: White PV modules fabricated at CSEM.

As shown in Figure 2, in order to make true white solar modules, the technology developed by CSEM combines various elements: (1) a solar cell technology able to convert solar infrared light into electricity; (2) a selective scattering filter which scatters the visible spectrum while transmitting infrared light.

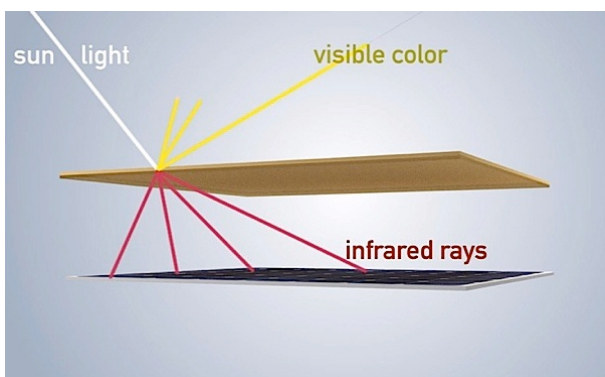


Figure 2: Schematic principle of the white PV module.

Crystalline solar cells are well suited for this application as more than 50% of the current generated under standard solar illumination comes from the infrared. The selective scattering filter has gone through a detailed optimization process, aiming at improving the efficiency, the visual aspect, the manufacturability, while performing all relevant reliability testing. Other colors than white can be produced by including colored pigments during the processing of the film.

As shown in Table 1, a performance of 11.4% has been achieved for a white solar module. The size of the module is 55 cm x 60 cm and it consists of 9 heterojunction solar cells interconnected in series. The loss in efficiency, i.e. comparing the same cell technology having usual or white appearances, is 40%. It is entirely due to losses in current as most of the visible light is reflected and therefore lost for current generation. The module presents a true white aspect. Neither the cells nor the connections are visible anymore.

Table 1: Summary of the performance parameters extracted for the reference and white modules.

Sample	Voc [V]	FF [%]	Jsc [mA/cm ²]	Efficiency [%]
Reference	0.727	71.8	36.56	19.1
White	0.714	74.7	21.38	11.4
Δ [%]	-1.8	4.0	-41.5	-40.2

At the beginning of 2015, a startup company Solaxess SA has been founded in Neuchâtel with the goal to manufacture and commercialize the white or colored PV technology developed by CSEM. Together with Solaxess, CSEM is now involved in the transfer from laboratory prototype fabrication to large scale industrial production. The two main technical objectives for the industrialization are the demonstration of the reliability of this new technology and the upscaling of the selective scattering filter fabrication at an acceptable production cost for the BIPV market. These two points are the subject of the CTI project NanoWhite which has been launched in autumn 2015. The targeted product is a specialty foil which, whose color can be easily adapted and which can be implemented by any module maker worldwide.

Photovoltaics for Hydrogen Production

J.-W. Schüttauf, D. Dominé, L. Löfgren, A. Faes, M. Despeisse, C. Ballif, J. Bailat

The SHINE Nano-Tera.ch project aims at the realization of a fully integrated solar-to-hydrogen system using thin-film silicon solar cells. Compared to a standard approach with discrete elements – with separate solar panels and electrolyzer – an improved efficiency might be expected thanks to the recycling of the dissipated heat from the solar cell using the same components.

A massive deployment of renewable energy technologies requires solving the present energy storage issue. This means finding a way to store a significant fraction of the annual world energy consumption.

A possible solution to elegantly store energy from sunlight in chemical bonds is the direct production of hydrogen using solar cells and water. Hydrogen can for instance be compressed, transported and stored; alternatively it can be injected in the gas distribution system as it is done, e.g., in a demonstration project in Germany.

The multi-disciplinary Nano-Tera.ch project SHINE involves several research groups within the fields of optics for solar, optics and fluidics, semiconductor solar cells, electrochemical materials and system simulation^[1]. A system engineering approach based on system simulation is adopted to demonstrate a prototype consisting of 4 key elements, as symbolized in Figure 1, to be integrated in a compact photo-electro-chemical (PEC) system:

- An innovative solar concentrator with self-tracking, where light is trapped in a waveguide through a local phase change of paraffin wax, thermally activated.
- A photovoltaic solar cell made of a thin-film silicon multi-junction device, operating at its maximum power point with enough voltage to enable the electrolysis of water.
- Microfluidic for water feedstock with solar heat management for the cooling needed by concentration photovoltaics and the production of water vapour.
- An electrolyzer based on hydrogen- and oxygen-evolving electrodes and on a solid electrolyte made of a proton exchange membrane.

CSEM is in charge for the photovoltaic element of the system. A triple-junction device has been developed. It is made of a stack of two amorphous silicon subcells and one microcrystalline silicon subcell, and is optimized to achieve sufficient voltage for water splitting when loaded with the electrolyzer.

At one sun illumination, its open-circuit voltage is 2144 mV and the power density produced at the maximum power point is 11.3 mW/cm², leading to a potential water splitting efficiency of

8.1%^[2]. This device has been successfully integrated in hydrogen production setups, so far leading to a stable solar-to-hydrogen conversion efficiency above 6% for over 20 hours.

In the project, alternative solutions to the triple-junction thin-film silicon will also be assessed, including a serial interconnection of small heterojunction crystalline silicon solar cells predominantly optimized for solar concentration. With this approach, solar-to-hydrogen conversion efficiencies above 15% can be expected, but making a fully integrated water splitting device is not desirable using this configuration due to the necessary cell interconnection. So far, we obtained direct solar-to-hydrogen conversion efficiencies up to 13.5%, fully relying on earth-abundant materials for device fabrication using a mini-module with three interconnected silicon heterojunction cells^[3].

Improvements towards efficiencies up to and above 15% can for instance be expected by specific fine-tuning of the silicon heterojunction solar cell properties for the application of water splitting. Operating under concentrated sunlight should even further enhance device performance. A monolithic, fully integrated device using silicon heterojunction cells could for instance be made using a triple-junction cell with a silicon heterojunction cell as stable bottom cell with an excellent infrared response^[4].

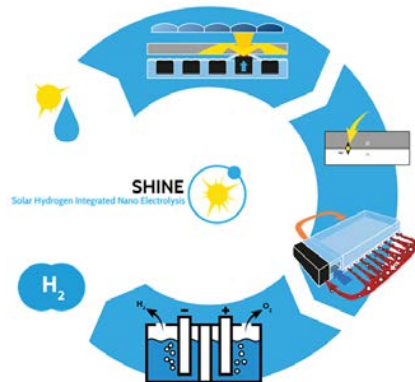


Figure 1: Conceptual view of the four elements of the integrated PEC device to produce hydrogen from solar energy and water^{[1][5][6]}.

CSEM thanks Nano-Tera.ch for its financial support received in the framework of the RTD project SHINE.

[1] www.nano-tera.ch/projects/367.php

[2] D. Dominé, *et al.*, Proc. of WC PEC 6, Kyoto, Japan (2014)

[3] J.-W. Schüttauf, *et al.*, Manuscript in preparation

[4] A. Smets, *et al.*, Presented at ICANS26, Aachen, Germany (2015)

[5] According to the IEA, the world final energy consumption in 2011 was equal to 9 Gtoe (105'000 TWh); see www.iea.org/publications/freepublications/publication/KeyWorld2013.pdf

[6] B. Burger, Fraunhofer Institute for Solar Energy Systems ISE, Electricity production from solar and wind in Germany in 2013, 12 August 2013

Perovskite Upscaling: from Cells to Modules

L. Löfgren, S.-J. Moon, D. Sacchetto, J. Bailat, C. Ballif, S. Nicolay

CSEM is upscaling perovskite solar cells from lab-scale cells to minimodules. The organic-inorganic perovskite is one of the most promising solar cell materials of recent years with a strong prospect to combine with crystalline silicon solar cells into very high efficiency tandem cells. The up-scaling to larger areas is a requirement for the formation of commercial perovskite/silicon tandem cells. Laser-scribed modules with 11.5% efficiency are demonstrated.

Efficiencies of solar cells based on organo-metallic halide perovskite absorber material have increased at a dramatic rate over the last few years, currently reaching more than 20% efficiency^[1]. However, most of the efficiencies reported so far have been obtained on solar cells with small lab-scale areas of less than 0.3 cm². Only a handful of studies have addressed the performances of mini-modules based on perovskite and none of them have used laser scribing, an industry standard for thin-film solar cells, to form interconnections.

This project, 'Systems for ultra-high performance photovoltaic energy harvesting' (Synergy), focuses on the up-scaling of perovskite processes and the creation of high efficiency mini-modules through laser scribing.

The overall module design is illustrated schematically in Figure 1, defining active- and dead-area widths as well as the aperture area i.e. the full area of the module including dead areas but without substrate borders and contacts.

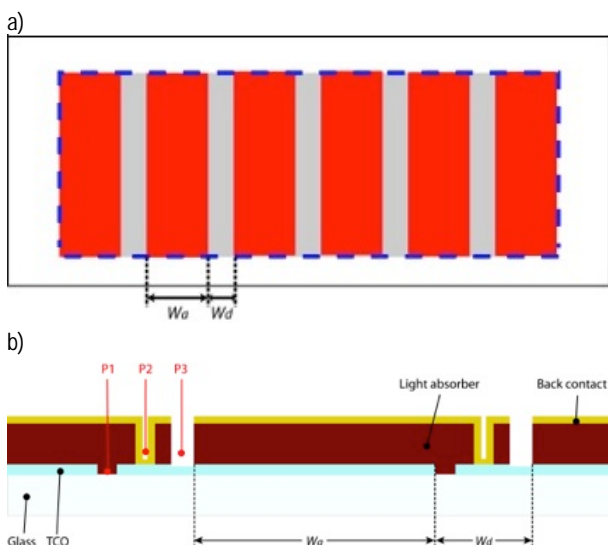


Figure 1: a) Schematic mini-module illustrating the width of active (W_a) and dead (W_d) areas, as well as the aperture area (dashed blue line). b) Module cross section defining the scribes P1-P3 and the active- and dead-area.

Initial attempts on 6 cm² large mini-modules produced a modest aperture area efficiency of 5.5%, owing to a highly resistive contact between adjacent segments^[2]. Still, this was to the best of our knowledge the world's first fully laser scribed perovskite mini-module, and the 16% dead-area fraction was the lowest reported value until then.

^[1] S.I. Seok, *et al.*, Science, 2015, 1234-1237

A set of measures were taken to improve module efficiency and increase module area.

- The P2 line processing is crucial for the inter-segment conduction and investigations pointed to residues of the highly resistive TiO₂ scaffold layer still present after laser scribing. The use of a thinner scaffold layer (150 nm instead of the original 300 nm) led to a P2 scribe free from residue and a module with drastically decreased resistance values.
- A change of anti-solvent led to improved perovskite homogeneity through spin-coating and the module size was doubled to 12 cm².
- Optimizations of the laser scribing process enabled denser scribing and dead-area ratios of less than 10%.

Altogether, these developments have allowed us to demonstrate a perovskite mini-module with 11.5% aperture area efficiency, the 2nd highest globally reported value at the time of presentation at EUPVSEC 2015. The main performance data of the mini-module are summarized in Table 1.

Table 1: Performance of optimized perovskite mini-module with voltage and current values given per module segment for easy comparison with the reference cell.

	Area (cm ²)	Eff. (%)	V _{oc} /seg. (mV)	J _{sc} /seg. (mA/cm ²)	FF (%)
module	10.9 (active area)	12.6			
	12 (aperture area)	11.5	1087	14.4	73.4
Ref.	0.49	15.5	1014	20.1	75.9

The module voltage (V_{oc}) and fill factor (FF) are close to, or even better, than the value of the reference cell while the current density (J_{sc}) is still comparatively low. Current is lost not only in the scribed dead-area but a delamination of the back-contact layer has also been observed, further reducing the current collecting area. Our development focus at present on back-contact adhesion and the transition from metallic to transparent back-contact layers in order to enable the formation of four-terminal perovskite/silicon tandem cells.

CSEM thanks Nano-Tera.ch, the Swiss Federal Office for Energy and Swiss Solar Connect for the funding of this work.

^[2] S.-J. Moon, *et al.*, JPV, 5, 2015, 1087-1092

Demonstrating Advanced PECVD Reactor for Uniform Coating on both Sides of a Substrate

A. Descoedres, L. Barraud, M. Despeisse, C. Ballif, F. Jeanneret •, A. Limouzin •, U. Kroll •, O. Shojaei •

The Mirror reactor is a new PECVD system invented and patented by the Swiss company INDEOtec, specifically dedicated but not restricted to the production of high-efficiency silicon heterojunction (SHJ) solar cells. Thanks to its innovative design allowing ultra-homogeneous coatings of wafers on both sides without breaking the vacuum, the handling of the substrates is significantly simplified, leading to higher production throughput and yield, reduced costs, and potentially to improved device performance. The experimental results obtained confirm the validity of this reactor concept, demonstrated by full-area 6-inch SHJ solar cells with efficiencies up to 21.5%.

The potential of the silicon heterojunction (SHJ) technology to reach high conversion efficiencies is well known, with a recent record efficiency for silicon solar cells above 25%. While the overall fabrication process for both-side-contacted SHJ solar cells is relatively simple, further cost reductions are still possible to render this technology even more competitive at the mass production level.

The Mirror reactor is a new concept of PECVD reactor, invented and patented by the Swiss company INDEOtec, and demonstrated by CSEM and INDEOtec in the frame of the CTI project "Mirror". The new reactor allows for uniform depositions on both sides of a substrate without the need of flipping it and of any vacuum break. By using a multi-chamber cluster tool equipped with such novel reactors and PVD chambers attached, the typical production process of SHJ cells would be significantly simplified. Fabrication costs would be decreased thanks to a reduction of process time (pumping and venting time), process steps (wafer flipping, loading and unloading), and equipment footprint. Furthermore, the removal of handling steps (flipping, loading) is also potentially beneficial for the device performance and production yield, as eventual surface contamination issues and risks of wafer breakage are significantly reduced.

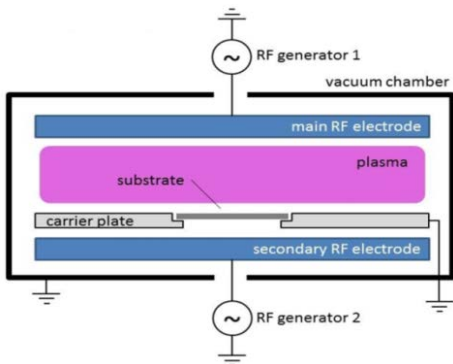


Figure 1: Schematic design of the Mirror PECVD reactor. A sister chamber with inversed position for the main and the secondary electrodes is used for deposition on the other side of the substrate.

In a classical PECVD reactor, the substrates are simply lying on an electrically-grounded metallic carrier-plate. Deposition is therefore only possible on one side of the substrates. In order to deposit on the second side, typically the substrates have to be taken out of the vacuum process chamber and mechanically flipped. In the Mirror reactor, the substrates are hanging in a carrier-plate with openings ("bi-facial" carrier-plate), making

depositions from both sides of the substrates possible. However, the use of such bi-facial carrier-plates induces additional challenges with regard to film uniformity. Indeed, the gap space below the substrate acts as an additional capacitor in the equivalent electrical circuit, which affects the global RF electrical field distribution and, finally, leads to film inhomogeneity on the substrate. This reduction of the deposition rate in the center of the substrate compared to its edges leads to considerable losses in performance and is therefore unacceptable for the production of high-performance SHJ solar cells.

The approach to overcome this problem is the use of a secondary RF electrode on the carrier-plate side (see Figure 1). A properly adjusted RF power level fed to the secondary electrode can compensate the undesirable voltage drop in the gap space and, hence, loss in local plasma power above the substrate. This compensation permits a film deposition as uniform as in the standard configuration.

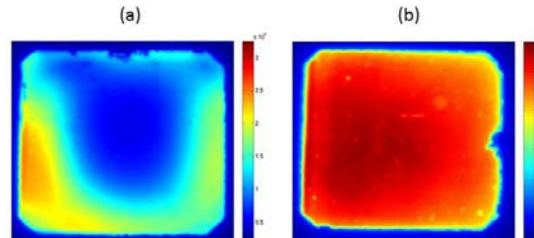


Figure 2: Photo-luminescence imaging of SHJ solar cell precursors produced in the Mirror reactor (a) without power compensation; (b) with power compensation.

Figure 2 shows lifetime mappings of 6-inch SHJ solar cell precursors, produced at CSEM in a Mirror reactor with and without the power compensation of the secondary electrode. Clearly, this compensation is mandatory to obtain homogeneous layer depositions in such bi-facial carrier-plates (corresponding layer thickness non-uniformity on the substrate surface: >40% without compensation, <4% with compensation). Complete full-area 6-inch SHJ solar cells with efficiencies up to 21.5% were produced in the Mirror reactor (busbar-less front grid design), on par with the best cells obtained in standard PECVD chambers using similar materials. These experimental results fully validate the concept of this reactor. Combined with PVD chambers directly attached to the same system, such multi-chamber cluster tools appear as extremely competitive for the production of high-efficiency SHJ solar cells. More details are available here^[1].

• INDEOtec SA, Neuchâtel, Switzerland

^[1] O. Shojaei, et al., Proceedings of IEEE Photovoltaic Specialists Conference 2015, New Orleans, USA

Metalization and Interconnection for Competitive Silicon Heterojunction Solar Cells

A. Faes, A. Lachowicz, N. Badel, C. Alleb  , F. Debrot, C. Ballif, M. Despeisse

The SwissInno-HJT Pilot and Demonstration project, funded by the Swiss Federal Office for Energy, focuses on the implementation of a R&D pilot production-line of silicon heterojunction (HJT) solar cell, and on the demonstration of the high performance of the developed technologies. In the frame of this project, CSEM develops advanced cell metallization technologies targeting both production cost reduction and module efficiency increase. Advanced materials, processes and concepts are developed on the semi-automatic high precision printer and on the electroplating R&D pilot-line acquired and installed at CSEM. Screen-printed cells with below 30 mg of silver per side were systematically demonstrated in combination with SmartWire interconnection, as well as industrial-size copper-plated cell with up to 22.8% (GridTouch) conversion efficiency.

Today's standard metallization process for silicon heterojunction (HJT) solar cells relies on screen-printing of low curing temperature silver paste. The 3 to 5 times higher resistivity of this paste as compared to high temperature silver paste demand larger volume of printed material to reach good line conductivity, therefore resulting into increased metallization costs. An important challenge for competitive HJT cell production is therefore the reduction of the metallization costs. Two routes are being followed at CSEM to reduce the silver laydown: combining fine-line printing with multiple wires interconnection, or switching to copper plating.

The use of multiple wires interconnection of HJT cells enables to reinvent the cell metallization, by relaxing the constraint onto finger conductivity by more than a factor 10. Fine-fingers can be used, enabling for increased current density (reduced shadowing) and reduced silver laydown without compromising on electrical performance. A production of 1'000 cells with an average of 30 mg of silver for the front side metallization was successfully done at CSEM (see Figure 1) for module integration, yielding no finger interruption and no impact on electrical performance, demonstrating that this approach enables to save up to 85 % of Ag with respect to busbar/ribbon interconnection (with typically 180 mg for front side). Pushing to the limits, bifacial HJT cells with as low as 15 mg silver per side were demonstrated, and ultra-fine fingers with 16 µm printed width and 10 µm height could be printed through ultimate screens with 12 µm openings (see Figure 1). Initial evaluation of copper paste for screen-printing shows further interesting results, with sufficient line resistance achieved for utilization with wire interconnection (see Figure 2). Modules done with such Copper paste metallization could demonstrate < 5 % degradation after 1000 hours of damp-heat and 200 thermo-cycling.

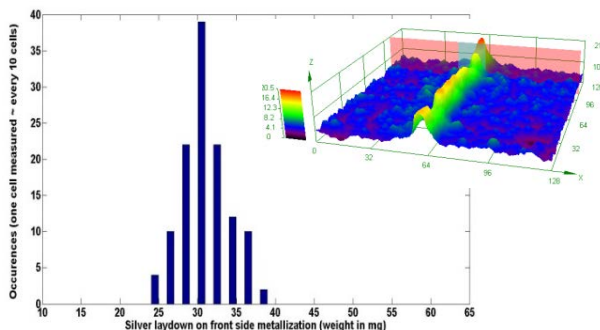


Figure 1: Distribution of silver laydown on front side of 1000 HJT cells (left). Printed silver finger of 20 µm width and 10 µm height (top-right).

The second approach takes advantage of copper electroplating to form the electrical grid; suppressing completely the use of silver while improving the finger conductivity (see Figure 2) and reducing the optical shadowing, as copper-electroplating can enable the fabrication of finer line (down to 8 µm width done at CSEM). Typical width and resistance of copper lines using the developed patterning and plating processes are shown in Figure 2. This metallization enabled performance gain with respect to standard screen printing thanks to reduced shadowing as shown in Table 2 with the increased current generation for busbar-less cells. Implementation in modules was done and long term reliability demonstrated with less than 5 % degradation after 2000 hours of damp heat and 400 thermo-cycles. Thanks to a low finger resistance of plated fingers, the use of 3 busbars design is possible without power losses increase; so that this developed metallization scheme is compatible with standard interconnection technology.

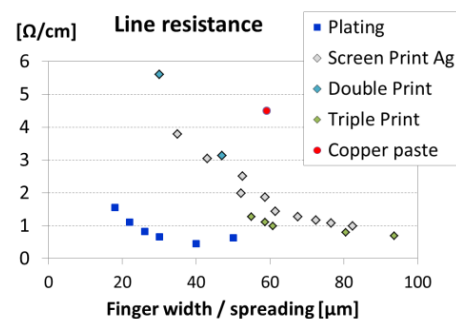


Figure 2: Line resistance versus line width of different metallization.

Table 1: Best cells performance for silver screen-printed and copper-plated cells in busbar-less (Grid Touch) metallization design [1].

HJT CELL	Voc mV	FF %	Jsc mA/cm ²	Eff %
Screen-Printed	735	79.3	38.7	22.6
PLATED NiCu	733	79.2	39.2	22.8

Alternative approaches for metallization and interconnection of HJT cells have been successfully developed in CSEM, with two competitive approaches set up demonstrating performance and reliability: fine-line printing and wire interconnection, and copper electroplating. Further developments on the reduction of indium in the wire for the first approach, and on the reduction of the patterning cost on the second approach are the next steps for further reducing HJT cells metallization and interconnection costs.

[1] A. Lachowicz, et al., Contact Resistance on Plated Silicon Heterojunction Solar Cells, 5th Metallization Workshop, 2014

Platform for High-efficiency Silicon Heterojunction Solar Cells

A. Descoedres, C. Allebé, N. Badel, L. Barraud, J. Champliaud, F. Debrot, A. Faes, A. Lachowicz, J. Levrat, S. Nicolay, B. Paviet-Salomon, L. Sansonnens, C. Ballif, M. Despeisse

CSEM has set up a complete platform for the production and the characterization of monofacial and bifacial both-side contacted silicon heterojunction solar cells, as well as for advanced back-side contacted devices. Innovative and industry-relevant solutions are continuously developed for the improvement of all cell processing steps, aiming for high conversion efficiencies at competitive costs. The technological topics covered at CSEM include wafer bulk quality improvements, wafer texturing and cleaning by wet-chemistry, PECVD depositions of ultra-thin passivating and contact layers, PVD depositions of low-cost and/or high-mobility transparent conductive oxides, advanced cell metallization and cell interconnection processes and various cell characterization techniques. Efficiencies up to 22.8% on industrial full-size 6", screen-printed, both-side contacted cells are demonstrated, as well as, in collaboration with EPFL, 22% back-side contacted cells (European record for such devices to date).

The silicon heterojunction (SHJ) technology is one of the most promising technologies for driving the costs of photovoltaic electricity lower. Compared to standard crystalline silicon solar cells, this type of cells is able to reach higher conversion efficiencies, while being fabricated with fewer fabrication steps at the same time. In addition, thanks to their symmetric structure, SHJ solar cells can easily be integrated in bifacial modules, leading to increased energy yield. Calculations show that, with SHJ solar cells, the average leveledized costs of energy could be below 4 €cts/kWh in sunny countries. These costs are comparable with base-load electricity produced from non-renewable resources.

Since 2013, a strong effort was put to establish a complete, performant and flexible platform at CSEM covering all aspects of production and characterization of such SHJ solar cells, from as-cut wafers to finished devices. This technological platform allows CSEM conducting advanced R&D projects on specific processing steps, to develop new processes, materials and cell concepts, and also to provide services and small batch production for its customers.

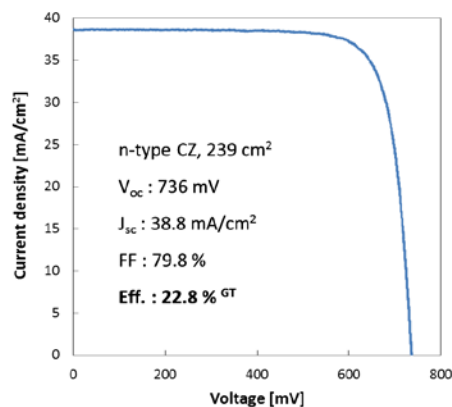


Figure 1: I-V curve of the best full-area 6" CSEM SHJ solar cell (busbar-less, screen-printed metallization, high-mobility TCO, measured with GridTouch).

Concerning the wafer preparation by wet-chemistry, special additives for the texturing baths are developed in-house, and simplification of the wafer cleaning process is also actively pursued. Depositions of advanced functional ultra-thin films by PECVD and ALD are investigated, in order to improve the wafer surface passivation and the carrier transport properties within the cell. The implementation of new high-mobility transparent conductive oxides (TCO) layers in the cells allows improving

their general optical properties. Finally, ultra-fine front metallization applied by screen-printing, stencil-printing, inkjet-printing or plating helps to minimize shadowing and thus improves the generated current. Applying all these developments, a 22.8% efficient large-area SHJ solar cell was fabricated, using industry-compatible processes (Figure 1)^[1].

In addition to classical both-side contacted devices, advanced interdigitated back-contacted (IBC) SHJ solar cells are also being developed, in collaboration with EPFL. In this configuration, the electrical contacts of both polarities are placed at the back side of the cell (Figures 2 and 3), permitting a gain in performance thanks to the complete removal of the front metallization shadowing. Nevertheless, the patterning of the rear contacts induces additional technical challenges. The approach developed at CSEM relies on mechanical hard masking during PECVD for the patterning of a-Si:H layers, and on hot-melt resist inkjet printing followed by wet etching for the patterning of TCO/metal stacks. Being completely photolithography free, this process flow permits to limit the fabrication costs of IBC SHJ cells, and represents a first step towards mass production. The best efficiency obtained so far is 22% on 9 cm² devices^[2], which represents the European record for IBC SHJ solar cells to date.

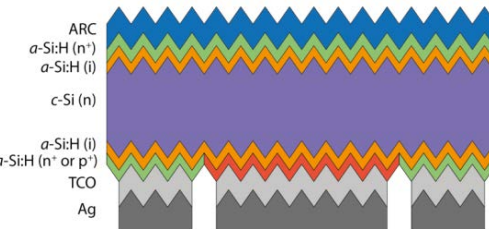


Figure 2: Schematic structure of an IBC SHJ solar cell.

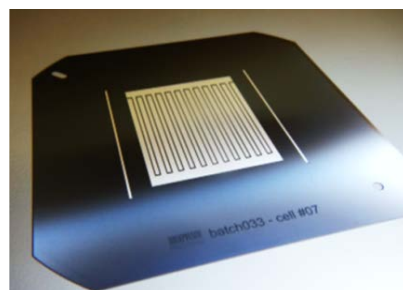


Figure 3: View of the back side of a 3 x 3 cm² IBC SHJ solar cell fabricated at CSEM-EPFL. The interdigitated pattern of the p and n contacts is clearly visible.

^[1] A. Descoedres, *et al.*, Energy Procedia, 77, 508 (2015)

^[2] B. Paviet-Salomon, *et al.*, IEEE J. Photovoltaics, 5, 1293 (2015)

Plastics Compounding Platform and the Formulation Development of PV Module Packaging Materials in CSEM

H.-Y. Li, C. Ballif, L.-E. Perret-Aebi

A compounding platform has been established in CSEM to develop the formulation of plastics for various applications, especially for the packaging materials of the PV modules. This platform opens up not only the possibility to develop reliable, processable and versatile packaging materials to meet the customized demands for special applications like BIPV, but also provides the possibility to study in-depth the degradation mechanism of PV encapsulant and thus to improve the life time of PV modules.

The reliability of PV modules, i.e. their life time, is critical for the further reduction of the levelized cost of PV electricity. A typical PV module mainly consists of front cover, stringed cells and back cover. For the structural integrity, those components are bonded with two layers of adhesive, commonly referred as the encapsulant. These thin encapsulants, normally 0.4-0.5 mm thick, bare multiple important functionalities within the module, like the mechanical bonding, optical in-coupling, UV blocking, water/oxygen barrier, etc. Moreover, their stability under the combinational effects of light, heat and moisture possesses significant impact on the reliability of PV modules [1]. The mostly used encapsulant in the past decades has been based on poly(ethylene-vinyl acetate) (EVA). It has been observed that EVA encapsulants of different grades from different manufacturers exhibit distinct outdoor reliability. The composition of the EVA base resins used therein is often similar, which has 26-32% of Vinyl Acetate. Therefore, the key factor causing the different reliability is the formulation. This is also true for the Polyolefin (PO)-based encapsulant, which is considered as a major alternative to EVA.

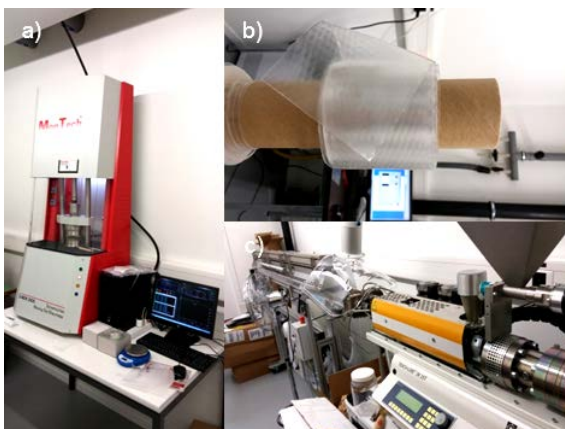


Figure 1: The compounding platform in CSEM. a) D-MDR 3000; b) compounder; c) extruded PO encapsulant.

Given the importance of mastering the formulation of PV encapsulants, CSEM has established a formulation development platform in house, to better serve the needs in various projects related to PV module technology. The platform includes mainly the following facilities (see Fig.1):

- Dr. COLLIN GmbH, TEACH-LINE twin-screw compounder ZK 25 x 24 L/D with co-rotating screws of 25 mm in diameter and 24D in length. Its max. throughput ranges from 0.3 to 4.0 kg/h. It is equipped with a slot die with adjustable opening width and a cooling belt system.

- Inversina 3D tumbler mixer
- Montech Dynamic Moving-Die Rheometer 3000
- Mettler Toledo DSC 1 Differential Scanning Calorimetry
- Chemical analysis facility (e.g. FTIR, GC/LC-MS, Raman, GPC, NMR, ...) partly in collaboration with external partners
- Extensive accelerating lifetime testing facilities: climate chambers to implement tests like damp heat, thermal cycling, humidity freeze, etc.; climate chamber with one-Sun irradiation to perform the test of UV+ damp heat; UV chamber; Ovens; highly accelerated damp heat testing setup (high-pressure cooker test)

Moreover, supply channels of base resins and additives have been built with multiple national and international chemical companies.

The compounding platform in CSEM can steadily extrude packaging foil of 0.1 to 2.5 mm thick with the maximum width of 12 cm. Extrusion processes have been developed for common grades of EVA and PO base resins for PV application.

At the moment, the compounding platform is supporting a few projects (internal, industrial and CTI). The examples of the applications are specified as following:

- Colourful PV-grade EVA encapsulant for applications in the BIPV field. Here the colour, stabilization and crosslinking additive packages are optimized for the selected EVA base resins to develop an encapsulant compatible with the building norms.
- PO-based packaging material for advanced PV module solution. Here besides the optimization of additive packages, the selection of a proper PO base resin with desired material properties (optical, rheological, UV stability, adhesion, ...) is critical for its processability and module reliability.
- Degradation mechanism study of PV encapsulants. Here with the capability of adjusting the material composition, it is possible to investigate the degradation mechanism of the encapsulants, especially for EVA. One focus is to understand the mechanism behind the yellowing and acetic acid production in EVA encapsulant under different environmental conditions.

Furthermore the expertise on the packaging material analysis has also been developed within the platform.

[1] H.-Y. Li, "Open the black box: understanding the encapsulation process of photovoltaic modules", Ph.D dissertation, EPFL 2013

Optimization of Quality of Supply in Demand-Response Schemes

P.-J. Alet, L. Bally, A. Hutter, C. Ballif, L.-E. Perret-Aebi, E. Olivero

Within the SEMIAH European project, CSEM is developing models to assess the available flexibility in power usage from home appliances and to optimize the quality of supply. Demand response can be used to mitigate some of the local issues associated with distributed power generation, which have been identified through measurement campaigns, as well as to provide power management services to distribution network operators. This capability opens business opportunities for demand-response schemes beyond trading on wholesale electricity markets.

The SEMIAH consortium is developing a demand-response (DR) framework based on the aggregation of the flexibility which is available at the household level. The purpose of such systems is to provide additional flexibility to the power system so that demand and production can be matched at all times without relying on expensive and polluting peaking power plants. Flexibility needs in the power system increase with the increasing use of variable, weather-dependent renewable power sources such as wind and solar power. Demand-response services can be monetized on wholesale electricity markets, through the market for ancillary services, or by providing savings to network operators or prosumers.

At the heart of demand-response systems lie forecasting and optimization algorithms to balance multiple objectives and constraints: user comfort, financial gains, regulatory constraints, etc. CSEM's contribution to the project focuses on two aspects: the modeling and forecasting of the flexibility that household appliances can provide, and the definition and validation of rules ensuring that the demand-response system maintains or improves the quality of supply.

In a first phase, CSEM investigated the number of households required to guarantee a minimum level of power reserve for tertiary control. Appliances in scope were white goods: washing machines, clothes dryers, and dishwashers.

For this purpose, a stochastic model of a typical user's consumption profile was developed based on measured data from a test site in Valais. The model was then used as load estimator and was integrated in a simulator to estimate the total load curve for a group of households. The number of households required to provide 5 MW tertiary control power was then evaluated with various time constraints for load shifting. The results are shown on Figure 1. Finally, a first scheduling strategy for load shifting was proposed.

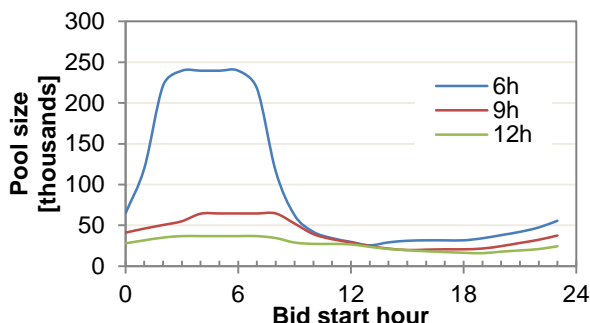


Figure 1: Minimum pool size to provide 5 MW of tertiary control power as a function of the hour at which the capacity is guaranteed (bid start hour) and the maximum shift in switch-on time (6 h, 9 h, 12 h).

While there are studies on the impact of demand response on overall system stability, few publications report on the local impact of DR systems on power quality. Yet local impacts can appear even in pilot stages, whereas system-wide disturbances are only likely to occur at high levels of deployment.

The major risks in low-voltage distribution networks which are relevant for a DR aggregation framework were then identified. The main risk from DR itself is current levels rising above the rating of transformers and lines, as already experienced with ripple control. Risks from distributed generation which can be managed with DR are reverse power flows and overvoltage. This assessment was validated through high-resolution power quality measurements on feeders with high PV penetration. Reverse power flows to the medium-voltage level at a transformer serving one of these feeders were indeed regularly observed between April and September (Figure 2).

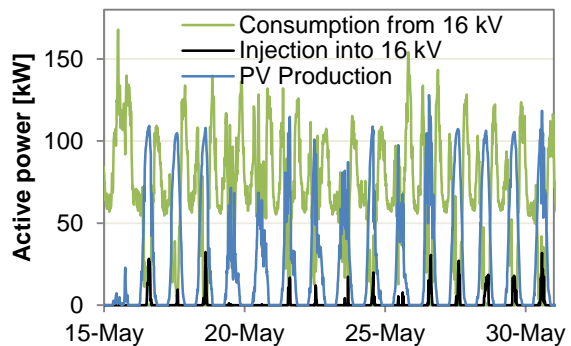


Figure 2: Net power consumption and injection from the low-voltage (seven feeders) to the medium-voltage level, and the production of a 145 kW_p PV system connected to one of the feeders.

Electrical sensing capabilities in the SEMIAH framework are limited to energy and exclude voltage or reactive power measurements. As a result, we formulated constraints for the scheduling algorithms which can operate solely on active power. In the next phases of the project, these formulations will be validated through modelling under Digsilent PowerFactory of SEMIAH's test sites and benchmark feeders.

The partners in the SEMIAH consortium are: Aarhus University (DK), Develco (DK), Misurio (CH), Netplus.ch (CH), Agder University (NO), Fraunhofer IWES (DE), CSEM (CH), HES-SO (CH), Devoteam (NO), Agder Energi (NO), SEIC (CH), and Enalpin (CH).

We thank Fabian Schmidhalter (Enalpin), Raymond Zuber (EVWR), Jürg Pargätsi (Parmeltec), and Camilla Seland Ellefsen (Agder Energi) for their support in the collection of power quality data.

The project has received funding from the European Union under the 7th Framework Programme (grant agreement number 619560).

Design and Control of DC Microgrid for Integrating PV in Built Areas

V. Musolino, L.-E. Perret-Aebi, C. Ballif, P.-J. Alet

Massively integrating PV in built areas raises both challenges for power quality and opportunities to solve them by local energy management. With photovoltaic generation, storage systems, and an increasing number of loads natively operating in direct current (DC), interconnection of this equipment in DC with a single interface to the AC grid opens new ways to locally manage power quality. Our approach, which is based on decentralized control, is particularly suitable for use in commercial or industrial buildings.

High penetration of photovoltaics in the power system raises several issues for the quality of supply due to fundamental differences between PV and conventional generation. The combination of weather-dependent fluctuations with the decentralized nature of PV creates issues for local power quality. Indeed, large up or down ramps of power can create rapid voltage variations in the distribution grid.

For PV to be systematically deployed on buildings, these power quality issues need to be dealt with. An opportunity is provided by the combination with local loads. In particular, more and more electric loads in buildings are either natively powered in DC (LED lighting, computing equipment, televisions, etc.) or have a DC stage in their power supply (variable-speed drives as used in energy-efficient appliances such as inverter heat pumps). Since both PV and battery storage are native DC components, DC interconnection within a building can reduce the number and complexity of power converters, and increase energy efficiency. Gains of 2% to 8% have been demonstrated^[1, 2].

The novelty of our approach consists in using this interconnection not only to increase energy efficiency but also to manage power quality. The proposed structure is shown on Figure 1. In this structure, the DC microgrid has a single interface to the larger AC grid: a bidirectional inverter. Whereas most microgrid approaches rely on a communication layer, here all the information on the status of the system is represented by the voltage on the DC bus. All PV generators are set to operate at their maximum power point and loads operate freely so any control can only be effected on the storage converter or on the bidirectional inverter.

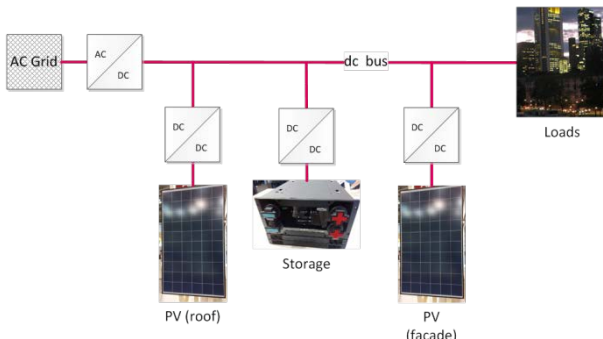


Figure 1: General architecture of a building DC microgrid without communication layer.

The coordination between the two controls is defined at the design stage; in operation, they operate independently based

[1] D. Fregosi, *et al.*, "A comparative study of DC and AC microgrids in commercial buildings across different climates and operating profiles," in 2015 IEEE First Int. Conf. DC Microgrids ICDCM, pp. 159–164 (2015)

on the local voltage. The main questions were whether voltage levels could be simultaneously managed on the DC and AC sides, and how much storage would be necessary.

Both the storage converter and the inverter use a proportional-integral (PI) controller based on the measured DC bus voltage and, for the storage controller, the state of charge. Parameters of the storage controller were set first for maximum responsivity to voltage fluctuations on the DC bus. Then three sets of parameters were defined for the inverter control, each leading to a different dynamics but all at least one order of magnitude slower than the storage controller.

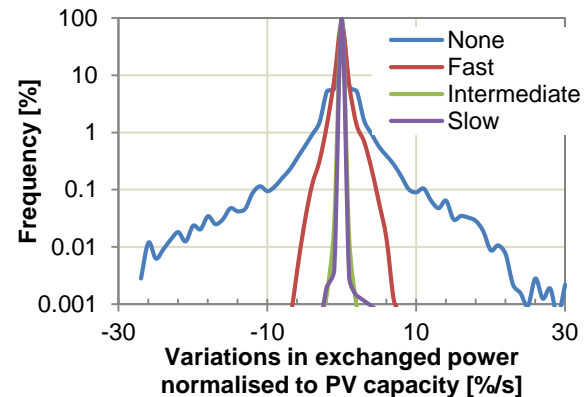


Figure 2: Power ramp rates at the interconnection with the AC grid as a function of the control applied on the bidirectional inverter.

With the "intermediate" control on the inverter, modeling with realistic grid parameters and measured load and solar irradiance shows that both DC and AC voltage levels can be maintained within $\pm 10\%$ of their nominal values. As shown on Figure 2, with this control the maximum ramp rates are divided by 15 as compared to direct power exchange without control. To achieve this outcome, a storage capacity equivalent to 40 min of PV production at nominal power is necessary. Dynamic battery technologies such as lithium-based ones are therefore best indicated for this purpose.

The modeling results have been obtained with data for a tertiary building with a 100 kW_p PV system. Indeed the potential impact of such systems on the grid, the local availability of loads, and the structured maintenance of their electricity infrastructure make them prime targets for using this approach of DC microgrids.

This project has received funding from Neuchâtel city authorities. We thank them for their support.

[2] U. Boeke, M. Wendt, "DC power grids for buildings," in 2015 IEEE First Int. Conf. DC Microgrids ICDCM, pp. 210–214 (2015)

Electrical Energy Optimization at District Level

Y. Stauffer, S. Arberet, M. Boegli, E. Onillon

The goal of the European project AMBASSADOR is to look for technological strategies to optimize the electric energy usage at district level. The proposed optimization aims at reducing the operational costs (i.e. global electricity bill) by taking into account all electric power generators and consumption elements of the districts and taking advantage of storage elements. In order to reach that goal, model predictive control (MPC) is applied. The latter relies on adaptive models that predict the energetic behavior (production and/or consumption) of the various elements. Extensive simulations were carried out under various simulation conditions and showed that significant savings can be achieved.

AMBASSADOR is a 48 months FP7 project that started in December 2012. It is coordinated by Schneider Electric and is composed of 15 partners from different European countries. The project's main objective is the reduction of exploitation cost of districts by maximizing the benefits linked to renewable production and storage. The emphasis is put on electrical flux management at district level. The cost reduction is achieved by exploiting the flexibility of the district. In the current context, the flexibility relies on storage elements such as batteries.

The district optimization is performed by DEMIS (District Energy Management Information System). Input to DEMIS are the predicted consumptions and productions of all district elements. These values are forecasted by the controllers of the various elements of the district, which are also called eNodes. In addition, DEMIS is running its optimization procedure aiming at reducing the costs by using the available batteries and their usage level in an optimal way. Once the best solution is found, the command signal is sent to the storage elements. This is illustrated in Figure 1.

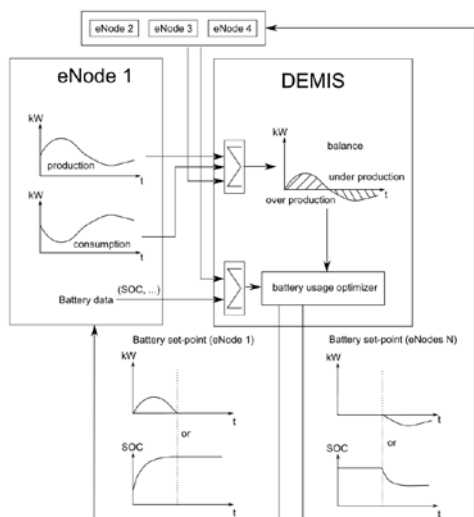


Figure 1: Ambassador district optimization procedure overview.

In the context of AMBASSADOR, eNodes for the following elements were developed and simulated:

- Wind turbines
- Photovoltaic panels
- Consumers (offices, villas and public lighting)

These eNodes are able to forecast the production/consumption of the corresponding system by using the available information,

such as weather forecast and time. All these eNodes rely on adaptive models that are continuously trained by minimizing the difference between the measured value and forecasted value. Forecasting results for a wind turbine are provided in Figure 2.

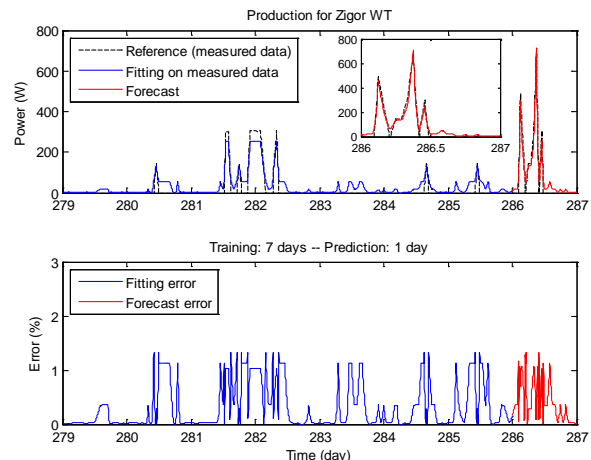


Figure 2: Wind turbine production, measurement and forecast (top) and relative error between the two values (bottom).

A validation of the district optimization concept was carried out under various simulation conditions:

- District size (ratio between consumption and production)
- Electricity tariffs (variable selling and buying tariffs)
- Different storage element sizes
- Allowing or preventing the usage of grid energy (i.e. not produced within the district) to load the storage elements

The benefits of the battery optimization (compared to the scenario to not using any battery at all) are maximal when:

- ratio between production and consumption is close to one;
- the battery size is large enough to cover one day of consumption
- tariffs are time-varying
- buying and selling tariffs differ

On a test site, where most of the above criteria are fulfilled, the simulation study point to a cost reduction of up to 80%. In very unfavorable cases (i.e. none of the above criteria is fulfilled), the benefits of optimizing the battery usage can drop drastically^[1]. In order to confirm the above mentioned simulation results, the deployment of DEMIS is foreseen on a Greek test site by the end of 2015.

^[1] Y. Stauffer, S. Arberet, M. Boegli, Centralized energy optimization at district level, Energycon 2016, submitted

Adaptive and Predictive Air Conditioning Control

Y. Stauffer, S. Arberet, E. Olivero, L. von Allmen, E. Onillon

The control of the hygro-thermal conditions within private and public buildings to maintain optimal user comfort is contributing to one third to the total energy consumption in Switzerland according the Analysis Report of the Swiss Federal Office of Energy. It also directly impacts the global carbon dioxide (CO_2) emissions and the user's energy bill. Given the ever increasing energy consumption and challenging objectives in terms of CO_2 reduction, there is an urge to minimize the energy linked to the hygro-thermal regulation without compromising user comfort. The objective of the project NeuroCool, is to drive the air handling unit in an efficient way that minimizes the exploitation costs and satisfies user comfort.

Two parallel trends exist in order to reduce the energy consumed for HVAC (heating, ventilation and air-conditioning). The first consists in retrofitting the building by, typically, replacing windows, insulation and other elements of the building structure. Even the impact of these retrofitting measures on the building structure is considerably reducing the energy consumption, the associated costs are high and the payback time often exceeds 10 years. The second approach consists in replacing the standard HVAC controller with a more efficient controller. The latter option can take advantage of weather forecasts and building characteristics in order to find an optimal heating or cooling strategy that minimizes the exploitation costs while maintaining user comfort. This option only requires the installation of a minimal set of additional sensors and the adaptation to an increased computational power, leading to shorter payback time than with the retrofitting option.

NeuroCool is a 24 months CTI project with Neurobat AG as industrial partner and the HEIG-VD and CSEM as research partners. NeuroCool is a novel Model-Predictive Control (MPC) based algorithm for HVAC^[1]. The algorithm relies on a self-adaptive data-driven model of the building hygro-thermal behavior which is used to predict the temperature and humidity in the building as a function of excitations that include the pulsed air (temperature, humidity and flow) and the weather (temperature and solar radiation). The model is used by the optimization procedure to guarantee that the indoor conditions are kept within the European norms in terms of zone temperature and humidity. The optimization procedure also takes into account the costs associated with heating/cooling and (de-)humidification in order to find the most cost efficient solution.

In the frame of this project, three test sites^[2] have been equipped with the developed solution: i) a climatic chamber facility at the HEIG-VD, ii) two tests rooms at CSEM facilities, and iii) one administrative building in Winterthur. The two first test sites have been modelled in Matlab-Simulink and extensive simulations under various climatic conditions and comfort settings have been carried out. For the CSEM facilities, simulation results are shown in Figure 1. The simulation conditions have been set to 100 days starting in June and with different comfort settings. The comfort is controlled by adjusting a weighting factor λ in the optimization loop. This factor controls the weighting between energy and comfort. The plot highlights

the energy consumption (kWh) and comfort (PMV, as defined in^[3]) for different values of λ . A perfect comfort corresponds to a PMV of 0. Note that if the comfort boundaries, as defined by the European norms, are respected, the PMV is comprised within -0.5 and 0.5. Figure 1 shows that the comfort can be controlled by adjusting (i.e. reducing) λ . As expected, lower comfort levels result in decreased energy expenditure.

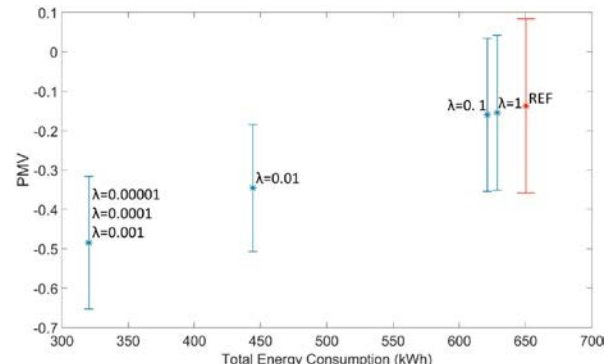


Figure 1: Simulation results for CSEM test facilities with comfort (PMV) versus energy consumption (kWh). NeuroCool (in blue), and standard controller (in red). For NeuroCool, different comfort settings are provided.

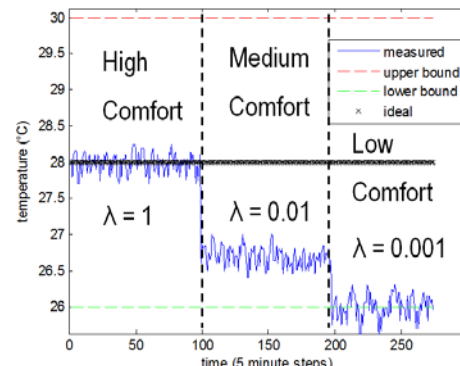


Figure 2: Test site facility results from HEIG-VD: the measured room temperature as a function of time is displayed for different comfort settings.

Preliminary test results from the HEIG-VD facilities are shown in Figure 2. As validated during the simulation study, various comfort levels can be achieved by controlling the weighting factor λ . Furthermore, stable operation is obtained even under unfavorable operating conditions. Deployment on the two remaining test sites are being undertaken in 2015 and detailed results will be provided with the end of the project in 2016.

[1] Y. Stauffer, et al., Neurocool: an adaptive, model-predictive control algorithm for ventilation and air conditioning systems, Clima 2016, abstract accepted

[2] Y. Stauffer, et al., Neurocool: field tests of an HVAC control algorithm, Clima 2016, abstract accepted

[3] ANSI/ASHRAE Standard 55-2010, Thermal environmental conditions for human occupancy

SYSTEMS

Jens Krauss

During the last decade the Systems research program has evolved from a project-oriented systems engineering approach into an application-oriented, interdisciplinary research program with an emphasis on the integration aspects of microsystems and of microelectronics technologies. In parallel, the Systems research program has become a pillar of CSEM's mission of transferring its technologies to industrial partners, preferably in Switzerland, and has interacted significantly in recent years with all the other CSEM research programs. Interaction with the other technology-oriented research programs—MEMS, ULP, and PV—has in particular been further intensified, leading to an unprecedented level of joint effort in CSEM's research strategy on topics such as compliant, hybrid micro-mechanisms (macro-MEMS); power-efficient, portable medical monitoring devices (wearable technologies); and energy-efficient building systems (smart grids). The collaboration within these multi-disciplinary research topics requires a great deal of coordination across disciplines and comprises the identification and development of new methods and modelling techniques. These methods make possible a better understanding of engineering systems as they grow more complex, and specifications as they tend toward physical limits. And in today's connected world, the role of system integration is becoming more and more important because the aggregation of different system components and subsystems is designed to cooperate and deliver the targeted functionality. Thus, the common denominator of the application-oriented Systems research program is system integration, and special emphasis is placed on applications that are demanding in terms of resource limitation (processing power), reduced power consumption, miniaturization, precision, reliability, comfort, production costs, and environmental conditions.

The most important aspects of the systems engineering activities at CSEM are their focus on the development of new and innovative micro- and nanotechnologies and the fact that they take into consideration all aspects of the lifecycle of the system, including manufacturability, installation, operations, maintenance, repair, and the disposal of a system. Systems engineering has always been situated at the end of the development cycle and at the interface between technology transfer and proof of full compliance with system-level quality assurance, risk assessment, and evaluation, as well as audited design, development, and test documentation. As a consequence, strict project management criteria are already applied during the early design and development phases, and the Systems research program has been certified according to the ISO-9001 and ISO-13485 quality standards, the latter certification concerning the strategy for further strengthening our research activities in the medical device technology domain. Our vision for the Systems research program is to promote innovative technologies and product concepts in (1) *Medical Device Technology*, (2) *Automation*, and (3) *Scientific Instrumentation*—application fields in which Switzerland has a well-proven competitive, industrial, and technological lead.

Long-term objectives

The *Medical Device Technology* research activity ranges from innovative sensing technologies for monitoring human vital

signs to bio-signal processing and active medical device technologies. Our aim is to create personal profiles by developing personalized diagnostic and trend-detecting algorithms. The major technological challenge is to operate these diagnostic algorithms so that personal sensor signals can be analyzed to give a reliable diagnosis of the health status of the person—so called personal, on-body biofeedback systems. Future monitoring systems will rely on greater miniaturization techniques with regards to sensor electronics and active medical devices. Our applied research activities aim at strengthening our know-how in biomedical engineering to encompass a broad range of disciplines, including the physics of environmental phenomena, sensor behavior, human motion, body size, ergonomics, manufacturability, and computer architecture, as well as wireless low-power and low-range communication.

The *Automation* research activity is focused on developing technologies for enhanced manufacturing and process flexibility, making high quality products in small to medium volumes possible. The activity aims to drive the competitiveness of easy-to-use automated solutions with facilitated man-machine interaction and eco-friendly production processes. The technologies we develop are designed around process and measurement solutions that lead to an optimum balance between flexibility, autonomy, and throughput including task programming and efficient processes. We put special emphasis on Industry 4.0 and the system efficiencies that result from integrated, advanced sensory feedback.

Our *Scientific Instrumentation* research activity targets complex multi-technology systems that involve multiple physical layers. Our main goal is to further evolve CSEM's competences in the design, simulation, development, and testing of complex, miniature, hybrid, precision systems into ever more applications in more and more branches of industry. These systems' complexity is emphasized by significant miniaturization and limited available resources in terms of energy, computing power, and space. Moreover, rapid progress and rising ambitions in terms of scientific instrumentation—calling for large numbers of ever-smaller and smarter mechanisms—have encouraged CSEM to invest further in this research domain. This puts us in a position to meet coming demands in the fields of astrophysics, space exploration, and watchmaking, as well as metrology and industrial instrumentation.

With the Systems program we coordinate our expertise across multiple research fields, including sensing and actuating, signal processing and control engineering, high-precision mechanisms and instrumentation, low-power electronics and software engineering, biomedical engineering, and automation. The application-driven synergies between these research domains, together with our competences in systems engineering and systems integration, are the key success factors of the Systems program, and its aim of offering new and innovative product concepts to our customers.

Highlights

The Systems research program has considerably increased its impact and technology portfolio during recent years. As per our mission to create high-tech businesses—Swiss where possible—the industrial impact of our research activities has been proven by the successful transfer of a dozen technologies to Swiss and foreign industry, and by the delivery of several key, micro-mechanical subsystems for space missions and for major astrophysics projects such as the telescopes at KECK and SOFIA. The expansion of our technology transfer activities has resulted in an increase in the head count within the Systems research program over recent years, across all three of our application-oriented research activities. The research teams of the Systems program maintain and valorize an IP portfolio of roughly 70 patents, and successfully execute—each year—more than a hundred applied research and development projects. Collaboration across all CSEM research programs has been further intensified during recent years, contributing to the following highlights from the last reporting period.

CSEM's *Medical Device Technology* research activity has a proven track record in transferring its core technologies to the Swiss medtech industry. Product development and industrialization have been successfully carried out in the health promotion domain with the privately funded start-up Actismile AG (www.actismile.ch), in the care-for-the-elderly domain with the privately funded start-up Limmex AG (www.limmex.ch), in the sports domain with the privately funded start-up SenseCore AG (www.senseyourcore.com), in the medical domain with the privately funded start-up Swisstom AG (www.swisstom.com), and in the fitness domain with the privately funded NOKIA spin-off PulseOn Oy (www.pulseon.com). It is also worth mentioning that Finland's PulseOn Oy also opened a subsidiary in the Canton of Neuchâtel during the last reporting period in order to reinforce its R&D teams, and won the Red Herring Award 2015—being ranked as Europe's most valuable start-up. Collaboration with a range of Swiss and foreign medtech companies on dedicated product development has been further intensified. A major highlight in 2015 was the collaboration with the American company ICON Fitness & Health—a perfect match for CSEM's mission to generate high-tech business within Switzerland. By the end of 2015, ICON Fitness & Health had launched—under its brand, iFIT—half a dozen new sports and smartwatches. Not only do these watches rely on CSEM's core technology for human vital sign sensing and on the center's miniaturization competences, some are being manufactured, assembled, and shipped by Swiss watchmaking industry partners—an ideal valorization of CSEM technologies along the value chain.

The *Automation* research activity develops innovative technologies that are designed around process and measurement solutions that lead to an optimum balance between flexibility, autonomy, and throughput—that is to say, ease of use, including task programming and efficient processes. The continued need for flexible manufacturing solutions is supported by the statistical department of the International Federation of Robotics (IFR), which has estimated a further growth in robot installations for 2014-2016 of 6%, on average, per year. The strong demand for automation solutions will create significant opportunities for Swiss (and foreign) companies, even more so if they succeed in expanding into

higher-value business sectors. Apart from the primary focus on flexible manufacturing systems and solutions, our different technology platforms are also exploited individually, including for system- and process-monitoring solutions, quality inspection, actuators and self-learning, or adaptive systems. A major highlight during the last reporting period was the successful completion of the European research project MegaRob with the implementation of a real-time external position measurement within the internal closed-loop control of an industrial robot. The resulting MegaRob technology makes it possible to overcome the limited absolute positioning accuracy of industrial robots and enables precision manufacturing tasks for large parts.

The *Scientific Instrumentation* research activity pursues its development efforts with flexure-based micro-mechanisms and miniature atomic clocks. The steadily increasing demand for CSEM's micro-mechanism devices has been confirmed by the launch of several large science mission projects. In this context—and in large part due to CSEM's 30 years of expertise in the design, simulation, realization, and testing of active precision opto-mechatronics systems based on compliant structures—CSEM secured, back in 2013, a major contract with Thales Alenia Space France (TAS-F) to provide instrumentation for a new generation of meteorological satellites. This contract will also benefit the several Swiss SMEs selected for specific manufacturing and assembly operations and other Swiss partners including RUAG Space in Nyon and Almatech in Lausanne. An entire network of smaller local companies and machine shops, such as Arcofil in St. Imier, will also benefit through subcontracts. Unsurprisingly given our heritage and the importance of the watchmaking industry in Switzerland, one of the major *Scientific Instrumentation* research topics is the hybridization challenges of silicon-based compliant components in high precision micro-mechanisms on the macro scale—so called macro-MEMS. Our expertise in “flextec” design is further enhanced by the activities of the MEMS research program and the focus is placed on the development of new, innovative mechanical components for watches. In this sense, CSEM offers—thanks to the excellent collaboration between the center's research teams—a unique environment in which to develop, fabricate, integrate, and characterize macro-MEMS components. The exceptional mechanical characteristics and precision of silicon watch components were proved with CSEM's proprietary and unique silicon mechanical regulator *Genequand*, which was announced by CSEM, together with our commercial Swiss partner Vaucher Manufacture Fleurier (VMF), on the occasion of the Swiss Society of Chronometry Conference in 2014. The Genequand regulator was invented, designed, developed, industrialized, and manufactured at CSEM, and outperforms existing products since there is no friction and no pivots, and since no lubrication is necessary for this mechanical regulator to run. The presented prototype, integrated within a VMF mechanical movement, needs to be wound only every 30 days, which makes it six times more efficient than the traditional Swiss anchor escapement. The Si-based compliant micro-mechanisms involved will, in the future, open new opportunities to improve the quality, reliability, precision, functionality, and energy consumption of mechanical watches.

Validation Results of the Long-term Medical Survey System (LTMS-S) for Antarctica

D. Ferrario, A. Falhi, J.-A. Porchet, R. Rusconi, O. Grossenbacher, M. Proen  a, R. Delgado-Gonzalo, J. Sol  , J. Cosandier, O. Ch  telat, C. Sartori •, N. della Ricca •

Since 2002, CSEM has been working for the European Space Agency (ESA) to develop and manufacture a system to study the adaptation of crewmembers in space analogues (like Concordia in Antarctica) in order to prepare future long-term manned missions. The latest project LTMS-S had the objective of extending the monitoring capabilities of CSEM's cooperative sensors with pulse oximetry and core body temperature (CBT), and to clinically validate the accuracy of the monitored signals.

LTMS-S is a new wearable system for the monitoring of several physiological signals – including a two-lead electrocardiogram (ECG) – and parameters, such as heart rate, breathing rate, peripheral oxygen saturation (SpO_2), core body temperature (CBT), and physical activity. As illustrated in Figure 1, all signals are measured using only three sensors embedded in a vest. The sensors are standalone with their own rechargeable battery, memory, wireless communication and with an autonomy exceeding 24 hours.



Figure 1: Overview of LTMS-S monitoring capabilities.

An important part of the project was devoted to the verification and clinical validation of the system. The LTMS-S electronics successfully passed the safety tests as well as the ECG performance tests of the international medical standards 60601-1 and 60601-2-47.

After approval of the ethics committee of the canton of Vaud (ref. CER-VD protocol 268/13), two protocols were performed at the HNE (Neuch  tel hospital) to evaluate the accuracy of the LTMS-S sensor against gold standard devices. The first one addressed the circadian rhythm that was evaluated by monitoring twenty healthy subjects in a closed environment during 24 hours. In the second protocol, 15 healthy subjects performed several activities while normobaric hypoxia was induced.

The statistics of the resulting performances are presented in Table 1. A more detailed version of the results was presented at EMBC 2015 [1].

- Centre Hospitalier Universitaire Vaudois (CHUV), Switzerland
- H  pital Neuch  telois (HNE), Val-de-Ruz, Switzerland

No significant difference was found between heart rate and activity class estimated by LTMS-S and the corresponding references, respectively the Polar RS800CX and a manual segmentation. The results obtained for breathing rate are slightly below the 95% that would consider the systems as equivalent. However, the comfort brought by the LTMS-S in comparison with the reference device (MetaMax), which requires the subject to wear a mask, is undeniable and should in most applications compensate the slight loss of accuracy.

Table 1: Summary of LTMS-S performances (mean \pm std. dev.).

Parameter	Evaluation criteria	Performance
Heart rate	Time percentage in ± 5 bpm	96 \pm 7.2%
Breathing rate	Time percentage in ± 3 rpm	92.5 \pm 4.6%
Activity class	Time percent. of correct class	98 \pm 0.3%
SpO_2	Root mean square error on all data points	3.7 \pm 0.9%
	Root mean square error after automatic rejection of unreliable signal	2.7 \pm 0.8%
CBT	Correlation	r=0.7, p=0
	Root mean square error	0.22 °C

The accuracy obtained with the SpO_2 sensor is within the requirements of ISO 80601-2-61 (<4%). Moreover, an unsupervised quality index algorithm was implemented increasing SpO_2 sensor performances from 3.7% to 2.7%, while rejecting 37% of the data automatically recognized as unreliable. Finally, the analysis showed a good agreement (r=0.7) between LTMS-S CBT and the ingestible temperature-sensor pill indicating that for the implemented conditions, the LTMS-S sensor was able to track circadian CBT variations.

This validation shows that the LTMS-S system can accurately monitor a large number of physiological parameters. Combined with the comfort of a vest, this system offers new opportunities for the monitoring of patients and athletes.

The financial support of the European Space Agency to the LTMS-S project is thankfully acknowledged.

[1] O. Ch  telat, et al., "Clinical validation of LTMS-S: a wearable system for vital signs monitoring", 37th Annual International Conference of the IEEE Engineering in Medicine and Biology Society—EMBC2015, Milan (IT), 25–29 August 2015

ECG12CS—12-lead ECG Monitoring System with Cooperative Sensors

M. Rapin, O. Chételat, C. Meier, J.-A. Porchet, J. Wacker, A. Falhi, A. De Sousa, M. Frosio, R. Rusconi

The goal of ECG12CS is to implement a wearable 12-lead electrocardiogram (ECG) monitoring system with dry electrodes. The system also fulfils international medical standards in terms of safety and signal quality. To that end, the system uses cooperative sensors. Cooperative sensors are a novel electronic architecture based on active electrodes that allows the acquisition of biosignals (e.g., ECG, electroencephalogram, bioimpedance, etc.) on patients in a comfortable and easy-to-integrate manner. One advantage of this technology developed and patented by CSEM is the extremely simple connection requirement that makes the sensors easy to integrate in a vest or any other garment.

In recent years, many different wearable sensor systems for measuring ECG have been developed and placed on the market. First sensor designs were relatively bulky (centralized electronics box, cumbersome connectors, shielded cables, etc.) and required the use of gel electrodes to get signals of best quality. Today, however, there is an increasing demand for systems which can be comfortably worn in daily life [1]. One of the main challenges in the development of such systems is the size and weight reduction of its elements. Additionally, the integration (in particular the cabling) of the sensors in a wearable monitoring device should be simple from a manufacturing and usage point of view.

Figure 1 shows the novel electronics architecture developed by CSEM (patent pending) for a 12-lead ECG monitoring system. This architecture includes one guard sensor and nine measuring sensors. Each measuring sensor measures the biopotential (e.g., ECG) at its specific location (measured as v_0 to v_8). All voltage measurements are referred to the same voltage potential picked up on the measurement wire (*meas. wire* in Figure 1) and controlled by the guard sensor thanks to the voltage source v_{cm} . By controlling this common mode voltage it is possible to compensate external electromagnetic noise. As a consequence external wires (*meas. wire* and *comm. wire*) do not require any shielding to get signals of best quality [2], even in an electromagnetically noisy environment, which is one of the main advantages of this novel architecture.

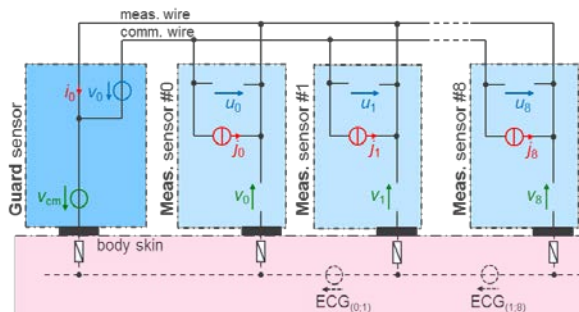


Figure 1: ECG12CS circuit with 1 guard and 9 measuring sensors.

Since ECG signals (measured at v_0 to v_8) are locally amplified and digitized in each measuring sensor, a duplex communication between sensors has been implemented to allow centralized data management (e.g., storage) in the guard sensor. To allow this duplex communication, a second wire is

used, namely the communication wire (*comm. wire*). This wire links together all sensors and is in parallel with the *meas. wire* (see Figure 1). For the communication between the guard (communication master) and measuring sensors, the guard sensor sends small voltage impulses with v_0 . These impulses are sensed by other sensors as v_0 to v_8 . The communication in the other direction is performed with small current impulses generated by j_0 to j_8 which are sensed as i_0 by the guard sensor. Since the current sources j_0 to j_8 are in parallel, each measuring sensor communicates in turn with the guard sensor to avoid current overlap [3].

A 12-lead ECG configuration including the guard sensor and nine measuring sensors is shown in Figure 2 (up left) as well as the final implementation of a measuring sensor (up right). Each sensor has its own electronics and power supply (e.g., a rechargeable battery). External wires (*meas. wire* and *comm. wire*) are two non-shielded conductive wires simply knitted in the garment and attached to sensors via snap buttons. These two wires are also used when the garment is not worn to simultaneously recharge all sensors without having to remove them from the garment.

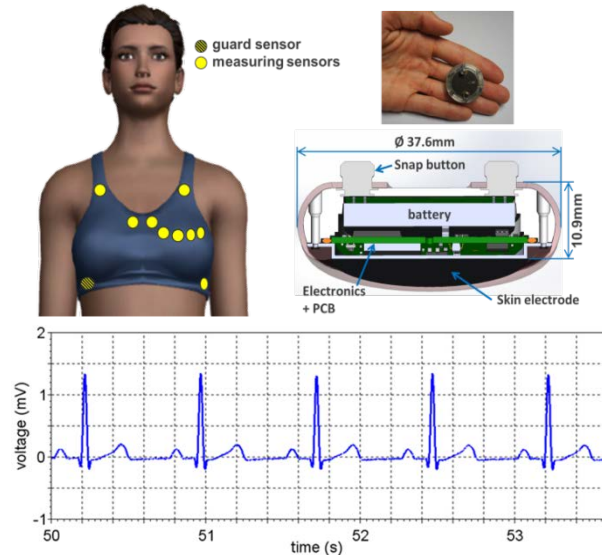


Figure 2: Sensors placement for a 12-lead ECG monitoring system (up left), final implementation of a measuring sensor (up right), and acquired ECG (from simulator) showing that the communication between sensors does not interfere with the measured signal.

[1] Y. L. Zheng, *et al.*, "Unobtrusive sensing and wearable devices for health informatics", IEEE trans. on biomed. eng. 2014, 61(5), 1538-54

[2] M. Rapin, *et al.*, "Cooperative dry-electrode sensors for multi-lead biopotential and bioimpedance monitoring" Physiol Meas. 2015 Apr. 36(4), 767-83

[3] M. Rapin, *et al.*, "Cooperative sensors: a new wired body-sensor-network approach for wearable biopotential measurement", MobiHealth Conference, London (GB), October 14–16, 2015

Activity-specific Step Counting and Energy Expenditure Models using 3D Wrist Acceleration

R. Delgado-Gonzalo, P. Celka, P. Renevey, S. Dasen, J. Solà, M. Bertschi, M. Lemay

CSEM developed a new physical activity profiling toolbox embedded in a wrist-located device. This toolbox includes step counting and energy expenditure models. Their performances, according to gold-standard validation, provide a significant improvement over the state of the art (total EE relative error of 5.5% against 26.8% for ActiGraph GT1M®) and represent a step forward for most of commercial wellness and training wearable devices.

Originally used by sports and physical fitness enthusiasts, pedometers are now becoming popular as an everyday exercise monitor and motivator (e.g. a total of 10'000 steps per day for an active lifestyle [1]). Because the distance of each person's step varies, a user-dependent calibration is usually required if presentation of the distance covered is desired (odometer). In the latest trends, step counters are being integrated into an increasing number of portable consumer electronic devices such as music players and smartphones. Energy expenditure (EE) measurements are important indicators to consider for the estimation of physical activity in combination with the energy intake to keep the body weight stable. The most used EE estimated methods are detailed activity/food diary, isotopic measurements, and direct and indirect calorimetry methods. Due to their cost, technical difficulties, or infrastructure requirements, none of them is suitable for daily-life EE monitoring. To overcome this issue, a large variety of methods based on diverse approaches (such as pedometry, actigraphy or electrocardiography) have been proposed. However, most of them are characterized by biased and inaccurate EE estimates that need specific user-dependent calibration protocols. CSEM has recently developed human activity-specific step counting and EE models. These calibration-free models based on subject's activity require 3D acceleration signals at the wrist and anthropometric parameters (e.g., weight and height) as inputs. The 3D accelerometer signals recorded on the wrist device are used for three purposes: physical activity classification, step count, and EE estimation.

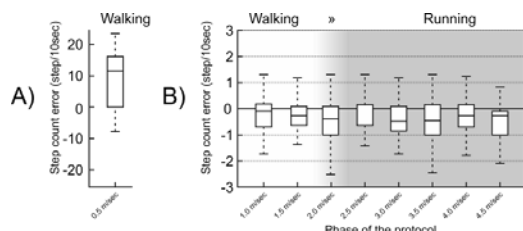


Figure 1: Performance of the step count model for each walking/running speed. Each distribution shows the 25th and 75th percentiles (lower and upper bounds of the box), the median (line within the box), and the minimum and maximum (lower and upper lines) values. Panel A displays the results for very slow walking, while panel B displays the results for walking to running.

Physical activity classifier—Several features are extracted from the accelerometer signals. These include signal strength, rhythmicity, and frequency stability among others. These features are used as predictors in a classification tree whose

[1] G. C. Le Masurier, C. L. Sidman, C. B. Corbin, "Accumulating 10,000 steps: does this meet current physical activity guidelines?", Res. Q. Exerc. Sport, vol. 74, no. 4, pp. 389–394, 2003

nodes depict different likelihoods for each activity. This tree was trained with a wide range of physical activities.

Step count model—This process starts by classifying the identified activities in two groups: rhythmic and non-rhythmic activities. Based on the result, a spectral analysis or a time-domain analysis is performed and the corresponding steps estimated from the time-window frequency (cadence) or single step is computed and added to the total step count.

Energy expenditure model—This human EE model is activity-dependent. For the activity classes *Rest* and *Other*, it uses a constant value of MET. For the activities classify as *Walk* and *Run*, it uses the so-called SPE2AR model, which uses a walking/running forward speed [2].

The performance of these two models and their activity classification sub-model were evaluated with respect to gold standards (ActiGraph GT1M® step counts, total energy expenditure estimated from indirect calorimetry) for a fixed protocol with activities including lying down, standing, sitting, walking, and running. The results are shown on Figures 1 & 2.

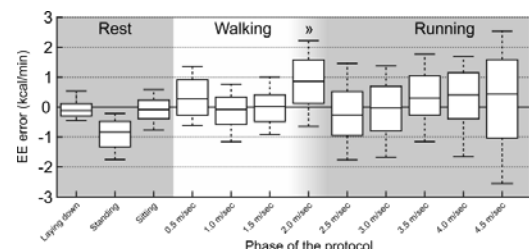


Figure 2: Performance of the EE model for each activity. The distributions have the same meaning as Figure 1.

Based on the presented results, we conclude that the proposed model for step count and EE offer a high accuracy as compared to off-the-shelf commercialized devices for walking and running activities at speeds larger or equal to 1.5m/s. More precisely, we achieve performance values of 0.71 ± 0.06 step/10s for the step-count model and 1.22 ± 0.34 kcal/min and a total EE relative error of 5.52% for the EE. These performances improve by an order of magnitude most of the commercial solutions based on actimetry sensor (total EE relative error of 26.8 % for ActiGraph GT1M®). However, rhythmic low-speed activities (walking at 0.5m/s) introduce misclassifications that limit the overall performance of the device. This limitation is being addressed by CSEM in the frame of its on-going research activity.

[2] R. Delgado-Gonzalo, et al., "Human Energy Expenditure Models: Beyond State-of-the-Art Commercialized Embedded Algorithms," Digit. Hum. Model. Appl. Heal. Safety, Ergon. Risk Manag. Lect. Notes Comput. Sci., vol. 8529, pp. 3–14, 2014

A Medical Compliant Wearable Monitoring System for 12-Lead ECG

M. Lemay, J.-A. Porchet, A. Falhi, G. Dubnik, M. Bertschi, M. Correvon

CSEM is developing a medical compliant multi-sensor monitoring device which specifically addresses the diagnostic of multiple health diseases related to metabolic syndrome conditions. By combining the monitoring of the cardiac activity (12-lead ECG), respiratory activity (thorax and abdominal impedance measurements) and physical activity (3D accelerometer), this innovative medical device aims at improving ambulatory long-term monitoring of patients in terms of diagnostic accuracy and, consequently, reducing medical outpatient follow-up costs. The entire product development is compliant to ISO 13485 and all the appropriate standards.

Metabolic syndrome is a disorder of body energy utilization and storage that increases the risk of developing cardiovascular disease and diabetes. The Nano-Tera project called ObeSense aims at developing low-power wearable multi-sensor monitoring systems permitting to better manage the therapies of this population group (estimated to be in the US one third of the adult population). The ObeSense solution will allow physicians to continuously monitor the most important medical parameters of patients suffering from metabolic syndrome and thus reduce medical follow-up costs of outpatients in ambulatory conditions.

The Wearable Electronic System (WES12) is a class IIa medical device dedicated to cardiac long-term clinical monitoring and integrating a 12-lead electrocardiogram, 3D accelerometers, and bio-impedance measurements. The device can be interfaced with fourteen standard male clips (e.g. gel or textile electrodes) and offers the possibility to store raw data and to automatically analyze synchronized long-term ECG, respiratory and body motion signals in terms of heart rate, rhythm and waveforms, ECG quality index, respiratory rate, and energy expenditure (see Figure 1).

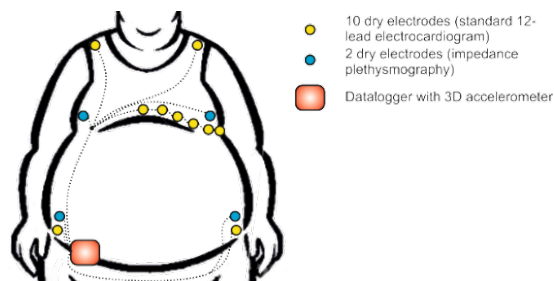


Figure 1: WES12 medical device setup.

The main functionalities of the WES12 includes: automatic recording, streaming, automatic transfer and low power warning. The internal recording is controlled via a push button or automatically trigger by the presence of ECG signals. All raw data are recorded internally without any compression. The medical staff (user) has access to the SD card with raw data. It is possible to stream and visually inspect the ECG signals via a dedicated mobile application. When placed on the docking station, an automatic data transfer and internal data management application is launched. Below a certain battery

level, a LED is switched on to warn the user. The final firmware and software design is based on the user specific needs and requests. The development of the product follows CSEM procedures compliant with ISO 13485 standard [1]. The Planning phase has been completed and has already provided the planning, the initial risk assessment, the risk management plan, the clinical use case, the user requirement specifications, the project management plan, the literature review, the software development plan, and the product quality plan documents. The feasibility phase is on-going and a prototype which respects both user requirements and essential requirements (standards IEC60601-1 [2], IEC60601-2-25 [3] and IEC60601-2-27 ed. 2.0b:2005 [4]) is being developed. The following list of documents is being finalized: risk analysis, usability- software- hardware-requirement specifications, feasibility analysis, verification and validation matrix documents.

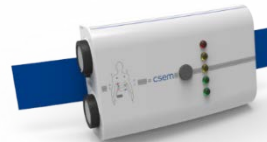


Figure 2: WES12 medical device demonstrator.

The clinical investigation of the approach—which shall be approved by SwissMedic and CHUV's Ethics committee—will be supervised by the cardiology institute at CHUV and validated on patients after an ischemic event or after an atrial fibrillation ablation procedure in long-term follow-up conditions. On the product aspect, this clinical investigation shall validate the user and patient acceptance. On the research aspect, it shall investigate on statistical relationship between cardiovascular and physiologic markers (including heart rate, heart rate variability, presence and recurrence of arrhythmias, beat-to-beat blood pressure variability, presence and recurrence of hypotensive periods, presence and recurrence of sleep apnea periods, physical activity patterns, and energy expenditure profiles) and symptoms as reported by the patient (including symptomatic fatigue and shortness of breath).

By offering such large scale of markers, WES12 aims at improving the actual management of metabolic syndrome medical issues.

performance of electrocardiographs", International Electrotechnical Commission standards, ed. 2.0, ICS 11.040.55/99, pp. 1–196, 2016

- [1] ISO 13485:2003, "Medical devices – Quality management systems – requirements for regulatory purposes", ISO standards, ed. 2.0, ICS 03.120.10, pp. 1–57, 2003
- [2] IEC 60601-1 ED.3.0:2005-12, "Medical electrical equipment – Part I: General requirements for basic safety and essential performance", International Electrotechnical Commission standards, ed. 3.0, ICS 11.040, pp. 1–408, 2005
- [3] IEC 60601-2-25:2011, "Medical electrical equipment – Part 2-25: Particular requirements for the basic safety and essential
- [4] IEC 60601-2-27:2011, "Medical electrical equipment – Part 2-27: Particular requirements for the basic safety and essential performance of electrocardiographic monitoring equipment", International Electrotechnical Commission standards, ed. 3.0, ICS 11.040.55, pp. 1–146, 2015

Cuffless Blood Pressure Monitoring: CSEM's Portfolio of Non-occlusive Technologies

J. Solà, M. Proença, F. Braun, M. Lemay, C. Verjus

During the last 10 years CSEM has intensively worked on the development of an innovative catalog of technologies that enable the monitoring of blood pressure in a comfortable and continuous manner. Either located at the chest or the wrist, these technologies open the door to a new era of cuffless blood pressure monitoring: improving patient's comfort and increasing the number of measurements per day. Several clinical validation studies are currently in progress, and a dedicated patent portfolio is available for licensing.

The non-invasive measurement of blood pressure in clinical practice is currently limited to the use of an inflation brachial cuff, providing only intermittent and uncomfortable readings of blood pressure. The race for alternative technologies that increase patient's comfort while providing actual 24/24h readings to physicians has started worldwide. The reward of the race will be a first-in-the-market wearable blood pressure monitor^[1]. In this technological race, CSEM's contribution resides on the introduction of two families of technologies (see Figure 1):

- A) chest-based technology relying on the analysis of optical and bioimpedance signals. Matching the needs of wearable systems, this technology estimates central continuous blood pressure values via the so-called Pulse Wave Velocity principle^[2].
- B) wrist-based technology relying on the analysis of optical signals. Matching the needs of smartwatches, this technology estimates peripheral blood pressure values via a proprietary analysis of arterial pulsatility patterns (physiological Pulse Wave Analysis)^[3].

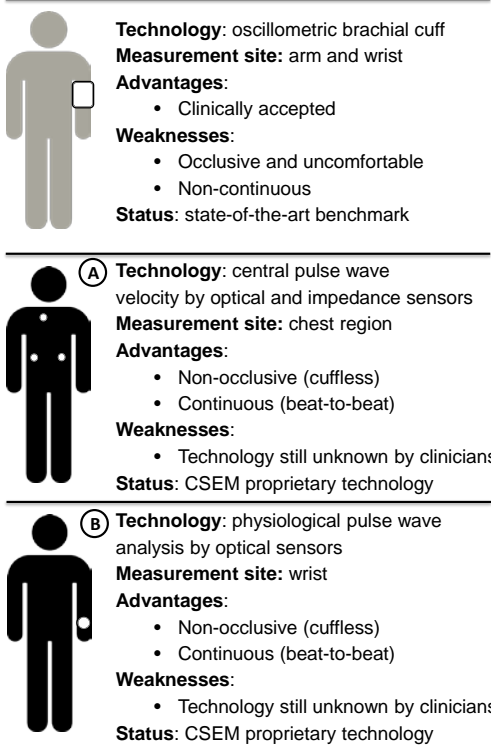


Figure 1: Summary of state-of-the-art and CSEM technologies for the non-invasive measurement of blood pressure.

[1] Mukkamala *et al.*, Towards Ubiquitous Blood Pressure Monitoring via Pulse Transit Time: Theory and Practice, IEEE TBME, 62(8), 2015.

Figure 2 illustrates the results of two pre-clinical studies involving healthy volunteers ($N=30$) when comparing CSEM's cuffless blood pressure estimations (vertical axis) to reference blood pressure values (horizontal axis). Different subjects are illustrated represented by different markers. Note that for both pre-clinical studies, cuffless blood pressure estimates correlate to the measured occlusive values, providing agreement scores that comply with AAMI and BHS standards.

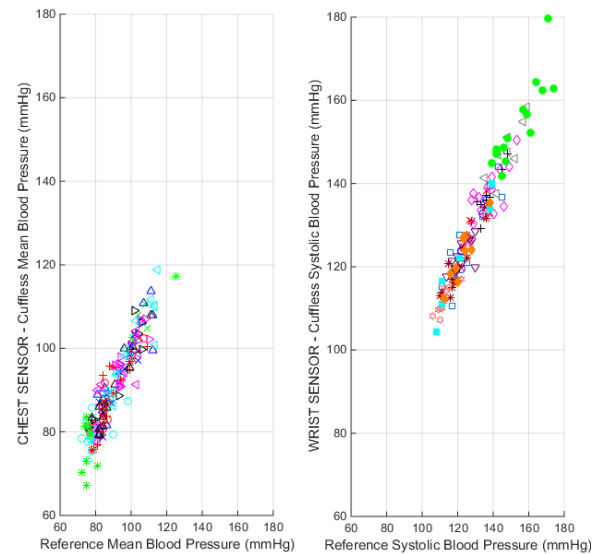


Figure 2: Correlation plots for cuffless versus reference blood pressure values for CSEM chest-based (left) and wrist-based (right) technologies.

Current efforts of CSEM's research team are put on in-depth clinical validation of these innovative cuffless technologies in different Swiss University hospitals. The implemented clinical studies involve a large palette of scenarios, ranging from anesthetized patients in the operating room to hypertensive patients in ambulatory settings.

The dedicated technology and patent portfolio differentiates CSEM as a key international player for the development of new blood pressure sensors for the wearable market.

[2] Solà *et al.*, Non-invasive and non-occlusive blood pressure estimation via a chest sensor, IEEE TBME, 60(12), 2013.

[3] Nichols *et al.*, McDonald's Blood Flow in Arteries: Theoretical Experimental and Clinical Principles, CRC Press, 2011.

Wrist-worn Optical Heart Rate Monitoring: a Comprehensive System Approach

C. Verjus, P. Theurillat, R. Delgado-Gonzalo, P. Renevey, P.-F. Rüedi, P. Persechini, E. Rincon Gil, M. Correvon, P. Pilloud

Optical heart rate monitoring has become a commodity in today's smartwatches with a limited measurement precision and reliability, especially during the presence of motion. Expertise in physiology, optical skin interface, electronics, mechanics, industrial design, and signal processing are essential to achieve high accuracy. CSEM solution has demonstrated excellent performance not only for heart rate (HR) monitoring during outdoor activities and exercising, but also for RR interval detection, heart rate variability analysis, perfusion, sleep analysis, and speed assessment.

While sports watches with an integrated optical heart rate sensor technology (OHR), based on photoplethysmography (PPG) have been commercialized for more than two years now, the market has seen recently a widespread use of such functionality within the smartwatch products of the microelectronic and smartphone giants such as Apple, Samsung, Huawei, LG and Sony. Unsurprisingly, not all of these smartwatch products reach the same accuracy and reliability, especially during the presence of motion. Actually, a comprehensive system approach is required to achieve the best heart rate measurement quality, and is even more critical to be able to measure additional parameter like RR intervals, heart rate variability (HRV) or perfusion, using a PPG sensor.

PPG is based on the measurement of the changes in light absorption of the subcutaneous tissue of the skin, typically illuminated with a LED. The light is actually modulated by capillary blood flow, which is used to monitor heart rate. However, even with well-designed sensor interfaces, two major issues are sources of error: ambient light and movement artefacts. Ambient light fast variations can become a major issue when its fluctuations show a high amplitude above the sampling frequency, which can occur with bright indoor lighting or when moving in sunny conditions. Today's available state-of-the-art solutions do not prevent the saturation of the input stage in every use case.

CSEM has been active in the OHR domain for more than 15 years now, and its first granted patent on this issue dates back to 2001. Multidisciplinary know-how and expertise in physiology, microelectronics, opto-mechanics and signal processing is key to success, and CSEM developed an innovative solution to overcome the ambient light variations, and which is implemented in the analog front end, using its latest application-specific integrated circuit (ASIC) generation.

Table 1: Mean performance of PulseOn HR Monitor in outdoor activities (N=number of recorded events).

Main activity	PulseOn	
	Reliability (%)	Accuracy (%)
Walking (N=3)	94.1	96.6
Running (N=17)	99.1	97.9
Cycling (N=4)	95.2	97.3
Mean (N=24)	97.8	97.6

Moreover, motion artefacts lead to small displacements in the sensor-skin contact and in the tissue, or induce variations in the blood flow itself. Advanced algorithms apply integrated 3D-accelerometer data to reduce motion artefacts and provide accurate HR estimation even during very intensive training,

spanning up to full running speeds and maximum HR levels. An experimental evaluation of the performance of CSEM's algorithms implemented in the PulseOn^[1] HR monitor on 19 healthy subjects obtained a mean accuracy and reliability above 97% for outdoor activities, as detailed in Table 1^[2]. Today's research activities at CSEM on PPG measurement at wrist target future health and medical applications. Figure 1 shows the HRV accuracy based on CSEM's proprietary RR interval detection algorithm and which performs within a standard deviation of 12ms when compared to ECG devices^[3].

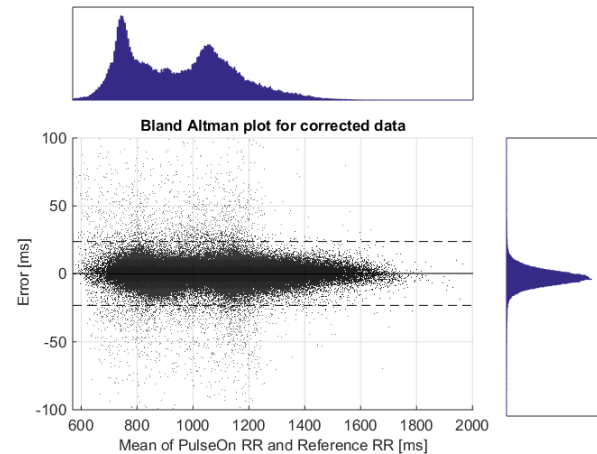


Figure 1: Bland - Altman plot comparing the reference ECG-obtained RR intervals to the PPG-obtained RR intervals. The confidence interval ($\mu \pm 2\sigma$, depicted by the dashed lines) is [-23.15,23.83] ms.

CSEM's health watch prototype is shown in Figure 2 and is providing not only HR, R-R intervals, perfusion, activity, and user's posture and speed but is also able to record and stream wirelessly raw PPG and accelerometer data during a period of more than 24hours before recharging.



Figure 2: Health watch prototype developed at CSEM for the monitoring of motion related and cardiac activity parameters.

The smartwatch activities are executed in the frame of CSEM's Medtech research activity and CSEM acknowledges and thanks the Swiss Confederation for its financial support.

[1] www.pulseon.fi

[2] R. Delgado-Gonzalo, et al. "Evaluation of accuracy and reliability of PulseOn optical heart rate monitoring device" EMBC 2015

[3] J. Parak, et al. "Evaluation of the Beat-to-Beat detection accuracy of PulseOn wearable optical heart rate monitor", EMBC 2015

Reliability of Integrated IMUs for Elbow-like Motion Patterns

T. Parkel, S. Follenier, J.-P. Baeyens •, R. Clijsen ••, T. Dai *, J. Steck **

Integrated sensor technologies are widely used in various self-monitoring devices for leisure and professional sports activities. Vital signals and general gait information are transferred into fitness and risk levels. Additional information of the musculoskeletal system coming from inertial measurement units (IMUs) can provide important information for a better holistic interpretation.

The aim of this study was to explore the reliability (precision, accuracy and reproducibility) of the 3 rotation axes of an IMU based motion capturing system currently used by the film-industries in animated movies for future use in medical applications.

Goniometric data from the right elbow was simultaneously recorded from the IMU based motion tracking system from Noitom (Perception Legacy from Noitom Ltd.) mounted on an industrial robot arm and on five subjects and from the optical IR imaging system from Vicon (as a reference system).

Vicon is a multi-camera infrared (IR) system using reflector balls to determine orientation in space. The Noitom system is based on 18 IMUs linked through a body model to wirelessly stream and record full body motion from head to toe.

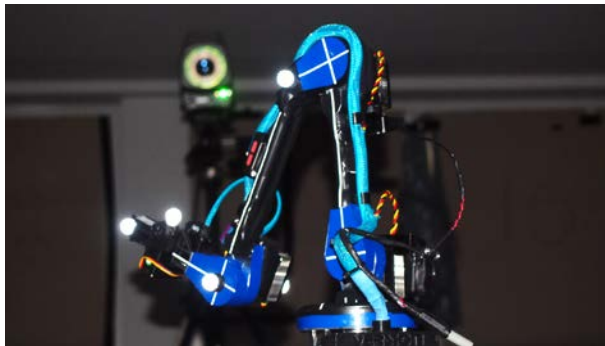


Figure 1: Robot arm with mounted reflectors and IMUs.

Using biomechanical aspects of the shoulder-elbow joints such as range of motion (ROM), velocity and orientation, a series of successive one minute motion patterns were programmed on the robot arm. The synchronized datasets were benchmarked to determine the reliability of the Noitom System compared to the gold standard Vicon.



Figure 2: Subject with mounted reflectors (silver) and IMUs (red).

5% of the 166,926 collected data samples from the 5 minute robot trials were within the acceptance window of +/- 0.75°. 3% of the 111,280 collected data samples from the 5 minute human trials were within the acceptance window of +/- 0.75°. 7% of the 333,840 collected data samples from the 1 hour robot trials were within the acceptance window of +/- 1°.

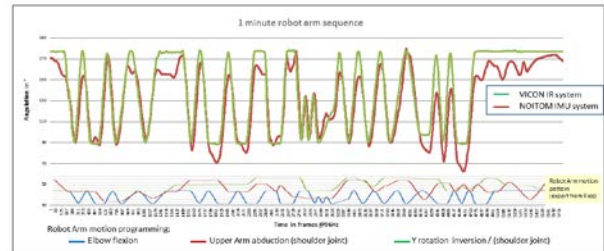


Figure 3: One minute angular data sequence showing deviation patterns between Vicon and Noitom systems.

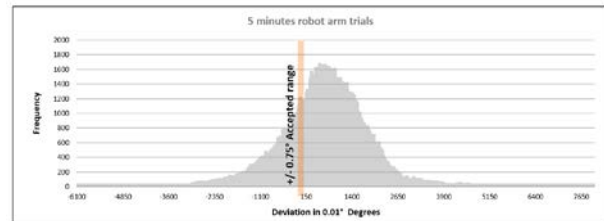


Figure 4: Histogram of 5 minute robot arm trials.

The Noitom IMU system has clear usability advantages such as working with obstacles around the subject (e.g. people, furniture), with much higher patient compliance (can be worn under clothes), with 1:10 time saving ratio on data post processing, with easier setup/equipment etc. Its current reproducibility still shows a far too high deviation rate for medical angulation monitoring over time. A distinct repetitive deviation pattern could be found on the multi axis rotation pattern. Nevertheless this lack of accuracy is still acceptable for monitoring motion patterns and detecting deviations caused by fatigue or by other systematic status changes.

The programmed motion pattern on the robot is closing the gap for a standardized approach to test the accuracy of IMUs regarding biomechanical properties of the human shoulder.

This thesis was conducted within the Berner Fachhochschule Medtech Master program and supported by CSEM, Department Biomechanics and Human Biometry, Vrije Universiteit, University College Physiotherapy, Noitom Pejig; SUPSI; and Ypsomed.

- Department Biomechanics and Human Biometry, Vrije Universiteit Brussel
- UCP University College Physiotherapy Landquart;
- * Noitom Pejig
- ** Ypsomed AG, Burgdorf

A Human Centred Design Approach for System Integration of Wearables

T. Parkel, F. Pereira, S. Generelli, N. Tscharner, D. Migorelli, M. Viviani, R. Junuzovic, K. Krasnopski, S. Sousa •

Together with the company Kenzen AG, CSEM is developing sensor patches for the analysis of unique biomarkers in sweat (including electrolyte imbalance, e.g. sodium, potassium) as well as monitoring sweat rate noninvasively on the skin, indicative of relevant health conditions. Integrating these electro-chemical sensors with advanced vital sensing technologies is key to the next generation of wearable patch devices to provide actionable insights on critical physiological indicators that directly influence one's health and well-being.

Determining the form factor design on wearable patch devices under the Usability IEC 62366 & Risk management ISO 14971 approach, provides valuable insights for the industrial partner when selecting the best matching technologies. This approach applies to medical device manufacturers in order to be compliant with the Medical Device Directive MDD 93/427EWG.

Engineering requirements are performed on the entire system to define the user's requirement specifications with the industrial partner. The specification list based on field of use (FOU) and intent of use (IOU), for example, ensures that the goals are understood prior to the start of the project.

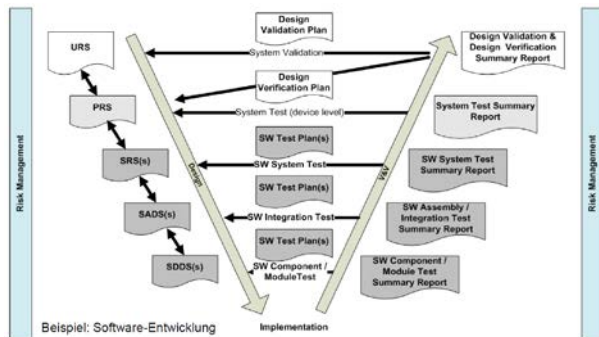


Figure 1: V-model of the product life cycle.

The modular system design approach to electronics and all interphases enables multiple nodes of communication and the accommodation of other sensor combinations due to its modular toolbox design approach (see Figure 2 below).

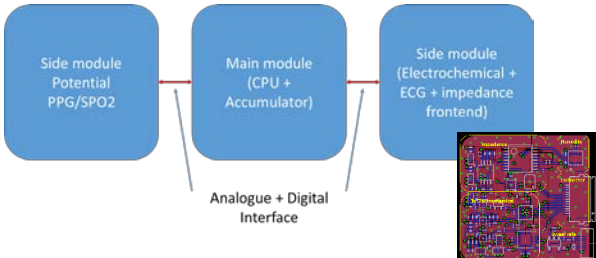


Figure 2: Modular architecture of a multi-purpose central node connected to function-specific side modules.

Early on, functional mock-ups of all components (transparent adhesive patch, electronics, housing, sensors) are tested and further developed in multiple iteration loops following the V-model of the product life cycle.

Regarding the disposable side of the system (Figure 3), screen printed electrodes are functionalized to measure e.g. Na, K, pH, or skin impedance providing information to determine dehydration status.

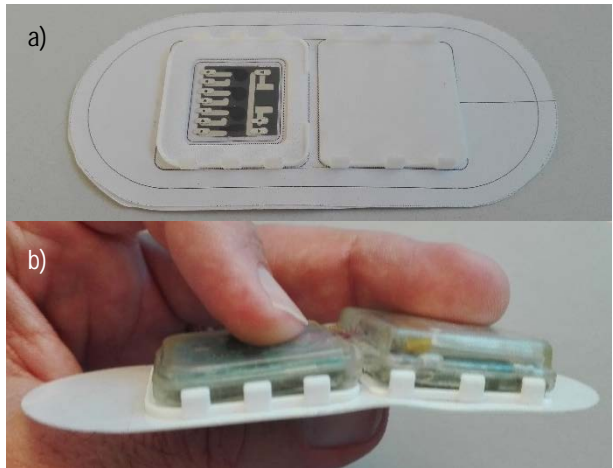


Figure 3: (a) Single use patch mock-up with electrochemical sensor and (b) clip mechanism with transparent flexible housing on adhesive patch.

The first results obtained by the Kenzen wearable patches for pH monitoring in sweat are displayed in Figure 4 below. Monitoring pH for several hours was demonstrated with the following specifications: pH range pH 8 – pH 3, rapid response (<1min) with a resolution of 0.1 pH unit.

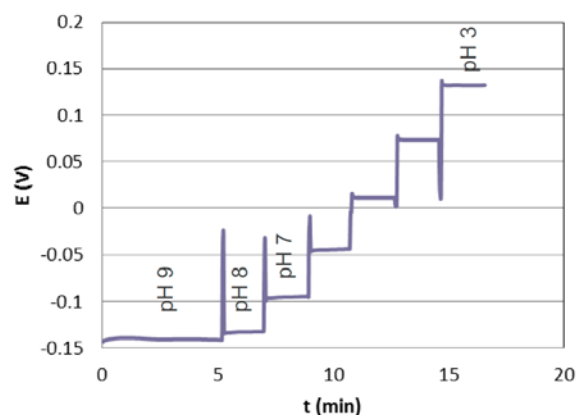


Figure 4: pH sweat monitoring using patch and sensor in Figure 3.

• Kenzen AG

LuCa Phantom Vent V2.0

T. Parkel, N. Tscharner

An anthropomorphic breathing phantom was initially built for the Paul Scherrer Institute (PSI) to explore and simulate tumour motion in the lungs for scientific exploration of proton radio therapy of moving organs. For the Radiotherapy Center at the Clinic Hirslanden, CSEM has built a newer LuCa phantom version with a redesigned ventilation system to perform explorative measurements on their CyberKnife, Hislanden's non-invasive, robot-controlled radio surgical system for the treatment of tumours in any part of the body.

With the prototype ventilation system V1.0, PSI was able to perform many explorative radiation tests on moving lung tumours using the LuCa Phantom. The vent V1.0 system has an overall size of 400x480x600mm and weighs 39kg. It is driven by a heavy duty ring blower and four servo valves. The entire ventilation system is controlled by an external PC connected by USB using LabView-based software.

During the last two years users have reported new requests for the system such as: new interfaces for other measurement equipment, a respiration wave-form generator, DICOM file-import functionalities, self-calibration of the ventilation system, a miniaturized and lighter, portable ventilator system.

To make this ventilator system ready for small serial production, the Usability IEC 62366 & Risk management ISO 14971 approach were applied to redesign the entire hard- and software of the ventilator system.

System description Vent 2.0

The control unit has been integrated into the new ventilation system, enabling standalone capabilities and thus independent of the computer and its performance. In this scenario the PC is only needed for the graphical interface.

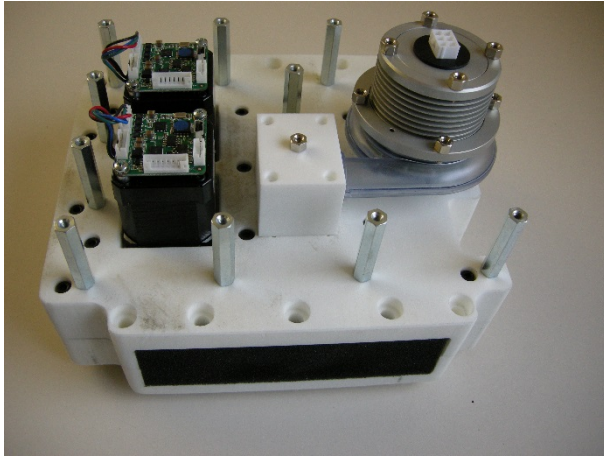


Figure 1: 3D printed air flow block with attached turbine and the two stepper-motors controlling the three-way valves.

All internal air ways and the mechanics of the valves are designed to be 3D manufactured by an additive manufacturing process (Figure 1).

To achieve the specifications, a powerful turbine, running at 35'000 rpm is integrated in a standard housing of 200x200x230mm, with a total weight of 8.1 kg. The maximum pressure levels that can be achieved with this system are +/- 30 mbars.

Figure 2 shows the programmed versus actual pressure in the lungs as displayed on the user interface. Motion of the tumour is directly correlated with the pressure and hence the volume of the lungs.

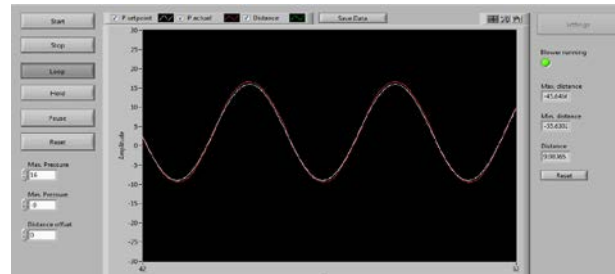


Figure 2: Main window of the GUI showing the pressure (applied and measured) and corresponding respiration curve.

The obtained results of the redesign fully match the requirements and its usability aspects. However at the current stage of miniaturization we experienced thermal issues running the ventilation system at full power for long periods.



Figure 3: Size comparison of the two ventilation systems.

In the third iterative development round we shall address the thermal problem of the turbine and try to reduce the noise caused by the air flow. Therefore a slight redesign of the hardware is envisioned.

Ultra-precision Manufacturing of XXL Parts

D. Boesel, P. Glocker

An innovative solution for machining of parts with large dimensions (up to 50 m) was implemented in a prototype. The solution is more precise and more flexible as well as considerably cheaper than currently available machines. Target applications include manufacturing of windmill wings, parts for civil construction and aerospace industries.

Parts with large dimensions, in the range of several tens of meters long, are commonly found in a number of industries, including aeronautics, energy and others. Machining of parts with these dimensions is usually performed manually, with very low geometrical tolerance, or with very large and expensive CNC machines, with cost and error growing more rapid than linear rate with machine dimensions.

The European project Megarob^[1] is developing an innovative solution for the manufacturing of such large parts based on standard industrial components: a three-axes overhead crane, a six-axes industrial robot arm and a laser tracker (see Figure 1). The robot is mounted upside down on the crane. The part to be worked on is placed under the area covered by the crane. Finally, the laser tracker is placed in the manufacturing hall so that the robot's end-effector is always in its field of view.

The use of only standard industrial components was a design decision. It lowers system development and operation costs while it increases acceptance and reliability. These components can be freely chosen by the end-user, avoiding technical restrictions emerging from commercial aspects.



Figure 1: The Megarob prototype with overhead crane, robot arm, and laser tracker.

Megarob uses two custom software components: a Robot Global Controller, implemented by CSEM, and a System Supervisor, implemented by project partner TeamNet International and CSEM.

The Robot Global Controller integrates the industrial robot arm with the laser tracker, enabling manufacturing large parts. The laser tracker gives the pose of the tool at the robot's end-effector. The difference between this position and the programmed robot pose is used to add an offset to the robot's target position. This cycle is repeated every milli-second on a real-time operating system running on a desktop PC.

The Robot Global Controller provides several features to the Megarob solution. Firstly, it continuously supervises the

manufacturing process and minimizes all static and dynamic positioning errors of the tool. Since the correction is performed online, the Global Controller guarantees first-time-right execution of a robot program. Furthermore, the correction is performed at the robot's joint motion controller. In this way, the correction is transparent at the robot's programming level. This leads to an easy deployment of the Global Controller, even in legacy systems.



Figure 2: Milling a circle with large disturbance in the system without real-time position correction (left) and with correction (right).

The System Supervisor is another piece of software developed for the Megarob system. It provides an interface to manually control every component of the system. The software can also be utilized as a process planning tool by working as CAM (computer aided-manufacturing). It calculates the 3D machining path of the tool taking into account the kinematic model of Megarob, composed of the crane and the robot. Finally, the System Supervisor also controls the machining process. It executes a planned program by automatically operating the components of the system in a synchronized form. In this way, the machining of a part can be split into several regions. In each region, the crane remains stopped while the robot performs the machining motions.

The resulting system provides a number of attractive technical and commercial features. The system has a better precision than currently available machines. The use of standard physical components lowers the cost of maintenance. Other features include flexibility for machining of complex geometries thanks to its nine axes as well as minimal footprint. Finally, Megarob costs about half of current machines.

The results achieved during the Megarob project are promising. Companies outside the consortium have expressed interest in testing and commercializing the system. The main target industries are civil construction, energy generation and aeronautical production.

This work is being co-financed by the EU under project reference 314015 and by the cantons of Central Switzerland. Their support is gratefully acknowledged.

[1] www.megarob.eu

Self-adaptation and Pre-maintenance Strategy in Industrial Production

I. Kastanis, D. Boesel, K. Krasnopski, P. Schmid, A. Steinecker, P. Glocker

Modern manufacturing systems consist of complex, heterogeneous and often distributed hardware components from a variety of vendors. The management of such systems has become more time consuming and requires expert knowledge typically only available from the system integrator. With the rise of Information Technology in the production floor of Industry 4.0, new solutions to these problems are becoming a reality. This new technology reduces the effort required for management of large production lines and provides new capabilities aiming to optimize their operation.

To meet the ever growing demands of industrial production, modern manufacturing systems must be capable of rapid product changes and product variations as well as maintaining a constant flow of production in order to reduce the associated costs. These complex systems consisting of heterogeneous collections of components often lack the important factors of ease of configuration and of a standardized management interface. The designer is faced with the problem of combining multiple components, from a variety of vendors that use their own proprietary software, in a single system that works in harmony. The European project PRIME [1] addresses this issue with the introduction of a multi-agent based framework.

In this framework each component is represented as an agent. Information about each agent can then be accessed in a generic manner. This approach offers a unified method for information retrieval which simplifies the process of creating a standardized Human Machine Interface (HMI) in the case of heterogeneous systems. The atomic skills of each component can be automatically detected and aggregated to build complex capabilities that encompass functionalities of one or more components. These advanced capabilities are compared to the product description for the system configuration to take place and replace or reduce the human effort required.

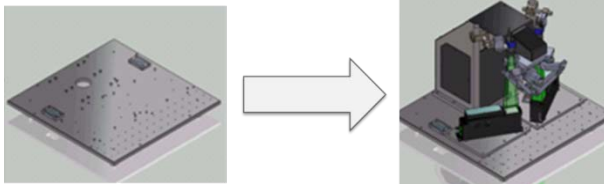


Figure 1: Demonstrator for system configuration. Image courtesy of Asyri [2].

A demonstrator (Figure 1) using an early version of the PRIME multi-agent framework has already been implemented [3] in collaboration with Asyri. Apart from the atomic skills that were used in this initial demonstrator component agents expose further information such as their status, execution times, and other measurements. This information can be processed with a variety of filters to provide real-time visualizations of historical data as well as prediction of future performance. Data from various sources can be combined to directly calculate Key Performance Indicators (KPI). These can be monitored and, once a predicted value falls under a certain level, a warning is issued and adaptation of the system can be performed.

CSEM in collaboration with ZHAW [4] is implementing a demonstrator that takes advantage of these capabilities of the

PRIME toolbox. The demonstrator (Figure 2) is based on a rotary indexing table where ball bearings are initially fed into the system, processed by pneumatic grippers, inspected by cameras and finally unloaded from the table.

The table can move at one or two positions per step depending on the existence and performance of the hardware components. A smart HMI displays information about the connected components by unifying the heterogeneous hardware into a standardized view. The operator can focus on different levels of detail observing information about individual components or groups of them. By monitoring components, the system can detect if some hardware is underperforming, an indicator of possible failure in the near future. In such a case, a warning is generated for the operator and the system automatically adapts its configuration to avoid using the potentially malfunctioning component. Speed is reduced at one position per step and the system is self-adjusted so that the underperforming hardware can be removed for maintenance without having to completely stop the process.

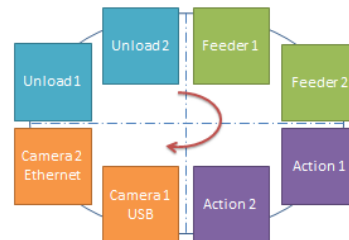


Figure 2: Diagram for rotary indexing table demonstrator.

This demonstrator utilizes the previous work on system configuration and extends it with the self-adaptation and pre-maintenance strategy. It offers a centralized management interface through the smart HMI that simplifies the process of operating a heterogeneous manufacturing system. With advanced process monitoring, proactive maintenance-schedule management can be performed in order to reduce the downtime of the system. This new strategy offers advantages in the optimization of complex assembly lines and aims to directly reduce the cost of such systems.

The work has been carried out in the collaborative project PRIME (University of Nottingham, Siemens, Simplan, TQC, Asyri, ZHAW, CSEM, UNINOVA, TTS, Introsys) supported by the European Commission under FP7, grant agreement number 314762. Co-financing by the EC and the cantons of Central Switzerland is gratefully acknowledged.

[1] www.prime-eu.com

[2] www.asyri.com

[3] I.Kastanis, et al., "Plug & Produce: Automatic detection and configuration of industrial devices", CSEM Scientific and Technical Report (2014), 110

[4] www.zhaw.ch

Robotic System for Integration of Electronics into Textiles

S. Widmer, M. Lützelschwab, P. Glocker, M. Höchemer

A system for automated assembly of electronic devices into fabrics has been developed. Conductive yarn for the power supply of LEDs is woven in the backside of the fabrics. Advanced vision algorithms have been used to identify the position of bonding spots on the yarn.

Direct integration of electronics in textiles is a topic which attracted major interest in recent time. Nevertheless, automated reliable low-cost assembly is technically challenging. We present a vision based approach for one sub-task: identification of bonding positions for LEDs.

Due to the flexibility of a textile the position of yarn and the bonding spots are not known a priori. Even if the textile pattern seems to be regular, each bonding area looks different (see Figure 1). To identify the correct bonding spots, an adaptive position recognition algorithm based on artificial neural networks was used.

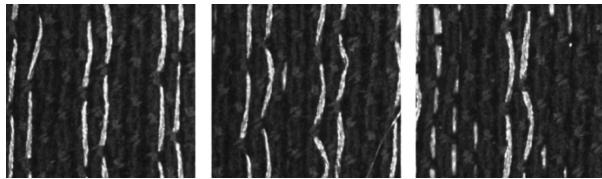


Figure 1: Images showing the different shapes of the conductive, bright wires. The LED's should be placed between two of them.

For image analysis we applied an algorithm based on a deep-belief network analysis. The goal is to find and track corresponding pairs of conductive yarn. The first step is a local image decomposition: At several points of interest a local log-polar-transformation is applied, and local (sharp, high resolution) and peripheral information (unsharp but still visible, similar to the perception of a human eye) is stored in a 16 x 16 pixel image (see Figure 2).

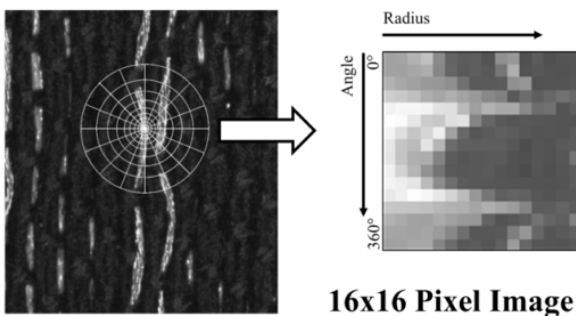


Figure 2: Symbolic representation of the log polar transformation.

Such transformed images serve as input for an initial training step. During this user-assisted process the systems learns the relevant features that are characteristic for a certain situation (Figure 3). The information is abstracted and the complexity is reduced. Only the significant information—appearance of a conductive wire—is considered.

In the next step of the training, the images are encoded with the previously learned procedure. The abstracted result is directly used to train the classifier ('what') and the localizer ('where') network (Figure 4).

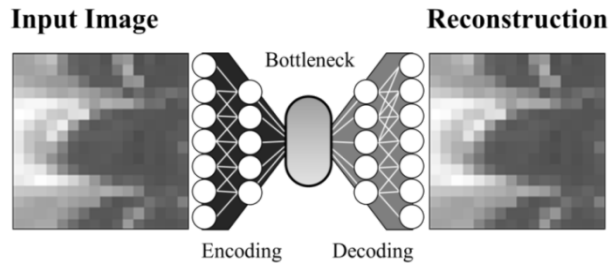


Figure 3: Illustration of the training where the image is encoded and decoded to reconstruct an image which is similar to the input image.

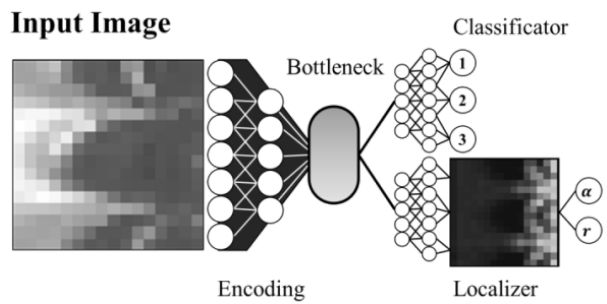


Figure 4: The two trained networks for classification and localization.

The localizer provides a jump map with the angle and the distance of interesting locations. Each map pixel stores the probability to be a point of interest. In Figure 5 the crosshair marks the current spot being analyzed. The circles are indicating where the next spots could be. Even when the starting spot is in a completely uninteresting place the jump map indicates peripheral POIs. With this efficient strategy an analysis of the entire image can be achieved within a few iterations in real time. The analysis of an image (Size 760x840) takes 182 ms.

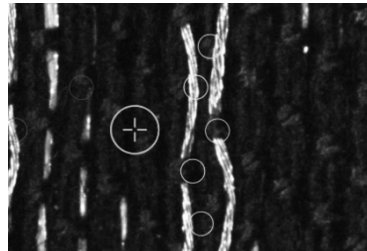


Figure 5: The cross-hair marks the spot which is analyzed, circles the interesting points.

This analysis yields precisely the position of bonding spots for the LEDs and the following automated assembly. The assembly process is described in "Process development for integrating electronics in textiles" in this volume.

We acknowledge the support of the work by the European Commission under contract 258724 "PASTA" and the cantons of Central Switzerland.

In-situ Tissue Identification by Ultrasonic Pulse Echo Analysis

K. Krasnopski, R. Limacher

This research aims at the development of a disposable hypodermic needle with embedded tissue identification. The measured response will ensure that specified locations for biopsies, drug dispensing or sensor/actuator placement are reached with superior confidence and false diagnoses or ineffective procedures are prevented. A first proposed application for this smart tool is fine- or core-needle biopsy.

The general motivation of the proposed technology is to add feedback during needle navigation based on viscoelastic properties of tissue either in addition to or as an alternative to imaging techniques. It is expected that this technology will result in an increased success rate of screening and reduced procedural efforts, hence contribute to early breast cancer detection^[1] and reduced health care cost. The concept is based on a remote sensing of tissue properties at the needle tip by acoustic emission and response detection at the needle base. Two different acoustic measurement principles are compared using mechanical FEM simulations and simple practical tests: needle resonance and ultrasound pulse-echo analysis.

Both, measurements and simulations, show that the material surrounding the needle body has a strong damping effect on the resonance quality of the needle. Hence, reliable, tip-sensitive tissue classification using needle resonance is very difficult.

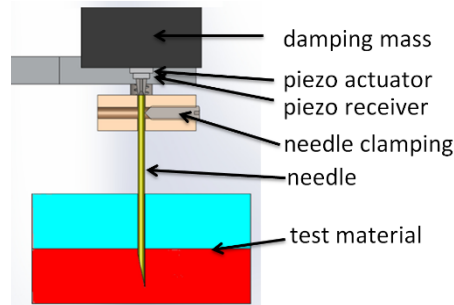


Figure 1: Pulse-echo test setup.

The ultrasound pulse-echo principle (Figure 1) enables spatial discrimination by time-windowing. Moreover, the longitudinal acoustic wave propagation minimizes interaction with tissue along the needle body provided that interface-friction is small. Significant reflection occurs at the needle tip depending on the tip-surrounding tissue.

In order to confirm the promising results of the simulation, various trials were conducted on artificial materials like rubber and silicone. In a first step, test samples made of homogenous materials were investigated. Significant differences in the signal's amplitudes were measured for most of the tested materials, allowing for a clear distinction (Figure 2). In a next step, combined test samples made of two different materials were analyzed to identify the transition from one to the other material. For this purpose, the needle was gradually immersed into the test sample and the signals were extracted related to the penetration depth. The transition between the two materials

in the sample could be identified (Figure 3) on the basis of the amplitude's course.

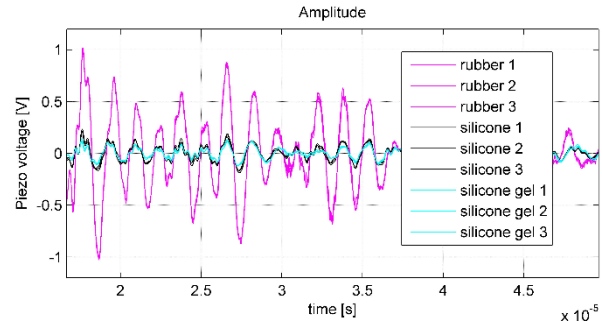


Figure 2: Measured signal for various test materials.

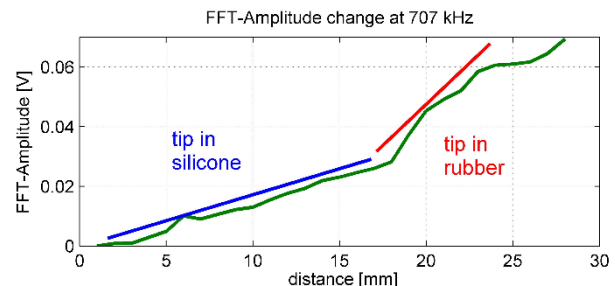


Figure 3: Measured signal at different penetration depth.

In a following step, similar investigations were performed on pig tissues like muscles and fat (bacon). As a result, the system's sensitivity was not sufficient to discern fat from muscle tissue. It is assumed that the characteristic acoustic impedances of both tissues are too similar in comparison with the sensitivity of the current experimental setup. A further increase of the system's sensitivity would require a significant modification of the needle tip and the needle's coupling to the excitation and sensing devices. Consequently, a commercially available disposable needle could not be used—one of the goal of this project. This calls into question the practicability of this method for the planned application area.

In conclusion, it could be shown that the measurement system based on the pulse-echo analysis in combination with a disposable needle allows to identify materials with different characteristic acoustic impedances as well as to detect the transition between two different materials. The applicability of this method for the planned application area is very challenging.

^[1] K. Krasnopski, et al., "In-situ Tissue Identification using Disposable Hypodermic Needles", CSEM Scientific and Technical Report (2013), 89

A Platform for a MEMS-based Laser Pointing System with Position Feedback

T. Burch, V. Revol, K. Krasnoplotski, A. Hoogerwerf, D. Bayat, P. Glocker

The Extreme Universe Space Observatory (JEM-EUSO) is a new type of observatory that will utilize the earth's atmosphere as a detector of ultra-high energy cosmic rays. An Elegant Breadboard of the Laser Pointing System for the JEM-EUSO space mission has been designed in order to demonstrate the achievement of the critical functionalities. The Laser Pointing System will be a key device to understand the atmospheric conditions in the field of view of the JEM-EUSO telescope.

The goal of the JEM-EUSO mission is to provide a solution to the problem of the origin of Ultra-High Energy Cosmic Rays (UHECR). Such cosmic rays, if entering the Earth's atmosphere, produce Extensive Air Showers (EAS) that consists of numerous electrons, positrons, and photons. EUSO captures the moving track of the resulting fluorescent UV photons and delivers information about the primary UHECR particles such as the arrival direction, the energy and also the type of the particles (Figure 1).

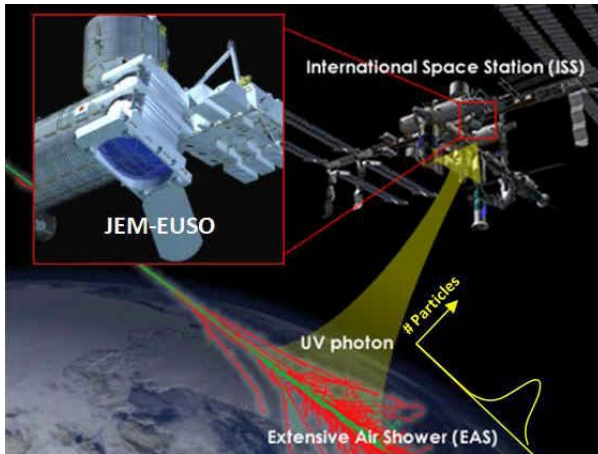


Figure 1: Principle of detection of UHECR from space with the EUSO telescope.

The intensity of the produced UV light depends also on the properties of the atmosphere, in particular on its transmittance and scattering characteristics in the UV band. Therefore EUSO will be equipped with a dedicated Atmospheric Monitoring System (AMS) which uses a LIDAR to probe the atmospheric conditions in the Field of View. In collaboration with the University of Geneva CSEM has designed an Elegant Breadboard (EBB) of the Laser Pointing System (LPS) for this LIDAR. The key specification of the LPS is the following:

- Laser Wave Length 355 nm
- Pulse Width 15 ns
- Pulse Energy: 20 mJ / pulse
- Beam Deflection: +/- 30° from vertical
- Beam Divergence: 2 mrad

The LPS will repoint the laser beam in the direction of the last triggered EAS and shoot the laser in several directions around this location. The focal surface detector of EUSO will receive the transient flashes of the laser and provides the data for the scattering and absorption profiles. The effective time available

to point the laser beam to a new location is typically a few tenths of seconds, thus requiring a lightweight MEMS mirror [1] with limited inertia and a fast control algorithm with a mirror position sensor in the feedback loop. A simplified block diagram of the LPS is given in Figure 2.

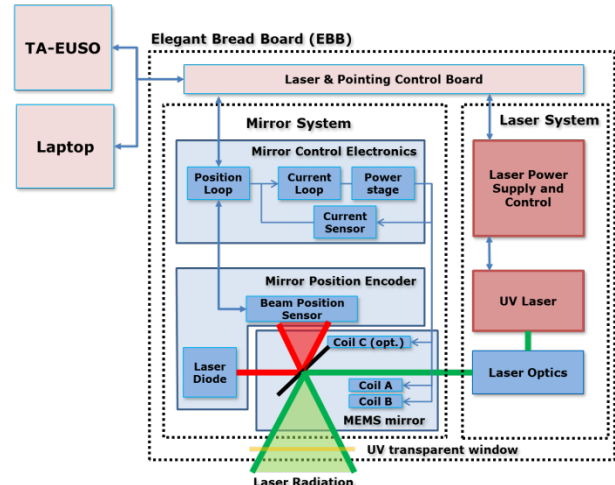


Figure 2: Block diagram of the laser pointing system (LPS).

The CAD Model of the EBB is shown in Figure 3. It is composed with the housing, the laser head, the optical system supporting the position sensor, the mems mirror and the electronics board. The red beam represents the UV laser beam, while the green one is the beam used to measure the position of the MEMS mirror through the position sensor and the supporting optical system.

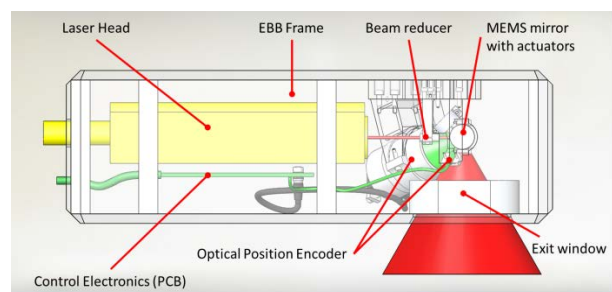


Figure 3: CAD model of the LPS elegant bread board.

The presented EBB design will be implemented during the next project phase and it is expected that a fully operational model will be available at the end of 2016. A qualification and flight model of the EUSO Laser Pointing System is planned for 2017

This work was funded by Swiss Space Office through a PRODEX program. CSEM thanks them for their support.

[1] A. Hoogerwerf, et al., "MEMS Mirror for High Power, Large Angle, 2D Laser Steering", this report page 25.

Integrated System and Proof of Concept of X-ray Phase Contrast Imaging for Inspection of Composite Materials

V. Revol, A.-M. Madrigal, T. Stadelmann, P. Niedermann, S. Droz, W. Glettig

The European project EVITA aims at bringing Grating-based Phase Contrast X-ray imaging technology^[1] to non-destructive evaluation and inspection of thick aeronautical composite structures. The demonstrator built within the project started operation in January 2015. The results confirm the high expectations on the applicability of this technology to the detection of critical defects in composite components such as cracks, porosity, missing plies and fiber waviness. Other industries (automotive, electronics or luxury) are also showing sign of interest.

Within the project EVITA^[2] (www.evita-project.eu), the requirements and needs of the aeronautics industry in terms of the non-destructive inspection of thick and thin composite components were collected and analyzed. From there, a customized demonstrator was designed and realized in order to benchmark this novel technique against the following non-destructive inspection (NDI) techniques: water jet ultrasonic, phased array ultrasonic, thermography and computed tomography.



Figure 1: Picture of the EVITA demonstrator at CSEM in Alpnach.

The demonstrator built within the project is depicted in Figure 1. The Phase Contrast X-ray imaging system is enclosed in a radiation protection cabinet to ensure the user safety. The measurement and the reconstruction of the images can be done entirely from the remote control desk.

The key parameters of the demonstrator are listed below.

Parameters	
Source acceleration voltage	40 – 70 kV
Maximal sample thickness (CFRP)	50 mm
System length (source to detector)	1.45 m
Measurement area (stitching mode)	1 m x 0.5 m
Effective pixel size	50 – 60 µm

Figure 2 shows the results obtained with a carbon fiber reinforced polymer sample, where the mid-plane ply was cut across the width of the laminate. The artificially induced defect can be detected in the scattering image using the EVITA

demonstrator (red arrows). This result was confirmed by the measurements done with the phased array ultrasonic system.

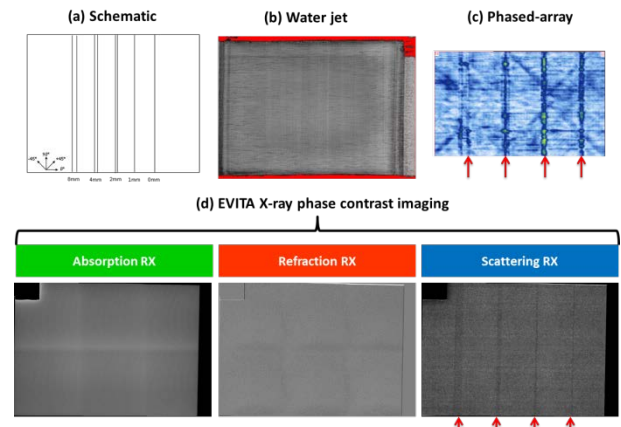


Figure 2: Results obtained on a sample with cut fibers (a) with the EVITA demonstrator (d) and with the benchmarking methods (b-c)

By increasing the level of detectability of defects in composite structures compared to standard non-destructive testing methodologies, this novel technique will play a major role during the whole life cycle of composite components, reducing their inspection cost and increasing their reliability endnote^[3].

The interest is now growing in other application domains, such as for the inspection of music instruments (see Figure 3).



Figure 3: Scattering image of a carbon fiber reinforced trumpet bell provided by the company DaCarbo, Switzerland.

Target industries for this method are:

- Aeronautics and aerospace
- Automotive
- Electronics and packaging
- Material science.

[1] V. Revol, et al., NDT&E International 58 (2013) 64–71

[2] Project financed by the European Union's Seventh Framework Programme under grant agreement n°314735 (Dassault Aviation, GMI Aero, the University of Manchester, the National Technical University of Athens and CSEM as coordinator).

[3] V. Revol, et al., Proceedings EASN workshop (2015)

Miniaturized Flash Imaging Lidar for Space Robotic

A. Pollini, C. Pache

Imaging LiDARs (light detection and ranging), or in other words three-dimensional (3D) vision-based sensors, are considered as key enabling technology for various space applications. Applications include the control of automatic descent, and soft and precise landing on celestial bodies such as Mars or asteroids, or the control of on-orbit rendez-vous or automated removal of space debris. CSEM extended its capacities from scanning LiDARs to flash imaging LiDARs in the past years.

Imaging LiDAR supports the relative navigation spacecraft-target by providing to spacecraft GN&C (Guidance, Navigation and Control) system information. It is containing at the same time distance to the target, 3D map and radiometric measurements of the target derived from time-of-flight (ToF) images and intensity images. Most of the existing imaging LiDARs use mirrors to scan a laser beam over a defined target area. The 3D image of the target is reconstructed from measurements made at different scanning directions. The major drawback of imaging LiDARs are their high mass (>12 kg) and power consumption (>75 W). And they require complex and bulky scanning mechanisms, and provide relatively low image spatial resolution and repetition rate (~400x400 points per frame in ~6 seconds). Hence, sophisticated motion compensation techniques shall be used at the same time as the spacecraft-target relative dynamics can be relatively high (up to 30 m/s). These systems are not able to achieve the desirable resolution (up to 1000x1000 points in one frame), the fast frame rate acquisition (frame rate >1 frame per second) and the relatively large observation field-of-view (>20 degrees) to meet the space mission requirements. The time available for the full image acquisition is a very critical parameter and is mainly limited by the measurement acquisition speed of the system (performing the scanning operation), the required high resolution of the image, the high velocities of the descent vehicle and, the time available and processing resources. Flash-type imaging LiDAR system is one possibility to overcome these drawbacks. In pure flash imaging LiDAR the target area is fully illuminated in one snapshot. ToF is measured on the LiDAR focal plane using a detector array with a high number of detector elements placed side-by-side in a 2D arrangements. Implementation of flash-type imaging LiDAR results in lower mass (4kg), lower power consumption (35 W) and lower system complexity and risk solutions. In addition, other effects such as image blur due to the motion can be minimized. In recent years CSEM became a recognized European innovator in the design of flash imaging LiDAR for space applications.

Today, CSEM is involved in several activities targeting the development of a flash imaging LiDAR to a Technology Readiness Level (TRL) of four. TRL4 means component and/or breadboard functional verification in laboratory environment.

In the mid-term, the objective is to maintain the leading role of CSEM in the design of flash imaging LiDAR for space applications and to cross the challenging gap between TRL4 demonstrators and engineering, qualification and flight models. In accordance with the Swiss space policy, these steps can only be achieved with the leading involvement of at least one Swiss industrial partner. In parallel, CSEM is investigating terrestrial applications fields such as metrology, driverless automotive vehicles and civilian applications of drones in order to identify additional potential markets for the technology.

CSEM was the coordinator of the project FOSTERNAV [1] which resulted in the demonstration of the first European multiple operation modes flash imaging LiDAR. The sensor architecture developed has now been scaled down to design a vision-based sensor that should be part in 2016-2017 of an in-orbit demonstration for Active Space Debris Removal [2].



Figure 1: FOSTERNAV demonstrator undergoing tests.

CSEM led the ESA MILS phase 1a project which aimed at investigating key technology bricks such as ToF matrix detectors, MOEMS mirror, Single Photon Counting (SPC) and In-Pixel Demodulation LiDAR architectures. This first project allowed CSEM to continue with the on-going MILA and CECILE ESA projects. MILA targets the development of a TRL4 traditional SPC flash imaging LiDAR, whereas CECILE aims at developing a TRL4 flash imaging LiDAR for space based on advanced image processing Compressive Sensing^[3] technique.

These activities have received the support of the EC, ESA as well as funding from the Swiss Government: we are grateful for the support received.

[1] www.fosternav.net

[2] RemoveDebris: an EU low cost demonstration mission to test ADR technologies. V.Lappas and all. IAC 2014.

[3] Compressive Sensing LIDAR for 3D Imaging. Howland and all. CLEO2011

Assessment of Precision Force Actuators and Non-contact Force Sensors for Astronomical and Medical Applications

S. Droz, W. Glettig, C. Hennemann, I. Kjelberg, H. Saudan, L. Voruz

In the frame of an internal research project, two demonstrators were conceived, manufactured, assembled, and tested: one for a simple, passive force sensor with non-contact read-out, for a potential medical application; another one to assess the true limits of resolution of a commercial motor-gear-spindle drive in a force actuation principle arrangement for typical Adaptive Optics application. For the latter, the demonstrator was assembled and tested within a Bachelor work at the HEIG-VD (Yverdon-les Bains) under the supervision of Professor Michel Girardin.

Non-contact read-out, simple, force sensor

Monitoring forces in a structure, or in an implant by simple means, remain a challenge. The sensor shall be simple, and passive, maintenance free, and require no power, etc.

How to simply interrogate, at distance, the tension of a spring force device, and the force evolution over time?

The response proposed is to use the spring coil structure as an inductance, add a two plate capacitor structure and thereafter analyze the electric resonance frequency, or complex impedance and associated changes, to correlate to the spring tension. A calibration of the system, before embedding, is required. The proposed principle applies to all pretension type force application devices, where a filament or wire is under pretension by a compressed spring.

At first, Finite Elements simulations were performed, on typical small (1cm^3) structures comprising a compression spring and a surrounding mechanical support acting also as a passive plate capacitance. The design was further enhanced by adding a supplemental coil to further increase the mechanical spring's low inductance. This increases the complexity of the solution but enhances the frequency domain resolution of the complex impedance measurement.

Typical force range is 0-100 N (adaptable by a spring stiffness change) and resonant frequency range of 6-12 MHz for such a sensor. Measurements show good concordance with performed simulations, as presented hereafter for the copper coil version under Figure 2 below.



Figure 1: With and without copper wire coil (diameter 12 mm).

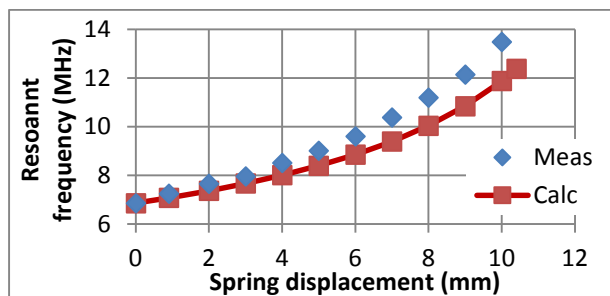


Figure 2: Typical response curve for copper coil version.

The feasibility is shown, allowing non-contact force measurements. It remains: to simplify the design and possibly pass into the GHz frequency domain.

Force actuator for adaptive optics

Adaptive optics is a way to improve the nanometric precision control of optical surfaces of mirrors and lenses, when these are deformed by thermal and gravity loads, i.e. in a telescope, or for space and satellite optics. One way, shown by astronomers at the Marseille Astrophysics Laboratory (LAM), is to attach a dozen of linear force actuators to a mirror structure. Switzerland has the most advanced miniature motor manufacturer proposing complete motors-gear-spindle position actuator arrangements.

How to best transform such a stiff position actuator into a compact force actuation systems and which force range and resolutions can one expect from existing industrial devices?

CSEM selected a system from maxon motor® EC/GP16, designed a simple flexure assembly to transform the position actuator into a force actuation scheme, and added a dummy representative membrane load. The test bed assembly with motor control and force range, and assessment of resolution and backlash was performed in the frame of a Bachelor work at HEIG-VD. The measurement results show a high linearity and resolutions (see under Figure 4). This series elastic force actuator transfers efficiently up to 25N force or some 6um displacement to the structure, with potentially nm resolutions, on a 4 N/um stiffness.

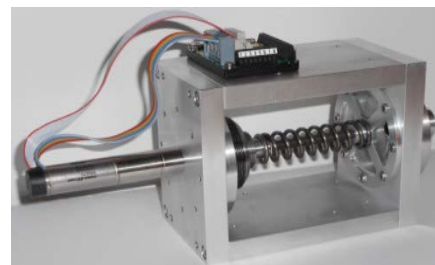


Figure 3: Force actuator test set-up based on a EC/GP16.

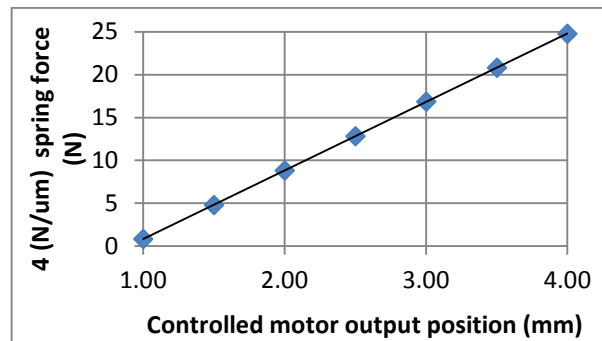


Figure 4: Spindle displacement versus mirror force and displacement.

This work was partly financed by the Canton of Neuchâtel and CSEM would like to acknowledge and thank for this support.

Optical Reference Cavities for Frequency Stabilization of Lasers

E. Portuondo, G. Buchs, S. Kundermann, S. Lecomte

Optical Reference Cavities are highly stable optical resonators, which can be used as etalons to stabilize the frequency of a laser down to a 1-Hz precision. This approximately represents a fraction of $1/10^{15}$ in terms of relative frequency stability. Such impressively stable optical sources find applications in domains where high-precision timing or distance measurements are required such as geo-positioning systems, RADARs, satellite formation flying, synchronization of large scientific facilities, as well as high-resolution optical spectroscopy. State of the art facilities for laser stabilization based on Optical Reference Cavities have been developed at CSEM in the last years and enable today further developments of high-precision instrumentation.

Optical Reference Cavities (ORC) constitute optical domain resonators of extreme frequency precision. As frequency references, ORCs outperform today all other types of resonators including mechanical, electro-mechanical (e.g. quartz), electronic and atomic in terms of relative frequency precision on a 1-second time scale.

An ORC is essentially constituted by a pair of highly-reflective mirrors fixed onto a spacer of high mechanical stability, facing each other in a Fabry-Perot interferometer configuration. Figure 1 presents a picture of such a cavity. The mirrors must be fabricated with the lowest possible losses (typically below 10 ppm), since this determines the width of the resonance line and hence the precision of the frequency reference. Also, the material (ultra-low expansion glass) and mechanical design of the spacer must be finely chosen to minimize the influence of external vibrations and temperature drifts of the cavity.

In order to obtain the ultimate laser stabilization performance, i.e., the highest frequency accuracy, it is necessary to operate the cavity in ultra-high vacuum ($\sim 10^{-8}$ mbar) and implement efficient sound, vibration and thermal insulation around it. In the end, it is the stability of the cavity length (distance between the mirrors) which determines the frequency stability of the resonator. When all the external perturbations are minimized, it is possible to reach a length stability level corresponding to the random thermal thickness fluctuations (thermal noise) of the mirror coatings. In this regime, the optical linewidth of a stabilized laser can reach the sub-Hz domain.

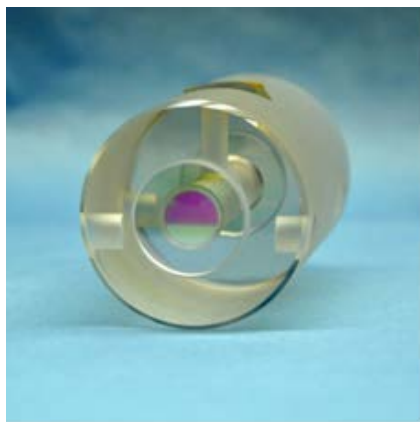


Figure 1: Optical reference cavity implemented at CSEM.

Two state of the art laser stabilization systems based on high-end Optical Reference Cavities were developed by CSEM

during the last years in collaboration with several industrial partners. Today, these systems constitute an essential part of CSEM precision-laser laboratory infrastructure, providing two independent Hz-linewidth-level optical sources in the telecommunications wavelength range of $1.5 \mu\text{m}$.

Highly precise optical frequency references can be directly applied to perform high resolution optical spectroscopy or as part of the local oscillator in optical atomic clocks. Also, the high precision of these optical oscillators can be transposed to the microwave domain thanks to the development of Optical Frequency Combs. By referencing a comb optical mode of a frequency comb to a cavity-stabilized reference laser, the pulse repetition rate of the frequency comb is stabilized with the same relative stability than the optical source. In this way, the optical frequency gets divided to the GHz-MHz range without loss of stability, enabling the generation of the purest microwave sources that can be obtained today^[1]. This technology can serve numerous applications that depend on timing accuracy such as Geo-positioning systems, RADAR, satellite formation-flying, synchronization of large scientific facilities and research in fundamental physics (Figure 2).

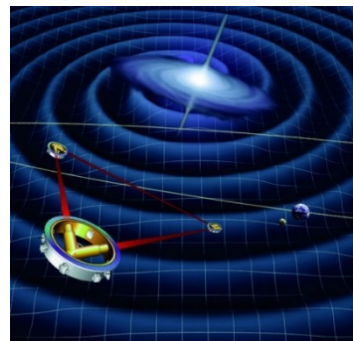


Figure 2: ESA mission candidate LISA will verify the existence of gravitational waves, relying on the accuracy of cavity stabilized laser sources. (Courtesy of ESA)

CSEM is today working in these fields as a research and development partner of several ESA and EU projects.

These activities have received financial support from the Swiss Commission for Technology and Innovation (CTI), the National Science Foundation, the Eurostars program and the Canton of Neuchâtel and CSEM would like to acknowledge and thank for this support.

^[1] T. M. Fortier, M. S. Kirchner, F. Quinlan, J. Taylor, J. C. Bergquist, T. Rosenband, N. Lemke, A. Ludlow, Y. Jiang, C.W. Oates, S. A. Diddams, "Generation of ultrastable microwaves via optical frequency division", Nature Photonics Vol. 5, 425-429, (2011)

Atomic Gyroscope for Enhanced Navigation

D. L. Boiko

Progress towards miniature atomic gyroscope with navigation grade performance based on a MEMS fabricated Rb vapor cell is reported. The gyroscope utilizes moderate pressure cell containing several hundred torrs of Xe and N₂ buffer that yield strong overlap of hyperfine absorption lines in Rb. Nevertheless we find that magnetic precession reveals large sensitivity to the pump-probe laser frequency. To overcome it, a dual frequency (DF) spin-polarized optical pumping for reduction of the laser frequency sensitivity is proposed. In addition, DF interrogation narrows the width of magnetic resonance and reduces bias.

Within the framework of the research project GYROCELL, we continue our efforts to establish a concept for low-cost navigation grade atomic gyroscope named AGEN (Atomic Gyroscope for Enhanced Navigation). Such micro-gyroscope has clear market prospects for small-size aircrafts and unmanned airborne vehicles.

Low manufacturing cost is inherent to wafer scale MEMS fabrication technique, which is envisioned as a key element of the gyroscope, a cell filled with noble gas and alkali metal atoms. Navigation performance is provided by measuring magnetic precession of nuclear spin in noble gas atoms. For operation of the gyroscope, the noble gas atoms have to be polarized in spin-exchange collisions with alkali atoms, which are under optical pumping with the circularly polarized light. Efficient and stable spin-exchange-optical pumping is vital for reaching navigation grade performance of such micro gyroscope. Here, we report on progress made in understanding the effects of optical frequency detuning from the absorption resonance and propose novel approach to reduce such sensitivity. Our optical test setup mimics the architecture of micro gyroscope physics package with a single frequency (SF) narrowband optical source. It consists of a 45° crossed circularly polarized pump and probe beams diverted from a DFB laser. Three-axis Helmholtz coil system provides a steady holding field in the pump beam direction and a second alternating magnetic field to drive the coherent spin precession in the orthogonal plane. We use a representative cell containing several hundred torrs of Xe and N₂ buffer and heated to 110°C to reach sufficiently high density of Rb vapor (Rb with natural isotopic abundance is used). The hyperfine features in the absorption line are strongly collision broadened and overlap (Figure 1, red curve). Once on resonance, one would expect no large sensitivity to small variations in laser optical frequency. Fixing the frequency of coherent magnetic field (120 kHz in Figure 2, red curve) and scanning the amplitude of the holding field, we recorded the electron spin resonance (ESR) curve for the two Rb isotopes in the cell. Under SF interrogation, ESR curve reveals bias, which can be attributed to the light shift effect. Fixing then both the frequency of coherent magnetic field and the amplitude of the holding field, we measured the impact of the laser frequency detuning on the amplitude of ESR (Figure 3). Surprisingly, despite smooth profile of the absorption spectrum in Figure 1, hyperfine ground state lines in Rb reappear in the ESR spectrum (Figure 3, red curve shows example for ⁸⁵Rb isotope). These features indicate that the laser frequency stabilization with MHz precision is required for navigation grade performance. This requirement implies an additional low-pressure reference cell in the architecture of such micro gyroscope.

We find what we believe a pioneering solution enabling us to avoid such tight stabilization of the laser frequency. It consists in modulating the laser drive current so as to produce a two

sidebands in the optical spectrum on resonance with the two hyperfine absorption lines in Rb. Dual frequency (DF) pumping and interrogation scheme flattens the ESR spectrum, reducing sensitivity to the carrier frequency detuning (Figure 3, blue curve). It also reduces the bias and the width of ESR resonances (Figure 2, blue curve). These findings will be crucial for the design of our micro gyroscope. They are also important for other miniature atomic sensors e.g. for chip-scale atomic magnetometers.

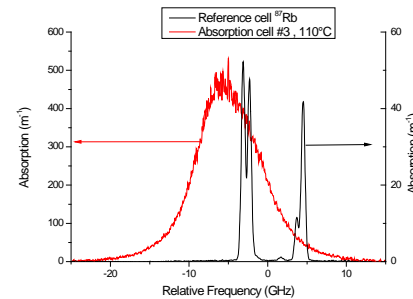


Figure 1: Measured absorption spectra of representative Rb-Xe-N₂ cell at 110°C (red curve) and of the reference cell with ⁸⁷Rb and no buffer (black curve).

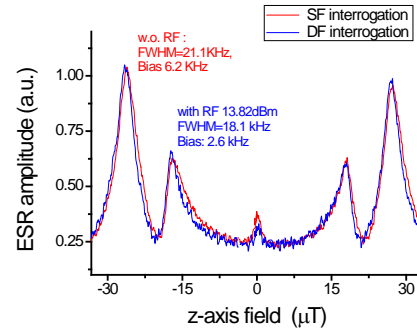


Figure 2: ESR amplitude vs holding field in a cell with natural abundance Rb. Coherent magnetic field oscillates at 120 kHz. Data are taken under SF (red curve) and DF (blue curve) interrogation.

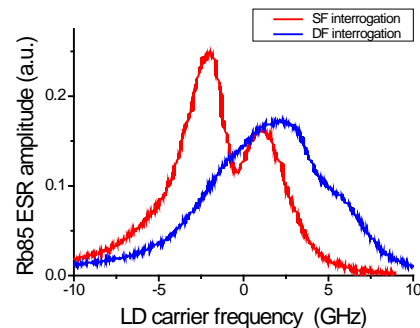


Figure 3: ESR in ⁸⁵Rb atoms at 145 kHz ($B_z=31\mu T$) vs carrier optical frequency under SF (red curve) and DF (blue curve) interrogation.

This work was partly financed by the Canton of Neuchâtel and CSEM would like to acknowledge and thank for this support.

Stratospheric Observatory for Infrared Astronomy (SOFIA): Flight Spare Mechanism for the Secondary Mirror

G. Perruchoud, J. Bennès, S. Droz, L. Giriens, L. Lisowski, I. Kjelberg

The performance of modern astronomical telescopes depends critically of the quality of their secondary mirror mechanisms. Over the years, CSEM has developed a particular expertise for this type of high-precision opto-mechatronics systems. In order to ensure continuity of the Stratospheric Observatory for Infrared Astronomy (SOFIA) observatory, CSEM was mandated to manufacture a spare system for the secondary mirror.

The (SOFIA) 2.5-m telescope is sponsored jointly by the US and German aerospace agencies NASA and DLR. The telescope is carried by a revised Boeing 747-SP aircraft in a special compartment, which can be opened during flight. The telescope is operated at about 14 km altitude, at temperatures down to -55°C and a pressure of 120 mbar.



Figure 1: SOFIA Boeing 747 with the telescope door opened.

The SOFIA Secondary Mirror Mechanism (SMM) has a diameter of 350 mm and comprises a complex mechanism providing precision motion control along 8 degrees of freedom, divided into two main sub-systems:

- The Focus-Centre Mechanism (FCM) which provides the static fine alignment capability for focus, centring and tip/tilt. The FCM consists of a hexapod mechanism of particular and compact geometry.
- The dynamic Tip/tilt-Chopping Mechanism (TCM) provides the fast tip-tilt-chopping actuation. The kinematics of the mechanism relies entirely on various flexure components: elastic rods, membranes, and cross pivots which provide original frictionless mechanical links.

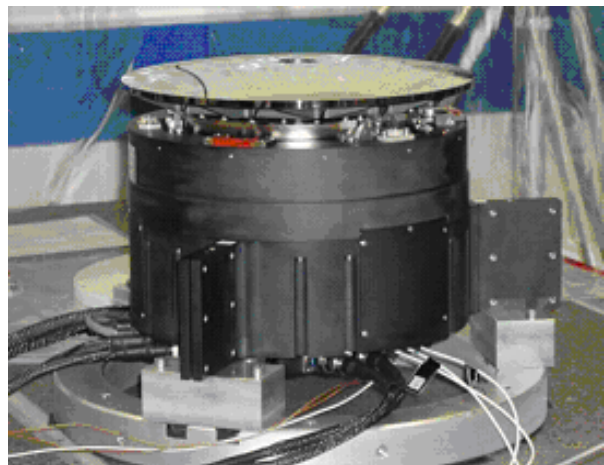


Figure 2: SOFIA SMM mechanisms (FCM + TCM).

The original SMM assembly was delivered in 2002 to the DLR. A major achievement in 2003 was the integration and final delivery and shipping to the USA of the full SOFIA Telescope. The first astronomical observation (first light) took place only in 2010.

The specifications of the SMM are given in Table 1.

Table 1: SMM main specifications.

Main Requirements	Measured performances
Focus-center mechanism	
Focus (z) range	$\pm 5 \text{ mm}$
Focus resolution	$\leq 0.5 \mu\text{m}$
Center (x,y) range	$\pm 3 \text{ mm}$
Center resolution	$\leq 1 \mu\text{m}$
Tip-tilt range	$\pm 0.312^{\circ}$
Tip-tilt resolution	$\leq 2 \text{ arcsec}$
Tilt-chop mechanism	
Tip-tilt range	$\pm 0.312^{\circ}$
Tip-tilt blind accuracy	< 2%
Tip-tilt resolution	$\sim 0.07 \text{ arcsec}$
Chop frequency	0-20 Hz
Chop rise (transition) time	< 7 ms
Chop stability	$\leq 1\% \text{ of chop excursion}$

Currently the SOFIA telescope is flying regularly, but without any spare items for the SMM. In case of failure, the full plane and telescope is stranded with associated high costs. In 2014, CSEM was mandated to manufacture a complete spare SMM (identical parts to those made 12 years ago), including the control electronics, updated to actual FAA flight standards.

All parts are made identical to the original ones to simplify the exchanges. Unfortunately, for the electronics, most parts and chips are no longer available. Therefore, the electronics is redeveloped with parts available today (with similar specifications) and, in the same time, is made fully NASA Aeronautic Quality compatible. The cabling, pinout and overall behavior shall be held identical to the old electronics to be fully compatible and exchangeable at rack level.

In order to obtain the same mechanics quality of the spare device the same Swiss manufacture providers were selected, as far as possible. A challenge is the procurement of the critical flexure hinge materials and their advanced surface treatments required to improve their corrosion resistance.

For the electronics, the main challenge was to find new equivalent circuits, and to make the new electronic racks fully compatible and interchangeable.

The first spare actuator will be assembled and thermally tested at CSEM premises in 2015, and fully assembled in 2016. Further qualification tests are planned at NASA AMES Centre in Palmdale, USA, in close collaboration with the DSI SOFIA team.

GENEQUAND, a Novel Watch Regulator based on Compliant Mechanisms

F. Barrot, G. Musy, F. Cosandier, I. Kjelberg, P. Renevey, L. Giriens, P. Schwab, P. Genequand[•], Y. Petremand, O. Dubochet, F. Ganny^{••}, T. Hamaguchi^{••}

Together with his industrial partner Vaucher Manufacture Fleurier, CSEM has developed a novel watch regulator which is six times more efficient than those used in traditional mechanical watches in term of mechanical losses. This breakthrough has been achieved by combining two fields of expertise of CSEM: the design of compliant mechanisms and the technology of silicon etching.

A watch regulator, which is made of the association of an oscillator and an escapement, is subject to losses due to friction and shocks. Limiting these losses can drastically increase the power reserve of mechanical watches.

Pierre Genequand, a former researcher at CSEM, had a long experience in the design of high precision mechanisms based on the use of "flexure hinges", also commonly referred to as "compliant mechanisms"; such an approach enables precise, frictionless and lubrication free movements. Several demanding mechanisms targeted for space or astronomy applications have been produced at CSEM with this approach. But Pierre Genequand had always in mind that, some of the small size and high precision components found in mechanical watches, could also greatly benefit from the "compliant mechanisms" design approach [1].



Figure 1: The Genesis of the Genequand regulator. From the 20:1 wood scale model (left) to the 1:1 silicon based prototype (right).

Based on this conviction, he designed the first version of his regulator and successfully implemented it on a 20:1 scale model wood based prototype. The hair spring and the ruby bearings of the classical oscillator were replaced by a flexure based pivot. In parallel, the classical Swiss anchor was replaced by a permanent contact anchor guided on a flexure based pivot and exhibiting flexible arms to cooperate with the escapement wheel. Convinced by the potential of the idea, CSEM worked to shrink down the prototype to the 5:1 scale before submitting this invention to several watchmakers. Seduced by the approach, Vaucher Manufacture Fleurier (VMF) decided to join the adventure and to work together with CSEM on the further miniaturization and the integration of the concept into a wrist watch.

That is when CSEM's knowhow, in silicon etching, comes into play [2]; CSEM's mastering of DRIE (deep reactive ion etching)

micro-structuration techniques made it possible to produce small size high precision mechanical parts taking full advantage of the excellent mechanical properties of silicon [3]. In this implementation several functions traditionally played by different components are gathered into one single part:

- At the oscillator level: a monolithic flexure based oscillator combines the functions of hair spring, oscillator pivot (ruby bearing + pivot shaft) and balance wheel into one single silicon component.
- At the anchor level: a monolithic flexure based anchor combines the functions of anchor pivot (ruby bearing + pivot shaft), pallet-stones and anchor into one single silicon component.

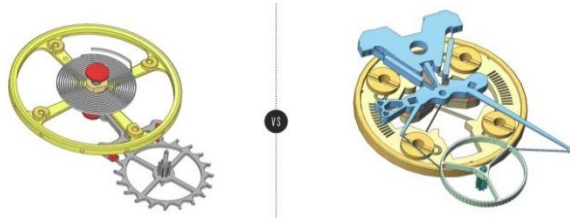


Figure 2: the classical Swiss anchor based regulator (left) versus the Genequand regulator implemented at the watch scale (right).

The first watch scale prototype was integrated in a VMF caliber in 2014 [4]. A first test campaign validated the strong innovation potential of this novel regulator which enables to foresee the creation of mechanical movements with up to 30 days of power reserve.

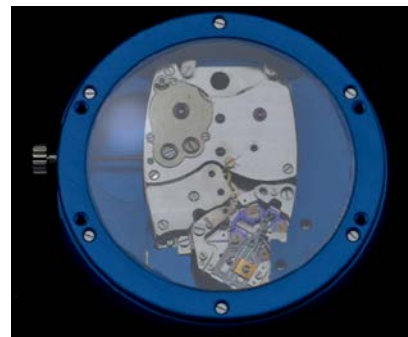


Figure 3: The Genequand regulator integrated in a VMF 6000 caliber.

[•] retired from CSEM

^{••} Vaucher Manufacture Fleurier

[1] P. Genequand, M. Bogdanski, I. Kjelberg, "Elements flexibles usinés pour applications microtechniques", Bulletin de la Société Suisse de Chronométrie, SSC, no. 33, 2000

[2] A. Perret, "Le silicium comme matériau dans la fabrication de pièces mécaniques", Bulletin de la Société Suisse de Chronométrie, SSC, Neuchâtel, CH, no. 38, 9 novembre 2001

[3] S. Jeanneret, A. Dommann, N. F. de Rooij, "Procédés de micro-fabrication avec application horlogère", développements récents, SSC, 2008

[4] F. Barrot, P. Genequand, I. Kjelberg, T. Hamaguchi, Un nouveau régulateur mécanique pour une réserve de marche exceptionnelle, SSC, 2014

ULTRA-LOW-POWER INTEGRATED SYSTEMS

Alain-Serge Porret

The Ultra-Low-Power (ULP) Integrated Systems program addresses the key challenges faced and the technologies required when building very low power, (often) wirelessly interconnected, embedded smart systems or remote sensing nodes. The availability of such components is central to several global technological trends, such as the Internet of Things (IoT) revolution, the advent of wearable technologies for wellness and medical applications (in line with the needs of an aging population), or the generalization of machine-to-machine (M2M) communications required by Industry 4.0.

It is generally recognized that the number of interconnected devices will continue to increase exponentially (as wearable items in our clothes or on our wrists, for implantable health monitors, at home in our appliances, to improve the security of our transport infrastructure, to track goods, etc.), to the point where they become essentially invisible to the end user (pervasive technology).

These trends are largely made possible by today's mature IC technologies, which allow the packing of an incredible number of interfaces and remarkable amounts of computational power in ever-smaller volumes, with constantly shrinking costs and lower power consumption. Therefore, the development of ASICs (application-specific ICs) is a significant element of the program's activities, although COTS (commercial, off-the-shelf) solutions are considered when suitable devices are available.

The overall technological realm of the program encompasses mixed-signal devices, embedded processing, sensor interfaces, wireless systems, and vision technologies with a mixed hardware and software approach. It is clearly aligned with the "More than Moore" paradigm, which is in line with the general directions being taken by the Swiss economy, its inventiveness (doing more with less), and its capabilities (investment requirements within the scope of SMEs' available resources).

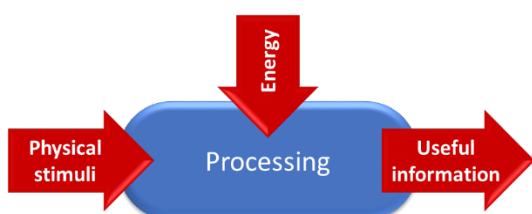


Figure 1: Basic structure and function of a generic sensing node.

Figure 1 shows the basic structure of a generic sensing node, which (1) collects and manages electrical energy to (2) acquire physical stimuli, (3) process them locally—both in the analog and digital domains—in order to extract the relevant information, and (4) communicate this information to a central unit, often wirelessly. The focus of the program is to provide solutions to these four key technical challenges as follows—

- *Energy management:* this includes the smart management of batteries, but also energy harvesting from photovoltaic cells, from thermo-electric generators, or from wireless power transmission, moving devices toward maintenance-free and environmentally friendly, zero-battery operation.

- *Sensing interfaces:* a great many different types of physical quantities may need to be sensed by the broad range of applications covered by the program. These monitored quantities are getting more varied and include environmental parameters (such as the monitoring of harmful gases) and non-invasive vital sign monitoring (for instance, heart rate at the wrist or with the help of advanced vision systems). These measurements require sophisticated electronic interfaces and processing, which are even harder to design within the additional constraints of the ULP context.
- *Processing and extraction of relevant data:* in many cases, transmitting the raw information from the sensors is not efficient or secure. Local pre-processing, event classification, and the encoding of data enable faster, much safer, and overall energy-efficient solutions that—moreover—will not generate unnecessary data "pollution" and will thus prevent the clogging of the precious, and shared, airwaves.
- *Transmission of extracted information, remote management, and coordination of distributed operations:* wireless communication requires a significant amount of energy. Optimized solutions need to be carefully devised, balancing various trade-offs for each specific application, both at the hardware and software levels. This also includes specific solutions for the integration and fusion of data from heterogeneous sensor networks, and the growing challenge of network security management.

The markets covered by the program are very diverse, as the generic nature of Figure 1 suggests, and are growing in scope with the development of the Internet of Things (IoT) paradigm, which is also aligned with the global trends of "wireless everywhere" and "smart everything". Applications include:

- Consumer electronics (Bluetooth Smart devices, GPS-enabled devices, home automation and security systems, and image classification);
- Industrial systems (high-performance sensor interfaces, sensor networks for harsh environments, and optical quality control);
- Metrology (integrated measurement microsystems or optical encoders for various purposes);
- Medical and wellness (implants, vital sign monitoring, and electronic prostheses).

The long-term objective of the program is to provide the unique technologies required to build commercially successful, state-of-the-art sensing platforms and remote sensing nodes, with a focus on very low power (or battery-less), low-voltage, miniaturized devices. Although the program has a strong ASIC design component, it also leverages off-the-shelf devices where suitable.

This objective is pursued not only by the continuous improvement of the components' performance, but also by system-level optimizations. All relevant hardware and software aspects—from signal acquisition to signal processing,

embedded software, and communication—are covered (all carried out in close conjunction with other CSEM programs).

A significant emphasis is placed on ensuring that the result is suitable for future industrialization without a major redesign or many compromises. Sometimes, the ultimate performance is therefore less central than the stability and reproducibility of the results in a real environment.

Many of the applications concerned cannot benefit from wired power, either because the device must be mobile or worn or because it is implanted, is not located near a suitable power source, or simply because the wiring necessary to connect a large number of remote nodes is impractical. Therefore, reducing power consumption to increase battery life, ultimately to the point where energy harvesting enables zero-battery solutions to be developed, is paramount to the whole program.

The ULP Integrated Systems program is sub-divided into three research activities, as follows:

- The *Vision* activity provides complete, embedded vision solutions that not only capture images, but also locally extract relevant features. It covers the complete acquisition chain from pixel sensing and electronics (components), via optics and processing hardware (system), to image processing and recognition tools (algorithms). In this area, better IC technologies also enable local processing and accurate pattern recognition, in an energy-efficient way, of the large amount of data generated. It is foreseen that imagers sensitive to much more than just visible light will eventually become mainstream—with applications in infrared, X-rays, or THz bands—and will be mixed with new multi-spectral capabilities and innovative optics.
- The *Wireless* activity similarly aims at providing complete solutions that wirelessly transmit information through a network at a low energy cost for the remote nodes and are tailored to specific applications. It includes the development of narrow- and wideband ULP radios and antennas (components), of dedicated protocols taking advantage of the specifics of the components and applications (algorithms), and of complete wireless sensing nodes and network architectures (system). The main markets targeted are wireless sensor networks (WSN and IoT) and wireless body area networks (WBAN). Emerging technologies supported include robust, flexible, and software-defined radios, as well as RF sensing in the radar and sub-THz bands.
- Finally, the *System-on-Chip* activity provides the missing elements to complete a fully integrated solution. It includes ULP sensor interfaces; power management and energy-optimized digital processing (components); embedded, real-time control and processing software (algorithms); and power-efficient design methodologies and design flow (system). Notable novel directions include vital sign monitoring, brain/neural system interfaces, and sub-/near-threshold logic circuits.

2015 has seen the continuation of our efforts in the field of near- and sub-threshold digital circuit design. Lowering the supply voltage of digital circuits to close to the value of the transistor threshold voltage has demonstrated the potential to provide a major energy-efficiency improvement over mainstream design

techniques. However, it also presents significant new challenges as leakage current become prevalent, some traditional circuit topologies stop operating properly, and statistical delay spreads increase to the point of challenging the usual timing analysis assumptions. Therefore, in order to benefit from the promised gains, the complete design flow needs to be reconsidered, including the synthesis methodology, standard cell libraries, memory (RAM and ROM) architectures, and power management schemes. Such a fundamental effort is now underway at CSEM for both 180 nm and 65/55 nm geometries. Some early and encouraging results for memories are discussed in the paper *Design and on-Silicon Characterization of a 6T SRAM Memory Operating at Subthreshold Voltage* (page 129). Further studies are ongoing on the other challenges mentioned above and already promise excellent results at the system level.

In *A 1 M-Pixel 2000 Frames/s Image Sensor* (page 107), a new generic sensor chip for high-speed, high dynamic-range cameras is shown to possess excellent characteristics. This platform will serve as a basis for building cameras for the growing number of applications requiring high-speed image capture, such as those in the industrial, medical, and automotive fields.

The paper *Feature Selection in Support Vector Machines for Cars and Pedestrian Detection* (page 109) is an example of our ongoing effort regarding the embedding of powerful image processing and recognition algorithms into small, resource-limited embedded nodes. A detector based on support vector machines (SVMs) has been successfully implemented on our new miniature "vision-in-package" platform and a processing time below 1s has been achieved with good result accuracy.

An ultra-wide-band chip that boasts significantly lower power consumption than existing commercial solutions is described in *A 6-8 GHz IR-UWB Transceiver ASIC in 65 nm CMOS for Ranging Applications* (page 122). The technology can be used for a variety of applications, including communication, ranging for security applications, and object localization/tracking. An energy consumption of a few tens of micro-joules per ranging operation, with a latency of only a few milliseconds, has been measured.

Finally, with the generalization of IoT devices, the ability to properly and conveniently secure wireless links has become a major concern that should not be understated. CSEM is developing its own solution—targeting embedded devices and resource-limited wireless nodes—in the form of a software library that can be customized for a variety of protocols, both proprietary and standard (such as 805.15.4-6 and Bluetooth LE), as discussed in the paper *Securing Wireless Links on Resource-Limited Devices* (page 120).

A 1 M-Pixel 2000 Frames/s Image Sensor

Y. Zha, H.-R. Graf, A. Bischof, C. Henzelin, B. Schaffer

A high-speed image sensor implementing 11 bit ADCs and pixels with a high Full-Well-Capacity of 150 ke- has been developed. It is capable of outputting up to 2000 frames/s at a 1 us row-time in global shutter mode. This sensor fits the needs of many industrial, medical and automotive applications requiring fast, high Dynamic-Range and high-SNR cameras. The building blocks have been developed in a tower 0.18- μ m CMOS process and serve as a basis for further high-speed camera projects as required for industrial automation, optical coherence tomography or process analysis.

High-speed image sensors are widely used for industrial, medical and automotive vision applications where fast moving objects have to be captured and analyzed. Most high-speed sensors on today's market implement a global shutter exposure to capture smear free images, 10 or 11 bit ADC's for reaching ~60 dB Dynamic Range and achieve row-times between 1-2 us. However, due to the reduction of the pixel pitch from 12 μ m to about 6 μ m, the pixel Fill-Factor and Full-Well-Capacity is lowered. Typical Full-Well-Capacity of these sensors is in the range of 20 ke- resulting in SNR levels of ~40 dB. This low SNR level is not sufficient for many applications because of the resulting low image quality.

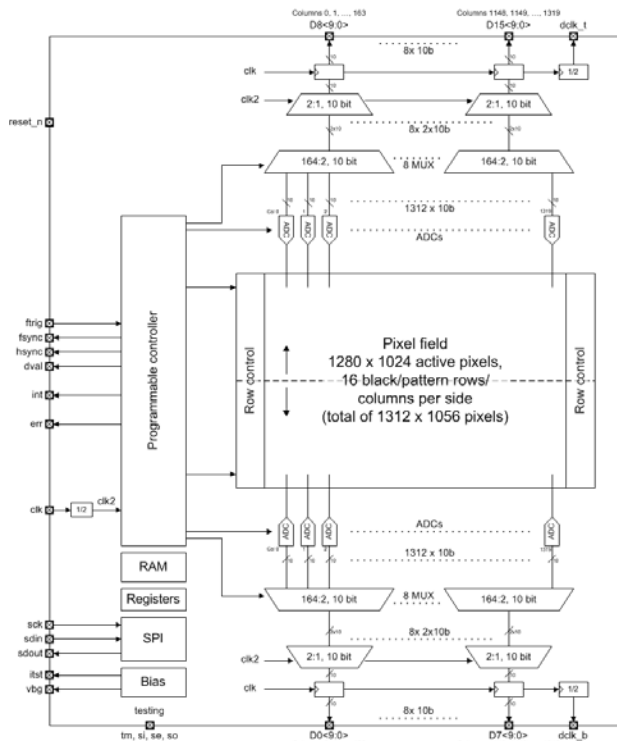


Figure 1: Sensor architecture of the 1.3 Mpixel sensor.

As part of the EU-project "VIAMOS—Vertically Integrated Array-type Mirau-based OCT System" we have developed an image sensor with a 12 μ m pixel pitch and a capacity as high as 150 ke-, achieving an SNR of ~51 dB, and including a readout path with a typical row-time of 1 us. This high SNR and short row-time is a strong requirement for our EU partners, whereas the Dynamic Range (>55 dB) is of lesser importance because the illumination level on the sensor pixel field is mainly constant.

The design is based on IP's developed in [1]. To reach the targeted 2000 frames/s a top/down readout architecture with

2 ADCs per column has been implemented. With this method the readout speed can be doubled (see Figure 1).

A major design effort has been spent on the digital backend to reach the 160 MHz clock speed within the big sensor area of 20 mmx20 mm. The sensor is packaged in a custom 356-pin LGA package and evaluated in a custom made test-bed (see Figure 2).

Different types and variations of pixels have been implemented in several test columns of this sensor. This includes pixels with LOG-functionality and pixels targeted for fluorescence lifetime imaging or time-of-flight applications. These pixels together with the blocks developed in this project will serve as a basis for future image sensor developments at CSEM.

The sensor has been evaluated according to the well-known EMVA1288 standard (Standard for image sensor characterization). The measured figures of merit are excellent and exceed the requirements given by the initial specification:

- Full-Well 137 ke-, Dynamic Range: ~60 dB, SNR: 51.5 dB
- Gain 177 e-/DN, Lag: 0%
- PRNU: 0.2%, Non-Linearity: 0.5%
- QexFF@600 nm: 0.5

This results in an excellent video quality which has been demonstrated in a high speed video capturing a rotating fan.

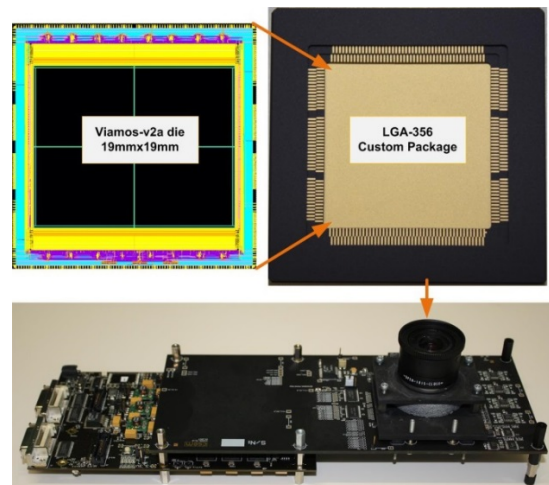


Figure 2: Sensor, test-bed and evaluation environment.

Thanks to the great contribution of all project members and our EU partners, this project can be characterized as a success.

[1] Y. Zha, et al., "A 256 x 256 pixels 4000 frames/s image sensor" CSEM Scientific and Technical Report, (2014) 122

Towards the Industrialization of the SunTracker

E. Grenet, P. Nussbaum, P.-A. Beuchat, E. Franzi, C. Gimkiewicz

The CSEM SunTracker has been fully redesigned to meet industrial specifications, among them the resistance to shocks and a wide operational temperature range, including a fabrication process for the optical front-end and an easily implementable calibration procedure. Additionally, its intrinsic performances were enhanced with an increased field of view, a lower power consumption and a sub-millidegree accuracy. The technology has been transferred to the industrial partner, who will now integrate CSEM SunTracker devices in various geo-localization products.

Based on the CSEM spaceCoder technology, a SunTracker prototype^[1] was realized in 2013, providing the azimuth and elevation angles of the Sun with high accuracy ($\pm 25.10^{-3}$) under a 120° field of view (FOV) with a power consumption of 800 mW. This prototype has been redesigned with industrial constraints such as the resistance to external shocks, the operability under a wide temperature range, a lower power consumption and a viable manufacturing process including calibration aspects.

A major point of this redesign was the optical front-end, which consists of an imager, an optical attenuation filter and the spaceCoder shadow mask. The Aptina imager was replaced by another version compatible with the required temperature range (-40°C to +50°C) and which has a better package: the smaller sensor-to-glass air gap increases the FOV up to 150° , and allows the use of a new shadow mask that provides a higher precision. This shadow mask was etched directly on the attenuation filter (NG1 substrate) with anti-reflective chromium.

The assembly process of the front-end was key, as it had to be both easy to manufacture with a high repeatability to simplify the calibration procedure, and shock-resistant to avoid a recalibration after an unexpected shock. The solution for this assembly was a gluing of the etched filter on the imager. As UV curing was not possible due to the OD4 attenuation filter, the assembly was realized with a high-precision mechanical setup by gluing the mask-filter reticle centered on the imager, and heat curing it. The repeatability of this process was perfectly satisfactory, as the assembly variations (offset and rotation) were small enough to be compensated by the calibration. Equipped with a reliable temperature sensor for metrological corrections, the optical front-end was mounted on a separate board with a flex connector to decrease the mass on glass, and thus increase the system sturdiness (Figure 1).

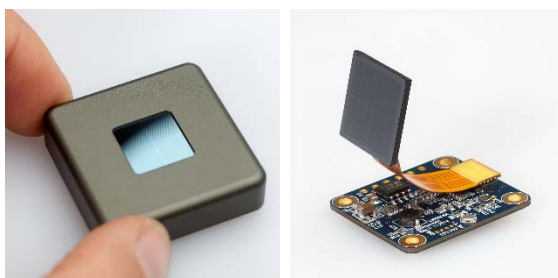


Figure 1: SunTracker prototype (left), front-end flex-board on its processing board (right).

The processing board was redesigned with two modes of operation and related supply voltages: RS232 under 3 V for programming, measurements and calibration, RS422 under up

to 24 V for industrial operational use. The image acquisition scheme has been re-implemented (acquisitions on request with a low-power standby mode in-between). The Sun angles measurement is performed by a cortex M4 ARM processor, including the front-end calibration and the temperature correction. Built from off-the-shelf components, the complete system in its aluminum package is compact (33x33x10 mm); it delivers accurate Sun angles in real time (30 ms after user request) and consumes 80 mW.

A new calibration process has been implemented that compensates most of the front-end variations, such as the hardware variations (thicknesses of imager air gap, glass parts and glue), the assembly imperfections (planarity, offset and rotation) and the internal reflections (NG1-Air, chromium and silicon). This resulted in a significant enhancement of the performances, achieving a sub-millidegree accuracy for the angle detection under a 120° FOV, and still $\pm 3.10^{-3}$ under the extreme 150° FOV. Based on a few measurements points, this calibration is compatible with an industrial production line. A compensation of the temperature effect has also been implemented: it allows to maintain an accuracy of $\pm 30.10^{-3}$ from -40°C to +50°C (Figure 2).

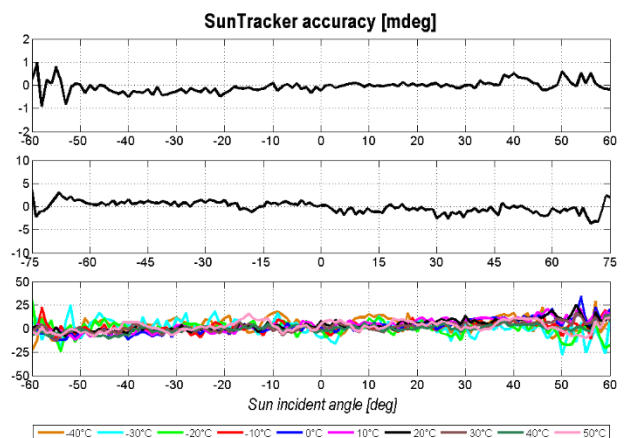


Figure 2: SunTracker accuracy [mdeg] under stable temperature (top and middle) and under large temperature variations (bottom).

Reshaped for industrialization, the CSEM SunTracker reaches very high performances in real time. It can be used in combination with other instruments (telescope, goniometer, theodolite etc.) or by itself. This achievement was made possible only with the support of the CTI office. The SunTracker know-how, based on the CSEM spaceCoder technology, has been fully transferred to the industrial partner, who will integrate SunTracker devices in various geo-localization products.

^[1] E. Grenet, et al., "Embedded sun tracker with extreme precision", CSEM Scientific and Technical Report, (2013) 100

Feature Selection in Support Vector Machines for Cars and Pedestrian Detection

V. Moser, A. Chebira

An application for cars and pedestrian detection has been developed to run on CSEM's vision-in-package (VIP), the world's smallest vision system. The detector is based on support vector machines (SVMs) and uses Haar features. Only thirty training images are needed to build a robust detector. To be embedded on the VIP, the speed of the detector and the required memory size had to be optimized. Hence, a feature selection mechanism has been designed, which also increases the efficiency of the detector. This application can be used to manage traffic lights at crossroads.

If a system for cars and pedestrian detection is to be deployed at crossroads, it must be cheap, low power, easily trainable and operate in real time. CSEM's VIP-429 fulfills these expectations in terms of cost and power consumption. Many algorithms exist for cars and pedestrian detection. The one we chose for this platform had to be able to make the decision in one second the most. Moreover, it should not require a large amount of labeled data for its training.

Even when used in a simple application, convolutional neural networks^[1] and Adaboost-based classifiers^[1] need a few hundreds of labeled training data to avoid overfitting. Moreover, the training must be done off-line, meaning that the classifier must be completely retrained if additional data become available. Deep networks^[1] can be trained from few images, but require a lot of computing power and are not suitable for small platforms. SVM based algorithms^[1] are likely to be less robust than the above-mentioned algorithm for complicated tasks, however they require less training data, and allow new data to be easily integrated into the detector later. The number of support vectors (SVs) and the type of features used can be parameterized, allowing us to tune the computing needs when used on an embedded platform. For our application, Haar features have been chosen for their well-known efficiency in object classification and their ease of computation.

The developed application detects, each second, from a single image, the presence of pedestrians and cars at specific positions. For example, a pedestrian waiting to cross the road or a car stopped at traffic lights. If the scanning zone is 10x10 pixels for each position, the usage of Haar features and SVM does not allow us to have more than 60 SVs for each detector.

The number of features is also a key point in the development of the application. From the observation that not all features are relevant to a specific SV, we decided to select, for each SV, only a subset of features that are specific to that particular SV. For example, as depicted on Figure 1, if the result of a feature on a positive SV (green image on Figure 1) is close to the result of the same feature on the negative SVs (red images on Figure 1), the feature is assumed not to be representative of the SV and can thus be removed.

The SVM training algorithm is configured to use 192 different Haar features for each input and a maximum of 60 SVs. The training database contains 30 labeled images and the testing database contains 100 labeled images. Tests have been performed with a different number of features for each SV. To assess the performance of the detection algorithm, we computed the number of misclassifications, and a "separability"

metric. The "separability" metric is computed by dividing the difference of the minimum value of the positive class $\min(pos)$ and the maximum value of the negative class $\max(neg)$, by the difference between the medians of both classes: $\frac{\min(pos)-\max(neg)}{\text{med}(pos)-\text{med}(neg)}$. This metric represents how well the two classes are separated given their SVs. A negative separability implies a non-zero misclassification.

For pedestrian detection, the results are the following:

- 192 features: 3 misclassifications, separability: -1.05
- 60 features: no misclassification, separability: 0.24
- 30 features: 1 misclassification, separability: -0.06

For car detection, the results are the following:

- 192 features: no misclassification, separability: 0.46
- 50 features: no misclassification, separability: 0.64
- 20 features: no misclassification, separability: 0.60

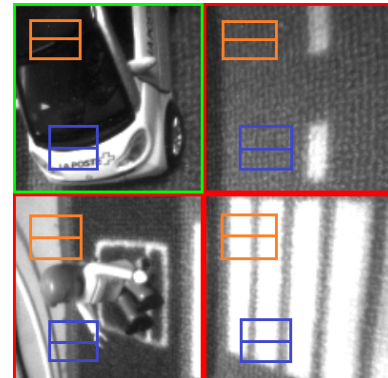


Figure 1: Example of feature selection for car detection: the green image represents positives while the red ones represent negatives. The blue feature is one that is representative of the positive while orange feature is not.

It is interesting to note that in the case where only 20 features are selected by each SV in the car detector, there are 13 features from the 192 initial ones that are never chosen by any of the 60 SVs. Those 13 features do not need to be computed, allowing an improvement in speed.

Due to the memory saved (SVs of size 50 instead of 192), this feature selection allows us to embed the detector on the VIP. In addition, our results show an improvement in the efficiency of the algorithm.

In a future work, the effect of integrating this feature selection during the training of the SVM could be studied.

^[1] C. Bishop, "Pattern recognition and machine learning", Springer ISBN 0-387-31073-8, (2006)

Scale-invariant Object Recognition from Industrial Light-field imaging

S. Cloix, D. Hasler, T. Pun •

A new approach to scale-invariant object recognition based on bag-of-visual-words is presented. Our method was tested on our new database of light-field images and assessed an excellent recognition rate greater than 90% despite a scale variation of about 200%. Our versatile light-field image dataset, CSEM-25, composed of 5 classes captured under several poses and backgrounds, was built with an industrial plenoptic camera, the Raytrix R5. It will be made available for research purposes.

Light-field imaging is an enhancement of conventional imaging that records not only the intensity of light but also the direction of every light ray hitting a camera [1]. In practice, the recording of a light field is either performed using arrays of cameras, or – as in our case – using a dedicated camera that includes a microlens array, also called a *plenoptic camera*. In our tests we used the industrial 4-megapixel Raytrix [2] camera.

The existing light field datasets, mostly capturing one object, are seldom suitable for classification purposes but 3D reconstruction. We aim at providing a dataset exhaustive enough to be used for many different vision and classification tasks. The dataset is composed of 5 classes of 5 objects of known and similar size. For each object, pose (72 angles) and distance (21 from 28 cm to 50 cm), four captures are acquired: two with a uniform background and two with a landscape background randomly picked from a database of high resolution images (Figure 1).



Figure 1: Our acquisition setup composed of a motorized linear stage, a motorized turntable, a background screen and a uniform colored ground.

The image recorded by the Raytrix camera is a group of micro-images lying on a hexagonal grid. An interesting feature of the recorded image is that the content of each micro-image does not vary a lot when highly increasing the distance of the object from the camera; only the number of times a pattern appearing inside a micro-image varies significantly (Figure 2) across neighbouring micro-images. We therefore aim at taking advantage of these pattern repetitions and the small variation in scale within the micro-images to develop a recognition system that is invariant to the scale induced by the distance.

Our object recognition method is based on bag-of-visual-words strategy: (i) a codebook is built from an unsupervised clustering method and (ii) is used to build a histogram of each image. The histograms of the test images are then compared to each of the training images of the labelled objects.

The codebook is a set of whitened pixel patches learnt from small patches extracted within each micro-image of a training-image set. The training set is made of segmented

• Computer Science Department, CVML, University of Geneva, Switzerland

captures of each object at the closest distance. A histogram is then extracted for each object. For each test image, the small patches are extracted at a fixed location within a fixed region of interest. Each bin of a histogram represents the number of occurrence of the corresponding visual word in the region of interest. The farther the object, the smaller the number of visual words belonging to the object. As the histogram of a test image is expected to have the same shape than of the training image but with lower amplitude, we scale up the test histogram and compare it with the histogram of the training images by minimizing a thresholded ℓ_1 distance.

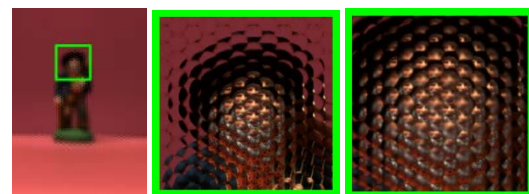


Figure 2: Dataset samples: on unified background, an instance of the "person" class is captured from the farthest distance (left), a zoom region (middle) of the left image and a zoom region at a closer distance to the camera.

We evaluate our approach on five objects, one instance of each class. The training images are composed of the ones with a uniform background. The test images are from four subsets, the first two with a uniform background and the last two with random backgrounds. At the closest distance, we obtain a recognition rate of 100%, the background not having a large impact. Using a fixed size detection window, the farther the objects, the lower the recognition rate, due to the noise introduced by the background that fills an increasing proportion of the detection window. We exceed 90% of correct recognition for each tested distance, the recognition rate expectedly decreasing with the distance (from 100% at the closest distance to 90% at the farthest one).

From the properties of our industrial plenoptic camera we designed a new real-time recognition approach that is robust to large scale variation of almost twice the size of the object when farthest from the camera. With a codebook of a few words (100 visual words), we reached a recognition rate greater than 90%. As next steps, we aim at scaling up the system to recognize more objects and also to classify objects by category. The dataset is available on demand.

This work is co-funded by the Swiss Hasler Foundation SmartWorld Program, grant Nr. 11083.

[1] E. H. Adelson, J. R. Bergen, "The plenoptic function and the elements of early vision", Computational models of visual processing, 1 (2) (1991) 2

[2] www.raytrix.de

System-on-chip for Nanometric-range, High-speed Optical Positioning Measurement

F. Kaess, A. Corbaz, B. Schaffer, S. Beer, B. Putter, C. Gimkiewicz, P. Masa, H.-R. Graf, D. Sigg, J.-L. Nagel, C. Monneron, R. Godinho Caseiro, C. Arm, Y. Zha, P.-A. Beuchat, T.-C. Le, L. von Allmen

A nanometric-range, high-speed optical positioning measurement system-on-chip was integrated in 0.18 μm CMOS image sensor technology to implement high-precision absolute optical encoders for metrological, automotive and harsh environment applications.

The spaceCoder technology [1] consists in computing the spatial position of a moving reference object from the position of the shadow image of a specific code pattern, which is projected on a sensor. Depending on the application constraints, this technology can be implemented with various hardware configurations: off-the-shelf components (sensor, optic, code pattern and lighting) or custom solutions. The shadow position measurement is done in two steps:

- A phase measurement of the shadow position for high-resolution position measurement
- Decoding of the absolute code interleaved with the phase pattern to extend the measurement range

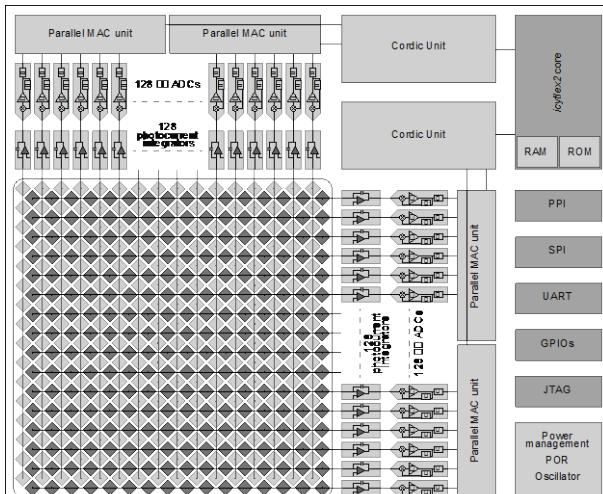


Figure 1: Block schematic of the spaceCoder system-on-chip.

A custom system-on-chip has been realized to fulfil the speed and temperature specifications of demanding applications that cannot be reached by assembling existing components. The block schematic of this ASIC is depicted in Figure 1. To achieve the high-speed requirement, a specific frontend composed of interleaved vertical and horizontal photodiodes was designed. The photocurrent of each photodiode is integrated and converted in parallel by row and column integrators, as well as ADCs placed at the edges of the photodiode array. A dedicated hardware unit (DHU) performs the phase computation in both the vertical and horizontal directions simultaneously by parallel multiply-and-accumulate operations, and two Cordic operators. With this optimized architecture, it is possible, under optimal illumination conditions, to compute the 2D phase position of the shadow in 5 μs , allowing a sampling rate of 200 kHz. The high-level application dependent algorithm is computed by an *icyflex2* processor and associated peripherals. For more demanding applications, a customized system-on-chip

embedding a hardwired high-level algorithm could be developed. The micro-photograph of the ASIC is shown in Figure 2 and its main specifications are summarized in Table 1.

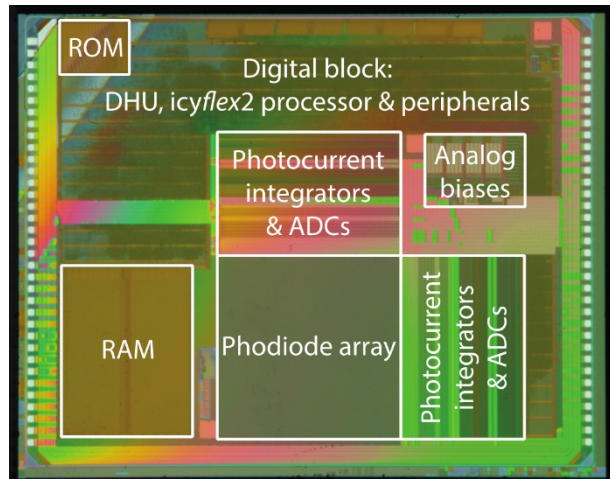


Figure 2: Micro-photograph of the spaceCoder system-on-chip.

Table 1: Summary of the system-on-chip characteristics.

Technology	0.18 μm CMOS Image Sensor
Size	20 mm ² (5 × 4 mm ²)
Power consumption	120 mW (full speed)
Temperature	140°C maximum operating temperature
Clock frequency	48 MHz
Number of pixels	128 + 128 interleaved horizontal and vertical pixels
ADC resolution	12 bit $\Sigma\Delta$ (1 ADC per pixel)
Integration time	Typically 1-5 μs (depending on lighting)
Sampling rate	Maximum 200 kHz, with 1 μs integration
Position resolution	10 nm (2D shadow position on the sensor)

For each targeted application, the spaceCoder system-on-chip is a core component that is implemented in a custom configuration including a dedicated lighting, optic and code pattern. Possible applications include:

- Metrological applications: linear, rotary, multi-dimensional high-speed, high precision encoders
- High-temperature automotive applications
- Harsh environment applications

This research was partially funded by the CTI program.

[1] E. Grenet, P. Masa, E. Franzi, P.-A. Beuchat, "spaceCoder: a nanometric 3D position sensing device", CSEM Scientific and Technical Report (2011) 89

HearRestore: Nanotracking for Image-guided Microsurgery

A. Chebira, E. Grenet, D. Hasler, P. Nussbaum, E. Franzi, P.-A. Beuchat

The goal of this work is to provide a highly precise and accurate tracking system for minimally invasive microsurgeries, such as cochlear implants. Our tracking system needs to compute the position of the surgical tool with respect to the patient at all times, in real time and under highly varying conditions. We designed an off-the-shelf hardware platform that control our LED targets, and embed the computation of the 2D position of each LED, based on the 2D spaceCoder technology. Moreover, we developed a 6D algorithm to derive the final target position.

In this work we aim at replacing invasive standard cochlear implantation surgeries with minimally invasive, image-guided ones, where a robotic arm drills a very small tunnel from the surface of the mastoid bone to the inner ear or cochlea, so as to allow the surgeon to easily insert the implant. Specifically, we need to derive a navigation system able to track the position of the robotic drill with respect to the patient. The drill is supposed to follow a specific trajectory, which is defined by the surgeon from the anatomy of the patient (e.g. using CT scans). Once in the operating room (OR), and using fixed references on the patient, the drill is positioned so as to follow the pre-defined trajectory. The 6D position of the drill has to be very accurate, precise, and robust, to avoid irreparable damages to, for instance, the facial nerve or the ear's external membrane. To this end, our HearRestore tracking system, coupled with a navigation system, should provide a 6D position with 80 μm accuracy, a 50 μm precision, and 0.015° angular accuracy. It should also run in real time, be easily integrable in the OR environment and be compact.

We built the first HearRestore demonstrator consisting of a camera, a 6D spaceCoder platform, a 6D tracking algorithm, a 4-LEDs target, and a navigation application.

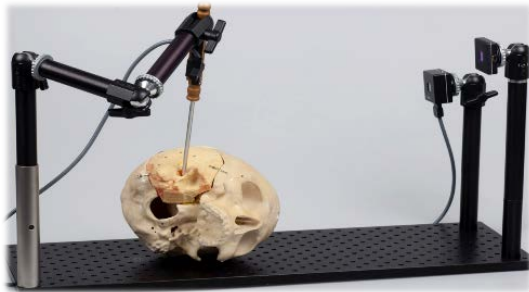


Figure 1: Initial HearRestore demonstrator for handheld medical devices. A 6D spaceCoder observes a 4-LEDs target. The 6D spaceCoder platform synchronizes the acquisition of the uEye camera with the LEDs and controls the target. The images are sent to a PC to estimate the 6D position.

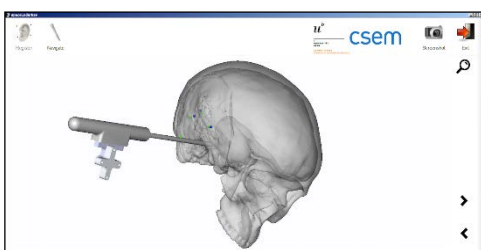


Figure 2: Navigation application representing the model with the moving surgical instrument. Joint work with ARTORG, Bern.

The platform drives the target and synchronizes the acquisition of the camera with the LEDs, whereas the navigation system

shows in real time the 6D position of the instrument w.r.t to the patient. The 6D tracking algorithm computes the 6D position of the target based on projective geometry methods and using the 2D positions of each LED of the target. The 2D spaceCoder technology consists of an optical sensor coupled with a shadow mask and a 2D pattern. A point light source creates a shadow image, the phase of which encodes the position of the light source. Using at least 4 light sources on a rigid target, we can thus compute their 2D positions and the 6D position of the target.

To compute a 6D position with a high accuracy and precision, we first need to understand the sources of noise and error: why, when and how they occur. We can then derive appropriate calibration and corrective measures. We have identified and studied several sources of error, amongst which those due to light reflection and refraction.

Assuming a fixed spaceCoder setup in front of which a light source moves in a circular manner from -60° to +60°, we observed that whether it is reflections from the sensor's Silicon or from the mask's Chromium, the errors can be as high as 40 mdeg, depending on the light's incident angle (see Figure 3). We also simulated the effect of the refraction index of the shadow mask (glass) and observed that a slight change in the index can lead to large errors in the computed position.

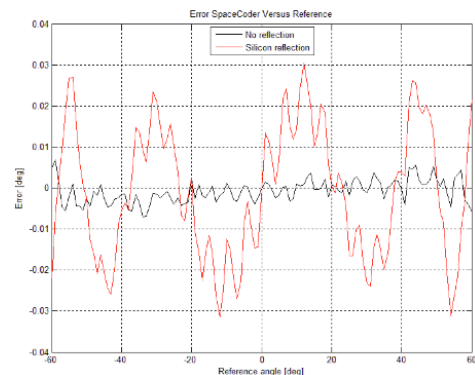


Figure 3: Errors due to the sensor's light reflections as a function of the incident angle. The large deviations from the center (red) are due to the Silicon's reflections.

The next steps in improving the overall tracking system consist of the following: estimate the refraction index instead of using the theoretical one, derive corrective measures for each source of error, design a new LED target with a larger baseline and add a non-planar LED to lift position ambiguity in the 6D optimization, and finally embed all 2D-position computation to increase the frame rate and the apparent rigidity of the target.

A US patent application has been filed^[1]. This work is supported by the NanoTera program.

[1] Patent: "6D positioning system using a shadow sensor", US number 14597434, filed 15-Jan-2015

Efficient Delineation of Curvilinear Networks from Biological Images

E. Türetken

Delineating networks of curvilinear structures is a challenging problem with numerous applications in the neuroscience, medical and biometrics fields. The large quantities of high-dimensional data produced by today's acquisition systems creates a growing demand for efficient data-mining and recognition algorithms to analyze these networks. The goal of this project is to develop a range of data-agnostic delineation tools that are simple, fast and require minimal user interaction.

Curvilinear networks, such as blood vessels and neurons, are ubiquitous in biology. Reconstructing them digitally is of great importance in the field of neuroscience to quantitatively analyze neuronal connectivity patterns, and in the medical sciences to study vascular pathologies or to assist surgeons in image-guided planning and navigation. However, despite many years of sustained efforts, existing solutions require extensive manual intervention that is both time-consuming and tedious.

We have developed a set of delineation algorithms that require minimal user interaction and can handle both tree-like and loopy networks in a variety of imaging modalities, such as confocal/bright-field micrographs and MRA/CT scans. The software supports visualising and processing a wide range of data including 2D images and 3D image stacks of various bit-depths as well as time-lapse sequences and color imagery.

The new delineation tools range from manual and interactive techniques that give the user full control over the results to automated ones that require only a few user clicks. This allows the user to take the most efficient approach depending on the data characteristics, such as spatial resolution, signal-to-noise-ratio and contrast.

A common feature of the tools is a novel "virtual mouse" algorithm, which estimates the 3D center location and radius of a curvilinear structure from a user-defined 2D point on the computer screen. The algorithm has no tunable parameters but involves a fast preprocessing step, which typically takes a few seconds for a 1 GB image stack on a modern laptop.

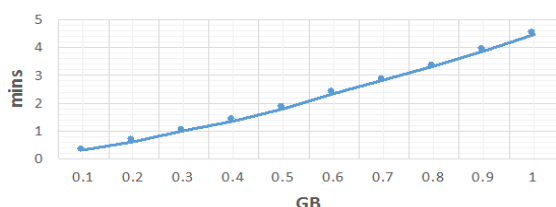


Figure 1: Image size versus tubular path preprocessing time.

Another preprocessing step common to the developed tools is the computation of tubular paths between all pairs of image locations. The computation and storage of the paths requires only $O(N)$ memory space, where N is the total number of image pixels. Furthermore, the running time of this step grows almost linearly with the image size as depicted by Figure 1.

The software operates mainly in four different delineation modes, namely manual, sliding-path, endpoint and one-click modes. The manual mode allows the user to sequentially connect points with tubes either with the help of the virtual

mouse algorithm or by manually picking the points in 3D. In the sliding-path mode, the user traces the filaments interactively by moving the mouse over them on the render window. The tool then automatically finds the most relevant 3D points and connects them with a smooth tubular path.

Unlike these two modes and existing solutions on the market, which require specifying intermediate points along the filaments, the endpoint tool finds a number of globally optimal paths connecting a given point (usually filament endpoints) to the delineation. The software then allows the user to view and select the best path on the render window. Finally, the one-click mode requires only a single point to be provided for each connected curvilinear network in the image.

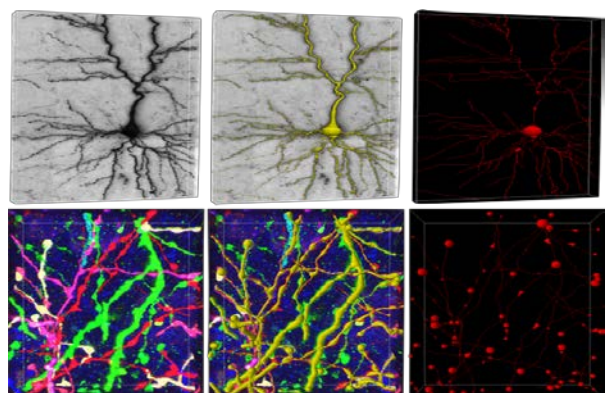


Figure 2: Neural structures delineated in the sliding-path and endpoint modes one at a time. Top: Brightfield micrograph of a biocytin-stained neuron. Bottom: Neurites acquired by the rainbow technique [1]. From left to right, intensity projections of the raw image stacks, delineations overlaid in yellow, and centerlines in red.

The combination of the sliding-path and endpoint tools represents a powerful strategy, which can handle both imaging noise and discontinuities along faint curvilinear filaments as shown in Figure 2. However, on cleaner data, such as high-resolution images of blood vessels, the one-click tool provides the most time-efficient approach (Figure 3).

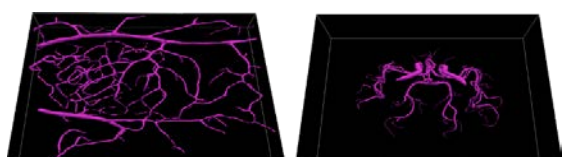


Figure 3: Two loopy networks produced in the one-click mode. Left: Reconstruction from a confocal image stack of blood vessels; Right: Reconstruction of a cerebral vasculature from an MRA scan.

[1] J. Livet, T. Weissman, H. Kang, R. Draft, J. Lu, R. Bennis, J. Sanes, J. Lichtman, "Transgenic strategies for combinatorial expression of fluorescent proteins in the nervous System," Nature, 450 (2007)

Data Muling for Remote Monitoring

P. Morel, M. Sénéclauze

Wireless Sensor Networks have been developed and deployed to collect data from sensors of any type. Those sensors need to be located at very precise places in order to ensure that the data collected is as relevant as possible. Unfortunately, in some cases, in remote areas, the link between the deployment location and the end user does not exist as the cellular network is not present. In such cases, someone has to manually go on site, extract the data, and bring it to the end user. The goal of this study is to facilitate the automation of this process by using a cell phone that will, without any intervention, copy the data when in the vicinity of the field, and populate the server when in range.

Muling data can be seen as "storing, carrying and forwarding" data. Typically, (Mobile Ubiquitous LAN Extension) MULEs are autonomous devices with wireless connection that travels between two endpoints. A MULE will download data from one endpoint, carry it until it reaches the second endpoint and forward it to the server [1]. If several MULEs are involved in the process, multi-hop routing between them is possible in order to attempt to reach the server faster, or to optimize the overall memory management between devices.

In order to evaluate what was possible to achieve, a set of scenarios were defined covering the different capabilities of a cell phone used as a MULE. The first scenario allows one MULE to transport the data from the field to the server, the second scenario allows more than one MULE transporting data from one field to the server and the third and last scenario allows many MULEs to collect and transport data from more than one field to the server (Figure 1).

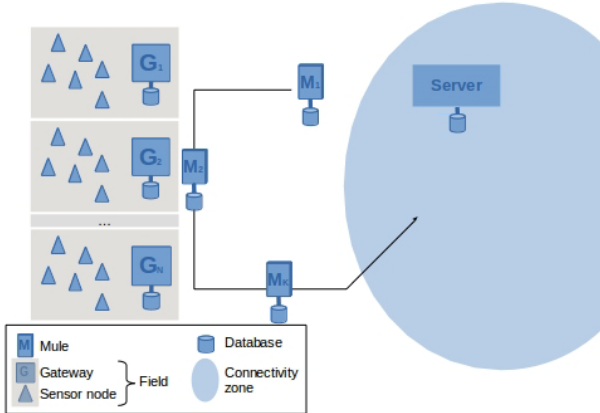


Figure 1: The most complex scenario allowing the monitoring of many fields with many MULEs.

A first test was conducted mixing different types of network protocols. Bluetooth was used between the gateway and the MULE and WiFi between the MULE and the server. The data transported between the gateway and the server (using the MULE) was coded in JavaScript Object Notation (JSON) simplifying not only the debugging but also the ability to expand

the number of measured data to be transported. Evaluation of this first test showed that using the MULE as a protocol gateway between Bluetooth and IP was probably not ideal (Figure 2) and that an end-to-end IP solution should probably be preferred.

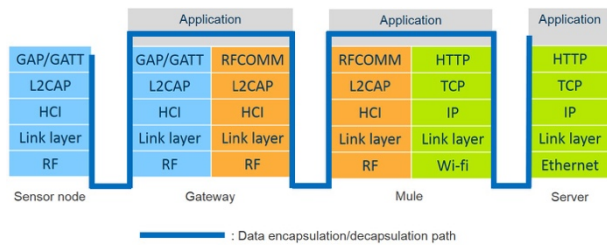


Figure 2: Heterogeneous network protocols.

The second setup was built to enable IP end-to-end. The gateway was responsible of formatting the data, making it available to the MULE through WiFi (Bluetooth was replaced) and in the same way, the MULE made the data available to the gateway. The data formatting, together with the application protocol needed to be homogenous and a HTTP-like protocol was used as the transport layer. This protocol is called Constrained Application Protocol or CoAP.

CoAP's goal is to enable Representational State Transfer (REST) environment on constrained devices like sensor nodes. It not only gives access to data in the same simple form as HTTP but also simplifies the interface with the database storing the data by including part of the database query in the Uniform Resource Identifier (URI) format. It also allows optimization of Machine-to-Machine applications.

This evaluation proved to be very successful. If only the first two scenarios were actually implemented, the results showed that choosing CoAP as a common application ease the implementation of the third scenario, in which part of the caching intelligence will have to be implemented in the MULEs themselves.

In order to generalize the end-to-end use of CoAP and thus to simplify even more the data representation, data handling and the network protocols, CoAP needs to be implemented in the sensors themselves. In addition, IP will be required on those sensors.

[1] U. Park, J. Heidemann, "Data muling with mobile phones for sensornets", Proc. ACM Conference on Embedded Networked Sensor Systems (SenSys), (2011) 162

IR-UWB in Intra-satellite Communications

P. Dallemande, J.-D. Decotignie, Y. Brunet, D. Piguet

CSEM has defined, implemented and evaluated an intra-satellite, low latency, and high throughput real-time wireless communication system. The system is highly reliable and operates in a difficult environment made of several metallic cavities. The solution is derived from an extension to the IEEE 802.15.4 MAC sublayer and the 802.15.4a IR-UWB physical layer.

Spacecrafts currently use wires to support the communication between sensors, controllers and actuators for the ground tests as well as in flight control applications, for which the rising cabling complexity due to the ever-increasing number of sensors has become unmanageable. The first use case is typical of a data acquisition scenario, in which data is acquired by the sensor and transferred to a central node. The second use case corresponds to the replacement of the MIL STD-1553 master-slave bus, in which the on-board calculator is often the bus master, while the other units (typically sensors) respond to the master's polls, transferring data cyclically from up to 40 sensors sampled at 32 Hz with a bounded latency (around 1 ms). A third use case aims at interconnecting busses (MIL STD-1553, CAN or Spacewire) used in the spacecraft or its launcher), which imposes bidirectional data transmission, with a maximum latency compatible with the response time of a MIL 1553 slave and a throughput greater than 10 Mbit/s full duplex.

Replacing wires by wireless networks corresponds to a real demand. However, current protocols do not fully meet the requirements in terms of timeliness, energy consumption and throughput. A satellite is composed of several cavities with metallic walls, forming a complex metallic structure, which lead to the choice of the IEEE 802.15.4a^[1]. Impulse Radio-Ultra Wide Band physical layer for its relative insensitivity to multipath.

IEEE 802.15.4^[2] is one of the most well-known wireless sensor network standards. Although the standard included real-time communications from the beginning, performance was limited^[3]. Due to restrictions on the number of Guaranteed Time Slots and on the beacon periods, the original IEEE 802.15.4 MAC is not able to meet the requirements. IEEE 802.15.4e^[4] introduced among other things, three new MAC behaviors that are possible solutions to the requirements: LLND (Low Latency Determinist Networks) for factory automation; TSCH (Time-Slotted Channel Hopping) for process automation; DSME (Deterministic and Synchronous Multichannel Extension) for general industrial application requiring robustness.

In short, the three schemes have advantages and limitations. In the absence of transmission errors, they are capable of covering most of the requirements, with the notable exception of some very short latency constraints. Due to the PHY

overhead of IR-UWB, throughput requirements can only be satisfied using two or more networks operating jointly on different channels. This shows that bandwidth should be used wisely. Satellites are made of different metallic cavities that create strong wave reflections. IEEE 802.15.4a is more resilient than narrow band transmission but does not eliminate transmission errors. The BER may be as high as 10-4. It is thus important to find an efficient scheme to recover from bit errors. Given the IEEE 802.15.4e principles, Forward Error Correction is not an option in the proposed MAC. The most logical choice is to use retransmissions. Possible error management principles include systematic repetition (babbling) and adaptive retransmission. The first option is typical of TSCH which statically assigns slots for retransmissions while the latter is used by LLND where these slots may be assigned dynamically. A comparison of the two schemes shows that the latter is much more efficient in particular when all links do not degrade simultaneously. To overcome some of the limitations of LLND, CSEM has designed a dynamic error retransmission scheme using a delayed acknowledge of correct reception in the beacons as well as on the fly slot assignments (in the beacon) for transmissions and retries.

The protocol is based on a TDMA approach (as LLND) with a slot duration of 1 ms and a configurable cycle duration. The protocol is not limited in terms of number of nodes. A scheduler performs a dynamic slot allocation as a function of the traffic requirements and transmission errors. The beacon indicates the cycle size and slot allocations. Based on this information, nodes send their data (or retries), which are not directly acknowledged in order to reduce transmission overhead. An example of the TDMA cycle is given below.

Beacon	SN21	SN22	SN23	SN24	SN25	empty or retransmissions	...
1 ms	1 ms	1 ms	1 ms	1 ms	1 ms		4 ms

Figure 1: UCS TDMA cycle.

The protocols have been implemented and tested by Airbus Space showing the excellent performance and robustness of the solution.

This work has been performed in the framework of the UWB4SAT project (ESTEC/Contract 4000107142/12/NL/AK).

[1] IEEE Std 802.15.4a™-2007. IEEE Standard for Information technology - Telecommunications and information exchange between systems - Local and metropolitan area networks - Specific requirements, Part 15.4: Wireless Medium Access Control (MAC) and Physical Layer (PHY) Specifications for Low-Rate Wireless Personal Area Networks (WPANs). Amendment 1: Add Alternate PHYs

[2] IEEE Std 802.15.4-2011 (Revision of IEEE Std 802.15.4-2006). IEEE Standard for Local and metropolitan area networks - Part 15.4: Low-Rate Wireless Personal Area Networks (LR-WPANs)

[3] S. Yoo, P. K. Chong, D. Kim, Y. Doh, M.-L. Pham, E. Choi, J. Huh, "Guaranteeing real-time services for industrial wireless sensor networks with IEEE 802.15.4," in IEEE Transactions on Industrial Electronics, 57 no. 11 (2010) 3868

[4] IEEE Std 802.15.4e-2012, Amendment 1: MAC sublayer (Amendment to IEEE Std 802.15.4-2011), (2012) 1

A Wireless Sensor Network for Safe Ship Evacuation

C. Kassapoglou-Faist, Y. Brunet, P. Dallemande

Real-time localization aboard large vessels is achieved using ultra-low power wireless sensor network technologies, enhancing safety through efficient decision support and emergency management. The system has been designed to meet requirements for high reliability, robustness, scalability and user acceptance, while being low-cost and low-maintenance. Small scale, real environment demonstrations have been performed.

The growing capacity of modern cruise ships raises serious challenges for efficient mustering and evacuation procedures in case of emergency. In the aftermath of recent mishaps, maritime security agents have identified the need to locate all persons on-board in all phases of a ship evacuation. The EU projects Lynceus (FP7, Support for SME and SME Associations) [1][2] and Lynceus2Market (Horizon 2020) propose the use of ultra-low power (ULP) wireless sensor network technologies for unobtrusive, real-time localization and tracking of people on-board and overboard.

The Lynceus concepts and technologies have been already described^[3]. The present article focuses instead on the localization tests that were recently performed in a real environment, on-board a cruise ship. Lynceus embeds low-cost, low-power, battery-powered radio-frequency (RF) devices in wearable items (life jackets, bracelets) and in fixed elements (gateways) that are interconnected to the ship wired infrastructure network (e.g. Ethernet). The current gateway demonstrators are designed to be integrated in smoke detectors and to use their communication network. The Lynceus devices are shown in Figure 1. They are based on ULP CSEM icyCOM technology and ULP communication protocols (WiseMAC). Sensors integrated on the devices provide additional information on person condition.

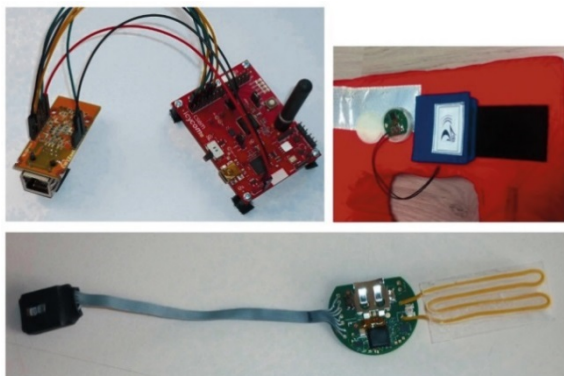


Figure 1: Lynceus devices.

On board, localization is based on received signal strength indicator (RSSI) of low-power RF signals. The mobile devices emit short-range, small periodic signals (beacons). The gateways know whether a mobile device is near them based on reception and power strength of its beacons. They send reports on the mobile devices in their vicinity to a central processing unit over the infrastructure backbone network of the vessel. In case of backbone failure, which is quite probable during emergencies, the gateways organize themselves into a multi-hop RF network and continue operating at a reduced data rate.

[1] www.lynceus-project.eu

[2] www.euronews.com/2014/05/05/don-t-panic

The localization algorithm is centralized, range-free and based on proximity detection. Its accuracy in such a harsh environment is not expected to be high but is still in accordance with the project requirements. The mobile locations are displayed in real-time on the Lynceus Graphic User Interface (GUI).

Small scale, real environment tests were performed on board Celestyal/Louis cruise ship Thomson Spirit, demonstrating the Lynceus concept and providing an opportunity to evaluate the system. Nine gateways were deployed at distances from 7 to 15 meters from each other, covering an area spanning over two contiguous decks, with corridors, cabins, open indoor and outdoor spaces. An Ethernet local area network was installed in the test area. The gateways also formed a multi-hop RF network to the central unit using three additional relay nodes. Crew members wearing mobile devices (11 life jackets and 4 bracelets) simulated an evacuation procedure that lasted 50 minutes. The locations of the nodes were displayed on the GUI and projected in the nearby ship cinema, where the central processing unit was placed. Three trajectories were pre-defined and their timing recorded, for result evaluation.



Figure 2: GUI snapshot onboard Thomson Spirit.

All devices were traced successfully throughout the tests. The accuracy achieved was on the order of 5 meters, with low latency (about 20 seconds over the backbone network, 40-60 seconds in multi-hop), yielding very satisfactory results.

The scalability of the system was shown through simulations conducted using the OMNeT++™ tool, assessing channel occupancy and delays in beacon reception. In the case of 200 nodes "competing" around two gateways, the medium was shown not to be overloaded with only 2% beacon losses, meaning that everybody could be located in a short time.

Lynceus2Market will deploy a large-scale demonstration of the system in 2017, involving 7000 devices.

[3] C. Kassapoglou-Faist, Y. Brunet , P. Dallemande, "Localization and Person Condition Monitoring on Board Cruise Ships for Safe Evacuation", CSEM Scientific and Technical Report (2014) ,137

WiseFly Routing—Reliability and Self-organization for Wireless Sensor Networks

D. C. Rojas Quiros, D. Piguet, J.-D. Decotignie

Worldwide experiments using wireless sensor networks have shown that these networks exhibit high end-to-end losses. Inadequate routing protocols are the main cause of this unreliability. WiseFly is a proactive routing protocol based on the ideas of CTP and takes full advantage of the low power operation of WiseMAC as the MAC layer. It corrects the deficiencies of classical WSN routing protocols.

WiseFly routing is CSEM's answer to the industry's need for Wireless Sensor Networks with a higher autonomy, flexibility and reliability. It provides an improvement to the current communication protocol stack (WiseNET^[1]) for networks that deliver critical information and therefore require a high service reliability. The protocol adds flexibility to the deployment and maintenance of the network by proactively and automatically handling locally changes such as broken links, adding or removing nodes and optimizing the current routes. Furthermore, local optimization of the topology enhances the scalability of the network.

Protocol Features

The protocol is inspired by the Collection Tree Protocol (CTP); a routing protocol that is considered as the state of the art in the area of self-organized routing for WSN. CTP has been shown to be very effective in providing a high reliability service while coping with the disturbances that a WSN may encounter in field deployments, providing Delivery Rates of 90-99.9% in 13 deployments^[2]. CTP combines adaptive beaconing and an efficient link quality estimator. However, CTP heavily relies on broadcast information which is very costly in terms of energy.

WiseFly removes this limitation, adapts beaconing and improves the link estimation efficiency. High reliability is enabled by the accurate identification of high quality routes thanks to a novel metric and the reactivity provided by the beaconing mechanism. As in CTP, the metric takes into account the packet success rate. WiseFly improves further by including statistical information about the received signal strength.

The protocol achieves efficient energy consumption by adapting the period of neighborhood explorations to the connectivity conditions. Furthermore, the protocol takes full advantage of the low power operation of WiseMAC.

Operating Principle

The nodes perform an exploration to gather information about their neighborhood as follows (Figure 1):

1. A node transmits a predefined number of beacons
2. The neighbors with a route to the sink will answer with a route proposal and a cost metric value, calculated from the beacons received
3. The node will choose the best route based on the cost

Every node, except the sink, will repeat periodically the "Neighborhood Exploration" process to find and optimize the routes. The period is increased progressively to reduce the energy consumption and protect isolated nodes from depleting their battery.

The exploration is the only opportunity for a node to change the next hop. This ensures that the decision of changing the current route is well founded on recent and statistical information.

WiseFly does not rely on the data traffic for updating the topology, since it could be scarce in some applications. It also does not require snooping packets or reporting the route changes, which results in simpler mechanisms than CTP.

Experimental Performance

The protocol was tested with the WiseNET stack in OMNeT++ simulations of the embedded code. It provided a Packet Delivery Ratio of 99% in networks of up to 100 nodes.

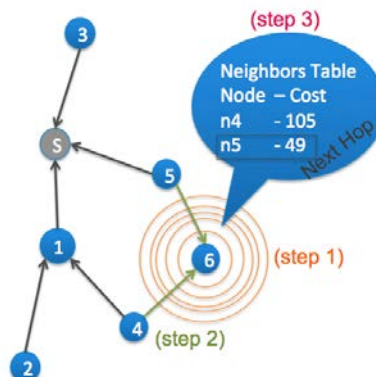


Figure 1: Operation diagram of WiseFly.

The same code was tested in a real deployment that consisted of 11 nodes at CSEM in Neuchâtel and lasted 5 days. Every node produced an application packet every 150s. All the nodes demonstrated a Packet Delivery Ratio of over 99%.

Application Domain

WiseFly is a promising solution for WSNs that convey sensitive information with reliability constraints in environments that are subject to change. Due to its self-organization capabilities and power efficiency, it is especially convenient for large scale deployments composed of hundreds of nodes that are difficult or expensive to access. This includes environmental, industrial and infrastructure monitoring. It also finds applications for IoT projects, such as home automation and body area networks.

^[1] C. C. Enz, A. El-Hoiydi, J.-D. Decotignie, V. Peiris, "WiseNET: an ultralow-power wireless sensor network solution," Computer, 37 no. 8 (2004) 62

^[2] O. Gnawali, R. Fonseca, K. Jamieson, M. Kazandjieva, D. Moss, P. Levis, "CTP: An efficient, robust, and reliable collection tree protocol for wireless sensor networks," ACM Transactions on Sensor Networks (TOSN), 10 no. 1 (2013) 1

Robust and Accurate Clock Synchronization for Wireless Sensor Networks

A. Restrepo Zea, B. Perrin, J.-D. Decotignie

Precise timing information is a key factor in computing and networking for applications that require a precise mapping of collected sensor data with the time at which the events were sensed. Clock synchronization is the process of ensuring that physically distributed nodes of a network have a common notion of time, despite the timing uncertainties (such as clock drifts, propagation delays, time-stamping mechanisms) from the transmitter to the receiver. Thanks to good models, it is possible to obtain accurate and also robust clock synchronization in practical settings.

Previous research or R&D activities on clock synchronization developed on top of the WiseMAC protocol has shown promising results. These have been further improved by removing the sources of uncertainty and better modelling of the variations.

When synchronizing clocks, timing uncertainties can degrade accuracy. Various different sources of uncertainty can be identified.

Time stamping is one of them. To reduce the timing uncertainty that it causes, time-stamping of the message is done at the physical layer instead of the MAC layer using the time capture capability of the used micro-controller (MSP430F5438A) to time-stamp radio transceiver interrupts. This removes most of the timing uncertainties due to the higher layers.

Propagation delay is a second source. The uncertainty is highly implementation dependent (IC, bit rate, modulation, event, etc.). We measured a CC1125 radio operating at 50 kbps every 5 seconds during 18 minutes and the results of the test showed that (Figure 1):

- The delay does not show a meaningful dependence on time
- It does not vary significantly. The maximum and minimum recorded values do not differ by more than 6.6 μ s.
- The value of 81.5 μ s (\pm 4 μ s) can be safely taken as a constant delay value
- Other tests using similar hardware platforms have shown that the communication delay shows similar behaviour at different bit rates

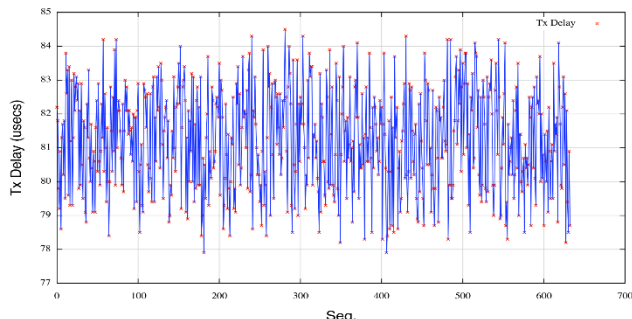


Figure 1: Transmission delay.

The Sink node inserts its clock value, with a granularity of 30.5 μ s, into a special flooded clock synchronization message. The reason of this value is that in the current hardware implementation of the nodes, the crystal oscillator has a frequency of 32768 Hz and, consequently, its granularity is of 30.5 μ s.

Upon reception of a clock synchronization message, a node stamps the message and estimates the corrections that should be applied to the clock. These corrections are applied in such a way that local clock monotonously increases.

In order to validate the accuracy of the CSEM Clock Synchronization Protocol, several experiments were performed. One of the experiments consisted of a Sink and a node placed in a room with ambient temperature. The Sink sent a Clock Synchronization Message every 10 minutes. The experiment ran for 3 hours and the measured clock error was found to be less than 150 μ s (Figure 2).

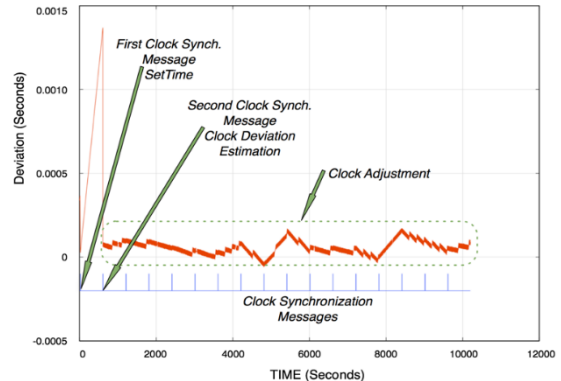


Figure 2: Clock adjustments under ambient temperature conditions.

A second experiment was performed in which a perturbation was introduced. This perturbation consisted of a cooling spray that was applied to the node after the fourth clock synchronization message. The clock deviation at that moment was about 1.3 ms, but three synchronization messages later, the measured clock deviation was again around 100 μ s (Figure 3).

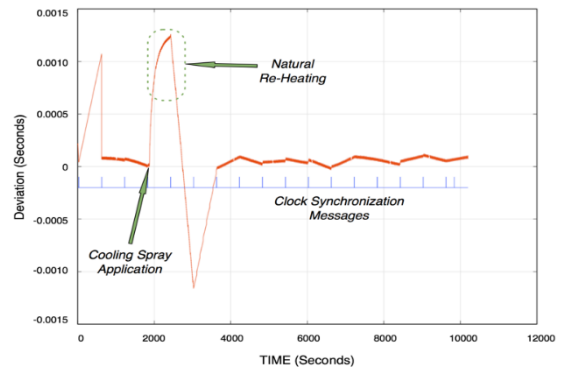


Figure 3: Clock adjustments under variable temperature conditions.

The experiments have shown that our protocol provides sub-millisecond accuracy with very little traffic even in the presence of severe temperature variations (shadow to light for instance). This does not degrade significantly with the number of hops.

Using Smart Phones for Remote Powering and Charging of Miniature Wireless Nodes

C. Hennemann, O. Vorobyov, J.-D. Decotignie

Wireless remote powering and charging is more and more used for daily life objects. It has been used at CSEM for wireless sensor network nodes when the nodes are hermetically sealed. Here, we present an application of the technology to power wireless sensors embedded in walls or structures.

In a number of applications, it is needed to embed sensors in structures and have the capability to read them remotely. RFID-based sensors are typically used in such a case and it is tempting to use NFC-enabled smart phones or tablets as readers. However, the available power is not sufficient to embed sensors too deeply. We present here an alternative that still use smart phones as readers but allows a larger range.

In this example, we assume that the sensor has a Bluetooth low energy interface (BTLE). The sensor is battery-less and will be powered once in presence of a remote energy source. This energy will be provided in this experiment by a tablet suitably equipped with a Near-Field Communication (NFC) transponder. This transponder supplies the necessary power to the BTLE sensor, which then wakes up and starts a task such as the measurement of the surrounding environment and then transmits the measured values to the tablet or to another BTLE receiver over greater distances.

For the demonstration, a wireless sensor provided by Texas Instruments, referred as the SimpleLink™ Sensortag, was used (Figure 1). The sensor tag includes multiple sensors: IR temperature, accelerometer, gyroscope, magnetometer, barometric pressure, temperature and humidity.



Figure 1: SimpleLink™ Sensortag from TI.

The system architecture (Figure 2) is based on the following blocks:

- Magnetic Resonant Interface. This interface harvests the maximum available power from the tablet and is based on magnetic coupling resonant technology.
- Rectifier circuit. This block transforms the high voltage output of the magnetic resonant interface into a continuous voltage.

- Power management. This device translates, with a high efficiency, the large dc voltage from the rectifier output to a suitable voltage for the sensor tag. It also delivers the power only when sufficient energy has been harvested. This is to prevent the BTLE from trying constantly to turn on and not succeeding because too much energy is required during the initial and startup phase.

For the demo, a Nexus 4 tablet was used as the power source. This device includes a NFC reader with an available output power of 200 mW as well as a BTLE interface. The tablet acts as a power source as well as a receiver for the measurements sent by the sensor tag. Both devices (NFC and BTLE) could also be two distinct devices.

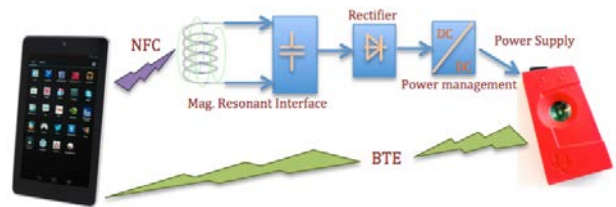


Figure 2: Architecture schematic.

Besides the embedded sensor case described earlier, there are many applications where the sensors are difficult to access, where it is complicated to change the batteries or where the sensors are completely encapsulated in a sealed enclosure making it impossible to change the batteries. The capability to remotely charge batteries that are close to depletion or depleted is a nice additional feature.

For such applications, the capability to do maintenance, such as updates or calibration, on the sensor remotely without soliciting the internal battery is key to long battery life. The principle described above can be used during all maintenance operations, thus avoiding to shorten the battery lifetime of the sensor.

The principle is also interesting when an increase of bandwidth is needed. NFC is much more limited in bandwidth than BTLE or equivalent technologies. Decoupling the remote powering technology from the communication technology gives the freedom to increase the bandwidth and possibly reduce interaction time.

The remote powering and charging of wireless sensors using NFC-enabled smart phone and tablets has a number of interesting applications. It has been tested with BTLE as the communication technology but it can be extended to other standards.

Securing Wireless Links on Resource-limited Devices

C. Kassapoglou-Faist

CSEM is completing its embedded security software library for wireless sensor networks, addressing entity authentication and key establishment. Solutions target mesh networks as well as point-to-point links and can be adapted to support standards (802.15.4-6, Bluetooth LE). This technology is being integrated in two CTI projects, on safety and industrial sensing applications.

Low-power wireless devices have become ubiquitous, ranging from simple remote sensors, to car keys, to health monitoring and embedded industrial-control devices, used in low-profile as well as in safety-critical applications. Nevertheless, the wireless medium is in essence an open communication channel—anyone in the vicinity can hear and produce messages. As a result, abnormal behavior, be it accidental or malicious, may lead to severe service malfunctions or even disruptions. There is an imperative need for appropriate security protection, tailored to the application requirements.

Adding to its expertise in wireless embedded systems, CSEM's objective is to acquire state-of-the-art practice in security solutions for wireless sensor networks (WSN) to build the corresponding software modules and to be able to propose adequate, thorough implementations that are easily integrated in an embedded communication protocol stack.

When two communicating devices establish a secure link (e.g. HTTPS), symmetric encryption is often used to protect the data, the key being established through an authenticated Diffie-Hellman (DH) exchange. This cannot be applied as such in the case of low-power wireless links, mainly due to the limited computing power and memory resources, driven by energy savings concerns and miniaturization requirements. Only elliptic curve DH can be considered, which still remains resource-demanding when compared to solutions based on symmetric cryptography. Moreover, the WSN communication model is often many-to-one (data collection) and one-to-many (commands from the sink), with possible pairwise links, notably for network organization and optimization purposes.

The proposed services are in line with WSN security requirements found in the literature:

- Message (or data) authentication, to guarantee that the data attributes are the ones claimed in the message. It also provides data integrity
- Confidentiality, which also enhances privacy protection
- Data freshness, for protection against replay of old valid messages (based on sequence numbers)
- Unilateral or mutual entity authentication for establishment of trust between the communicating parties, preventing man-in-the-middle attacks

In addition, access control and authorization must be implemented—in particular, the rejection of any non-expected message type or any non-expected behavior—to prevent node capture or system intrusion.

Cryptography is based on the Advanced Encryption Standard symmetric block cipher (AES-128). Data protection uses AES-CCM mode^[1] (counter mode for encryption and cipher

block chaining mode for data authentication). We have adopted the parameterizations taken in IEEE802.15.4 and Bluetooth LE.

The use of symmetric cryptography raises the issue of sharing secret keys. To make key compromise difficult, session keys, used to protect the messages, have time limited validity. They are derived from a master key, which is solely used for this purpose (and thus never exposed to cryptanalysis attacks), and from ephemeral data (nonces) exchanged by the devices in a mutual authentication and key establishment process, such as the one shown in Figure 1. Being already available, the AES function is also used in this phase (e.g. $E(K, \cdot)$ is AES, AES-CMAC as a hash function).

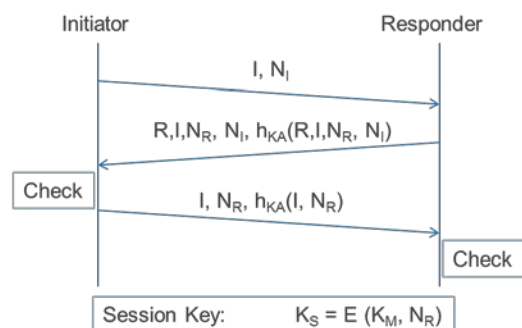


Figure 1: Typical mutual authentication scheme with symmetric key agreement (AKEP2).

There are several possibilities to distribute the master keys. They can be derived from pre-installed and/or configuration data or be established during a pairing procedure. For example, in Bluetooth LE, the parties first engage in a pairing procedure to establish a short-term key involving a process similar to Figure 1, then use this key to transport the long-term key (or master key) encrypted from one device to the other.

End-to-end data protection is proposed for WSNs: the messages are encrypted at their origin and decrypted/verified at final destination. Although the network level headers are thus transmitted in clear, all end-to-end data are authenticated. An individual, pairwise key per node-sink link is recommended for better robustness and easy key revocation. Depending on network topology, group keys are also needed. Either they are transmitted over the already secured sink-to-node link, or they are established between one-hop neighbors based on initial configuration data during network set-up, when an attack is considered very improbable.

Our security software runs on commercial (MSP430) as well as in-house (icyCOM) platforms. It is tested within WiseStack (the protocol stack around ULP medium access protocol WiseMAC). In addition, a BTLE implementation on an MSP430-icytrx platform successfully engages in pairing and exchange of encrypted data with an iOS i-pad.

[1] D. Whiting, et al., "Counter with CBC-MAC" IETF RFC3610, (2003)

Motion Sensing Behind Walls and Obstacles Using Radio Waves

O. Vorobyov, C. Heneman, J.-D. Decotignie

Changes in radio wave propagation may be used to sense movement. A concept for sensing the movement of people or objects hidden behind walls or objects was rapidly prototyped and tested with the aid of a flexible SDR platform combined with a MISO antenna system. Tests successfully demonstrated the feasibility of using radio waves to sense the motion of persons or objects hidden behind walls or obstacles.

Alterations of wave transmission have been used for decades to detect objects and movements. This is the basic principle of radar. The results presented in a recent paper by MIT^[1] demonstrate that narrowband transmission in the 2.4 GHz ISM band (i.e., WiFi) can be used to detect the movement of people and their relative locations behind walls without their having to carry any active or passive RF identification devices. The concept relies on the use of two transmitters and one receiver behind the wall (opposite to the person whose motion we wish to detect). The transmitters operate jointly so that, in the absence of movement, the signal at the receive antenna is nulled. However, in case of movement, the differential signal from the transmitters seen at the receive antenna does not cancel; enabling movement to be detected. This has been verified at CSEM using a software defined radio (SDR) platform.

The first objective of the project was to reproduce the results of the behind walls sensing system proposed by MIT^[2] and assess the potential to develop a solution that can be built with low-power CSEM technology. The second objective was to setup a versatile platform for rapid prototyping of ideas and algorithms for RF sensing based on a SDR platform, in our case, the well-known Universal Software Radio Peripheral (USRP), and to learn how to use the open source software "GNU Radio". The ability to perform the necessary signal processing in a compact and efficient way is a key challenge.

The idea behind of motion sensing through walls and opaque obstacles is similar to that of radar or sonar imaging. The RF signal is transmitted towards the obstacle in question, where part of the RF signal penetrates the obstacle, reflects off of the moving object on the other side and returns to the receiver. The received signal contains information about what is hidden behind the obstacle. Losses may be large though and indeed the major problem with detection through walls and behind obstacles is that the received signal is very weak compared to the signal reflected off of the wall or obstacle.

The solution relies on the ability to cancel the strong signal components reflected off of the wall, or obstacle, leaving the weak signal reflected off the target person or object behind the wall (or obstacle). For this purpose, a type of Multiple Input Multiple Output (MIMO) antenna system known as a Multiple Input Single Output (MISO) antenna is used to cancel or null the signal from obstacle reflection. In this case, the MISO test system consisted of two transmit antennas and one directive receive antenna pointed towards the wall or obstacle. The antennas were connected to the USRP device and the PC with installed SDR platform for controlling, data acquisition and processing. The test setup is illustrated in Figure 1.

In order to demonstrate the feasibility, two SDR platforms were tested: 1) commercially available MATLAB/SIMULINK software and 2) open-source GNU radio. A block diagram of the nulling algorithm is presented in Figure 2. In addition to the fact that the GNU radio platform is an open source software, it also demonstrated better flexibility compared to that of SIMULINK.



Figure 1: Setup for test and demonstration of motion sensing behind obstacles using an SDR platform and MIMO principles.

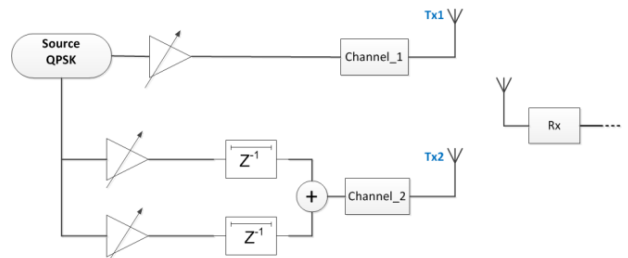


Figure 2: Functional block diagram of the nulling algorithm implemented in GNU Radio.

Using the test platform, we demonstrated the ability to detect hidden persons or objects moving behind walls. The results are promising. In principle, the sensing system could be implemented in commercial WiFi base stations (e.g. WiFi base stations using OFDM signals in the 2.4 GHz ISM band) equipped with multiple antennas without the need for additional hardware. Additionally, the SDR platform proved to be a very useful tool for rapid prototyping and experimentation with different algorithms (i.e., before implementing them in optimized hardware). However, before the results can be exploited, improvements are required including: new hardware with increased operational bandwidth and better channel isolation (in order to avoid crosstalk), as well as, calibration and recognition mechanisms for different RF transparent obstacles.

[1] web.mit.edu

[2] A. Fadel, "See through walls with WiFi", Proc. ACM Special Interest Group on Data Communication (SIGCOMM), (2013)

A 6-8 GHz IR-UWB Transceiver ASIC in 65 nm CMOS for Ranging Applications

D. Barras, D. Ruffieux, A. Vouilloz, F. X. Pengg, J.-L. Nagel, C. Arm, R. Godinho Caseiro

Starting from an existing Impulse-Radio Ultra-Wideband (IR-UWB) wireless transceiver prototype crafted with off-the-shelf components and aiming at demonstrating roundtrip time-of-flight (RTOF) distance measurements, DENEB2 had the objective to develop a fully integrated ASIC in a CMOS 65 nm technology. Although optimized for point-to-point distance measurements, DENEB2 is very versatile and fits a wide range of applications.

IR-UWB continues to gain momentum, mostly driven by the proliferation of location-aware applications and by the emergence of wireless indoor positioning systems for asset tracking, emergency, health monitoring, home and industrial automation, augmented reality, sensor networks and the Internet of Things (IoT).

CSEM has been active for many years in the field of UWB with its proprietary FM-UWB solution for communication^[1]. The latter solution is now complemented with activities in low-power IR-UWB radio technology for distance measurements conducted in collaboration with 3DB ACCESS AG (3DB), a start-up company based in Zurich. After a successful FPGA-based demonstrator, CSEM and 3DB have now developed a highly integrated and low-power solution addressing the worldwide UWB frequency bands between 6 and 8.5 GHz.

In order to cope with the challenges posed by the generation and the reception of impulses a couple of nanoseconds long at multi-GHz center frequencies, CSEM developed a new complete IR-UWB RF front-end and investigated several new radio components such as: a) wideband carrier synthesis with digital control; b) fully programmable UWB impulse transmitter and wideband power amplifier; c) high-gain and low-power wideband analog radio-frequency front-end; d) high-speed and low-power analog-to-digital converters (ADC).

To ensure a maximum flexibility in the generation of UWB impulses, the radio-frequency synthesis is based on a digital transmitter. This transmitter is able to accurately generate impulses of lengths ranging from less than a nanosecond to more than 10 ns, with controlled envelope shape and with a carrier frequency that covers a range of approximately 2 GHz from 6.0 GHz to 8.0 GHz. An example of the pulse shaping capability of the transmitter is depicted in Figure 1.

The transmitter also features several modulation modes such as amplitude modulation, frequency modulation enabled by the frequency agile synthesis and phase-shift modulation.

The receive path consists of a frequency down-conversion circuit (RF front-end) comprised of low-noise amplifiers and mixers, a digitally controlled variable gain wideband amplifier with an automatic gain control and an analog-to-digital conversion. The latter features ADC's operating at up to 1 gigasample per second. This high sampling rate enables distance resolution in two-way time-of-flight ranging down to 15 cm. The DSP implementation is able to process the sampled IR-UWB signals in a power-efficient way and allows signal synchronization with an accuracy down to one nanosecond for physical distance measurement and data communication.

Figure 2 shows results of distance measurements conducted in an indoor environment with dense multipath (hallway). With an energy consumption of a few tens of micro-Joules per measurement and a latency of a few milliseconds, DENEB2 demonstrates that real-time ranging with decimeter accuracies is feasible at very low-power consumption.

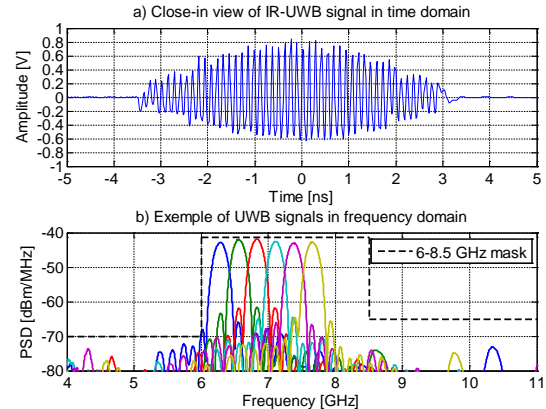


Figure 1: IR-UWB signal in time and frequency domain vs. ETSI mask (example for impulses having -10 dB bandwidth of approximately 300 MHz and six different center frequencies ranging from 6 to 8 GHz).

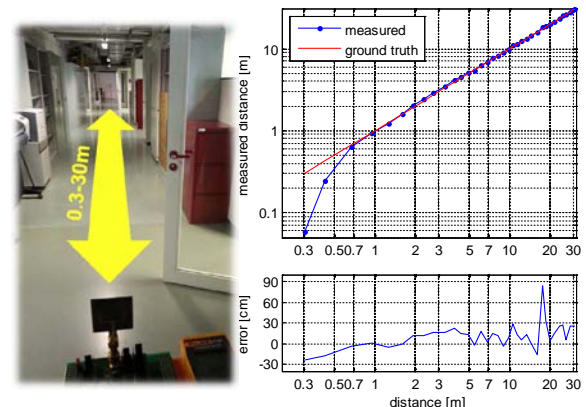


Figure 2: 30 cm to 30 m indoor measurement in a CSEM hallway. The mean absolute error is 15 cm.

Owing to its strong performance, the ASIC is suitable for use in a wide variety of applications, especially, where real time and energy consumption are at a premium, for example, electronic tags and key-fobs, wrist-watches, three-dimensional indoor localization for micro-robots and/or drones.

This project was made possible owing to the support of CTI/KTI grant no. 15416.1 PFES-ES.

^[1] J. F. M. Gerrits, et al., "Principles and limitations of ultra-wideband FM communications systems", EURASIP Journal on Applied Signal Processing, 3 (2005) 382

A Miniature Timing Module Embedding its XTAL within the CMOS Substrate

D. Ruffieux, N. Scolari, F. Giroud, T.-C. Le, P.-A. Beuchat, J. R. Farserotu, S. Dalla Piazza •, F. Staub •, K. Zoschke ••, C. A. Manier ••, H. Oppermann ••, J. Dekker •••, T. Suni •••, G. Allegato *

MEMS oscillators have recently successfully entered the timing market owing to the packaging revolution enabled by wafer scale technologies. This paper explores how XTAL resonators could similarly benefit from such technologies with the demonstration of a miniature timing module.

One of the main goals of the Go4Time EC-funded FP7 project was to demonstrate how post-CMOS wafer scale technology could be applied to the packaging of miniature tuning fork XTALS. Embedding the later directly within the CMOS substrate leads to the ultimate miniaturization of timing modules which are at the heart of almost any electronic system. In order to develop a versatile module, 131 kHz XTALS were combined with 2 GHz BAW resonators to enable the generation of both a low power sub- μ W real time clock (RTC) and of an on-demand low jitter clock of high spectral purity that could support the requirements of radio applications such as for Bluetooth Low Energy (BLE). Furthermore, the hybrid packaging approach which was developed is applicable to any sensor that should be put in intimate contact with its CMOS read-out circuit in an air tight or vacuum-sealed cavity.

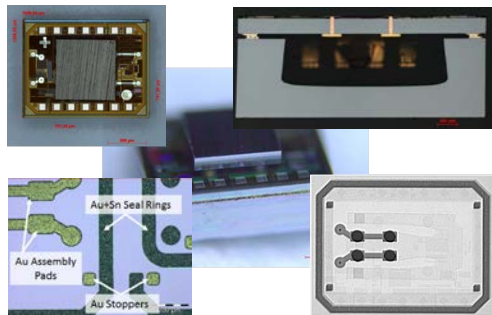


Figure 1: Timing module photographs: center, side view showing wafer stack and BAW die on top of CMOS; top-left, top view showing IC IOs, RDL and TSVs; top right, cross section revealing TSV, XTAL, and cap; bottom-left, CMOS backside, bottom right, X-ray picture.

Pictures of the fabricated modules, which were produced on 8" wafers following a standard 180 nm CMOS process flow, are shown in Figure 1. In order to generate through silicon vias (TSV), holes are first etched from the CMOS side of the wafers to a depth of 100 μ m through the BEOL metallization and silicon before being filled with copper. A redistribution layer (RDL) is then deposited and patterned to redirect the original frontside circuit IOs to the wafer backside with the help of the newly formed vias. The later are revealed after grinding the CMOS substrate, which has been previously glued to a temporary holding glass wafer, down to a residual thickness of 100 μ m. A backside Au-RDL is then electro-plated to connect the TSVs, define the XTAL landing patterns and form mechanical stoppers. Gold-tin seal rings are subsequently plated and Au-studs are bumped on top of the landing patterns completing the post-CMOS processing. The XTALS are then individually attached using a die bonder. In parallel, cap wafers

plated with Au seal rings of matched geometries are formed by etching cavities to accommodate the protruding XTALS after the wafers are bonded together at 280°C [1]. Eventually miniature BAW resonators are reflow-soldered on pads lying on the front CMOS side after removal of the temporary bonded glass wafer. The resulting complete timing modules measure only 1.6x1.2x0.6 mm³, hence about the dimensions of a single miniature radio XTAL.

Wafer level measurements of the timing modules prior to BAW assembly were performed at room temperature in order to assess the packaging manufacturing yield. Figure 2 provides two wafer maps depicting the yield. The multi-layer mask CMOS design was shared equally between the XTAL/BAW and a Silicon Resonator-based version arranged in a chessboard configuration (related black sites not populated). Dummy sites containing foundry test structures are colored in yellow. Only the central wafer area was populated with XTALS forming 2600 XOs. White cells denote know-good dies (KGD) with fully functional, hence properly sealed and interconnected XOs. Red cells represent non-functional DUT while blue cells are those having suffered from probe-card contacting/alignment issues. Overall, the yield reaches ~70%, while large areas are found mostly defect free. The mean core current consumption of the 131 kHz XO from the best wafer reached ~60 nA with a deviation of 12%. This is 2.5 times higher than what was obtained with XTALS packaged in standard ceramic packages, glued on a standard CMOS wafer and wire-bonded to the ICs. The difference is due to a larger package parasitic capacitance from the TSV and RDL and a higher residual cavity pressure lowering the Q-factors.

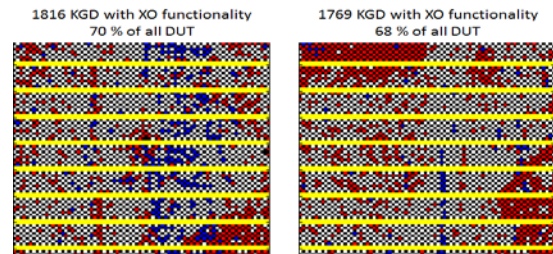


Figure 2: Wafer map showing timing module manufacturing yield.

This work demonstrated the potential manufacturability of a leading edge European timing solution. It was performed within the project Go4Time that was funded by the EC FP7 research program. The consortium led by CSEM was formed of Micro Crystal, ST, Fraunhofer IZM, VTT, Polimi and TuD.

• Micro Crystal AG, Switzerland
•• Fraunhofer IZM, Germany
••• VTT Technical Research Centre of Finland LTD, Finland
* STMicroelectronics, Italy

[1] K. Zoschke, *et al.*, "Application of TSV integration and wafer bonding technologies for hermetic wafer level packaging of MEMS components for miniaturized timing devices," in Proc. IEEE Electronic Components and Technology Conference, (2015) 1343

Bluetooth Low Energy, from Integrated Circuit to Application

E. Le Roux, F. X. Pengg, N. Scolari

The BLIM4SME FP7-SME-2013 project develops an optimized integrated solution targeting the rapidly growing number of SME's and industries that require low-cost, highly integrated and ultra-low-power BLE radios for their next generation healthcare, sports and fitness product or even for industrial applications.

The target applications require standardized connectivity for plug-and-play interconnection with other devices, ultra-portability with tiny modules for maximal comfort for the wearer, ultra-low-power consumption for long autonomy and flexibility for simple integration with a heterogeneous set of other components like sensors, signal processors, energy harvesters.

The designed RF IC integrates the hardware part of an RF transceiver compliant with Bluetooth 4.2 assembling two pre-existing IP in TSMC 65 nm:

- CSEM's icyTRX-65 Bluetooth Low Energy RF transceiver [1] which provides the Physical Layer, Bit Stream Processing and Air interface Packet assembly and disassembly. It can also support IEEE802.15.4 and proprietary standards from 62.5 kbps to 4 Mbps.
- RivieraWaves's Bluetooth Low Energy 4.2 protocol engine

The software part is implemented into a companion microcontroller communicating with the BLIM RF IC via SPI and IRQ. The choice to not co-integrate the controller has been made to provide maximum flexibility (e.g. memory size) for evolution by opportunistic use of COTS controllers.

The resultant IC also implements dedicated power management and ultra-low-power time keeping functionalities for minimum size and cost:

- A capacitive DC-DC voltage converter supplies the IC core from the 2.4-3.6 V supply voltage (typ. LiMnO₂ coin cell).
- A fully-integrated Ultra-Low-Power 32 kHz low-jitter oscillator transparently precisely re-calibrated each time the RF quartz crystal oscillator is on.

The complete assembly targets state-of the art performances with minimized power consumption in active and standby modes thanks to the optimized architecture, clock gating, power domains and use of retention cells.

A module has been designed to embed the RF IC and an off-the-shelf Cortex M0+ controller with 128 kB of Flash memory. It embeds also, in less than half of a cm³, an antenna designed by VTT Technical Research Centre of Finland for minimum constrain on supporting PCB with a dedicated Integrated Passive Device for impedance matching and filtering.

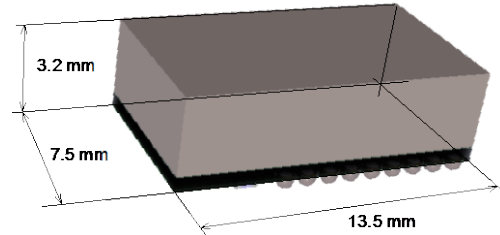
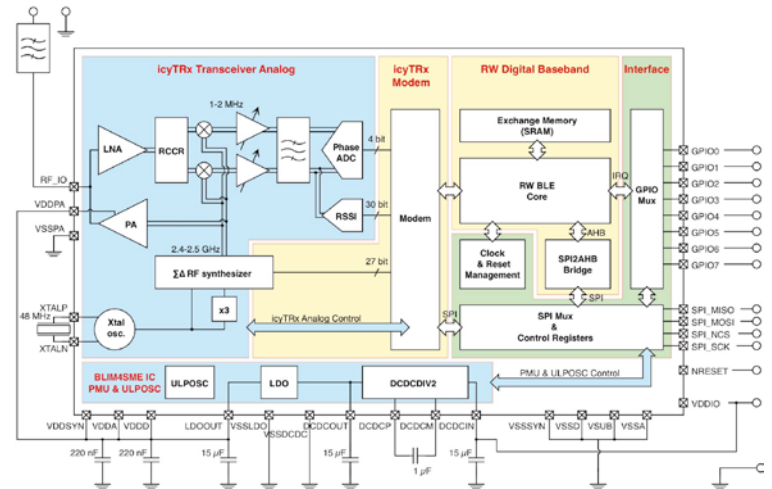


Figure 1: BLIM module dimensions.



Operation frequency	2.36-2.5 GHz	
Voltage supply	2.4-3.6 V	
Interface	RF: single 50 Ω interface, Digital: SPI & GPIO	
External components	A 48 MHz quartz and 6 ceramic capacitors	
Transmission	0 dBm, 4.5 mA	
Reception	-97 dBm, 3.0 mA after 0.5 ms crystal oscillator startup	
Standby current	300 nA Including RTC based on 32 kHz osc.	

Figure 2: BLIM RF IC block diagram and preliminary specifications.

[1] N. Raemy, et al., "icyTRX-65, a 2.4 GHz silicon RF IP optimized for low-power bluetooth low energy", CSEM Scientific and Technical Report, (2014) 127

icyTRX-55, an Evolution of the Bluetooth Low Energy (BLE) RF IP

N. Raemy, F. X. Pengg, N. Scolari, A. Vouilloz

As a direct derivative of the 65 nm version, the icyTRX-55 transceiver benefits from all of the previous successful achievements and the know-how gained previously. The new technology node (CMOS ULP 55 nm) offers the huge advantage to provide access to an EFLASH memory, which opens new opportunities for SoC developers. Due to the newly implemented features, together with the benefits of the shrink to 55 n, this new version of the icyTRX has already triggered substantial interest from major semiconductor major players and is foreseen to remain among the most attractive BLE IP's available on the market.

Compared to the icyTRX-65 silicon, which achieved last year state-of-the-art sensitivity at minimal current consumption and supply voltage, the 55 n IP version does not claim to improve those transceiver performance characteristics dramatically. Rather, the choice of the CMOS ULP 55 nm process (TSMC and Global Foundries) is based on the intrinsic access to the EFLASH memory offered by those technology nodes. This process option together with the outstanding transceiver performance opens the door for the icyTRX-55 IP to enter the huge IoT (Internet of Things) market. In order to increase icyTRX attractiveness, a reduced 7 metal stack (5 thin, 1 think and 1 ultra-thick) was chosen for the porting to the 55 nm technology, lowering the fabrication cost significantly.

SoC (System on Chip) assemblers are looking for low cost reliable high performance IPs available in an EFLASH capable technology node, which makes the icyTRX-55 a perfect candidate. At the same time, they also need a robust IP with silicon proven characteristics. Based on the experience obtained with the 65 nm version of the IP and the large amount of measurements performed, several major enhancements have then been made to the icyTRX-55 IP. First of all, a new carrier recovery algorithm has been designed. It is based on the correlation over the access address in order to have a precise estimation of the carrier offset. The results are impressive; the maximum frequency offset tolerance of the receiver, i.e. the maximum deviation of the transmitter center frequency tolerated by the receiver, covers a range of ± 250 kHz around the nominal value without observable degradation on the Packet Error Rate (PER). In other words, icyTRX can comply with a ± 50 ppm error on both the receiver and the transmitter reference clocks, as often seen in the case of low cost BLE (Bluetooth Low Energy) devices.

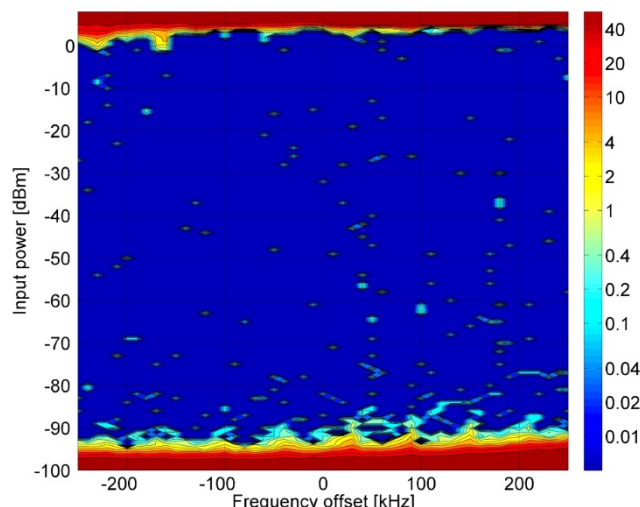


Figure 1: PER in % versus frequency offset and versus input power.

The second major enhancement is a new algorithm for the sub-band selection to overcome the problems of temperature dependence and selection ambiguity observed in the previous version. The new algorithm is faster, more accurate and even provides fractional information on the sub-band to be selected. The finer algorithm allows narrowing of the margins previously taken to accommodate the extreme PVT (process, voltage, temperature corner) cases, hence reducing, for example, the PLL bandwidth and thus the emitted noise at a given frequency offset from carrier. Compared to the BLE 4.2, ETSI EN 300 328 and FCC CFR47 part 15 certified 65 nm version, this modification provides more margin with respect to the spurious emission characteristics required by these standards.

The robustness against close interferers was also improved thanks to an interferer detector (called "peak detector") located in parallel with channel filter. In the presence of a strong interferer, an attenuation step will be triggered by the AGC (Automatic Gain Control) algorithm, reducing the Rx gain, thus preventing the saturation of the receiver blocks. An improvement of up to 7 dB is expected on the interferer rejection characteristics (at <10 MHz offset).

In parallel with these enhancements, several other features have been added, such as new interfaces (AMBA APB and AHB light 32-bit) and the inclusion of the AES CCM coding for the BLE. Although the encryption algorithm is not mandatory and can be implemented in software, internal tests have shown that calculations required to encrypt packets can take as long as 30 ms. By comparison, hardware implementation of the algorithm does not generate any latency and is completely transparent with respect to the upper layers of the BLE stack.

For customers interested in ultra-low-cost solutions, the integrated oscillator circuit is now capable of addressing low cost crystals (XTAL) with high ESR (equivalent series resistance of up to 200Ω) thanks to a special operation mode, if at the cost of a higher power consumption for this block.

Last but not least, icyTRX-55 is foreseen to be "out of the box" BLE 2 Mb/s compliant, as soon as the Bluetooth 5.0 is released in 2016. All tests conducted so far show that changing a few configuration registers will be sufficient to switch from the original BLE data-rate of 1 Mbps to the enhanced BLE data-rate (2 Mbps). The attractiveness of the icyTRX-55 IP is thus reinforced and its success assured for the years to come.

A Modeling Technique for Simulating Power Supply Noise Coupling in a Complex System

J. Deng, E. Le Roux, P.-F. Rüedi

A methodology based on Verilog-A modeling is studied to efficiently simulate the power supply noise coupling in a complex system. The modeling tools have been implemented.

The purpose of this study is to find a generic and efficient way of verifying the supply noise coupling between different blocks in a complex system. The interest of this work is coming from the fact that running transistor-level simulation for complex functional blocks, having very different frequency of operation (e.g. transceiver with 2.45 GHz carrier frequency, audio analog processing, DC-DC converter, etc.), can be too resource-hungry.

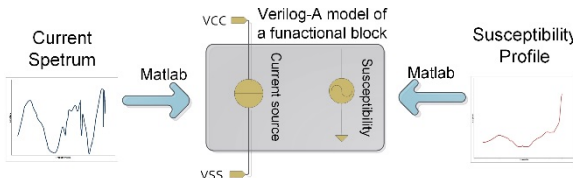


Figure 1: Modeling.

Rebuilding the performances of blocks by Verilog-A behavioral models is considered as a good approach, which is compatible with different design environments. A simple Verilog-A model for supply noise coupling simulation is shown in Figure 1. It consists of two key elements:

- A current source based on the given spectrum of the current flowing through the supply pin of the functional block: with these current sources and the intended regulators, the supply noise can be simulated
- An internal AC voltage source based on the given susceptibility profile: it gives the maximum accepted supply noise level (frequency dependent) of the functional block as a victim, and is used as the reference to judge the acceptance of the supply noise

The chart flow of the modelling is presented in (1) of Figure 2. The two major steps are:

- Approximating current spectrum and susceptibility in Matlab
- Rebuilding the approximation results with Verilog-A

Approximating the current spectrum and the susceptibility over a wide frequency range is the major challenge of this work, considering the accuracy and stability limitations of conventional approximation approaches [1]. In this project, the approximation approach based on the frequency range segmentation is used: applying the approximation over a small frequency subrange, and summing approximation results.

$$(1) \left(\sum_{n=1}^N \frac{c_n}{s - a_n} + d + s \cdot h \right) \approx \left(\sum_{n=1}^N \frac{\bar{c}_n}{s - a_n} + 1 \right) f(s)$$

By solving Equation (1) with complex conjugate zero and pole pairs, the frequency range segmentation is automatically achieved; and boundary issue of segmentation is solved.

Equation (1) is a nonlinear problem, as the unknowns, " a_n ", appear in the denominator. The "vector fitting" methodology [1] solves the Equation (1) as a linear problem in two stages (as shown in (2) of Figure 2): 1) pole identification and 2) residue identification.

To rebuild the approximation results obtained by Equation (1) with Verilog-A, 2nd order Laplace transform is used for each zero/pole pairs:

$$(2) H(s) = \sum H(s)_i + d, \quad H(s)_i = \frac{n_2 s^2 + n_1 s + n_0}{d_2 s^2 + d_1 s + d_0}$$

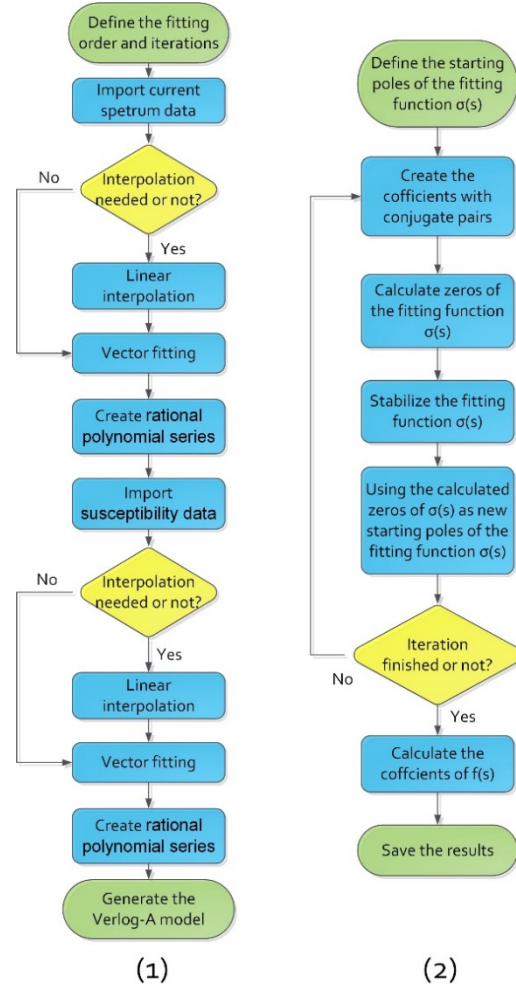


Figure 2: (1) Flow chart of the modeling procedure; (2) Flow chart of the vector fitting procedure.

One modeling example has been carried out based on the supply noise measurement results of the transceiver of icyTRx65 chip: with 90th-order approximation, a Verilog-A model with an approximation error of less than ±5% over the frequency range from 100 Hz to 2.5 GHz is achieved.

[1] B. Gustavsen, A. Semlyen, "Rational approximation of frequency domain responses by Vector Fitting", IEEE Trans. Power Delivery, 14 no. 3 (1999) 1052

An Off-chip Capacitor-free LDO with Fast Transient Response

J. Deng, P.-F. Rüedi, C. Monneron, P. Persechini

A LDO has been implemented for achieving good line and load regulation, fast transient reaction to large load current and supply voltage step, good noise and PSRR performances without off-chip capacitor.

The regulator is a linear low-dropout regulator (LDO), providing 1.2 V output voltage with a load current capability up to 100 mA with an input voltage range from 1.6 V to 5.5 V. It is designed for security applications, presenting the following features:

- Capability of driving either on-chip or off-chip blocking capacitor
 - Fast reaction (meaning <50 mV output voltage drop in nominal case) to a large load current step (i.e. ± 10 mA in 2 ns) or a large supply voltage step (i.e. ± 0.5 V in 2 ns)
 - Good line regulation and load regulation
 - Good noise and PSRR performances

The conventional regulator structure is not capable of meeting the above requirements without a large off-chip capacitor. However, due to packaging constraints, no external capacitor can be accommodated. Thus, only on-chip blocking capacitor can be used. Stability and fast transient reaction are the two major challenges of this LDO.

The LDO structure is shown in Figure 1, implemented basing on a modified nested structure with zero-pole cancellation technique (indicated in Figure 2):

- Indirect feedback of the miller capacitor C_1 is to generate the dominant pole (p_1), as well a LHP (Left Hand Plane) zero (z_1)
 - C_2 together with CG_2 is to fine adjust the position of z_1
 - C_3 is optional, to reduce the Q factor of the conjugate complex pole pair, $p_4 \& p_5$
 - A low impedance node, marked as "A" in Figure 1, is available for adding the "Transient Enhancement" block to improve the transient performance when a large load current step or a large supply voltage step occurs

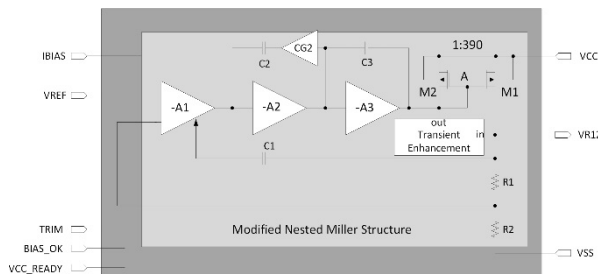


Figure 1: LDO block diagram.

The stability is achieved with zero-pole cancellation for the specified on-chip capacitor range, as shown in Figure 2. The pole of "p₂" is located at the LDO output, while the "p₃" pole is due to the C_{gs} of the output transistors "M1". Depending on the load current and the load capacitor, "p₂" shifts along the real-axis. The zero of "z₁" is carefully positioned so that the phase margin >50° is achieved under all conditions.

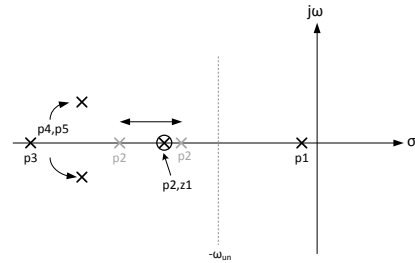


Figure 2: Zero-pole cancellation.

The GBWP of the LDO is about 50 kHz, which is not sufficient to achieve the required transient reaction against fast load current step or supply voltage step. The "Transient Enhancement" circuit is therefore introduced to improve the transient performance. The block diagram is presented in Figure 3.

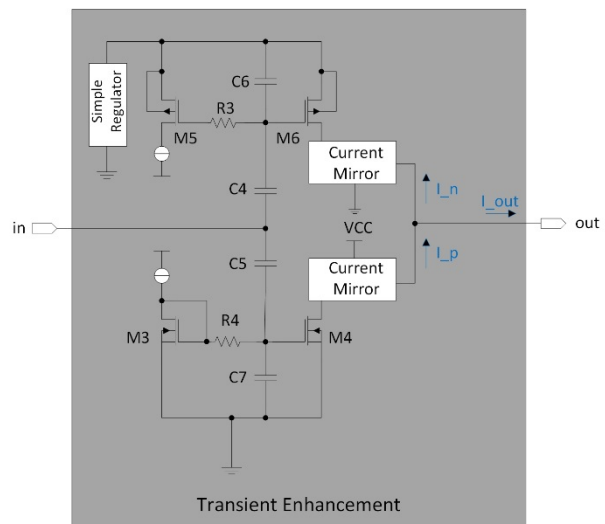


Figure 3: Transient enhancement block diagram.

The table below shows a summary of the LDO performances.

Technology	90 nm CMOS
Operation temperature	0°C to 105°C
Supply voltage	1.6 V to 5.5 V
Load capacitor	10 nF to 40 nF
Load current	0 mA to 100 mA
Step current	upto ± 10 mA
Step supply voltage	upto ± 0.5 V
Line regulation	<50 mV/V
Load regulation	<0.5 mV/mA
Integrated noise	<275 μ V from 10 to 100 kHz
PSRR	>30 dB @ 1 < freq < 100 kHz >12 dB @ 100 k < freq < 1 MHz
Current consumption	<0.5% * I_{load} + 0.25 mA
Area	0.2 mm ² (excluding blocking capacitor)

A Versatile Sensor Interface for IO-Link Applications

P. Heim, A. Vouilloz, Y. Zha, F. Giroud, T.-C. Le, C. Monneron, B. Putter, P.-F. Rüedi, C. Schuster •, S. Meier •, P. Vaucher •, C. Eichenberger •, S. Tahary ••, F. Tanner ••

The actual IO-Link Standard version 1.1 was launched at the end of 2010. In the meantime, IO-Link has applied for acceptance as an IEC-norm, and became a world-wide accepted norm in automation. CSEM designed a sensor interface composed of a novel versatile capacitance to voltage converter (C2V), two programmable gain amplifiers (PGA) with sample and hold (SH) and a low-pass filter (LP) incorporated in HMT Microelectronics' HMT872 ASIC. This ASIC also encompass an 18-bit ADC, a 14-bit DAC, a temperature sensor, a serial-parallel interface (SPI) and an IO-Link interface.

IO-Link is the first standard IO technology worldwide (IEC 61131-9) for the communication with sensors and actuators [1]. It is based on the long established 3-wire sensor and actuator connection without additional requirements.

The sensor interface is illustrated on the following block-schematic together with the whole IO-Link ASIC.

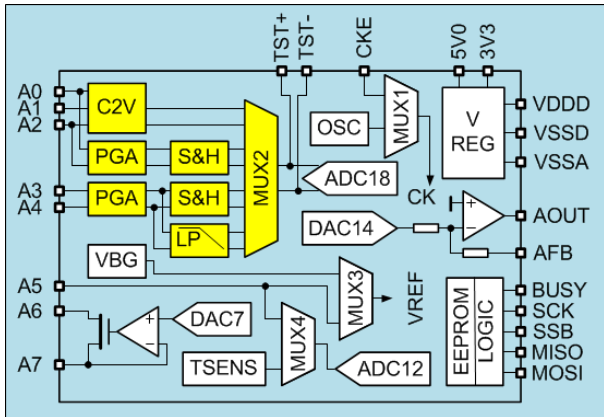


Figure 1: Block-schematic of the HMT872 IO-Link compatible ASIC with the sensor interface part highlighted.

The ASIC includes the following characteristics:

- Wide temperature range from – 40 to + 125°C
- Versatile Programmable Gain Amplifier (PGA) stage with 14 μ V input referred noise and programmable gain from -6 dB to 48 dB
- Capacitance to voltage converter with high input capacitance range from 1 pF to 100 pF and tuneable bandwidth up to 10 kHz
- High precision DAC for actuators yielding 14-bit resolution with 20 kHz sampling rate
- High resolution ADC: From 12 effective bits and 10 kHz bandwidth to 18 effective bits and 1.2 kHz bandwidth

The most unusual circuit of the ASIC is the C2V converter. The challenge of this block is to handle a wide range of capacitive sensors. Differential capacitive sensors have a mid-point electrode that is not trivial to handle with a differential circuit. It has been made possible only with a dedicated multi-phase structure comprising a difference differential amplifier (DDA) that is used alternately on either input pairs. The result is a truly

differential circuit with inherent correlated double sampling operation that suppresses the 1/f noise.

The C2V block can handle various differential or single-ended capacitive sensors, with a total capacitance of up to 100 pF.

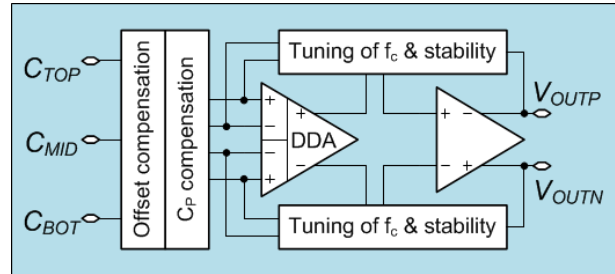


Figure 2: Simplified block-schematic of the fully differential C2V.

All capacitive sensors possess both sensitive and parasitic capacitances (C_S and C_P). In order to ensure linearity, the C2V interface can compensate C_P up to 40 pF with a resolution of 10 bits. There is also an offset cancellation of 16 pF with 10 bits resolution. Finally, a tuning that acts on the cut-off frequency f_c is used to ensure the stability of the circuit for large capacitance sensors. The tuning strategy dispatches a total capacitance amongst the various pairs of the differential circuit's capacitors such that none of it is wasted. This results in a wide sensor capacitance range and optimal noise performances.

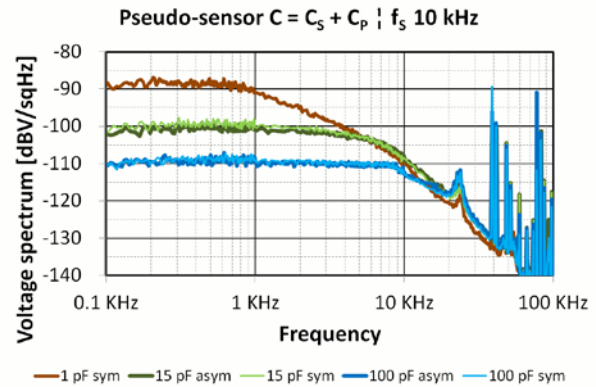


Figure 3: Noise measurement of the C2V with pseudo-sensors.

The noise measurements above are made with pseudo-sensors made of fixed capacitors. After compensation (i.e cancellation) of C_P, this is the active sensor capacitance C_S which is relevant for the noise estimation.

This work was supported by a CTI/KTI grant.

• HMT Microelectronic AG, Switzerland
•• EPFL, ESPLAB, Switzerland

[1] IO-Link System Description – Technology and Application, www.io-link.com

Design and on-Silicon Characterization of a 6T SRAM Memory Operating at Subthreshold Voltage

M. Pons Solé, T.-C. Le, C. Arm, D. Séverac, S. Emery, C. Piguet

Subthreshold designs reduce power consumption by working down to lower voltage levels than classical design (i.e. 0.4 V). This allows for instance a longer battery life, or even better, replacing the battery by energy harvesting (e.g. photovoltaic cells can generate 0.4 V directly). However SRAM blocks limit the minimum voltage at which the whole design can be supplied. SRAM bit-cell noise margins are highly degraded in subthreshold operation due to the increased sensitivity to process, voltage and temperature variations. This motivated the optimization of an SRAM memory for subthreshold operation with special attention to manufacturability. The SRAM on-silicon measurements for a 180 nm technology are presented here.

Subthreshold 6T bit-cell design

The trend for subthreshold SRAM design is to add some or several transistors to the classical 6T bit-cell to overcome low-voltage limitations. In the literature, solutions can be found spanning from 7T to 14T bit-cells. However, adding transistors leads to more variability, noise and power consumption. Our proposal is to change the read protocol at an architectural level based on the "Random Access Memory" CSEM patent [1] where the read access is performed from a single side (Figure 1). Both bit-lines (*b11* and *b12*) are used for a write operation, however only *b11* is used for reading. Doing so, the reading static noise margin is improved as only one side of the internal loop is aggressed. Moreover no sense amplifiers are required as full voltage swing is applied to the bit-line and only simple tri-state gates are used. This also simplifies and increases the robustness and manufacturability at subthreshold voltage. Bit-cell transistors are also upsized to optimize them for subthreshold effects. This optimization is based on our previous works for subthreshold standard cell design [2]. For this work in 180 nm, the minimum channel length has been determined to be 420 nm. To refine transistor sizing, Spice simulations have been performed taking into account process variations, voltage from 0.4 V to 0.9 V and temperature from -40°C to 125°C. The worst read static noise margin is 40 mV for 0.4 V operation and over 130 mV for 0.9 V (for 0.4 V and a minimum channel length sizing of 180 nm, it is 20 µV and the bit-cell is not operating anymore).

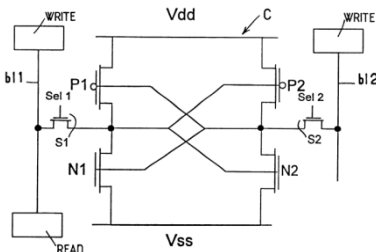


Figure 1: 6T bit-cell. WRITE and READ circuits indicated as boxes.

Subthreshold 1 kib SRAM memory design

The 1 kib SRAM block (total area of 22'350 µm²) includes:

- A full custom decoder implemented using standard cells able to sustain the bit-cell subthreshold voltage operations
- Pre-charge switches and tri-state gates for reading controlled by an "output enable" signal to decrease read power consumption

- Write-mode tri-state gates to drive the *b11* and *b12* signals controlled by "byte enable" signals to decrease write power consumption
- A bit-cell array composed of 16 rows of 8 bytes that can be individually addressed for a total of 1 kib memory size

On-silicon characterization of the SRAM

The SRAM was tested using a March algorithm that activates all the addresses and forces worst-case paths. Measurements at room temperature for supplies up to 0.6 V are shown in Figure 2. The SRAM is 100% functional (i.e. all the output bits tested in the March test are correct) at a minimum voltage of 0.27 V, with a maximum frequency of 530 Hz, with only 3.1 nA of total current and 2.4 nA of leakage. It can be observed how the ratio of total and leakage current is small for sub-threshold operation (that is why bit-cell robustness is critical). This ratio increases with supply voltage. For lower voltages and higher frequencies, correct read and write operations were observed, however the March test did not complete satisfactorily. As expected, the bit error degradation occurs when reaching deep sub-threshold supply voltage levels (see Figure 3).

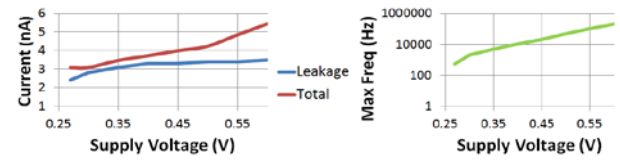


Figure 2: SRAM leakage, total current and maximum frequency.

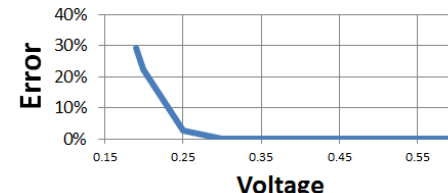


Figure 3: SRAM measurements for bit errors degradation.

Conclusion

A 1 kib 180 nm 6T subthreshold SRAM has been designed with a focus on manufacturability, then integrated and measured satisfactorily. The design operates without errors down to 0.27 V which allows a seamless use of this SRAM block in combination with energy harvesting techniques.

[1] J.-M. Masgonty, et. al., "Random access memory," US 6366504 B1 patent, (2002)

[2] M. Pons, et. al., "Ultra low power standard cell design using planar bulk CMOS in subthreshold operation," in the International Workshop on Power And Timing Modeling Optimization and Simulation (PATMOS), (2013) 9

Telemetry Unit for a Neuro-prosthesis Stimulation Chip

J.-L. Nagel, M. Morgan, C. Hennemann, D. Séverac

The combined expertise of micro-/nano-technology and neuroscience opens new opportunities in the development of neuro-prostheses, i.e. devices designed to restore sensory and motor functions after injury or disease to the nervous system. The SpineRepair project, involving a multidisciplinary consortium of experts, aims at developing a miniaturized spinal cord neuro-prosthesis in the hope of someday offering a solution to paraplegics.

The SpineRepair project proposes to optimize, manufacture, assemble and validate a fundamentally different technology to produce an electrical stimulation of the spinal cord via a neuro-prosthetic system based on ultra-compliant microelectrode arrays, embedded ultra-low-power analog electronics and an efficient telemetry unit. This type of device could also be applied to epilepsy, Parkinson's disease or pain management.

Spinal cord injury causes a loss of function below the level of the lesion. The goal of the neuro-prosthesis is to restore motor function and potentially to provide sensory feedback. Stretchable and flexible electrodes are connected to a stimulator chip which generates epidural current pulses to stimulate the spinal cord below the point of injury. The micro-electrode array and the flexible electrodes must withstand demanding mechanical loading and yet present low resistivity.

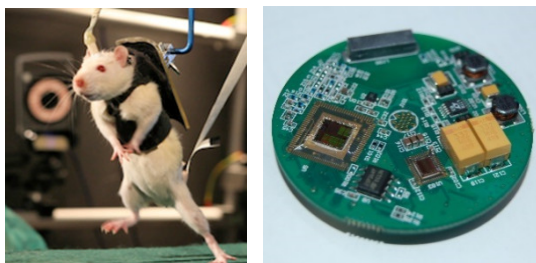


Figure 2: Left: rat walking with electrical stimulations on spinal cord (EPFL [1]). Right: First version of PCB for neuro-prosthesis.

The SpineRepair implantable device addresses important technical challenges: ultra-low-power consumption, miniaturization and bio-compatible encapsulation to cite a few. The neuro-prosthesis is composed of electrodes, a stimulation chip, an ultra-low power microcontroller with radio transceiver, and a rechargeable battery.

For the purposes of the project, the neuro-prosthesis is driven by a lab computer. A radio link between the PC and the prosthesis relays commands to the stimulation chip to test different forms of stimulation patterns on the spinal cord.

The stimulation chip was developed by Prof. Hierlemann's group [2] at ETHZ and drives 15 independent channels which can generate monophasic or biphasic current pulses with up to 3 mA amplitude at up to ± 6 V each. CSEM too has proven experience in designing similar neural stimulation and sensing chips, e.g. collaborations with Nano Retina [3] (retinal implant), the Wyss Center for Bio- and Neuro-engineering [4] (brain implant) and 3Brain (in vitro monitoring).

A state of the art ultra-low power 868-915 MHz radio link is provided by CSEM's icycom [5] system-on-chip which provides a radio transceiver (4 mW at 1 V), local processing capability with the icyflex1 processor and SPI connectivity to the stimulation chip (on the neuro-prosthesis side) or an Ethernet interface (on the PC side of the radio link).

A simple software API was defined for the host PC to send commands to the stimulator. The icyflex1 processor on the icycom SoC then parses the UDP command strings, recodes them in the form of stimulation commands and transmits them over-the-air to the implantable receiver. The radio on the receiver node continuously listens for commands and sends them to the stimulation chip.

In terms of power budget, the receiver system-on-chip consumes less than 2.5 mA in continuous-receive mode (on a 3 V battery), which is on the same order as the average power consumption of the stimulation chip (typically 4 mA). However, the impulsive nature of the current delivered and drawn by the stimulation chip (up to ~50 mA peaks on ± 6 V) implies important constraints on the power management. Large capacitors are coupled to the +6 V and +12 V step-up converters to avoid large peak currents on the 3 V battery.

Transmission delays are also very important for an efficient use of the system. The overall delay from commands on the host PC to the resulting stimulation spikes is currently around 10 ms. Whereas the timing on the icycom controller depends essentially on the processing done on the icyflex1 CPU, the time from host PC to the icycom radio varies more as it is dependent on the host hardware and its operating system (MS Windows) which is not a real time OS.

An antenna was designed specifically for the radio link and the wireless charging of the battery. Its operation on or under the skin poses specific challenges. Experiments with bio-compatible packaging (silicone rubber) were carried out at EPFL on an antenna module. CSEM characterized the antenna properties of this packaged version, connected to the 868 MHz radio. The dielectric packaging impacts the matching of the antenna. Additional experimentation will be undertaken to model the effects of surrounding tissues and to fine tune the antenna circuits before the finalization of the device.

The electronics for the neuro-prosthesis have been validated in the lab, with the stimulation channels connected to a load. A first in-vivo test is planned for Nov 2015 on a rat to validate the whole command chain from the host PC to the spinal cord.

[1] cnp.epfl.ch, Center for Neuroprosthetics, EPFL

[2] www.bsse.ethz.ch/bel, Bio Engineering Laboratory, ETHZ

[3] www.nano-retina.com, Nano Retina, Inc.

[4] www.wysscenter.ch, Wyss Center for Bio- and Neuro-engineering

[5] www.csem.ch/docs>Show.aspx/12228, icycom flyer

ANNEXES

Publications

- [1] P.-J. Alet, F. Baccaro, M. De Felice, V. Efthymiou, C. Mayr, G. Graditi, M. Juel, D. Moser, M. Petitta, S. Tselepis, G. Yang, "Photovoltaics merging with the active integrated grid", European Photovoltaic Technology Platform, White paper, June 2015
- [2] F. Braun, M. Proen  a, M. Rapin, M. Lemay, A. Adler, B. Grychtol, J. Sol  , J.-P. Thiran, "Aortic blood pressure measured via EIT: investigation of different measurement settings", *Physiological Measurement*, 36 (6), June 2015, 1147-59
- [3] G. Buchs, S. Kundermann, E. Portuondo-Campa, S. Lecomte, "Radiation hard mode-locked laser suitable as a spaceborne frequency comb", *Optics Express*, 23 (8), April 2015, 9890-9900
- [4] G. Cattaneo, A. Faes, H.-Y. Li, F. Galliano, M. Gragert, Y. Yao, R. Grischke, T. S  derstr  m, M. Despeisse, C. Ballif, L.-E. Perret-Aebi, "Lamination Process and Encapsulation Materials for Glass-Glass Photovoltaic Module Design", *Photovoltaics International*, May 2015, 82-90
- [5] S. De Wolf, J. Holovsky, S.-J. Moon, P. L  per, B. Niesen, M. Ledinsky, F.-J. Haug, J.-H. Yum, C. Ballif, "Organometallic Halide Perovskites: Sharp Optical Absorption Edge and its Relation to Photovoltaic Performance", *The Journal of Physical Chemistry Letters*, 5, November 2014, 1035-1039
- [6] A. Descoedres, C. Alleb  , N. Badel, L. Barraud, J. Champliaud, F. Debrot, A. Faes, A. Lachowicz, J. Levrat, S. Nicolay, L. Sansonnens, M. Despeisse, C. Ballif, "Silicon heterojunction solar cells: towards low-cost high-efficiency industrial devices and applications to low-concentration PV", *Energy Procedia*, 77, March 2015, 508 - 514
- [7] J. R. Farserotu, J.-D. Decotignie, et. al., "Tactile Prosthetics in WiseSkin", Nano-Tera publication, March 2015
- [8] M. Filipi  , P. L  per, B. Niesen, S. De Wolf, J. Kr  , C. Ballif, M. Topi  , "CH₃NH₃PbI₃ perovskite / silicon tandem solar cells: Characterization based optical simulations ", *Optics Express*, 23 (7), February 2015, A263 - A278
- [9] B. Gallinet, J. Butet, O. J. F. Martin, "Numerical methods for nanophotonics: standard problems and future challenges", *Laser and Photonics Reviews*, 9, November 2015, 577-603
- [10] T.E. Gartmann, F. Kehl, "Experimental Validation of the Sensitivity of Waveguide Grating Based Refractometric (Bio)sensors", *Biosensors*, 5 (2), April 2015, 187-198
- [11] J. Geissbuhler, J. Werner, S. Martin de Nicolas, L. Barraud, A. Hessler-Wyser, M. Despeisse, S. Nicolay, A. Tomasi, B. Niesen, S. De Wolf, C. Ballif, "22.5% efficient silicon heterojunction solar cell with molybdenum oxide hole collector", *Applied Physics Letters*, 107 (8), August 2015, 081601
- [12] J. Geissb  hler, S. De Wolf, A. Faes, N. Badel, Q. Jeangros, A. Tomasi, L. Barraud, A. Descoedres, M. Despeisse, C. Ballif, "Silicon heterojunction solar cells with copper-plated grid electrodes: Status and comparison with silver thick-film techniques", *IEEE J. Photovoltaics*, 4, November 2014, 1055
- [13] H. Gold, A. Haase, A. Fian, C. Prietl, B. Striedinger, F. Zanella, N. Marjanovi  , R. Ferrini, J. Ring, K.-D. Lee, R. Jiawook, A. Drost, M. K  nig, R. M  ller, K. Myny, J. Genoe, U. Kleb, H. Hirshy, R. Pr  t  t, J. Kraxner, R. Schmied, B. Stadlober, "Self-aligned flexible organic thin-film transistors with gates patterned by nano-imprint lithography", *Organic Electronics*, 22 (7), July 2015, 140-146
- [14] C. Hannesschl  ger, V. Revol, B. Plank, D. Salaberger, J. Kastner, "Fibre structure characterisation of injection moulded short fibre-reinforced polymers by X-ray scatter dark field tomography", *Case Studies in Non destructive Testing and Evaluation*, 3, April 2015, 34-41
- [15] P. D. Heinstein, Z. Tiefert-Reckermann, "Ein Durchbruch in der geb  udeintegrierten Photovoltaik: Weisse PV-Module vom CSEM in Neuenburg entwickelt", K  nstlerh  user und Ateliers, (k+a 2015.1), March 2015, 70-71
- [16] P. D. Heinstein, "Geb  udeintegrierte Photovoltaik", *TEC21 - Schweizerische Bauzeitung*, 24, June 2015, 28-30
- [17] S. Heub, N. Tscharner, V. Monnier, F. Kehl, P. S. Dittrich, S. Follonier, L. Barbe, "Automated and portable solid phase extraction platform for immuno-detection of 17beta-estradiol in water", *Journal of Chromatography A*, 1381, February 2015, 22-28

- [18] A. Hokkanen, I. Stuns, P. Schmid, A. Kokkonen, F. Gao, A. Steinecker, J. Budczies, P. Heimala, L. Hakalahti, "Microfluidic sampling system for tissue analytics", *Biomicrofluidics*, 9 (5), September 2015, online journal
- [19] C. Jud, S. Ahmed, L. Mueller, C. Kinnear, D. Vanhecke, Y. Umehara, S. Frey, M. Liley, S. Angeloni, A. S. Fink, B. Rothen, "Ultrathin ceramic membranes as scaffolds for functional cell co-culture models on a biomimetic scale", *Biores Open Access*. 2015; 4(1): 457-468
- [20] F. Kehl, D. Bischof, M. Michler, M. Keka, R. Stanley, "Design of a Label-Free, Distributed Bragg Grating Resonator Based Dielectric Waveguide Biosensor", *Photonics*, 2 (1), January 2015, 124-138
- [21] M. Ledinsky, P. Löper, B. Niesen, J. Holovsky, S.-J. Moon, J.-H. Yum, S. De Wolf, A. Fejfar, C. Ballif, "Raman spectroscopy of organic-inorganic halide perovskites", *Journal of Physical Chemistry Letters*, 6 (3), May 2015, 401-406
- [22] H.-Y. Li, Y. Luo, C. Ballif, L.-E. Perret-Aebi, "Effect of Cooling Press on the Optical Transmission Through Photovoltaic Encapsulants", *Polymer-Plastics Technology and Engineering*, 54, February 2015, 416-424
- [23] H.-Y. Li, Y. Luo, C. Ballif, L.-E. Perret-Aebi, "Fast and Nondestructive Detection on the EVA Gel Content in Photovoltaic Modules by Optical Reflection", *IEEE Journal of Photovoltaics*, 5 (3), February 2015, 759-765
- [24] P. Löper, M. Stuckelberger, B. Niesen, J. Werner, M. Filipic, S.-J. Moon, J.-H. Yum, M. Topic, S. De Wolf, C. Ballif, "Complex Refractive Index Spectra of CH₃NH₃PbI₃ Perovskite Thin Films Determined by Spectroscopic Ellipsometry and Spectrophotometry", *Journal of Physical Chemistry Letters*, 6 (1), February 2015, 66-71
- [25] P. Löper, S.-J. Moon, S. Martín de Nicolas, B. Niesen, M. Ledinsky, S. Nicolay, J. Bailat, J.-H. Yum, S. De Wolf, C. Ballif, "Organic-inorganic halide perovskite/crystalline silicon four-terminal tandem solar cells", *Physical Chemistry Chemical Physics*, 17, 2015, 1619-1629
- [26] P. Löper, B. Niesen, S.-J. Moon, S. Martín de Nicolas, J. Holovsky, Z. Remes, M. Ledinsky, F.-J. Haug, J.-H. Yum, S. De Wolf, C. Ballif, "Organic-Inorganic Halide Perovskites: Perspectives for Silicon-Based Tandem Solar Cells", *IEEE Journal of Photovoltaics*, 4, November 2014, 1545-1551
- [27] Y. Luo, C. Ballif, L.-E. Perret-Aebi, H.-Y. Li., "Modeling of voids evolution in the encapsulation process of photovoltaic modules", *Polymers and Polymer Composites*, January 2015, 375-388
- [28] F. Lütolf, M. Stalder, O.J.F. Martin, "Up-scalable method to amplify the diffraction efficiency of simple gratings", *Optics Letters*, 39 (23), November 2014, 6557-6560
- [29] S.-J. Moon, J.-H. Yum, L. Löfgren, A. Walter, L. Sansonnens, M. Benkhaira, S. Nicolay, J. Bailat, C. Ballif, "Laser-scribing patterning for the production of organometallic halide perovskite solar modules", *IEEE J.of Photovoltaics*, 5 (4), July 2015, 1087-1092
- [30] D. Müller, S. Cattaneo, F. Meier, R. Welz, A. J. de Mello, "Nanoparticle separation with a miniaturized asymmetrical flow field-flow fractionation cartridge", *Frontiers in Chemistry*, 3, July 2015, 45
- [31] G. Nisato, O. Fernàndez, R. Ferrini, S. Nicolay, "Les OLED ou la lumière dans tous ses états—Un atout de taille dans la course à l'éclairage durable", *Bulletin Electrosuisse*, 1, January 2015, 36-40
- [32] B. Paviet-Salomon, A. Tomasi, A. Descoeuilles, L. Barraud, S. Nicolay, M. Despeisse, S. D. Wolf, C. Ballif, "Back-Contacted Silicon Heterojunction Solar Cells: Optical-Loss Analysis and Mitigation", *IEEE Journal of Photovoltaics*, 5 (5), September 2015, 1293-1303
- [33] O. Perez-Anguiano, B. Wenger, R. Pugin, H. Hofmann, E. Scolan, "Controlling Mesopore Size and Processability of Transparent Enzyme-Loaded Silica Films for Biosensing Applications", *ACS Applied Materials & Interfaces*, 7 (4), January 2015, 2960-2971
- [34] O. Pérez-Anguiano, B. Wenger, R. Pugin, H. Hofmann, E. Scolan, "Controlling mesopore size and processability of transparent enzyme-loaded silica films for biosensing applications", *ACS Appl Mater Interfaces*, 7 (4), February 2015, 2960-71
- [35] E. Portuondo-Campa, G. Buchs, S. Kundermann, L. Balet, S. Lecomte, "Ultra-low phase-noise microwave generation using a diode-pumped solid-state laser based frequency comb and a polarization-maintaining pulse interleaver", *Optics Express*, 23 (25), December 2015, 32441-32451

- [36] M. Proen  a, F. Braun, M. Rapin, J. Sol  , A. Adler, B. Grychtol, S. H. Bohm, M. Lemay, J.-P. Thiran, "Influence of heart motion on cardiac output estimation by means of electrical impedance tomography: a case study", *Physiological Measurement*, 36 (6), June 2015, 1075-91
- [37] M. Rapin, M. Proen  a, F. Braun, C. Meier, J. Sol  , D. Ferrario, O. Grossenbacher, J.-A. Porchet, O. Ch  telat, "Cooperative dry-electrode sensors for multi-lead biopotential and bioimpedance monitoring", *Physiological Measurement*, 36, March 2015, 767-783
- [38] L. Rossini, E. Onillon, O. Ch  telat, Y. Perriard, "Closed-loop magnetic bearing and angular velocity control of a reaction sphere actuator", *Mechatronics*, 30, September 2015, 214-224
- [39] H. Rossmann, F. Zanella, N. Marjanovic, M. Schnieper, T. A. Jung, E. Meyer, J. Gobrecht, R. A. Minamisawa, H. Bartolf, "Simulations and fabrication of novel 4H-SiC nano-trench MOSFET devices", *Swiss Nanoscience Institute Annual Report 2014 - Supplement*, March 2015, 62-63
- [40] B. Schyrr, S. Boder-Pasche, R. Ischer, R. Smajda, G. Voirin, "Fiber-optic protease sensor based on the degradation of thin gelatin films", *Sensing and Bio-Sensing Research*, 3, March 2015, 65-73
- [41] M. Stuckelberger, B. Perruche, M. Bonnet-Eymard, Y. Riesen, M. Despeisse, F.-J. Haug, C. Ballif, "Class AAA LED-Based Solar Simulator for Steady-State Measurements and Light Soaking", *IEEE J. Photovoltaics*, 4 (5), November 2014, 1282
- [42] A. Tomasi, B. Paviet-Salomon, D. Lachenal, S. Martin de Nicolas, A. Descoeuilles, J. Geissb  hler, S. De Wolf, C. Ballif, "Back-contacted silicon heterojunction solar cells with efficiency >21%", *IEEE J. Photovoltaics*, 4, November 2014, 1046
- [43] J. Werner, G. Dubuis, A. Walter, P. Loper, S.-J. Moon, S. Nicolay, M. Morales-Masis, S. De Wolf, B. Niesen, C. Ballif, "Sputtered rear electrode with broadband transparency for perovskite solar cells", *Solar Energy Materials and Solar Cells*, 141, October 2015, 407-413
- [44] X. Zeng, L. Sulmoni, J.-M. Lamy, T. Stadelmann, S. Grossmann, A. C. Hoogerwerf, N. Grandjean, D. L. Boiko, "Solitary Pulse-on-Demand Production by Optical Injection Locking of Passively Q- Switched InGaN Diode Laser Near Lasing Threshold", *Applied Physics Letters*, 106 (7), February 2015, 071101

Proceedings

- [1] A. Adler, F. Braun, J. Sol  , "Distinguishability as a noise performance metric for EIT algorithms", *EIT2015*, Neuch  tel (CH), June 2015, 21
- [2] P.-J. Alet, V. Musolino, C. Meier, Y. Stauffer, A. Hutter, L.-E. Perret-Aebi, C. Ballif, "Electrical design for systematic integration of PV construction elements in newly-built blocks", *Congr  s national photovolta  que*, Basel (CH), 16-17 March 2015
- [3] P.-J. Alet, V. Musolino, M. Despeisse, L.-E. Perret-Aebi, B. Strahm, C. Ballif, "Outdoor benchmarking of silicon heterojunction (HJT) modules", *Congr  s national photovolta  que*, Basel (CH), 16-17 March 2015
- [4] P.-J. Alet, F. Baccaro, M. De Felice, V. Efthymiou, C. Mayr, G. Graditi, M. Juel, D. Moser, F. Nemac, M. Petitta, S. Tselepis, G. Yang, "Quantification, challenges and outlook of PV integration in the power system: a review by the European PV Technology Platform", *EUPVSEC 2015*, Hamburg (DE), 14-18 September 2015
- [5] P.-J. Alet, J. Escarr  , G. Cattaneo, H.-Y. Li, P. Heinstein, L. Sansonnens, S. Nicolay, J. Bailat, V. Musolino, C. Ballif, L.-E. Perret-Aebi, "Products and system design for making PV a natural component of the building envelope", *Reaching out for opportunities in BIPV: technology and industry developments*, Hamburg (DE), 15 September 2015
- [6] C. Alleb  , J. Levrat, J. Champliaud, M. Despeisse, A. Descoeuilles, L. Barraud, A. Faes, A. Lachowicz, N. Badel, F. Debrot, J. Geissb  hler, S. De Wolf, C. Ballif, "Silicon Heterojunction Solar Cells with Plated Contacts for Low to Medium Concentration Photovoltaics", *IEEE PV Conference*, New Orleans (US), 14-19 June 2015
- [7] C. Ballif, *et al.*, "Crystalline Silicon Heterojunction: Advances in Research and Opportunities for Low Electricity Costs", *SNEC*, Shangai (CN), April 2015

- [8] C. Ballif, *et al.*, "Hetero-Junction PV Technology, Basic Principles, Manufacturing ", IEEE PV Conference, New Orleans (US), June 2015
- [9] C. Ballif, *et al.*, "Advances in Crystalline Silicon Heterojunction Research and Opportunities for Low Manufacturing Costs", IEEE PV Conference, New Orelans (US), June 2015
- [10] C. Ballif, L.-E. Perret-Aebi, *et al.*, "When PV modules are becoming real building elements: White solar module, a revolution for BIPV", IEEE PV Conference, New Orelans (US), June 2015
- [11] C. Ballif, *et al.*, "R&D from material preparation up to next generation manufacturing:opportunities for local companies", Swiss Photovoltaic Conference, Basel (CH), March 2015
- [12] C. Ballif, *et al.*, "Solar cells with higher efficiencies and lower production costs : the role micro and nanotechnologies", Nanoconvention, Neuchâtel (CH), May 2015
- [13] C. Ballif, *et al.*, "Towards ultra-high efficient photovoltaics with perovskite/crystalline silicon ", EUPVSEC 2015, Hamburg (DE), September 2015
- [14] P. Berthoud, M. Haldimann, A. Michaud, S. Kundermann, D. Boiko, S. Lecomte, V. Hermann, M. André, "Development of a transportable optically-pumped cesium beam clock", European Frequency and Time Forum (EFTF) and Frequency Control Symposium (FCS), Denver (US), April 2015
- [15] M. Bertschi, P. Celka, R. Delgado-Gonzalo, M. Lemay, E.M. Calvo, O. Grossenbacher, P. Renevey, "Accurate Walking and Running Speed Estimation Using Wrist Inertial Data", 37th Annual International Conference of the IEEE Engineering in Medicine and Biology Society (EMBC'15), Milano (IT), 25-29 August 2015, 8083-8086
- [16] F. Braun, M. Proen  , M. Rapin, X. Alba, K. Lekadir, M. Lemay, J. Sol  , A. F. Frangi, J.-P. Thiran, "Stroke volume measured via electrical impedance tomography (EIT): a simulation-based feasibility study", 2015 Annual Meeting of the Swiss Society of Biomedical Engineering (SSBE), Neuch  tel (CH), August 2015
- [17] F. Braun, M. Proen  , M. Rapin, X. Alba, K. Lekadir, M. Lemay, J. Sol  , Alejandro F. Frangi, J.-P. Thiran, "4D Heart Model Helps Unveiling Contributors to Cardiac EIT Signal", EIT2015, Neuch  tel (CH), June 2015, 107
- [18] G. Buchs, S. Kundermann, E. Portuondo-Campa, S. Lecomte, "Radiation Hard Optical Frequency Comb from a Diode-Pumped Solid-State Femtosecond Laser", European Frequency and Time Forum (EFTF) and Frequency Control Symposium (FCS), Denver (US), April 2015
- [19] G. Buchs, S. Kundermann, E. Portuondo-Campa, S. Lecomte, "Radiation hard optical frequency comb from a diode-pumped solid-state femtosecond laser", CLEO Europe 2015, Munich (DE), June 2015
- [20] H. Cai, A. Hutter, E. Olivero, P. Roduit, P. Ferrez, "Load shifting for tertiary control power provision", Powereng 2015, Riga (La), 11-13 May 2015
- [21] M. Cermack, O. Ch  telat, V. Fontana, "Health and safety monitoring in extreme environments: technology capabilities and real needs", 13th International Symposium on Maritime Health - ISMH13, Bergen (NO), 23-26 June 2015
- [22] O. Ch  telat, M. Rapin, C. Meier, A. Bischof, M. K. Augustyniak, "Synchronization and communication of cooperative sensors", 37th Annual International Conference of the IEEE Engineering in Medicine and Biology Society - EMBC2015, Milan (IT), 25-29 August 2015
- [23] O. Ch  telat, D. Ferrario, M. Proen  , J.-A. Porchet, A. Falhi, O. Grossenbacher, R. Delgado-Gonzalo, N. Della Ricca, C. Sartori, "Clinical validation of LTMS-S: a wearable system for vital signs monitoring", 37th Annual International Conference of the IEEE Engineering in Medicine and Biology Society - EMBC2015, Milan (IT), 25-29 August 2015
- [24] R. Delgado-Gonzalo, J. Par  k, A. Dan Tarniceriu, P. Renevey, M. Bertschi, I. Korhonen, "Evaluation of Accuracy and Reliability of PulseOn Optical Heart Rate Monitoring Device", 37th Annual International Conference of the IEEE Engineering in Medicine and Biology Society (EMBC'15), Milano (IT), 25-29 August 2015, 430-433
- [25] R. Delgado-Gonzalo, P. Celka, P. Renevey, S. Dasen, J. Sol  , M. Bertschi, M. Lemay, "Physical Activity Profiling: Activity-Specific Step Counting and Energy Expenditure Models Using 3D Wrist Acceleration", 37th Annual International Conference of the IEEE Engineering in Medicine and Biology Society (EMBC'15), Milano (IT), 25-29 August 2015, 8091-8094

- [26] A. Descoedres, C. Alleb  , N. Badel, L. Barraud, J. Champliaud, F. Debrot, A. Faes, A. Lachowicz, J. Levrat, S. Nicolay, L. Sansonnens, M. Despeisse, C. Ballif,
"Silicon heterojunction solar cells: towards low-cost high-efficiency industrial devices and applications to low-concentration PV", 5th International Conference on Crystalline Silicon Photovoltaics (SiliconPV 2015) and 5th nPV workshop, Konstanz (DE), 22-27 March 2015,
- [27] M. Despeisse, A. Faes, A. Lachowicz, N. Badel, C. Alleb  , A. Descoedres, L. Barraud, F. Debrot, J. Champliaud, J. Levrat, P.-J. Alet, F. Galliano, L.-E. Perret-Aebi, T. S  derstr  m, Y. Yao, C. Ballif, "Advanced Metallization and Interconnection for Silicon Heterojunction Cells and Modules", 6th World Conference on Photovoltaic Energy Conversion (WCPEC-6), Kyoto (JP), November 2014,
- [28] M. Despeisse, A. Lo, M. Bonnet-Eymard, Y. Riesen, J. Levrat, P.-J. Alet, C. Ballif,
"Large-Area LED/Halogen hybrid solar simulator and Silicon Heterojunction solar modules indoor to outdoor performance monitoring", 6th World Conference on Photovoltaic Energy Conversion (WCPEC-6), Kyoto (JP), November 2014
- [29] M. Despeisse, C. Alleb  , J. Champliaud, J. Levrat, A. Descoedres, A. Faes, L. Barraud, F. Debrot, A. Lachowicz, N. Badel, C. Ballif,
"Silicon Heterojunction Solar Cells with Plated Contacts for Low Concentration Photovoltaics", 24th International Photovoltaic Science and Engineering Conference (PVSEC-24), Kyoto (JP), November 2014
- [30] M. Despeisse, C. Alleb  , J. Champliaud, J. Levrat, A. Descoedres, A. Faes, L. Barraud, F. Debrot, A. Lachowicz, N. Badel, C. Ballif,
"Silicon Heterojunction Solar Cells with Plated Contacts for Low Concentration Photovoltaics", 6th World Conference on Photovoltaic Energy Conversion (WCPEC-6), Kyoto (JP), November 2014
- [31] M. Despeisse, A. Faes, A. Lachowicz, N. Badel, C. Alleb  , A. Descoedres, L. Barraud, F. Debrot, J. Champliaud, J. Levrat, P.-J. Alet, F. Galliano, L.-E. Perret-Aebi, T. S  derstr  m, Y. Yao, C. Ballif,
"Advanced metallization and interconnection for silicon heterojunction cells and modules", 24th International Photovoltaic Science and Engineering Conference (PVSEC-24), Kyoto (JP), November 2014
- [32] M. Despeisse, A. Faes, J. Levrat, J. Escarr  , J. Champliaud, V. Chapuis, N. Badel, T. S  derstr  m, Y. Yao, J. Ufheil, P. Papet, G. Cattaneo, J. Cattin, Y. Baumgartner, A. Hessler-Wyser, C. Ballif, "SmartWire Solar Cell Interconnection Technology", 24th International Photovoltaic Science and Engineering Conference (PVSEC-24), Kyoto (JP), November 2014
- [33] M. Despeisse, A. Faes, J. Levrat, J. Escarr  , J. Champliaud, V. Chapuis, N. Badel, T. S  derstr  m, Y. Yao, J. Ufheil, P. Papet, G. Cattaneo, J. Cattin, Y. Baumgartner, A. Hessler-Wyser, C. Ballif, "SmartWire Solar Cell Interconnection Technology", 6th World Conference on Photovoltaic Energy Conversion (WCPEC-6), Kyoto (JP), November 2014
- [34] D. Domin  , L. L  fgren, M. Modestino, J.-H. Yum, P. Kohler, M. Benkhaira, L. Sansonnens, S. Nicolay, J. Bailat, C. Ballif, "Thin-Film Silicon Triple-Junction Solar Cells For Hydrogen Production", Technical Digest - WCPEC6, Kyoto (JP), November 2014
- [35] V. Fakhouri, J. Hiller, R. Ambigapathy, J. Levrat, P.-J. Alet, M. Despeisse, "I-V characterization of bifacial PV devices", SNEC PV Power expo, Shanghai (CN), April 2015
- [36] O. Fernandez, F. Zanella, R. Ferrini, P. Evanschitzky, S. Ivanovici, "Thin-Film Light Management System for Intelligent Large-Area LED Luminaires", LED Symposium 2015, Bregenz (AT), 22-24 September 2015
- [37] O. Fern  ndez, R. Ferrini, P. Evanschitzky, V. Agudelo-Moreno, "Large-Area Solid State Intelligent Efficient Luminaires", 8th International Conference on Energy Efficiency in Domestic Appliances and Lighting EEDAL'15, Luzern (CH), 26-28 August 2015
- [38] W. Glettig, S. Droz, Q. Longchamp, R. Rabe, J.-M. Breguet, "A 3-DOF force measurement device for quality inspection applications of microsystems", euspen's 15th International Conference & Exhibition, Leuven (BE), 1-5 June 2015, 111
- [39] E. Hammes, J. Gonzalez-Chavarri, G. Garcia Mandayo, H. F. Knapp, P. Ryser, "The Transport Phenomena within the Intasense Indoor Air Quality Monitor Design", 15 AIChE Spring Meeting, Austin TX (US), April 2015, 213a

- [40] E. Hammes, J. Gonzales-Chavarri, L. Henwood-Moroney, G. Garcia Mandayo, P. Ryser, H. F. Knapp, "A Smart Air Quality Monitor for Energy Efficient Buildings", Smart Systems Integration, Copenhagen (DK), 11-12 March 2015, 157-164
- [41] S. Hänni, J. Persoz, B. Niesen, M. Boccard, G. Bugnon, M. Ledinsky, L. Löfgren, J. Bailat, C. Ballif, "Highly Crystalline Microcrystalline Silicon Solar Cells for Enhanced Near-Infrared Absorption", Technical digest - WCPEC 6, Kyoto (JP), November 2014
- [42] S. Heub, X. Mao, P. S. Dittrich, L. Barbe, "A functionalized poly(dimethylsiloxane) chip for solvent-free, temperature actuated solid phase extraction", 19th micro-TAS conference, 2015
- [43] R. Hylsberg Jacobsen, D. Gabioud, G. Basso, P.-J. Alet, A. G. Azar, E. S. M. Ebeid, "SEMIAH: An aggregator framework for European demand response programs", Euromicro Conference on Digital System Design (DSD), Funchal (PT), 26-28 August 2015
- [44] J. Kruis, P. Gentsch, P. Theiler, F. Barrot, F. Cosandier, S. Henein, "6 DOF repeatability measurement setup for measuring position of assembled silicon parts with nanometric resolution.", euspen's 15th International Conference & Exhibition, Leuven, (BE), June 2015
- [45] S. Kundermann, S. Lecomte, "Comparison of different carrier-envelope frequency stabilization methods for a high performance DPSSL frequency comb", European Frequency and Time Forum (EFTF) and Frequency Control Symposium (FCS), Denver (US), April 2015
- [46] S. Kundermann, S. Lecomte, "Comparison of different carrier-envelope offset frequency stabilization", CLEO Europe 2015, Munich (DE), June 2015
- [47] A. Lachowicz, A. Faes, P. Gröninger, J. Champliaud, J. Levrat, L. Barraud, C. Allebé, M. Despeisse, C. Ballif, "Contact Resistance on Plated Silicon Heterojunction Solar Cells", 5th International Conference on Crystalline Silicon Photovoltaics (SiliconPV 2015), Constance (DE), 23-26 March 2015
- [48] S. Lani, F. Cardot, Y. Petremand, G. Bergonzi, P.-A. Clerc, M. Amine, S. Ischer, V. Ruhaut, A. Guillet, M. Dadras, A. Pezous, O. Dubochet, "L'hybridation du silicium: vers une simplification de l'intégration de composants silicium dans les mouvements horlogers", SSC, September 2015
- [49] M. Ledinsky, P. Löper, B. Niesen, F.-J. Haug, J. Holovsky, S.-J. Moon, J.-H. Yum, S. De Wolf, A. Fejfar, C. Ballif, "Degradation of organometallic halide perovskite photovoltaic absorbers probed by Raman spectroscopy", Materials Research Society Fall, November 2014
- [50] J. Levrat, K. Thomas, C. Allebé, A. Faes, J. Champliaud, N. Badel, L. Barraud, F. Debrot, A. Descoeuilles, A. Lachowicz, M. Despeisse, C. Ballif, "Metal-free c-Si solar cells in module", IEEE PV Conference, New Orleans (US), 14-19 June 2015
- [51] P. Löper, S. J. Moon, S. Martin de Nicolas, M. Ledinsky, B. Niesen, J. Bailat, S. Nicolay, J. H. Yum, S. De Wolf, C. Ballif, "Si-based tandem solar cells with organometallic lead halide high-band gap top-cells", The 6th World Conference on Photovoltaic Energy Conversion, Kyoto (JP), November 2014
- [52] Y. Michou, B. Deleglise, F. Lebrun, E. Scolan, A. Grivel, R. Steiger, R. Pugin, M.-C. Merienne, Y. Le Sant, "Development of a Sol-Gel Based Nanoporous Unsteady Pressure Sensitive Paint and Validation in the Large Transonic ONERA's S2MA Windtunnel", Proceedings of the 31st AIAA Aerodynamic Measurement Technology and Ground Testing Conference, June 2015, 2408
- [53] S.-J. Moon, J.-H. Yum, L. Sansonnens, L. Löfgren, S. Nicolay, J. Bailat, C. Ballif, "Organometallic perovskite toward high performing and upscale solar cell", The 6th World Conference on Photovoltaic Energy Conversion, Kyoto (JP), November 2014
- [54] S.-J. Moon, J.-H. Yum, L. Löfgren, A. Walter, L. Sansonnens, M. Benkhaira, S. Nicolay, J. Bailat, C. Ballif, "Organometallic perovskite toward high performing and upscale solar cell", Technical Digest - WCPEC6, Kyoto (JP), November 2014
- [55] V. Musolino, P.-J. Alet, L.-E. Perret-Aebi, L. Piegari, "Alleviating Power Quality Issues when integrating PV into built areas: design and control of DC microgrids", IEEE Conference on DC Microgrid, Atlanta (US), 7-10 June 2015, 1-6
- [56] V. Papapanagiotou, C. Diou, L. Zhou, J. den Boer, M. Mars, A. Delopoulos, "Fractal Nature of Chewing Sounds", New Trends in Image Analysis and Processing – ICIAP 2015 International Workshops, V. Murino, M. Cristani, E. Puppo, C. Sansone, D. Sona, Genoa (IT), 7-8 September 2015, 401-408

- [57] J. Pará k, A. Dan Tarniceriu, P. Renevey, M. Bertschi, R. Delgado-Gonzalo, I. Korhonen, "Evaluation of the Beat-to-Beat Detection Accuracy of PulseOn Wearable Optical Heart Rate Monitor", 37th Annual International Conference of the IEEE Engineering in Medicine and Biology Society (EMBC'15), Milano (IT), 25-29 August 2015, 8099-8102
- [58] B. Paviet-Salomon, A. Tomasi, S. De Wolf, M. Despeisse, D. Lachenal, C. Ballif, "Analysis and mitigation of Jsc losses in back-contacted silicon heterojunction solar cells", 5th International Conference on Crystalline Silicon Photovoltaics (SiliconPV 2015) and 5th nPV workshop, Konstanz (DE), 22-27 March 2015
- [59] L.-E. Perret-Aebi, "Integrated Design, Architecture and Sustainability", IDEAS Seminar, Lausanne (CH), 02 February 2015
- [60] L.-E. Perret-Aebi, "When PV modules are becoming real building elements : White solar module, a revolution for BIPV", EU PVTP Conference "Energy Efficiency and BIPV: Where sustainability meets aesthetics", London (GB), 8 July 2015
- [61] L.-E. Perret-Aebi, J. Escarré, H.-Y. Li, L. Sansonnens, F. Galliano, G. Cattaneo, P. Heinstein, S. Nicolay J. Bailat, S. Eberhard, C. Ballif, "When PV modules are becoming real building elements: White solar module, a revolution for BIPV", EUPVSEC 2015, Hamburg (DE), 14-18 September 2015
- [62] C. Piguet, M. Pons, D. Séverac, "Sub-Threshold Design and Architectural Choices", IEEE Computer Society Annual Symposium on VLSI, Montpellier (FR), 8-10 July 2015
- [63] B. Planck, C. Hanneschlaeger, V. Revol, J. Kastner, "Characterisation of anisotropic fibre orientation in composites by means of X-ray grating interferometry computed tomography", 30. Symposium on Verbundwerkstoffe und Verksstoffeverbund, Wien (AU), July 2015
- [64] M. Pons, T.-C. Le, C. Arm, D. Séverac, S. Emery, C. Piguet, "A 1kb single-side read 6T sub-threshold SRAM in 180 nm with 530 Hz frequency 3.1 nA total current and 2.4 nA leakage at 0.27 V", SOI-3D-Subthreshold Microelectronics Technology Unified Conference - S3S, Rohnert Park (US), 5-8 October 2015, 213-214
- [65] M. Pons, T.-C. Le, C. Arm, D. Séverac, S. Emery, C. Piguet, "A 10 kgates sub-threshold stream cipher in 180 nm with 6.1 kHz frequency 70 nA total current and 46 nA leakage at 0.33 V", SOI-3D-Subthreshold Microelectronics Technology Unified Conference - S3S, Rohnert Park (US), 5-8 October 2015, 244-245
- [66] E. Portuondo-Campa, G. Buchs, S. Kundermann, S. Lecomte, "Ultra-low phase noise microwave generation from a diode-pumped solid-state laser", European Frequency and Time Forum (EFTF) and Frequency Control Symposium (FCS), Denver (US), April 2015
- [67] E. Portuondo-Campa, J. Bènnes, S. Kundermann, S. Lecomte, "Dual frequency comb interferometer for fast and high resolution optical spectroscopy", CLEO Europe 2015, Munich (DE), June 2015
- [68] M. Proençā, F. Braun, M. Rapin, J. Solà, M. Lemay, J.-P. Thiran, "Non-invasive pulmonary artery pressure monitoring: a pulse wave velocity approach", 2015 Annual Meeting of the Swiss Society of Biomedical Engineering (SSBE), Neuchâtel (CH), August 2015
- [69] M. Proençā, F. Braun, M. Rapin, J. Solà, M. Lemay, J.-P. Thiran, "Feasibility of EIT-based pulmonary arterial pressure monitoring", EIT2015, Neuchâtel (CH), June 2015, 108
- [70] M. Rapin, M. Proençā, F. Baun, J. Solà, O. Chételat, "Cooperative sensors: a new approach towards wearable EIT systems", EIT 2015, Neuchâtel (CH), 2-5 June 2015
- [71] M. Rapin, J. Wacker, O. Chételat, "Cooperative sensors: a new wired body-sensor-network approach for wearable biopotential measurement", MobiHealth 2015, London (UK), 14-16 October 2015
- [72] N. Rebeaud, J. Rochat, J. Hiller, V. Fakhfouri, R. Ambigapathy, J. Levrat, M. Despeisse, "A novel approach to contact busbarless, IBC and MWT solar cells", SNEC PV Power expo, Shanghai (CN), April 2015
- [73] L. Rossini, E. Onillon, A. Boletis, S. Mingard, R. Wawrzaszek, J. Serin, C. Ortega, "Development and Closed-loop Experimental Results of a Reaction Sphere Elegant Breadboard", 16th European Space Mechanisms and Tribology Symposium, Bilbao (SP), 23–25 September

- [74] R. Smajda, G. Voirin, G. Andreatta, S. Ramjlak, R. Frisvold, A. Pfützner, M. Liley,
"Interference Test Results for an Osmotic Pressure Sensor for Interstitial Glucose Assessment ",
Dianetes Technology Society Bethesda ML (US),
October 2015
- [75] P. Spanoudakis, P. Schwab, L. Kiener, H. Saudan, G. Perruchoud,
"Development challenges of utilizing a Corner Cube mechanism design with successful IASI flight heritage for the Infrared Sounder (IRS) on MTG",
16th ESMATS 2015, L. Ouwehand, Bilbao (ES),
23-25 September 2015
- [76] Y. Stauffer, L. von Allmen, E. Onillon, S. Arberet, E. Olivero, D. Lindelof,
"Model Predictive Control Based Air Handling Unit Control Algorithm", CISBAT, Lausanne (CH),
9-11 September 2015
- [77] I. Texier, S. Xydis, D. Soudris, P. Marcoux, P. Pham, M. Muller, M. Correvon, G. Dudnik, G. Voirin, J. Kristenssen, M. Laurenza, A. Raptopoulos, C. Saxby, T. Navarro, F. Di Francesco, P. Salvo, M. Romanelli, L. Lymberopoulos,
"SWAN-iCare project: Towards smart wearable and autonomous negative pressure device for wound monitoring and therapy", 2014 EAI 4th International Conference on Wireless Mobile Communication and Healthcare (Mobihealth), Athens (GR),
3-5 November 2014
- [78] N. Vuković, J. Radovanović, V. Milanović, D. L. Boiko,
"The Role of Carrier Diffusion in RNGH Instabilities of Quantum Cascade Lasers ", CLEO/Europe-EQEC 2015, Munich (DE), 21-25 June 2015, ef-p.10-thu
- [79] J. Wacker, O. Chételat, M. Rapin, C. Meier, J.-A. Porchet, Y. L. Chang, B. K. Pierscionek, R. Kayyali, S. Elnabhani, N. Philip,
"Electrical and Mechanical Design of a Vest Measuring a Large Set of Physiological Signals", 4th International Conference on Wireless Mobile Communication and Healthcare - "Transforming healthcare through innovations in mobile and wireless technologies" - MobiHealth, Athens (GR), 3-5 November 2014
- [80] X. Zeng, L. Sulmoni, N. Grandjean, D. L. Boiko, "Solitary Pulse-on-Demand Production by Optical Injection Locking of Passively Q-Switched InGaN Laser Diode ", CLEO/Europe-EQEC 2015, Munich (DE), 21-25 June 2015, cb-8.1-thu

Conferences and Workshops

- P.-J. Alet,
"Smart Grid Integration of Photovoltaics", Smartgrids for a Competitive Europe, Brussels (BE),
29 April 2015
- P.-J. Alet, L. Bally, E. Olivero, F. Schmidhalter, C. S. Ellefsen, L.-E. Perret-Aebi, A. Hutter, C. Ballif, "Low-voltage grid assessment for demand-response systems", 2015 SCCER-FURIES Annual Conference, Lausanne (CH), 25 November 2015
- P.-J. Alet, F. Baccaro, M. De Felice, V. Efthymiou, C. Mayr, G. Graditi, M. Juel, D. Moser, M. Petitta, S. Tselepis, G. Yang, "Challenges, quantification and outlook of PV integration in the power system: a review by the European PV Technology Platform", 5th Solar Integration Workshop, Brussels (BE), 19-20 October 2015
- G. Andreatta, R. Smajda, S. Angeloni, S. Ramjlak, R. Frisvold, A. Pfützner, M. Liley, "Optimization of Core Sensor Components for an Osmotic Pressure Sensor for Interstitial Glucose Assessment ", Diabetes Technology Meeting, Bethesda, Maryland (US), 22-24 October 2015

- S. Angeloni,
"Intelligent insert as scaffolds for functional biological barrier models on a biomimetic scale", EUSAAT 2015, Linz (AT), 20-23 September 2015
- D. Bayat, I. Kjelberg, G. Spinola Durante, D. Schmid, "Investigation of ion interactions and space charge effects in a time of flight ion trap resonator", Comsol Conference, Grenoble (FR), 14-16 October 2015
- N. Blondiaux, G. Andreatta, R. Pugin, E. Scolan, "Manufacturing of Functional Nanostructured Polymer and Hybrid Components", PRN 2015, Copenhagen (DK), 18-19 May 2015
- G. Buchs, "Engineering of the Electronic and Opto-Electronic Properties of Carbon Nanotubes via Artificially induced Defects and Electrostatic Doping", DIPC Physics Seminars, San Sebastian (ES), 2 June 2015
- S. Cattaneo, D. Müller, "SMART-NANO: Sensitive measurement, detection and identification of engineered nanoparticles in complex matrices", i-net Technology Event "Innovation Landscape Nano", Muttenz (CH), 9 September 2015

- M. Dadras, O. Sereda, S. Biselli, L. Boulat, R. Viennois, N. Fréty,
"Development of Diffusion Barrier for Thermoelectric Material ", CMI DAY, Lausanne (CH), 5 May 2015
- M. Despeisse, *et al.*,
"Silicon Heterojunction: status on technology developments in Neuchâtel", n-PV workshop, Konstanz (CH), March 2015
- M. Despont,
"MEMS, Enabler in Product Innovation", Semiconductor EMEA Leadership Council meeting, Amsterdam (NL), 24 March 2015
- L. A. Dunbar, B. Timotijevic, L. Duchêne, R. Eckert, Ross P. Stanley,
"Plasmonic structures for infrared wavelength applications", Frontiers in Nanophotonics, Monte Verità, Ascona (CH), 30 August – 4 September 2015
- L. A. Dunbar,
"Miniaturized Enhanced Sensing Systems", 42nd Freiburg Infrared Colloquium, Freiburg (DE), 3-4 March 2015
- A. Faes, N. Badel, M. Despeisse, C. Ballif,
"Screen-printing for High Efficiency Solar Cells", Asada Workshop, Stiges (ES), 30.09-01.10 September 2015
- A. Faes, N. Badel, M. Despeisse, C. Ballif,
"Solar Cells with Diverse Metallization Schemes Enabled by SmartWire Connection Technology for Module Integration", EUPVSEC 2015, Hamburg (DE), 13-18 September 2015
- A. Faes, N. Badel, M. Despeisse, C. Ballif,
"Ultra-Fine Screen and Stencil-Printed Line for Silicon Solar Cells", EUPVSEC 2015, Hamburg (DE), 13-18 September 2015
- A. Faes, M. Despeisse, J. Levrat, J. Champiaud, A. Lachowicz, N. Badel, H. Watanabe, K. Söderström, Y. Yao, J. Ufheil, P. Papet, B. Strahm, J. Hermans, A. Tomasi, Y. Baumgartner, J. Cattin, M. Kiaee, A. Hessler-Wyser, *et al.*,
"Diverse Metallization Schemes Enabled by SmartWire Connection Technology", EUPVSEC 2015, Hamburg (DE), 14-18 September 2015
- M. Höchemer,
"CresaCheck-Tileye: Self Learning Algorithms", Credimex Tech Days, Alpnach Dorf (CH), 28-29 October 2015
- R. Jose James, G. Spinola Durante, C. Bosshard, S. Mohrdiek,
"Micropackaging of long-term implantable Active Medical Devices", IMAPS - 2nd Advanced Tech. Workshop on Microelectronics, Systems and Packaging for Medical Devices, Lyon (FR), 10-12 December 2014
- J. Kaufmann,
"Using industrial ps-pulsed laser for micro-machining", Posalux Symposium on Glass Micro Machining, Biel (CH), 23 November 2015
- H. F. Knapp,
"CSEM, a regional and national catalyst", Swiss BiotechTM Innovation Day 2015, Zug (CH), 19 August 2015
- G. Kotrotsios,
"International R&D as an enabler of disruptive innovation", Swiss-Korean Technology Cooperation Seminar Organised by the Embassy of Switzerland in the Republic of Korea, Korea Institute for Advancement of Technology (KIAT), Seoul (KR), 20 May 2015
- G. Kotrotsios,
"Développer de nouveaux modèles pour stimuler le secteur de la santé ", Journée de l'Innovation et des PME 2015 – Health Valley, Lausanne (CH), 22 May 2015
- G. Kotrotsios,
"In Katalysatoren der Gesundheitsregion", Erster Plattform Gesundheit der Hauptstadtreion Schweiz, Fribourg (CH), 17 November 2015
- J. B. La Cour, D. Migliorelli, S. Prill, S. Generelli, L. Barbe, C. Duschl, O. Guenat,
"Electrochemical sensors for hepatotoxic assessment in a modular microfluidic system", Hemibio Symposium, Leuven (BE), 2-3 December 2015
- S. Lani, D. Bayat, M. Despont,
"2D tilting MEMS micro mirror integrating a piezoresistive sensor position feedback", Photonics West 2015, San Francisco (US), 8 February 2015
- H.-Y. Li, L.-E. Perret-Aebi, Y. Luo, C. Ballif ,
"Fast and Non-Destructive Detection on the EVA Gel Content in Photovoltaic Modules by Optical Reflection", EUPVSEC 2015, Hamburg (DE), 14-18 September 2015
- L. Lombardo, N. Tschnarner, D. Migliorelli, D. Caminada, N. Donato, S. Generelli,
"Development of a Wearable Electronic Interface for Electrochemical Sensors", International workshop on Micro-Nano-Bio-ICT Covergence, Otranto (IT), 13-15 July 2015
- D. Migliorelli, S. Paoletti, S. Generelli, N. Glaser, D. Caminada,
"Sensor System for Saliva Monitoring", 9th European Congress on Tropical Medicine and International Health , Basel (CH), 6-10 September 2015
- S.-J. Moon, L. Löfgren, D. Sacchetto, M. Benkhaira, J. Bailat, S. Nicolay, C. Ballif,
"Organometallic Halide Perovskite Solar Modules by Laser Patterning Technology", EUPVSEC 2015, Hamburg (DE), September 2015
- T. Morf, U. Drechsler, L. Kull, D. Corcos, D. Elad, N. Kaminski, U. Pfeiffer, H. Keller, J. Grzyb, A. Bischof, J. Farserotu, *et al.*,
"Room Temperature THz Camera in micro machined CMOS", German THz Conference 215, Dresden (DE), June 8-10, 2015

V. Musolino, P.-J. Alet, L.-E. Perret-Aebi, C. Ballif,
 "Characterising the accuracy of measurements by PV micro-inverters", EUPVSEC 2015, Hamburg (DE),
 13-18 September 2015

B. Paviet-Salomon, A. Tomasi, D. Lachenal,
 A. Descouedres, L. Barraud, G. Christmann, N. Badel,
 S. Nicolay, M. Despeisse, S. De Wolf, B. Strahm, C. Ballif,
 "Development of photolithography-free, large-area, back-contacted silicon heterojunction solar cells", IBC Workshop Freiburg, Freiburg-im-Breisgau (DE), 4-5 November 2015

L.-E. Perre-Aebi, F. Galliano, F. Sculati-Meillaud,
 E. Annigoni, H.-Y. Li, M. Jankovec, C. Ballif,
 "In-situ monitoring of moisture ingress in PV modules", SPIE Optics 2015, San Diego (US), 9-13 August 2015

L.-E. Perret-Aebi, J. Escarré, H.-Y. Li, L. Sansonnens,
 F. Galliano, G. Cattaneo, P. Heinstein, S. Nicolay, J. Bailat,
 S. Eberhard, C. Ballif,
 "When PV modules are becoming real building elements: White solar module, a revolution for BIPV", SPIE Optics 2015, San Diego (US), 9-13 August 2015

J.-W. Schüttauf, E. Moulin, D. Dominé, J. Bailat, F. Meillaud,
 F.-J. Haug, C. Ballif,
 "Triple- and quadruple-junction thin-film silicon solar cells", ICANS26, Aachen (DE), 13-18 September 2015

E. Scolan, A. Bionaz, A. Grivel, N. Blondiaux, R. Pugin,
 D. Szabo, S. Grimm, M. Schneebeli,
 "Design of Icephobic coatings", SGO Annual Review, Colombes (FR), 1-3 July 2015

R. Stanley,
 "Tunable optical gas sensors using MEMS devices", Optical Gas Sensing Workshop, Dübendorf (DE), 15 January 2015

A. Steinecker,
 "Bio-Compatible Microsystem Packaging of VCSEL Laser for Implantable Devices", IVAM Forum at COMPAMED fair "Laser & Photonics Applications", Düsseldorf (DE), 12 November 2014

A. Steinecker,
 "Process Monitoring and Control in Lab Automation", labotec 2015, Lausanne (CH), 6 May 2015

A. Steinecker,
 "Integration of Electronic Devices into Textiles", EPoSS Annual Forum 2015, Leuven (BE), 13 October 2015

A. Steinecker, P. Schmid,
 "Monitoring vital signs with implantable pressure sensors", COMPAMED High-tech Forum by IVAM, Düsseldorf (DE), 17 November 2015

M. Tormen, B. Timotijevic, Y. Pétremand, M. Lützelschwab, D. Bayat, Y. Jacquat, L. Aebi,
 "MEMS acceleration sensor with remote optical readout for continuous power generator monitoring", ISOT 2015, Neuchâtel (CH), 14-16 October 2015

G. Weder, J. Cottet, R. Ischer, L. Le Reste, M. Favre, C. Martin Olmos, H. Heinzelmann, M. Liley,
 "Mechanical profiling of biopsies by parallel AFM for rapid sensing of cancer", 21st Congress of the European Society of Biomechanics, Prague (CZ), 5 July 2015

G. Weder, R. Ischer, L. Le Reste, M. Favre, M. Liley, P. Albert,
 "DEMOX a miniature optical oxygen sensor", BioInnovation Day, Lausanne (CH), 23 June 2015

G. Weder, B. Wenger, R. Ischer, L. Le Reste, M. Favre, R. Smajda, C. Martin Olmos, M. Liley, P. Albert,
 "DEMOX: a miniature optical oxygen sensor", MEMS Executive Congress Europe, Copenhagen (DK), 9 March 2015

G. Weder, J. Cottet, M. Favre, R. Ischer, L. Le Reste, M. Liley, H. Heinzelmann,
 "Demonstration of parallel AFM read-out for rapid sensing of cancer", Nano-Tera annual meeting, Bern (CH), 4-5 May 2015

G. Weder, J. Cottet, M. Favre, R. Ischer, L. Le Reste, M. Liley, H. Heinzelmann,
 "Parallel AFM read-out for rapid sensing of cancer ", Swiss Nano Convention , Neuchâtel (CH), 27-28 May 2015

F. Zanella, J. Schleuniger, N. Marjanović, G. Nisato, J. Pallares, F. Vila, J. Carrabina, R. Ferrini,
 "Design kit toolset development for gravure printed organic thin-film transistors", 7th International Exhibition and Conference for the Printed Electronics Industry - LOPEC, München (DE), 3-5 March 2015

Research Projects

3R Research Foundation Switzerland	EndothelialChip – An in-vitro microvascular model of the endothelial barrier
Canton de Neuchâtel	NECAN – Développement de solutions PV pour le bâtiment
CCEM – Electricity	CONNECT-PV – Conductive transparent electrodes: a competence cluster for highly efficient thin film photovoltaics
CCEM – Mobility	DURACAT – Highly durable oxide-based catalysts for polymer electrolyte fuel cells

CCMX-NMMC – Analytical Platform	FANOSENSE – Ultrasensitive sensing transducer based on Fano interferences in plasmonic metamaterials
CCMX-NMMC – Analytical Platform	GANTRY – Gantry-based X-ray phase contrast scanner for microCT application
CCMX-NMMC – Analytical Platform	OMNY – Tomography nano cryo stage
Eurostars	ALBIREO – Low-power impulse-radio ultra-wideband module for remote control and keyless access
Eurostars	HICOLA – Highly coherent laser for coherent communication and sensing
Eurostars	LAMMIC – Production of laminin-521™ coated microcarriers for stem cell expansion
Eurostars	MTGA – Modular trace gas analyzer (MTGA) consisting of MEMS grating tuned infrared laser module for enhanced photo-acoustic spectroscopy
Eurostars	ORCA – Development of ultra-stable high-finesse cavity
Eurostars	REMIQUA – Scalable and reconfigurable systems for microassembly and quality inspection
Eurostars	SENSMOTION – Patch-like sensor system for skeletal muscle and motion monitoring
Fondation Suisse pour les Téléthèses	LISOMAD – Pour des services et des produits favorisant l'autonomie et les possibilités de maintien à domicile des personnes âgées
Foundation The Ark	PREDMAINT II – Maintenance predictive pour des installations hydroélectriques
Hasler Fondation	EYEWALK – Mobile ultra-light vision system for the handicapped
InterReg	PIMENT – Plastique injection micro et nano technologie
InterReg	RHIN-SOLAR – Aufbau eines Exzellenzclusters für organische Solarzelle Region Oberrhein, inkl. Herstellung von Demonstratoren
Ligue Pulmonaire Suisse	OxySmart – Validation of portable SpO2 sensor by reflective means
Nano-Tera	3D-SENSTEX – 3D Large scale Integration of sensors into smart textile
Nano-Tera	BREATHE – High throughput transducers to measure in-vitro muscle contraction
Nano-Tera	FLUSITEX – Developing a wound dressing with an integrated sensing layer for non-invasive wound monitoring using fluorescence lifetime detection
Nano-Tera	HEARRESTORE – Image-guided micro surgery for hearing aid implantation
Nano-Tera	ICYSOC – Inexact sub-near-threshold systems for ultra-low power devices
Nano-Tera	MINIHOLTER – Photoplethysmography-based ambulatory heart rate monitor device embedded into a smart watch
Nano-Tera	NAMBП – Night ambulatory monitoring of blood pressure
Nano-Tera	NEWBORNCARE – Reducing the false alarms of neonate vital sign monitoring via a computer vision-based approach to accurately measure heart and respiratory rates in a contactless way
Nano-Tera	OBESENSE – Monitoring the consequences of obesity
Nano-Tera	PARATEX – Novel smart textile to non-invasively monitor pressure, oxygenation and perfusion of tissue to prevent pressure ulcers in paraplegics
Nano-Tera	PATLiSci II – Developing rapid diagnostic tools for cancer, using highly parallelized mechanical sensors to investigate biopsy samples efficiently
Nano-Tera	SHINE – Solar to hydrogen integrated nano-electrolysis

Nano-Tera	SPINERPAIR – Hybrid CMOS-polymer neural interfaces for restoration of sensorimotor function after spinal cord injury
Nano-Tera	SYNERGY – Realizing photovoltaic energy harvesting systems based on tandem solar cells with efficiency beyond that achievable with state-of-the-art industrial single-junction cells
Nano-Tera	WISESKIN – Wise Skin for tactile prosthetics
NCCR-Nanoscale Science	NCCR-VI – Applied projects in nanoscience and nanotechnology (Module 6)
SNI – Argovia Program	ELE-NA – Silica nanoparticles coloured electronic ink (e-ink)
SNI – Argovia Program	NanoSiCTrenchFet – Physical studies of SiC nano-trench-MOSFETs
SNSF	Novel generation perovskite devices
SNSF	PV2015 – Photovoltaics into the built environment: from semi-transparent PV glazing to high efficiency roof integrated solutions
SNSF	ACTIVE INTERFACES – Holistic strategy to simplify standards, assessments and certifications for building integrated photovoltaics
SNSF	FASTIQ – Ultrafast infrared emitter on a quantum cascade
SNSF	HEMODYNAMEIT – Subject-adapted 3D dynamic bio-impedance models: application to blood pressure monitoring
SNSF	NOVIPIX – Novel integrated pixel X-ray detectors
SNSF	RB-GAN2 – Establish a concept and demonstrate novel active atomic clock based on mode-locked semiconductor laser with alkali vapor cell saturate absorber
SNSF	RB-GANX – Active atomic clock based on mode-locked laser with atomic vapor cell absorber
Swiss Space Center	E-GRIP – Einstein gravitational red-shift probe (E-GRIP) mission study

Swiss Commission for Technology and Innovation (CTI)

18101.1 PFNM-NM	3D NANOMET	Surface micro-nanostructuring of metallic surfaces for improved tribological performances
16025.1 PFIW-IW	APPROBATE	Automatisierte approbierte Qualität für manuelle Montage von kleinen Stückzahlen auf der Basis von selbstlernenden Bildverarbeitungsalgorithmen zur Arbeitsschrittkontrolle
17486.1 PFNM-NM	ATIPS	Advanced aircraft tire pressure sensing
13865.2 PFNM-NM	aTORCH	Active optical resonator chip – Innovative concepts for next generation high sensitivity label-free bio-sensors
16901.1 INNO-13-16-LS	CELLECTRIC	Enable bioimpedance sensing within UCUP perfusion bioreactor culture device
17623.1 PFNM-NM	CNT-SENSE	Surface enhanced Raman scattering sensor for airborne carbon nanotubes in workplaces
15971.1 PFNM-NM	COMSTEER	Compact beam steering unit
16372.1 PFIW-IW	COTTON	Development of sorting systems with self learning algorithm and optical detection systems for foreign materials in cotton flakes
16692.2 PFIW-IW	CUMAPRO	Massenproduktion von kundenspezifischen PV-Modulen für die Gebäudeintegration, Customised Mass Production
17507.1 PFEN-NM	DAYGLAZING	Daylight and heat management foil for high quality illumination in buildings

17266.2 PFIW-IW	DEFIA	Development of novel electrode foil solution for solar cells interconnected with smartwire connection technology applied in the glass-glass module configuration
14954.1 PFNM-NM	DELIGHT	Development of energy-efficient lighting technology based on organic solid-state light sources
15416.1 PFES-ES	DENEBO2	Development of integrated IR-UWB technology for secure distance measurement
15558.1 INNO-13-16-IW	DIAMONDWIRE-PRE	Drahtbeschichtung mit Mikro-Diamanten
17324.1 PFLS-LS	DRDO	Device to reliably detect ovulation
17490.1 PFIW-IW	DSC-FAB	Production technology of durable dye-sensitive glass-modules for building integrated photovoltaic power generation
17708.1 PFNM-NM	ELECTROLUMINATI	Electro-illumination of dive watches through mechanical power generation
17288.1 PFNM-NM	FELCOLAP	Fabric-based electrodes for large-area commercial OLED-based products for lighting applications
13822.2 PFNM-NM	FILMS4GLAZING	Seasonal heat management films – passive smart glazings
16689.1 PFEN-IW	FLEXBAT	Process evaluation and implementation for production of flexible batteries
17246.1 PFIW-IW	FLEXHEAT	Stretchable heating element based on printed conductors for a shape-customizable feature in novel pointing devices
13485.1 PFFLE-NM	FLEXLAM-COMPLEMENT	Improve cost & quality for manufacturing flexible LCD display by simpler handling of sheets and process robustness
16862.2 PFNM-NM	HIFLOW	High sensitivity flow sensor for extended flow range
18099.1 PFNM-NM	HIPERSTEER	High performance beam steering unit
10894.1 PFNM-NM	ICYAMR 2	Development of an automatic meter reader (AMR) for retrofit applications on existing meters
17142.2 PFEN-NM	IOTLOC	Development of a network for advanced low power localization using LoRa technology
15532-1 PFNM-NM	LARS	System zur Überwachung der Webzone auf Webmaschinen
16188.1 PFNM-NM	LASGRAT	High contrast gratings in vertical external cavity surface emitting lasers for gas sensing
18062.1 PFIW-IW	LETOP	Feasability study: Lever topologies for load cell
17508.1 PFNM-NM	LICOFO	Large-area light collecting foils for solar light concentration in photovoltaic devices
16871.1 PFNM-NM	LIDTDOS	LIDT und Degradations Prüftechnik für industrielle Anwendungen
16044.2 PFNM-NM	LORNOFOX	A high performance time bounded fire hydrant network
15862.1 PFNM-NM	MEASOS2	Measurement system for mechanical watch oscillator (next generation)
16711.1 PFNM-NM	MICRO-FAS	Integrated fiber optics acceleration sensor
17728.1 INNO-16-NM	Microgravity test	Testing and validation of miniaturized fluid handling system for microgravity research

16373.1 PFIW-IW	MIRROR	Development of a new PECVD reactor for efficient production of high-quality silicon heterojunction solar cells
13482.1 PFFLI-NM	MULTISENSE PHASE 2	Design of a high-speed, high-precision miniaturized mechano-optical touch-trigger probe for use on 3D coordinate measuring machines
18088.1 PFNM-NM	NANOWHITE	Process development and reliability of white solar module for BIPV
159541.1 PFEN/IW	NCOOL2	novel HVAC
17372.2 PFNM-NM	NOVACAMERA	An infrared multispectral camera for gas detection and quantification
17896.1 PFIW-IW	OILGUARD	Oil in water monitoring
1618.1 PFNM-NM	PASS	Particles free sealing system
16049.1 PFNM-NM	PICOFAB	Fabrikation von Komponenten für die Präzisionsmechanik mit Picosekunden-Ultrakurzpulslasern
16111.1 PFNM-NM	PIFPAF	Pipetting system with flowsensor and microelement for passive flow control
17625.1 PFNM-NM	POMICLED	Powerful micronic light emitting diode for next generation micro-projectors
17244.1 PFLS-LS	POSBONE	Compact and flexible system for total knee replacement surgery
17705.1 PFNM-NM	PUNCH	Production-ready, next generation back-contacted silicon heterojunction solar cells and modules
11290.1 PFNM-NM	QUADLINE	A novel micro mark register head camera based on ultra-high-speed multi-linear image sensor
16108.1 PFNM-NM	SAIGA	Small antenna integrated in hearing aids
14782.1 PFLS-LS	SARENAPATCH	Micro patch portable pour l'injection en continu d'insuline
16584.1 PFEN-IW	SILVERLINE	Next generation production processes and quality controls for watch batteries
15826.1 PFIW-IW	SMARTWIRE	Development of multi-wire module design technology and production equipment
16050.2-PFNM-NM	SPINBEAT-II	Leistungsmessgerät mit integrierter Trittanalyse und Effizienzfeedback für Radfahrer
12628.1 PFIW-IW	SST	Single shell tunneling
16694.2 PFIW-IW	STABILITY	Dynamische Lageregelung für Hydraulikmodule demonstriert an einem Stelzentrator im Rebberg
15708.2 PFNM-NM	SUBGRATPOL	Magical watch dial
16853.1 PFNM-NM	SUNTRACKER	An accurate sun sensor for earth geographical north detection
17518.1 PFEN-NM	SUPERTC	SuPeRTC, a super high performance temperature compensated miniature real time clock module
12215 PFNM-NM	SWARM	Smart water resource active management
1799.1 PFNM-NM	SWW	OEM module and new algorithms (speed, sleep)
16637.2 PFNM-NM	TACOS	Development and integration of alternative transparent conductive oxides for silicon heterojunction solar cells
16185.1 PFNM-NM	VALIPLATE	Calorimetric tool for validating the liquid volume dispensed by liquid handling instruments

18091.1 PFEN-NM	WISEROCK	Low-cost WSN with GNSS capability for long-term landslide monitoring
17170.1 INNO-13-16-NM	WISEROCK-PRE2	Ultra-Low Power Felsüberwachung

European Commission Projects

FP7 – ICT	ACTION	Active Implant for optoacoustic natural sound enhancement
FP7 – TRANSPORT	AGEN	Atomic gyroscope for enhanced navigation
FP7 – NMP	AMBASSADOR	Autonomous management system developed for building and district
FP7 – ICT	ARROWS_COMPLEMENT	Advanced interfaced micro-systems research for analysis of real-world clinical, food, environmental and waste samples
FP7 – ICT	BIOFOS	Microring resonator-based biophotonic platform for food analysis
FP7 – SECURITY	BONAS	Bomb factory detection by networks of advanced sensors
FP7 – ICT	D-LIVER	Monitoring of patients with liver diseases
FP7 – SPACE	ELSA	European levitated spherical actuator
FP7 – SECURITY	ESPONDER	A holistic approach towards the development of the first responder of the future
FP7 – TRANSPORT	EVITA	Non-destructive evaluation, inspection and testing of primary aeronautical composite structures using phase contrast X-ray imaging
FP7 – ICT	FLEXNET-COMPLEMENT	Network of excellence for building up knowledge for improved systems integration for flexible organic and large area electronics (FOLAE) and its exploitation (FLEXNET)
FP7 – ICT	FLEX-O-FAB	Pilot-scale hybrid roll to roll/sheet to sheet manufacturing chain for flexible OLEDs
FP7 – ICT	FLEXTILES	Self adaptive heterogeneous manycore based on flexible tiles
FP7 – JTI	FLITE-WISE	Wireless sensor nodes for continuous flight test measurements
H2020 – MG 2014	FUTURESKY	Smart, Green and Integrated Transport
H2020 – ICT 2014	GATEONE	Innovation Service for European Smartization by SMEs
FP7 – ICT	GO4TIME	Global, flexible, on-demand and resourceful timing IC & MEMS encapsulated system
FP7 – ICT	GO4TIME-COMPLEMENT	Global, flexible, on-demand and resourceful timing IC & MEMS encapsulated system
FP7 – ICT	HEARTCYCLE-COMPLEMENT	Compliance and effectiveness in HF and CHD closed-loop management
FP7 – HEALTH	HEMIBIO	Hepatic microfluidic bioreactor
FP7 – ENERGY	HERCULES	High efficiency rear contact solar cells and ultra-powerful modules
SP1 – JTI – CleanSky	ICEAGE	Ice phobic coating associated to low power electromechanical deicers
FP7 – NMP	IMPRESS-COMPLEMENT	Flexible compression injection moulding platform for multi-scale surface structures
FP7 – SECURITY	INGRESS	Innovative technology for fingerprint live scanners
FP7 – NMP	INNOVABONE	Novel biomimetic strategy for bone regeneration

H2020 – SC5 2014	INREP	Materials for electronic devices
FP7 – ENVIRONMENT	INTASENSE	Integrated air quality sensor for energy efficient environment control
FP7 – ICT	LASSIE-FP7	Large area solid state intelligent efficient luminaires
H2020 – MG 2014	LYNCEUS2MARKET	Safer and more efficient waterborne operations through new technologies and smarter traffic management
H2020 – ICT 2014	M3TERA	Micromachined terahertz systems -a new heterogeneous integration platform enabling the commercialization of the THz frequency spectrum
H2020 – ICT 2014	MEDILIGHT	Miniaturized smart system for light stimulation and monitoring of wound healin
FP7 – NMP	MEGAROB	Development of flexible, sustainable and automated platform for high accuracy manufacturing operations in medium and large complex components using spherical robot and laser tracker on overhead crane
FP7 – NMP	NANODIARA-COMPLEMENT	Development of novel nanotechnology based diagnostic systems for rheumatoid arthritis and osteoarthritis
FP6 – NMP	NANOSECURE-COMPLEMENT	Advanced nanotechnological detection and detoxification of harmful airborne substances for improved public security
FP7 – ICT	NEPHRON	Wearable artificial kidney and personal renal care system
FP7 – SME	ORION	Organic waste management by a small-scale innovative automated system of anaerobic digestion
FP7 – ICT	PASTA	Integrating platform for advanced smart textile applications
FP7 – ICT	PEGASO	Personalised guidance services for optimising lifestyle management in teen-agers through awareness, motivation and engagement
FP7 – SPACE	PHASER	High speed, high frequency electro-photonic ADC for space enabled routers
FP7 – ICT	PLAISIR-COMPLEMENT	Plasmonic sensing in the infrared
FP7 – NMP	PLIANT	Process line implementation for applied surface nanotechnologies
FP7 – ICT	POSITIVE-COMPLEMENT	A highly integrated and sensitive porous silicon based lab on a chip for multiple quantitative monitoring of food allergies at point of care
FP7 – NMP	PRIME	Plug and produce intelligent multi agent environment based on standard technology
FP7 – KBBE	RADAR	Rationally designed aquatic receptors integrated in label-free biosensor platforms for remote surveillance of toxins and pollutants
H2020 – ICT 2014	RAWFIE	Road-, Air- and Water-based Future Internet Experimentation
FP7 – ENVIRONMENT	RECONCILE-COMPLEMENT	Reconciliation of essential process parameters for an enhanced predictability of arctic stratospheric ozone loss and its climate interactions
FP7 – SPACE	REMOVE-DEBRIS	A low cost active debris removal demonstration mission
FP7 – SP1 – JTI	RESACC	Development of a readout circuit for a resonant accelerometer
FP7-SECURITY	SAVE-MED	Tackling counterfeit medicines and related criminal networks
FP7 – NMP	SELFMEM-COMPLEMENT	Self-assembled polymer membrane

FP7 – ICT	SEMIAH	Scalable multi-criteria energy management infrastructure for aggregation of households
H2020 – ICT 2014	SMARTER-SI	Smart access to manufacturing for systems integration
FP7 – NMP	SMART-NANO	Sensitive measurement, detection, and identification of engineered nanoparticles in complex matrices
FP7 – NMP	SMARTRONICS	Development of smart machines, tools and processes for the precision synthesis of nanomaterials with tailored properties for organic electronics
FP7 – SECURITY	SNIFFER	Sensory devices network for food supply chain security
FP7 – SPACE	SOC-2	Towards neutral-atom space optical clocks: Development of high-performance transportable and breadboard optical clocks and advanced subsystems
FP7 – ICT	SPLENDID	Personalized guide for eating and activity behavior for the prevention of obesity and eating disorders
FP7 – ENVIRONMENT	STRATOCLIM	Stratospheric and upper tropospheric processes for better climate predictions
FP7 – ICT	SUNFLOWER	Sustainable novel flexible organic watts efficiently reliable
FP7 – ICT	SWAN-iCare	Smart wearable and autonomous negative pressure device for wound monitoring and therapy
FP7 – ICT	TERATOP	Terahertz photonic imager on chip
FP7 – ICT	THERMINATOR-COMPLEMENT	Modeling, control and management of thermal effects in electronic circuits of the future
FP7 – NMP	TRIBUTE	Take the energy bill back to the promised building performance
FP7 – ICT	VIAMOS	Vertically integrated array-type Mirau-based OCT system for early detection of skin pathologies – Small or medium-scale focused research project (STREP)
FP7 – ICT	WELCOME	Wearable sensing and smart cloud computing for integrated care to COPD patients with comorbidities

European Space Agency (ESA), Swiss Space Office and CNES Projects

ESA Projects

ADR-QB50	Pre-study of vision based technologies for ADR proximity navigation
AMIGO	Autonomous medical monitoring and diagnostics
CCM_MTG	Development and manufacture of corner cube mechanisms for MTG satellite
CECILE	LiDAR integrating compressive sensing
CLUPI2 C D	Clupi instrument for Exomars
C-MAC	Ceramic miniature atomic clock physics package – C-MAC PP
DANOE	High-dynamic absolute nanometric optical encoder technology assessment for space
DATA_FUSION	Sensor data fusion for hazard mapping and piloting
DELIAN	Detrous lightweight arm for exploration
ENRUM	Space and energy resources utilisation mapping (EnRUM)
FGU	Micro-optoelectronic frequency generation unit (FGU)
IHMDS	Integrated vehicle health management system demonstrator

IHMSD-2	Integrated vehicle health management system demonstrator – Phase 2
JEM-EUSO	Laser pointing system
LTMS-S	Long-term medical survey system
MEMS_GC-MS	MEMS-based gas chromatograph and mass spectrometer
MEMS-QUAL	Validation and experimental verification of ESA MEMS qualification methodology
MEMS-REAL	MEMS reliability assessment
MHIPIS	Miniature high performance imaging spectrometer for remote sensing
MILA	Miniaturised imaging laser altimeter (Miniature imaging LIDAR system, Phase 1)
MILS	Miniature imaging LIDAR system for GN&C space application
MLSCL	Sub-picosecond model-locked semiconductor laser for space missions
MTS	Miniature Timing Source (mTS): miniature atomic clock, MEMS vapor cells, ASIC specifications
NIRS	NIR immersed grating in transmission for high resolution spectroscopy
NPI-CELL	PhD on fabrication of miniature atomic cells
NPI-EIT	Wearable physiological sensor network – non-invasive and non-occlusive blood pressure (BP) measurement based on Electrical Impedance Tomography (EIT)
OCOR-VACUUM	Optical correlator testbed for high resolution imaging from geostationary orbit
OEO	Ultra-low phase noise reference oscillator
SAMTWO_5	Space active maser – five
SAMTWO_6	Space active maser – six
SPHM_EQM	Industrialisation of the passive hydrogen maser for the Galileo navigation payload
STE-QUEST-A-PLUS	STE-QUEST class M ESA mission candidate: assessment study
SWIRS	New generation SWIR immersed grating (Phase1)
UWB4SAT	Ultra-wideband as a multi-purpose robust and reliable
WALES-PLUS	Wafer level encapsulation for microsystems-PLUS
WATERLENS	Water availability – Improved monitoring, forecasting and control of water availability, quality and distribution

Swiss Space Office Projects

3D-EEE	EEE components produced by additive manufacturing
HYBSAT	Hybrid lightweight and flexible circuit boards (FCBs) for satellites and space

CNES Projects

IASI-FM3PHASE 1B	IASI-FM3 Travaux préparatoires complémentaires à la réparation du mécanisme CCM
IASI-FM3REFUB	Perform refurbishment of actuator on IASI-EM at CSEM and IASI-FM3 at TAS
IASI-FM3SUP	Support for refurbishment of IASI-FM3
IASI-FM3VC	IASI-FM3 refurbishment stator procurement and manufacture

Industrial Property

Creativity

In 2015, 19 invention reports were submitted for examination.

Patent portfolio

CSEM inventions have led to 16 patent applications in 2015 (14 regular applications and 2 provisional applications). The patent portfolio has been further enhanced by the extension of different countries of 5 patent files based on prior patent applications.

Collaboration with Research Institutes and Universities

<i>University</i>	<i>Institute</i>	<i>Professor</i>	<i>Field of collaboration</i>
Aristotle University of Thessaloniki	Laboratory of Medical Informatics	N. Maglaveras	Collection of large set of physiological signals
Bern University of Applied Sciences	MSE	V. Koch	Sensory processing prosthetics
Berner Fachhochschule (BFH)	Institute for Energy and Mobility Research	A. Vezzini	BFH-CSEM Energy Storage Research Center (ESReC): electrochemical storage
Brown University	School of Engineering	A. V. Nurmikko	Integrated circuits for brain implants
Carleton University	Systems and Computer Engineering	A. Adler	Electrical impedance tomography
CEA	INES	P. Bernaud	Building energy management
CEA-LETI	Capteurs et Actionneurs	M. Le Prado	Atomic gyroscopes
CEA-LETI	Service conception pour les microtechnologies émergentes	R. Lemaire	Multicore systems-on-chips
Christian-Albrechts-Universität zu Kiel	Klinik für Anästhesiologie und Operative Intensivmedizin	I. Frerichs	Electrical impedance tomography
CHUV	Service de cardiologie	E. Pruvot	Cardiac arrhythmias
CHUV	Internal medicine	C. Sartori	Sleep analysis
CHUV	Département anesthésiologie	P. Schoettker	Blood pressure
CIRO Center of Expertise for chronic organ failure	Physical activity, exercise training & rehabilitation	M. A. Spruit	Clinical validation
Croydon Healthcare NHS Trust	Trust R&D	J. Chang	Clinical validation
EMPA	Department of advanced materials and surfaces	P. Görning	X-ray read out circuits
EMPA	Swiss federal laboratories for materials science and technology	P. Hoffmann	Solid state lighting
EMPA	Protection and Physiology	S. Lukas	Dry-electrodes in textile
EMPA	Biocatalysis group	M. Richter	Fluorescence lifetime imaging microscopy
EMPA	Medical textiles	L. Scherer	Fluorescence lifetime imaging microscopy

<i>University</i>	<i>Institute</i>	<i>Professor</i>	<i>Field of collaboration</i>
EPF Lausanne	Embedded Systems Laboratory	D. Atienza	C-Compilers for reconfigurable processors; ECG monitoring
EPF Lausanne	IMT/PVLAB	C. Ballif	Passivated contacts
EPF Lausanne	Integrated Circuit Laboratory	C. Bruschini	Microlens on vision chips
EPF Lausanne	TCL	A. Burg	Good enough circuits
EPF Lausanne	Laboratory of advanced semiconductors for photonics and electronics	N. Grandjean	Solid state lighting; GaN-based semiconductor lasers
EPF Lausanne	Instant-Lab	S. Henein	Precision mechanics
EPF Lausanne	Laboratory of Photonics and Quantum Measurements	T. J. Kippenberg	Optical microresonators and frequency combs
EPF Lausanne	Laboratory for Soft Bioelectronic Interfaces	S. Lacour	Artificial skin; restore spinal connections
EPF Lausanne	Nanophotonics and metrology laboratory	O. Martin	Development of plasmonic sensors
EPF Lausanne	Peripheral Systems Laboratory	R. Rossier	Moiré security devices
EPF Lausanne	Laboratoire de Production Microtechnique	P. Ryser	Compact 3D force sensor; Indoor air quality sensor system
EPF Lausanne	Hemodynamics and Cardiovascular Technology Laboratory	N. Stergiopoulos	Cardiac output monitoring
EPF Lausanne	Signal Processing Laboratory 2	P. Vanderghenst	Signal processing; Newborn vital signs monitoring based on multiple vision sensors
EPF Lausanne	Applied signal processing group	J.-M. Vesin	Signal processing; Newborn vital signs monitoring based on multiple vision sensors
EPF Lausanne	IMT, Galatea Laboratory	Y. Bellouard	Femtolaser micro-structuring
EPF Lausanne	Laboratoire de Technologie des Poudres	H. Hofmann	Porous films for biosensing
EPF Lausanne	Institute of Materials science and Engineering	R. Logé	New Iron based materials and characterization
EPF Lausanne	Signal Processing Laboratory 5	J.-P. Thiran	Electrical impedance tomography
EPF Neuchâtel	Institute of Microengineering	N. de Rooij	Microsystems and sensors
EPF Neuchâtel	ICLAB	C. C. Enz	Approximate arithmetic; ULP Radio and protocol for WiseSkin
EPF Neuchâtel	Institute of Microengineering	H. Shea	Microstructural characterization
ETH Zurich	Integrated Systems Laboratory	L. Benini	Sub-near-threshold multicore
ETH Zurich	Chemistry and applied biosciences	P. S. Dittrich	Microfluidics for sample preparation
ETH Zurich	Integrated Systems Laboratory - Analog and Mixed-Signal Design	Q. Huang	Analog design in advanced CMOS technology

University	Institute	Professor	Field of collaboration
ETH Zurich	Institute of robotics and intelligent systems	B. Nelson	Fluorescence lifetime imaging microscopy
ETH Zurich	Photonics laboratory	L. Novotny	Development of plasmonic antennas
ETH Zurich	Laboratory for solid state physics	H. von Känel	X-ray read out circuits
ETH Zurich	Chemistry and Applied Biosciences	A. de Mello	Nanoparticle analysis
Fraunhofer Society	Group for Automation in Medicine and Biotechnology	B. Grychtol	Electrical impedance tomography
Hochschule für Technik, Rapperswill (HSR)	Institute for solar technology (SPF)	M. Rommel	Hybrid solar thermal collector
Hôpital neuchâtelois HNE	Hôpital de Landeyeux	N. Della Ricca	Validation of biomedical sensors
INPG Institut Polytechnique Grenoble	TIMA Laboratory	M. Nicolaidis	Fault-tolerant processor cores
Kingston University London	Science, Engineering and Computing	B. Pierscionek	Collection of large set of physiological signals
National Institute of Standards and Technology (NIST)	Optical Frequency Measurements group	S. A. Diddams	Optical frequency combs and their applications
Paul Scherrer Institute (PSI)	PSI	S. Abolhassani	Study of mechanism of oxidation
Paul Scherrer Institute (PSI)	Laboratory for Micro- and Nanotechnology	J. Gobrecht	Microstructuring NanoArgovia project
SUVA Care	Clinique Romande de Réadaptation	O. Deriaz	Prevention of obesity through different monitoring methods
Technical University of Kaiserslautern	Chair of real-time systems	G. Fohler	Real-time networking
University Hospital of Bern (Inselspital)	Department ENT Surgery	M. Caversaccio	Image-guided micro surgery for hearing aid implantation
University Hospital of Bern (Inselspital)	Department of Pulmonary Disease	T. Geiser	Oxygen therapy
University Hospital of Bern (Inselspital)	Cardiovascular Department	S. F. Rimoldi	Blood pressure
University Hospital of Hamburg (UKE)	Klinik und Poliklinik für Anästhesiologie	D. Reuter	Electrical impedance tomography
University Hospital of Zurich	Division of Neonatology	J.-C. Fauchère	Newborn vital signs monitoring based on multiple vision sensors
University Hospital of Zurich	Biomedical optics research laboratory	M. Wolf	Newborn vital signs monitoring based on multiple vision sensors
University Hospital of Zurich	Clinic of Neonatology	M. Wolf	Neonate monitoring
University of Applied Sciences and Arts (FHNW)	Hochschule für Life Sciences	M. de Wild	Security / branding / implants

<i>University</i>	<i>Institute</i>	<i>Professor</i>	<i>Field of collaboration</i>
University of Applied Sciences and Arts (FHNW)	Hochschule für Life Sciences	U. Pieles	Biology and sensing
University of Applied Sciences and Arts, Lucerne (HSLU)	CC Aerospace biomedical science & technology / CC Mechanische Systeme / CC Electronics	M. Egli, C. Haack, O. Schälli	Micro gravity incubator
University of Applied Sciences and Arts, Lucerne (HSLU)	CC Mechanische Systeme	U. Lang	Nanofoils
University of Applied Sciences and Arts, Lucerne (HSLU)	Zentrum für Integrale Gebäude Technik	U. P. Menti	Building energy management
University of Applied Sciences and Arts, Lucerne (HSLU)	CC Electronics	E. Niederberger	Solid state lighting
University of Applied Sciences and Arts, Lucerne (HSLU)	Envelopes & Solar Energy	S. Wittkopf	BIPV
University of Applied Sciences, Valais (HES-SO)	Institut Systèmes industriels	P. Roduit	Smart grid and water distribution
University of Applied Sciences, Yverdon (HEIG-VD)	Microtechnique	M. Girardin	Actionneur de force de haute précision
University of Applied Sciences, Yverdon (HEIG-VD)	Systèmes Industriels de Bioénergie	J.-B. Michel	Building energy management
University of Applied Sciences, Zurich (ZHAW)	Institute of computational physics	B. Ruhstaller	Solid state lighting
University of Basel	Dept. of Physics	E. Mayer	Nano Argovia project
University of Basel	Dept. of Physics	C. Schöneberger	Development of organic solar cells
University of Bern	ARTORG Center for Biomedical Engineering	O. T. Guenat	Monitoring of in-vitro tissue models
University of Bern	ARTORG Center for biomedical engineering	S. Weber	Guided surgery; Image-guided micro surgery for hearing aid implantation
University of Bern	SPACE research & planetary sciences division	P. Wurz	Mass-spectrometry
University of Fribourg	Adolphe Merkle Institute	C. Weder	Nanosensors
University of Geneva	Computer vision and multimedia laboratory	T. Pun	Obstacle detection for the elderly based on stereo vision
University of Liège	Building Energy Monitoring and Simulation (BEMS)	P. André	Space and energy resources utilisation mapping
University of Neuchâtel	Institute of Chemistry	R. Deschenaux	Synthesis of nano particles

<i>University</i>	<i>Institute</i>	<i>Professor</i>	<i>Field of collaboration</i>
University of Neuchâtel	Institute of Biology	P. Junier	Ultrastructural investigation in microbial ecology
University of Neuchâtel	Laboratoire Temps-Fréquence	G. Miletí	Cell-based atomic clocks
University of Rennes I	CAIRN and IRISA Lab	O. Sentieys	Tools for programming multicores
University of Sheffield	Center Computational Imaging and Simulation Technologies in Biomedicine	A. Frangi	MRI segmentation for electrical impedance tomography
University of Zurich	Musculoskeletal research unit	B. von Rechenberg	Fluorescence lifetime imaging microscopy
University Pierre et Marie CURIE	Institut des Systèmes Intelligents et Robotique (ISIR)	S. Régnier	Haptic feedback for positioning system
WSL Institute for Snow and Avalanche Research SLF	Physique de la neige	M. Schneebeli	Icephobic coatings

Teaching

	<i>Title of lecture</i>	<i>Context</i>	<i>Location</i>
J.-M. Buforn	Ingénierie de la Qualité (Expert)	Microtechniques	HE-ARC Neuchâtel
M. Dadras	TEM and AFM nanotools	Master program	HE-ARC Neuchâtel
	Microscopy	Master of biology	UNINE
	AFM, TEM and SEM	Doctoral school	EPFL
J.-D. Decotignie	Informatique du Temps Réel	Bachelor informatique	EPF Lausanne
	Real Time Networks	Master computer and communication systems	EPF Lausanne
J. R. Farserotu	Satellite Communication Systems and Networks	Master degree course under Communication systems and space technology	EPF Lausanne
W. Glettig	Projet Goniomètre	Conception de mécanismes II	EPF Lausanne
	Projet PRIGO		
G. Nisato, O. Fernández, T. Offermans, N. Marjanović	Introduction to printed electronics	Training FSRM	IMT-Neuchâtel
C. Piguet	Microelectronics for Systems-on-Chips	Master, EPFL, Autumn semester	EPF Lausanne
	Green Electronics	Invited course	ISEP Paris
	ICT for Sustainable Development	Invited course	ISEP Paris
	Microelectronic Technology	ALaRI course on embedded systems	University of Lugano
D. Schmid	Von der Idee zum Produkt – mit Mikro- und Nanotechnologie für die Zukunft	SCNAT: Research live	Davos
	Lichtschranken – wie funktionieren sie?	Kinderlab	Landquart Bibliothek
E. Scolan	Nano-/Micro-structuration de revêtements élaborés par voie sol-gel : design, fabrication, intégration et application industrielles	Maîtriser le procédé Sol-Gel et ses applications industrielles aux matériaux multifonctionnels	Ecole Polytechnique, Paris

	<i>Title of lecture</i>	<i>Context</i>	<i>Location</i>
G. Weder	Introduction à la culture cellulaire	Diplôme fédéral ES de technicien en analyses biomédicales	Ecole Supérieure du Canton de Neuchâtel
F. Zanella, N. Marjanović	Organic Thin-Film Transistors (OTFTs): Basics, Applications, Sustainability	Module sustainable production and clean technologies – Printed organic electronics	FHNW, School for Life Sciences, Basel

Theses

PhD Degrees Awarded in 2015

<i>Name</i>	<i>University</i>	<i>Title</i>
S. Heub	ETH Zurich	Integrated and automated sample preparation for the monitoring of pollutants in water
K. Kanoun	EPF Lausanne	Energy-efficient co-design optimization of many-core platforms for big-data streaming applications
F. Kehl	ETH Zurich	Theory, development and validation of a novel label-free waveguide grating based biosensor system
F. Lütolf	EPF Lausanne	Optical properties of asymmetric, partially metallic gratings
O. Pérez-Anguiano	EPF Lausanne	Innovative optical lactate biosensing through the design of nanostructured materials
L. Rossini	EPF Lausanne	Electromagnetic modeling and control aspects of a reaction sphere for satellite attitude control
B. Schyrr	Université de Fribourg	Development and characterization of thin sensitive films for optical (bio)chemical sensing, and implementation as fiber-optic sensors for wound monitoring application
P. Teerapanich	LAAS-CNRS, Toulouse	Fluorescence-based nanofluidic biosensor platform for real-time monitoring of protein binding kinetics
X. Zeng	EPF Lausanne	Active atomic clockwork: Mode-locked GaN QW laser with Rb atomic vapor cell absorber

CSEM Employees carrying out a PhD

<i>Name</i>	<i>Professor / University</i>	<i>Theme / CSEM Unit</i>	<i>Start year</i>
F. Braun	J.-P. Thiran / EPF Lausanne	Estimation of hemodynamics via electrical impedance tomography / Systems	2013
S. Cloix	T. Pun / University of Genève	Stereoscopic computer vision / Integrated & Wireless Systems	2012
L. Dümpelmann	L. Novotny / ETH Zurich	Deep-subwavelength plasmonic nanostructures for light harvesting / Thin-Film Optics	2013
E. A. Hammes	P. Ryser / EPF Lausanne	Design, implementation and integration of an indoor air quality sensor system / Microrobotics & Packaging	2012
S. Heub	P. S. Dittrich / ETH Zurich	Integrated sample preparation for label-free Immunoassays / Landquart	2011
S. Karlen	G. Miletí / University of Neuchâtel	MEMS cells for atomic clocks / Systems	2014
F. Kehl	J. Vörös / ETH Zurich	Waveguide grating biosensing / Landquart	2011

Name	Professor / University	Theme / CSEM Unit	Start year
V. Kopta	C. C. Enz / EPF Lausanne	FM-UWB radio for high-density wireless sensor networks / Integrated & Wireless Systems	2014
J. Kruis	S. Henein / EPF Lausanne	Hybridization of silicon micro-components / Systems	2012
J. B. Larsen	O. Guenat / University of Bern	Electrochemical in-vitro metabolites sensing / Landquart	2011
F. Lütolf	O. Martin / EPF Lausanne	Optical properties of asymmetric, partially metallic gratings / Thin-Film Optics	2011
J. Mayer	C. Schönenberger / University of Basel	Light Management and harvesting for photovoltaic and sensing applications / Thin-Film Optics	2014
D. Müller	A. de Mello / ETH Zurich	Miniaturization of asymmetrical flow field-flow fractionation / Landquart	2012
O. J. Perez Anguiano	H. Hoffman / EPF Lausanne	Innovative optical lactate biosensing through the design of nanostructured materials / Micro & Nano Systems	2010
M. Proenca	J.-P. Thiran / EPF Lausanne	Estimation of hemodynamics via electrical impedance tomography / Systems	2012
M. Rapin	J. Snedeker / ETH Zurich	Wearable EIT system / Systems	2013
D. C. Rojas Quiros	J.-D. Decotignie / EPF Lausanne	Development of MAC and routing protocols for dense wireless sensor networks / Integrated & Wireless Systems	2014
F. Sorba	H. Shea / S. Henein / EPF Lausanne	MuscleLab: cell population stiffness measurements / Micro & Nano Systems	2014
J. Sun	H. Lissek, X. Falourd / EPF Lausanne	Anomaly detection in time varying signals for the quality inspection of electromotors / Microrobotics & Packaging	2011
R. Thirunarayanan	C. C. Enz, D. Ruffieux / EPF Lausanne	Ultra-low power flexible frequency synthesizers / Integrated & Wireless Systems	2011

Commissions and Committees

P. Albert	Expert, Electronic Components and Systems for European Leadership Joint Undertaking (ECSEL)
P.-J. Alet	European Photovoltaic Technology Platform: member of the Steering committee, leader of the Grid Integration working group IEEE International Conference on DC Microgrids: member of the technical committee
F. Amez-Droz	CSEM Representative, EARTO Communication Group CSEM Representative, Swiss Association of Science Journalism
C. Bosshard	CSEM Representative, European Photonics Industry Consortium (EPIC) Innovation Network Switzerland: Member of Advisory Board and Technology Field Leader Nano Managing Director of the Swissphotonics NTN Photonics21, Board of Stakeholders
P. Dallemagne	Secretary and Swiss representative of Technical Committee 5 "Information Technology Applications", International Federation for Information Processing (IFIP)

J.-D. Decotignie	<p>ISO TC 65 Swiss Committee</p> <p>ISO TC 65C, WG16 convenor, Wireless Industrial Communication Standardization Program Committee, Design Automation in Europe (DATE), Grenoble, France.</p> <p>Program Committee, IEEE Real-Time Systems Symposium (RTSS), San Antonio, TX, USA</p> <p>Program Committee, Real-Time Networks and Systems, Lille, France</p> <p>Program Committee, Workshop on Factory Communication Systems, Palma de Mallorca, Spain</p>
M. Despont	<p>Board member of the Swiss-MNT network</p> <p>Chairman of the IEEE International Conference on Micro ElectroMechanical Systems (MEMS), 2018</p> <p>Chairman of the Swiss Nanoconvention (Neuchâtel, 2015)</p> <p>CSEM and HTA representative at the Micro- and Nano- Technology Workgroup, European Spatial Agency (ESA)</p> <p>External Expert at PhD Thesis, EPFL</p> <p>Member of the Technical Program Committee of European Solid-State Device Conference, ESSDERC (Lausanne, 2016)</p> <p>Member of the editorial board of Microelectronic Engineering Journal (Elsevier)</p> <p>Member of the executive board of the Swiss research program NanoTera</p> <p>Member of the Industrial Advisory Board, Nanotechnology Program, Prof H. Bahaskaran, Oxford University, UK</p> <p>Member of the Int'l Steering Committee of the Micro- and NanoEngineering (MNE) conference</p> <p>Senior Member of the IEEE Society</p>
M. El-Khoury	<p>CNCI Chambre Neuchâteloise du Commerce et de l'Industrie, Neuchâtel</p> <p>Concours International de Chronométrie, Le Locle, Membre du Comité d'honneur</p> <p>Conseil de l'Université de Neuchâtel</p> <p>Emirati-Swiss Friendship Platform, Abu Dhabi</p> <p>Nano-Tera, Member of the Steering Committee</p>
H. F. Knapp	<p>Delegate for cluster initiative Toolpoint for Lab Science</p> <p>Member of the Executive Board of biotechnet, Switzerland</p>
J. R. Farserotu	<p>Chair and Research Co-ordinator The Hermes Partnership</p> <p>Chair of ETSI Technical Committee Smart Body Area Networks (TC SmartBAN)</p> <p>Expert, Bachelor projects, WiseSkin, BFH, July 2015</p> <p>Member of the Steering Committee and Technical Committee, IEEE International Symposium on Medical Information and Communication Technology 2015 (ISMICT 2015)</p> <p>Opponent, Doctoral Thesis Defence, H. Karvenen, Oulu University, Oulu, Finland, March 2015</p>
R. Ferrini	<p>Chair of the Swissphotonics Solid State Lighting – (SSSL) Swiss National Laboratory for Solid State Lighting</p>
E. Györvary	<p>Advisory Board Smart Frame</p> <p>Extended Board Member CSEM Brasil</p> <p>Extended Board Member HTA</p> <p>Member of the Finnish Chamber of Commerce</p> <p>Member of the Latin American Chamber of Commerce</p>
H. Heinzelmann	<p>Program Committee, MNE Micro Nano Engineering 2015, Den Haag</p> <p>Program Committee, SSI Smart Systems Integration 2015, Copenhagen</p> <p>Steering Committee, CCMX Competence Center for Materials Science and Technology</p> <p>VP Nanotechnology, Swiss Society for Optics and Microscopy SSOM</p>
C. Julia-Schmutz	<p>Communication Coordinator within the Heterogeneous Technology Alliance (HTA)</p> <p>CSEM Representative, BioAlps</p>

G. Kotrotsios	<p>Le Réseau, Advisory Board</p> <p>Member of the Board of Directors of CSEM do Brazil</p> <p>Member of the Board of Directors of Femto Innov, Besancon, France</p> <p>Member of the Board of the Heterogeneous Technology Alliance (alliance federating the Fraunhofer (microelectronics), VTT, CEA-Tech and CSEM)</p> <p>Member of the Executive Board of EARTO, the European Association of Research and Technology Organisations</p> <p>Member of the Executive Board of EREA (the European Association of Aeronautics Research Centers)</p> <p>Member of the International Advisory Board of the Samara Space and Aeronautics University (SGAU), Russian Federation</p> <p>Micronarc, member of the expert group</p>
J. Krauss	President, Swiss Society of Biomedical Engineering (SSBE)
M. Krieger	<p>CSEM Representative Greater Zurich Area (GZA)</p> <p>CSEM Representative Zürcher Handelskammer (ZHK)</p> <p>CSEM Representative, Advanced Factory Automation workgroup of Swissmem (AFA)</p>
S. Lecomte	European Time and Frequency Forum (EFTF) scientific committee member
A. Madrigal	<p>CSEM Delegate in the Aviation and Security Research Groups of EREA (Association of European Establishments in Aeronautics)</p> <p>CSEM Representative, General Forum Clean Sky</p> <p>CSEM Representative, Network of European Research Organisations on ESA Issues (NERO)</p> <p>CSEM Representative, Swiss Aeronautics Security and Defense Division of Swissmem (Swiss ASD)</p> <p>CSEM Representative, Swiss Space Industries Group of Swissmem (SSIG)</p> <p>Expert for the evaluation of proposals for the Comité Consultatif pour les Technologies Spatiales (CCTS) of the Swiss Space Office (SSO)</p> <p>Member of the Steering Committee of the Swiss Space Centre (SSC)</p> <p>Members of the Advisory Board of the new Space exhibition of the Museum of Transport of Lucerne</p>
S. Mohrdiek	<p>Member of Phonotics21 Work Group 6 – Design and Manufacturing of Components and Systems</p> <p>Swissphotonics, Head of Swiss Photonic Packaging Laboratory</p>
G. Nisato	Board member of the Organic and Printed Electronic Association (OE-A)
A. Perret	<p>Euripides Scientific Adviser of the Board, Council Member and Adviser of the Council</p> <p>Member of the ESA's Future Technology Advisory Panel</p> <p>Program Committee of Smart System Integration Conference</p> <p>Secrétaire de la Fondation du Prix Omega</p>
L.-E. Perret-Aebi	<p>CTI expert in the micro-nano commission</p> <p>Vice President of the Swiss Solar Connect association</p>
C. Piguet	<p>Membre du Conseil d'Administration de Centredoc, Neuchâtel, Suisse (until June 2015)</p> <p>Steering Committee of the ALARI Master Course, University of Lugano</p>
D. Ruffieux	Member of the International Technical Program Committee of the International Solid State Circuit Conference (ISSCC) in the Technology Directions sub-committee
E. Schaller	Member of the Executive Board of sensors.ch, Switzerland
P. Steiert	<p>Advisory Board Member for Institute für Chemistry and Biological Chemistry at the ZHAW</p> <p>Advisory Council for cluster initiative Toolpoint for Lab Science</p> <p>Member of the Executive Board for microPark Pilatus</p>

Prizes and Awards

- May 2015 The LYNCEUS project received the 2014 Award for Best European innovative project of the Valencian Region (Valencia, SP).
- June 2015 Gilles Weder has been awarded the BiolInnovation-Eclosion Prize 2015 for his work on a rapid, efficient, and non-invasive device for determining oxygen concentrations in cell and tissue cultures (Lausanne, CH).
- June 2015 Young researcher Fabian Braun, a PhD student at CSEM, took home the Best Student Paper Award at the 16th International Conference on Biomedical Applications of Electrical Impedance Tomography (EIT 2015) for his work entitled "4D Heart Model Helps Unveiling Contributors to Cardiac EIT Signal" (Neuchâtel, CH).
- June 2015 The Quantum Electronics and Optics Division (QEOD) of the European Physical Society (EPS) has awarded the 2015 Thesis Prize for applied aspects to Dr. Tobias Herr for his work on "Solitons and dynamics of frequency comb formation in optical microresonators" (Munich, DE).
- July 2015 Luc Dämpelmann received the Best Talk Award at the International Nanoscience Student Conference, INASCON 2015, in Basel for his presentation "Large-Scale Plasmonic Color Substrates" (Basel, CH).
- August 2015 The young researcher Martin Proenca has received the SSBE Best Poster Award from the Swiss Society of Biomedical Engineering (www.ssbe.ch) for his work, entitled "Non-invasive pulmonary artery pressure monitoring: a pulse wave velocity approach" (Neuchâtel, CH).
- November 2015 Silvia Angeloni has been awarded the Neode Special Prize by the jury 2015 for her work on enabling a technology transplant from the watchmaking industry to the field of innovative labware manufacturing for nanotoxicity studies and nanomedicine development (Neuchâtel, CH).

CSEM SA
Jaquet-Droz 1
CH-2002 Neuchâtel

CSEM Alpnach
Untere Gründlistrasse 1
CH-6055 Alpnach Dorf

CSEM Landquart
Bahnhofstrasse 1
CH-7302 Landquart

CSEM Muttenz
Tramstrasse 99
CH-4132 Muttenz

CSEM Zurich
Technoparkstrasse 1
CH-8005 Zurich

www.csem.ch
info@csem.ch
jobs@csem.ch

